GEOLOGICAL SURVEY OF DENMARK AND GREENLAND BULLETIN 35 • 2016

Review of Survey activities 2015

Edited by
Adam A. Garde, Ole Bennike, Kristine Thrane and W. Stuart Watt

GEOLOGICAL SURVEY OF DENMARK AND GREENLAND
MINISTRY OF ENERGY, UTILITIES AND CLIMATE

Geological Survey of Denmark and Greenland Bulletin 35

Keywords
Geological Survey of Denmark and Greenland, survey organisations, current research, Denmark, Greenland.

Cover photographs from left to right

1 3D anthroprogenic model of urban infrastructure with buildings and pipes for combination with geological data.
2 Elevated plain (*c*. 800 m a.s.l.) across Precambrian basement cut by a deep valley, Torngat Mountains, Labrador, Canada. Source: Google Earth.
3 The geothermal energy potential in Denmark is substantial and a WebGIS portal for exploration of deep geothermal energy based on geolocial and geophysical data has been launched. An interactive 3D tool in the portal gives an intuitive overview of the variations of subsurface topography.
4 After drilling two or more overlapping holes in the sea ice, a so-called Kajak core with seabed sediments is retrieved for investigations of past climate. Photo: Jesper Hoffmann.

Frontispiece: facing page
Field investigations at the Sulugssut intrusive complex in the alpine terrain of East Greenland. The rocks formed during the initial stages of the opening of the North Atlantic Ocean at *c*. 55 Ma. The field camp in the background was pitched on top of a glacier. Photo: Thomas F. Kokfelt.

Chief editor of this series: Adam A. Garde
Editorial board of this series: John A. Korstgård, Department of Geoscience, Aarhus University; Minik Rosing, Geological Museum, University of Copenhagen; Finn Surlyk, Department of Geosciences and Natural Resource Management, University of Copenhagen
Scientific editors: Adam A. Garde, Ole Bennike, Kristine Thrane and W. Stuart Watt
Editorial secretary: Jane Holst
Referees (numbers refer to first page of reviewed article): Katrine Juhl Andresen, DK (27); Anonymous (59, 75); Per Bergmo, NO (87); Albertas Bitinas, LT (47); Lars Ole Boldreel, DK (35); C. Kent Brooks, UK (59); Mikael Calner, SE (39); Andy Chadwick, UK (87); Jacob Q. Christensen, DK (9, 47); Stefan Claesson, SE (103); William Colgan, CA (71); Lynn Dafoe, CA (83); Christian Deibjerg, DK (17); Mikael Erlström, SE (23); Ida Fabricius, DK (43); Wesley Farnsworth, NO (71); Jens Galsgaard, DK (31); Christopher Harrison, CA (63, 83); Jens Havskov, NO (79); Michael Houmark-Nielsen, DK (35); Julie Hollis, GL (95); Jan Jeppesen, DK (13); Reinhard Kirsch, DE (23); Margrethe Kristensen, DK (9); Mats Larsbo, SE (17); Gert Laursen, DK (13); Jerry Lloyd, UK (67); Anders Mattias Lundmark, NO (103); Sebastian Mernild, NO (75); Thorsten Nagel, DK (99); Allen Nutman, AU (55); Asger Ken Pedersen, DK (63); Toby Rivers, CA (91); Anders Scherstén, SE (55); Denis Schlatter, CH (99); Vera Schlindwein, DE (79); Iain Sinclair, CA (91); Jasna Sinigoj, SL (95); Jette Sørensen, DK (27); Svend Stouge, DK (39); Sander Suicmez, DK (43); Nicolas R. Thibault, DK (51); Clemens Ullmann, UK (51); Tod Waight, DK (31); Jacob C. Yde, NO (71).
Illustrations: Jette Halskov, Stefan Sølberg, Susanne Rømer, Adam A. Garde and Benny M. Schark
Layout and graphic production: Jane Holst and Annabeth Andersen
Printer: Rosendahls-Schultz Grafisk A/S, Albertslund, Denmark
Manuscripts received: 8 January – 29 February 2016
Final versions approved: 11 February – 1 May 2016
Printed: 15 July 2016

ISSN (print) 1604-8156, ISBN (print) 978-87-7871-438-1
ISSN (online) 1904-4666, ISBN (online) 978-87-7871-439-8

Citation of the name of this series
It is recommended that the name of this series is cited in full, viz. *Geological Survey of Denmark and Greenland Bulletin*.
If abbreviation of this volume is necessary, the following form is suggested: *Geol. Surv. Den. Green. Bull*. 35, 106 pp.

Available from
Geological Survey of Denmark and Greenland (GEUS), Øster Voldgade 10, DK-1350 Copenhagen K, Denmark
Phone: +45 38 14 20 00, fax: +45 38 14 20 50, e-mail: *geus@geus.dk*
and at *www.geus.dk/publications/bull*

© De Nationale Geologiske Undersøgelser for Danmark og Grønland (GEUS), 2016
For the full text of the GEUS copyright clause, please refer to *www.geus.dk/publications/bull*

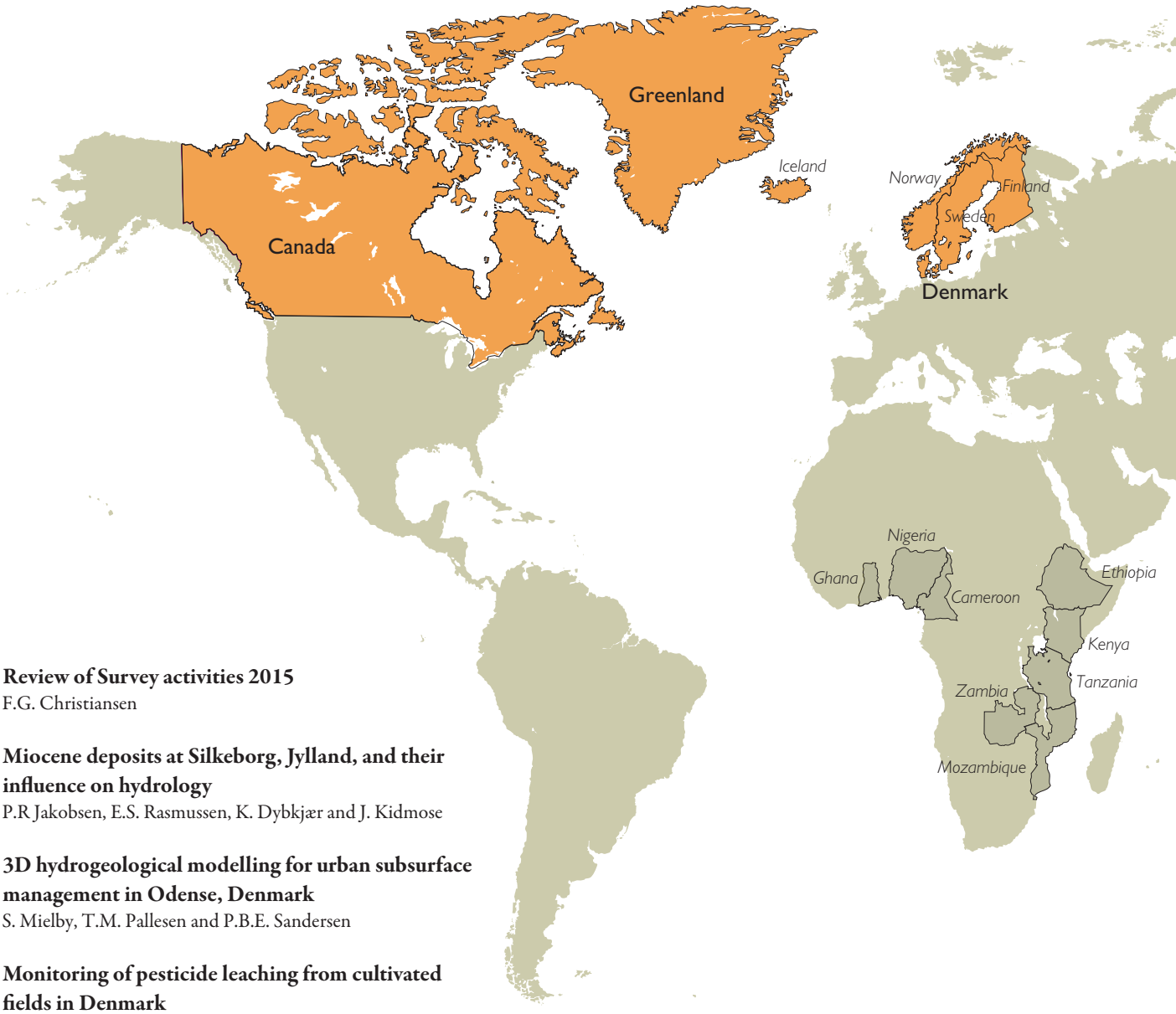

7 Review of Survey activities 2015
F.G. Christiansen

9 Miocene deposits at Silkeborg, Jylland, and their influence on hydrology
P.R Jakobsen, E.S. Rasmussen, K. Dybkjær and J. Kidmose

13 3D hydrogeological modelling for urban subsurface management in Odense, Denmark
S. Mielby, T.M. Pallesen and P.B.E. Sandersen

17 Monitoring of pesticide leaching from cultivated fields in Denmark
W. Brüsch, A.E. Rosenbom, N. Badawi and P. Olsen

23 A WebGIS portal for exploration of deep geothermal energy based on geological and geophysical data
H. Vosgerau, A. Mathiesen, M.S. Andersen, L.O. Boldreel, M.L. Hjuler, E. Kamla, L. Kristensen, C.B. Pedersen, B. Pjetursson and L.H. Nielsen

27 Towards a national 3D geological model of Denmark
P.B.E. Sandersen, T. Vangkilde-Pedersen, F. Jørgensen, R. Thomsen, J. Tulstrup and J. Fredericia

31 Pre-Quaternary rocks and sediments with a high level of radioactivity in Denmark
P. Gravesen and P.R. Jakobsen

35 Tectonic control on the formation of Roskilde Fjord, central Sjælland, Denmark
S.A.S. Pedersen and P. Gravesen

39 Middle–Upper Ordovician and Silurian stratigraphy and basin development in southernmost Scandinavia
N.H. Schovsbo, A.T. Nielsen and M. Erlström

43 Types of formation water and produced water in Danish oil- and gasfields: implications for enhanced oil recovery by injection of 'smart' water
N.H. Schovsbo, H.D. Holmslykke, C. Kjøller, K. Hedegaard, L. Kristensen, E. Thomsen and K.H. Esbensen

47 Middle Pleistocene interglacial deposits near Herning, Jylland, Denmark
B.V. Odgaard, K.L. Knudsen, O. Bennike and H.J. Granat

51 Geochemistry of the Maastrichtian Rørdal Member, Jylland, Denmark: Ce anomaly as a palaeo-redox proxy
C. Knudsen and B.W. Lauridsen

Grey indicates countries where GEUS has ongoing or recently completed projects.

Orange indicates countries with GEUS projects described in this volume.

55 New zircon U-Pb and Hf isotopic constraints on the crustal evolution of the Skjoldungen region, South-East Greenland
T.F. Kokfelt, T. Næraa, K. Thrane and L. Bagas

59 *In situ* fractionation and inward migration of the solidification front in the Skaergaard intrusion, East Greenland
T.F.D. Nielsen

63 Palaeovalleys at the basal unconformity of the Palaeoproterozoic Karrat Group, West Greenland
P. Guarnieri, C.A. Partin and D. Rosa

67 Investigations of past climate and sea-ice variability in the fjord area by Station Nord, eastern North Greenland
N. Nørgaard-Pedersen, S. Ribeiro, N. Mikkelsen, A. Limoges and M.-S. Seidenkrantz

71 Placing Greenland ice sheet ablation measurements in a multi-decadal context
D. van As, R.S. Fausto, J. Cappelen, R.S.W. van de Wal, R.J. Braithwaite, H. Machguth and the PROMICE project team

75 Regional climate-model performance in Greenland firn derived from *in situ* observations
C. Charalampidis, D. van As, P.L. Langen, R.S. Fausto, B. Vandecrux and J.E. Box

79 Crustal structure over the Nagssugtoqidian deformation front in West Greenland: Receiver Function analysis
T. Dahl-Jensen, P.H. Voss and T.B. Larsen

83 New geophysical and geological mapping of the eastern Baffin Bay region, offshore West Greenland
U. Gregersen, P.C. Knutz and J.R. Hopper

87 Mapping of the CO_2 storage potential in the Nordic region
K.L. Anthonsen, P. Frykman and C.M. Nielsen

91 Burial and exhumation history of the Labrador-Newfoundland margin: first observations
P. Japsen, P.F. Green, J.M. Bonow, A.M. Hinchey and D.H.C. Wilton

95 The Greenland Mineral Resources Portal – another step forward
M. Pedersen, M. Hansen, B.H. Heincke and L. Thorning

99 aFieldWork – an Android app for offline recording of geological information and data display
M. Hansen, M.N. Petersen, T.F. Kokfelt and B.M. Stensgaard

103 jAgeDisplay: software for evaluation of data distributions in U-Th-Pb geochronology
T.B. Thomsen, T. Heijboer and P. Guarnieri

Review of Survey activities 2015

Flemming G. Christiansen
Deputy Director

2015 was a tough year for many geologists around the World, and the years to come may be even tougher. Low prices of oil, gas and other energy sources, and also of many mineral commodities have led to a significantly lower level of investments in exploration and production than seen in previous years. Both society and industry suffer from much lower income, so cost reduction is the new buzzword; and many geologists have lost their jobs – also in Denmark and at GEUS. Investments in data, projects and knowledge – including many typical products from the Geological Survey of Denmark and Greenland (GEUS) – are worryingly low and will eventually reduce the level of knowledge for decision makers in both the private and public sectors.

Commodity prices are, however, cyclic by nature, and it is very important for GEUS to continue to collect and compile new data, build up new knowledge and models based on research projects – and prepare for a future that will still rely on traditional resources but with a strong focus on a transition towards new green technologies that can reduce the consumption of fossil fuels and the emission of CO_2.

This issue of GEUS' Review of Survey activities has a broader content and a total of 24 four-page articles, more than seen for several years. It reflects that GEUS works on many different subjects and is preparing for a future where geology still plays an important part in the planning of important activities in Denmark and Greenland. Eleven papers are on Denmark, eight on Greenland and five on international and general themes.

Activities in Denmark

GEUS' Danish activities and research cover a wide range of topics within our specific programme areas: data, water, energy, mineral resources and nature and climate, as well as many other basic research projects.

The use of groundwater is very important for Denmark, and GEUS carries out many studies on water resources, their protection and possible future challenges due to changes in climate and use. As a follow-up on previous studies of the Miocene sedimentary succession in Jylland, one paper focuses on deposits at Silkeborg and their influence on hydrology. Another paper describes 3D hydrogeological modelling important for the urban subsurface management in Odense. A third paper is on the monitoring of pesticide leaching from cultivated fields in Denmark, an activity that has been carried out for several decades.

Denmark has a large potential for subsurface geothermal energy. Following several regional studies and many local case stories in preparation for drilling campaigns, GEUS has developed a WebGIS portal for exploration of deep geothermal energy based on geological and geophysical data. One paper describes this portal where the relevant geological and geophysical maps, data and key information from drilling are easily accessed.

Many of the applied studies emphasise the strong need for a comprehensive national 3D geological model of Denmark. Similar models are being developed in several other European countries in order to provide the best possible background for large resource and infrastructure projects. One paper describes the strategy behind the effort that GEUS is currently putting into developing such models and gives examples of how existing data and geological models can be applied.

Sediments and rocks in Denmark generally have a low content of radioactive minerals and radon. Some of the highest levels of radioactivity on Mors and Bornholm have been studied in detail to understand their geological control and distribution in space. This is described in one paper. Another paper describes how the terrain in the Roskilde area, and in particular the Roskilde Fjord, is controlled by deeper tectonic features that are clearly recorded in subsurface maps of the Danian limestone and Paleocene chalk, marl and clay. After several studies of the Palaeozoic succession in Denmark, it is now possible to make a complete Middle–Upper Ordovician and Silurian stratigraphy and basin model for all of southern Scandinavia. This is described in another paper using wireline logs as a correlation tool.

Several methods of enhanced oil recovery, e.g. injection of 'smart' water, have the potential to significantly increase oil production, and thereby income for Danish society. To do this, a detailed understanding of different types of reservoirs is required, as shown in a paper describing the distribution and composition of primary formation water and produced water in the North Sea oilfields.

© 2016 GEUS.

Interglacial marine deposits are fairly common in Denmark but for the first time such deposits are described from Kibæk in the Herning area, where they occur several metres above present sea level. Chalk is a very important rock for Denmark. It is the reservoir for most of the oil and gas resources in the North Sea, it is important as a groundwater reservoir in large areas onshore, and it is an important resource for cement production. One paper provides new details of geochemical stratigraphy as a tool to understand the depositional environments and their geographical correlation.

Activities in Greenland

Once again there was a high level of activity in and about Greenland in 2015. Many large and small projects were carried out, studies that are important for evaluating and marketing the resource potential in Greenland. The level of industrial activity in both oil and mineral exploration is very low at the moment, but it is important to prepare for a future when prices of the most important commodities will eventually rise again.

For the last few years GEUS has focused on mapping and mineral evaluation activities in South-East Greenland; this emphasis is now changing to West and North-West Greenland. Two papers give new information from South-East Greenland. One paper describes new geochronological data using Hf isotopes in zircon to unravel Archaean crustal accretion processes in the Skjoldungen region, and another provides entirely new insight into the fractionation processes of the world-famous Skaergaard intrusion, which has been discussed for many decades. The last paper on Greenland bedrock geology describes Palaeoproterozoic palaeovalleys underlying the Karrat Group in the Uummannaq region of West Greenland, where new field activity has started.

Studies and monitoring of the Greenland ice sheet and studies of marine sediments in the fjords around Greenland result in important contributions from GEUS to global climate models. One paper investigates past climate and sea-ice variability in the remote eastern part of North Greenland close to Station Nord. Results from the important PROMICE monitoring project with its focus on temperature sensitivity of ice sheet-ablation are presented in another paper. A third paper is on climate models based on *in situ* observations of Greenland firn.

Passive, so-called Receiver Function analysis of seismological signals from natural earthquakes around the World can be used to information on the deep crustal structure, e.g. the depth to Moho. One paper presents results from such a study across the Nagssugtoqidian front in West Greenland where a significant change in Moho is recorded across an ancient plate boundary and subduction zone.

Systematic mapping of offshore sedimentary deposits and evaluation of the petroleum potential is crucial for planning and marketing of licensing rounds and for advice on subsequent exploration activities. After several successful licensing rounds and a relatively high level of activity, the seismic data coverage in Baffin Bay is now relatively high compared to many other regions around Greenland. Based on a systematic updated interpretation and mapping, one paper outlines some interesting possibilities for future exploration but also describes the main risks and uncertainties.

International and broader technical themes

GEUS also works overseas in many different countries with a variety of projects and is involved in broader thematic studies.

Over the years GEUS has been involved in several projects of carbon dioxide capture and storage (CCS), especially with European Union and industrial funding. One paper summarises mapping of the storage capacity of sandstone aquifers in Denmark and the Nordic Region, based on a large Nordic collaboration project. Another paper describes a preliminary study of the burial and exhumation history of the Labrador-Newfoundland margin using apatite fission track analysis and thermal maturity methods similar to previous studies on the Greenland side of the Labrador Sea.

GEUS is constantly developing databases and facilities for easier access to and use of data, as well as new methodologies and technologies to make research easier, quicker and better for our geologists. One paper describes the Greenland Mineral Resources Portal; a new version of this was launched by GEUS and the Ministry of Mineral Resources in Greenland (MMR) in April 2015. The portal is based on decades of work and re-organisation of previous databases with an ambition of securing data and making them easily accessible through the internet. Another paper is on a new app – aFieldWork – that has been designed specifically for field work in Greenland to make digital capture of data as easy and efficient as possible. The last paper presents the development of special software for evaluation of data distribution in U-Th-Pb geochronology – jAgeDisplay.

Miocene deposits at Silkeborg, Jylland, and their influence on hydrology

Peter Roll Jakobsen, Erik Skovbjerg Rasmussen, Karen Dybkjær and Jacob Kidmose

A motorway was constructed in 2010–2016 through the suburbs of the city of Silkeborg (Fig. 1). The Danish Road Directorate wished to climate-proof the motorway against adverse future climate changes. The directorate collaborated with the Geological Survey of Denmark and Greenland (GEUS) to study the hydrological conditions. Studies of historical and projected climate-change-driven variations in groundwater levels in relation to urbanised hydrological fluxes were conducted by Kidmose *et al.* (2013, 2015). During the construction of the motorway, Miocene and Quaternary deposits were exposed in the slopes of the Gudenå valley and late-glacial glaciofluvial deposits were found in the valley floor. This paper focuses on the Miocene sediments and their influence on the local hydrological conditions.

At Silkeborg the Gudenå valley is *c.* 35 m deep (Fig. 1). The surrounding terrain is a till plain. In the slope of the valley, glaciofluvial sand is found below the till. Miocene deposits are found below the glaciofluvial sand. The floor of the Gudenå valley is covered by *c.* 15 m thick glaciofluvial deposits, which rest on Miocene deposits. In borehole no. DGU 87.907 49 m of Miocene deposits belonging to the Vejle Fjord Formation are recorded, consisting primarily of marine clay with minor occurrences of sandy deposits.

About 12 km south of Silkeborg lower Miocene deposits are seen in outcrops and boreholes (Fig. 2). Here the fluvial Addit Member of the Billund Formation (Rasmussen *at al.* 2010) is separated from the underlying marine Vejle Fjord Formation by a sharp erosional contact (Rasmussen 2014).

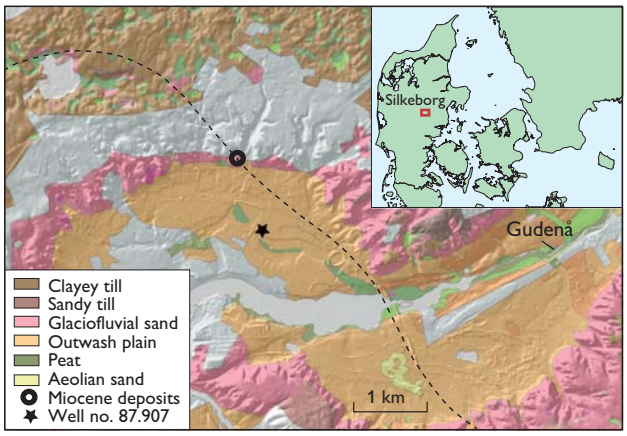

Fig. 1. Geological map of the Silkeborg area. Dashed line: motorway.

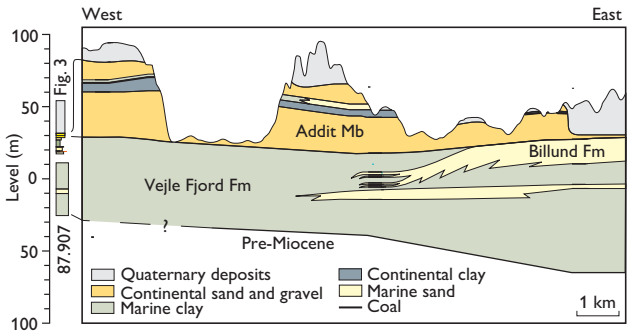

Fig. 2. East–west profile about 12 km south of Silkeborg (from Rasmussen 2014). A composite log from Silkeborg (Fig. 3) and data from well no. DGU 87.907 are shown to the left.

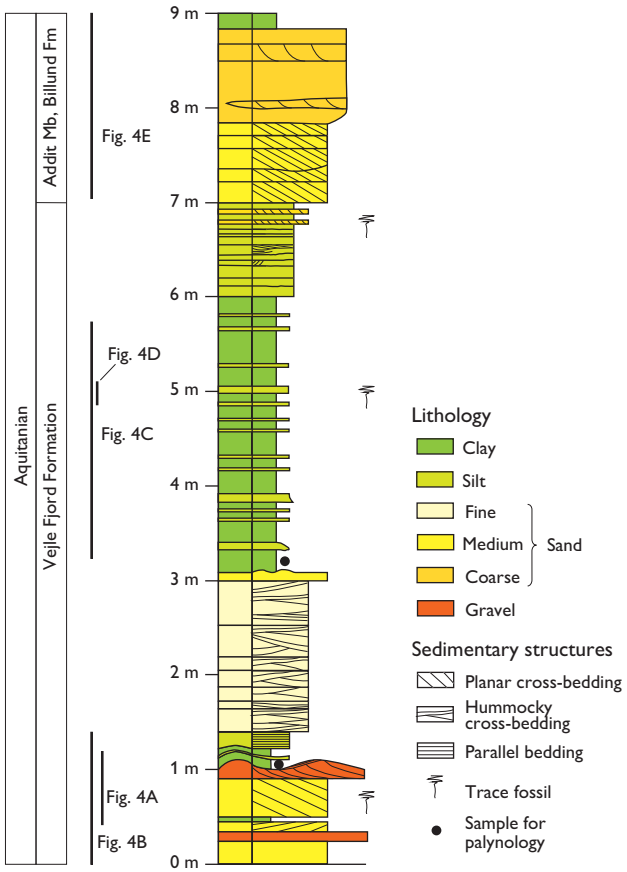

Fig. 3. Composite sedimentological log of the temporarily exposed Miocene deposits.

© 2016 GEUS.

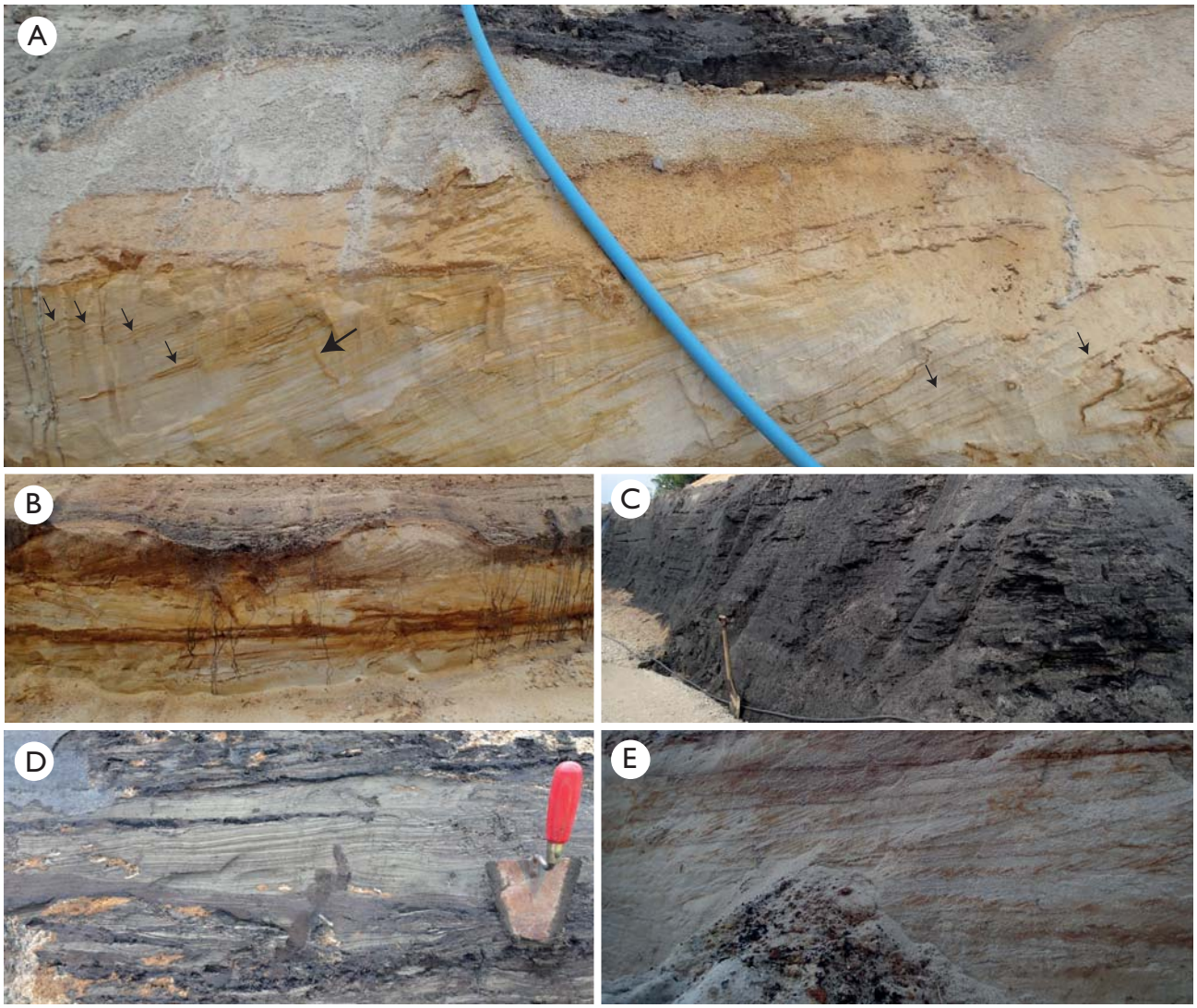

Fig. 4. Details of the Miocene deposits. The stratigraphic positions of the photos are indicated on Fig. 3. **A:** Cross-stratified medium grained sand. Double clay layers are indicated with small arrows. Trace fossil is indicated with larger arrow. **B**: Wave-formed, coarse grained ripples. **C**: Thick dark mud succession. **D**: Hummocky cross-stratification (HCS). **E**: Tabular co-sets of cross-stratified beds.

Sedimentology

The section along the motorway comprised 9 m of Miocene deposits (Fig. 3). The lower part is characterised by cross-stratified medium-grained sand, dipping *c.* 30° towards the north (Fig. 4A). A few trace fossils (*Skolithos*?) are seen. The cross-stratified sand is sharply overlain by wave-formed, coarse-grained ripples. The crests of the ripples strike SE–NW, and crest-to-crest spacing is in the range of 250 cm with amplitudes up to 35 cm (Fig. 4B). The ripples show tangential cross-bedding towards the SW. In a nearby exposure, tidal bundles form the base of the section. The presence of clay layers varies systematically and is commonly characterised by double clay layers (Fig. 4A). Dips of cross-bedding are both SW and NE. The coarse-grained ripples are in turn overlain by a dark brown mud. The mud is succeeded by silt and fine-grained sand, *c.* 1.5 m thick. Hummocky cross-stratifications (HCS) are common, especially in the upper part of the section. These are superimposed by 3 m of dark brown mud (Fig. 4C) showing a slight increase in grain size upwards where hummocky cross-stratified sands are common (Fig. 4D). A sharp boundary separates the mud from an overlying 2 m thick section of medium- to coarse-grained sand and gravel. This coarse-grained section is composed of tabular co-sets of cross-stratified beds dipping towards the south (Fig. 4E).

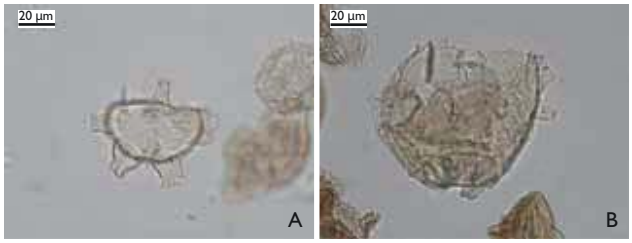

Fig. 5. **A**: *Homotryblium*? *additense*. **B**: *Chiropteridium galea*.

Bio- and chronostratigraphy and depositional environment

In order to confirm the Miocene age of the described succession and to achieve a more precise dating, two sediment samples were selected for palynological analysis. The stratigraphic positions of the samples are shown in Fig. 3.

One of the samples was almost barren, while the other contained a rich assemblage of organic particles dominated by bisaccate and non-saccate pollen. In addition, the sample contained a moderately rich and diverse dinoflagellate cyst (dinocyst) assemblage together with a few wood particles, cuticle, acritarchs and freshwater algae. This assemblage indicates a marine, inner neritic depositional environment with a high influx of freshwater (Tyson 1995).

The dinocyst assemblage is dominated by two species of the genus *Homotryblium*: *H.*? *additense* (Fig. 5A) and *H. plectilum*. Among several other dinocyst taxa, a single specimen of the stratigraphically important species *Chiropteridium galea* was found (Fig. 5B). The dinocyst assemblage refers the sample to the *Chiropteridium galea* Zone (Dybkjær & Piasecki 2010). This dinocyst zone is dated to the early Aquitanian (earliest Miocene) and the age of the sample is 23.03–22.36 Ma.

Palaeogeography

The sand and gravel in the lower part of the section were deposited during an overall regression of the Billund Formation in the early Miocene (Rasmussen *et al.* 2010). The gravel was probably originally deposited in a fluvial environment during the most extended regression. The cross-stratified sand in the lower part was formed in a marine bar that migrated landwards. The tidal bundles were formed by both ebb and flood currents, as indicated by the bipolar dips of cross-bedding, in an adjacent tidal inlet. The overlaying wave-formed, coarse-grained ripples were formed by marine reworking (Leckie 1988) of the coarse-grained fluvial sediments laid down during maximum regression and now forms a transgressive lag (Plint 1988). The depositional water depth of the coarse-grained ripples may lie in the range of 15 to 60 m (Leckie 1988) – most likely in the lower end as the sea-level changes during this part of the Miocene was *c.* 25 m (Miller *et al.* 2005). The strike of the crests of the coarse-grained rippels, SE–NW, indicates the trend of the palaeo-shoreline (Leckie 1988). The succeeding mud and HCS-dominated silt and fine-grained sand were deposited in slightly deeper water, in the offshore transition zone. The mud-dominated part with few intercalations of HCS's was deposited offshore near the storm wave base.

The assemblage of organic particles indicates that the sediment was deposited in a marine depositional setting near the coast. The two *Homotryblium* species further indicate that the palaeoenvironment was marine but probably with lowered salinity (Dybkjær 2004). These interpretations support the sedimentological interpretations and palaeogeographic maps for the earliest Miocene of Jylland, indicating that large river and delta systems existed, which transported large amounts of freshwater and sediment from the north to the middle part of Jylland (Rasmussen *et al.* 2010).

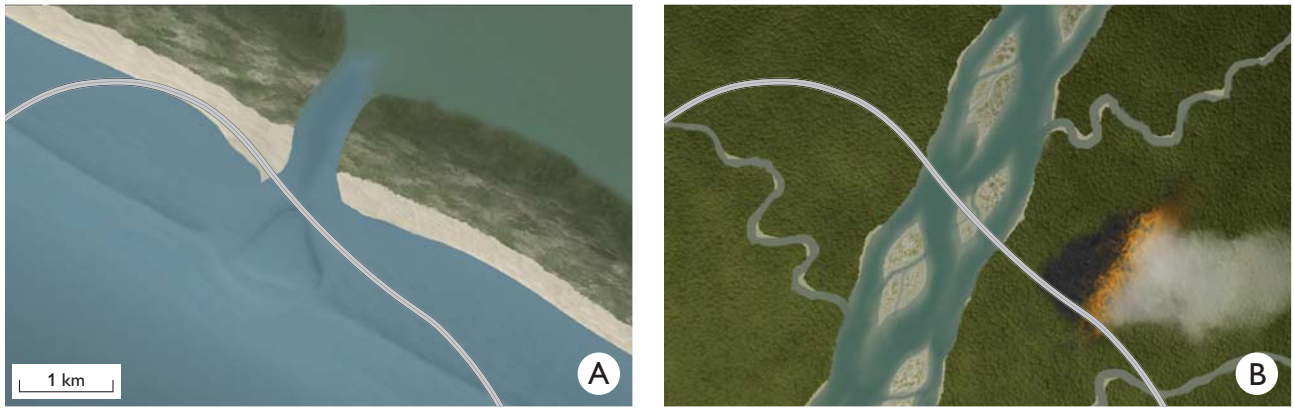

Fig. 6. Palaeogeographical reconstructions of the Silkeborg area. **A**: Early Aquitanian (earliest Miocene, Vejle Fjord Formation) tidal-dominated marine-barrier system. **B**: Late Aquitanian (Addit member, Billund Formation) fluvial environment. Grey line: motorway.

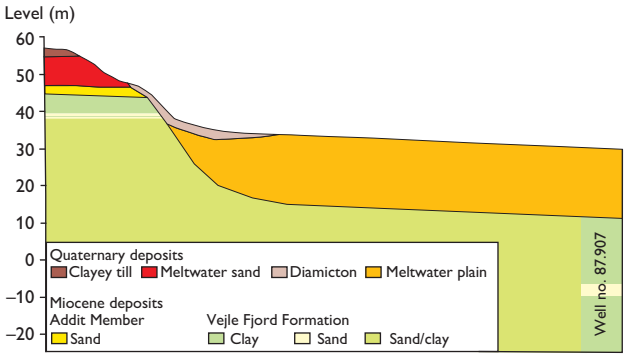

Fig. 7. Conceptual geological model along the motorway alignment.

The coarse-grained sand and gravel at the top of the studied succession, that sharply overlie the marine deposits, were deposited in a fluvial environment, the Addit Member of the Billund Formation (Rasmussen *et al.* 2010; Fig. 6). The dramatic change in the depositional environment was partly a result of an eustatic sea-level fall and partly a result of inversion of the Norwegian–Danish Basin (Rasmussen 2014). The latter resulted in marked incision in the middle and northern part of Jylland during the late Aquitanian. The Miocene succession in Silkeborg shows a strong resemblance to successions in boreholes and exposures about 12 km south of Silkeborg (Fig. 2).

Hydrology

On the floor of the Gudenå valley, wells with screens in the Miocene deposits have artesian hydraulic heads, whereas the hydraulic head in the overlying glaciofluvial sediments is in hydraulic contact with the Gudenå. This shows that the alternating Miocene layers of the Vejle Fjord Formation form a hydraulic barrier between deeper groundwater and the surficial glaciofluvial aquifer that is in contact with the motorway (Fig. 7).

In the higher terrain the measured hydraulic head in the Quaternary glaciofluvial sand is very different from the hydraulic head measured in the underlying Miocene deposits. This is because the 3 m thick Miocene mud unit (Fig. 4C) acts as a barrier. The Addit Member, however, is in hydraulic contact with the glaciofluvial sand (Fig. 7).

The hydraulic connection between the glaciofluvial sand found in the slopes of the valley and the glaciofluvial deposits in the valley floor is also affected by the Miocene deposits as the 3 m thick mud unit separates them.

The hydrogeological relations between the Miocene deposits and the Quaternary deposits illustrate the importance of applying detailed field-site geological evidence to get an impression of the local groundwater flow.

Acknowledgement

The Danish Road Directorate is thanked for access to the field site and funding.

References

Dybkjær, K. 2004: Morphological and abundance variations in *Homotryblium*-cyst assemblages related to depositional environments; uppermost Oligocene – Lower Miocene, Jylland, Denmark. Palaeogeography, Palaeoclimatology, Palaeoecology **206**, 41–58.

Dybkjær, K. & Piasecki, S. 2010: Neogene dinocyst zonation in the eastern North Sea Basin, Denmark. Review of Palaeobotany and Palynology **161**, 1–29.

Kidmose, J., Refsgaard, J.C., Troldborg, L., Seaby, L.P. & Escrivà, M.M. 2013: Climate change impact on groundwater levels: ensemble modelling of extreme values. Hydrology and Earth System Sciences **17**, 1619–1634.

Kidmose, J., Troldborg, L., Refsgaard J.C. & Bischoff, N. 2015: Coupling of a distributed hydrological model with an urban storm water model for impact analysis of forced infiltration. Journal of Hydrology **525**, 506–520.

Leckie, D. 1988: Wave-formed, coarse-grained ripples and their relationship to hummocky cross-stratification. Journal of Sedimentary Research **58**, 607–622.

Miller, K.G. *et al.* 2005: The Phanerozoic record of sea-level changes. Science **310**, 1293–1298.

Plint, A.G. 1988: Sharp-based shoreface sequences and "offshore bars" in the Cardium Formation of Alberta; their relationship to relative changes in sea level: In: Wilgus, C.K. *et al.* (eds): Sea-level changes: an integrated approach: SEPM, Special Publication **42**, 357–371.

Rasmussen, E.S. 2014: Development of an incised-valley fill under the influence of tectonism and glacio-eustatic sea-level change: valley morphology, fluvial style and lithology. Journal of Sedimentary Research **84**, 278–300.

Rasmussen, E.S., Dybkjær, K. & Piasecki, S. 2010: Lithostratigraphy of the Upper Oligocene – Miocene succession in Denmark. Geological Survey of Denmark and Greenland Bulletin **22**, 92 pp.

Tyson, R. 1995: Sedimentary organic matter: organic facies and palynofacies, 615 pp. London: Chapman & Hall.

Authors' address

Geological Survey of Denmark and Greenland, Øster Voldgade 10, DK-1350 Copenhagen K, Denmark. E-mail: *prj@geus.dk*

3D hydrogeological modelling for urban subsurface management in Odense, Denmark

Susie Mielby, Tom Martlev Pallesen and Peter B.E. Sandersen

The subsurface material in urban areas comprises the original geological succession together with anthropogenic modifications and deposits. The Geological Survey of Denmark previously performed geological mapping in selected Danish cities (e.g. Mertz 1974), but this practice stopped in the mid-1980s. The lack of recent systematic mapping in urban areas is apparent not only in Denmark but also in most other European countries (COST 2015). However, there is a growing demand for knowledge of the subsurface beneath our cities for a number of reasons: increased urbanisation, infiltration of excess surface water and other climate-change related measures, thermal storage, groundwater cooling and abstraction, subsurface infrastructure, infrastructure projects, etc. The physical properties of the subsurface material are in constant change due to urban growth and infrastructure development. This can strongly influence the geotechnical properties and handling of excess surface water. In order to manage both challenges and opportunities of the ground beneath the cities there is a growing need for 3D hydrogeological models that can encompass all relevant parts of the physical subsurface system and act as operational tools in its management.

With the main focus on hydrogeology and the urban water cycle, the Municipality of Odense, the local waterworks (VandCenter Syd), the Geological Survey of Denmark and Greenland (GEUS) and two consultants (Alectia and I-GIS) have made a joint effort to systematically map the subsurface layers and build a 3D hydrogeological model of the subsurface of the city of Odense (Fig. 1). This paper provides an overview of the project rationale and an outline of the major results.

The sedimentary succession beneath Odense

The uppermost 50 to 100 m of the subsurface of Odense is dominated by Weichselian clay till with intervening sand layers (e.g. Jørgensen & Piotrowski 2003, Mertz 1974), which form three groundwater reservoirs of varying extent and thickness. There are also late- to postglacial, near-surface, sandy outwash plains and heterogeneous infill of erosive channels and depressions (Sandersen *et al.* 2015). Historical maps from the late 1800s show that postglacial bogs and wetland areas have also earlier been present.

The urban development of Odense has mainly taken place within the past 200 years (Fig. 1). The switch to the industrial era increased its population and led to expanding residential and paved areas, installation of water supply and sewage systems, creation of waste dumps and an accelerated abstraction of groundwater. The drainage and lowering of the groundwater table dried out some of the former wetlands and created new agricultural and urbanised land, and in other areas caused subsidence due to the decay of organic matter. Since the 1980s, a growing environmental awareness and increased taxes have resulted in a marked decrease in groundwater abstraction, and former

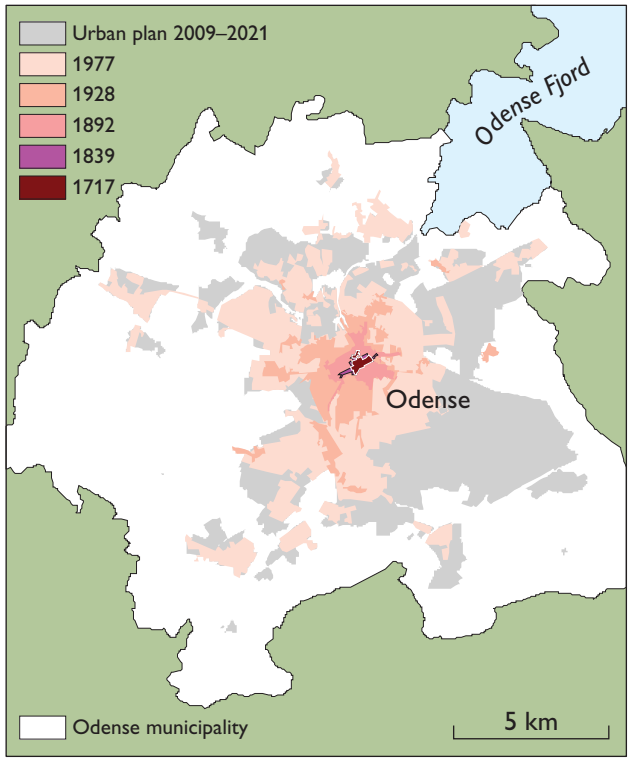

Fig. 1. Urban development of Odense Municipality (Laursen & Mielby 2016).

© 2016 GEUS.

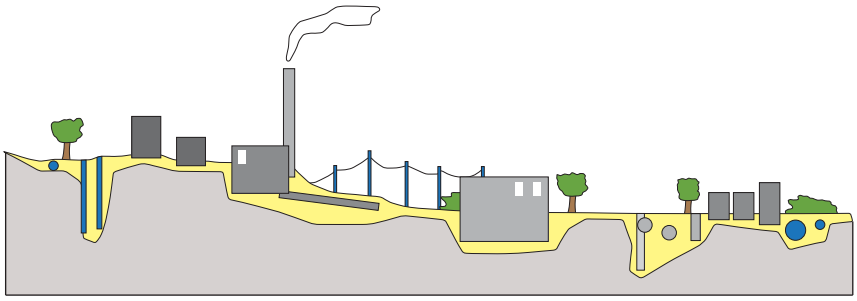

Fig. 2. Simplified picture of the subsurface elements in the man-made urban layer, where the original geological sediments (light grey) are replaced by infill (yellow), basements of buildings, wells, pipes, sewers, etc. forming the anthropogenic layer.

wetland areas are beginning to return to their original wet state. The urban activities within the last 200 years created a heterogeneous man-made layer consisting of backfill of excavations, modified terrain, landfill, waste dumps, etc. Parts of this anthropogenic layer rest on top of the original geological formations, whereas other parts replace them.

Building the 3D model

The man-made modifications of the urban subsurface, along with the ongoing climate change, affect the urban water cycle and must therefore be carefully evaluated. For instance, in areas with sustainable urban drainage systems (SUDS), the local infiltration potential and its consequences on the hydraulic heads in adjacent areas must be known (Jeppesen 2014; Mielby *et al.* 2015a), and this implies a need for a close integration of regional and local geological information.

In order to build a comprehensive subsurface model for Odense both the natural and man-made layers were mapped, but due to their different nature, different mapping and modelling approaches were needed. A standard framework-model approach where layer boundaries were mapped all the way to the surface was employed for the original geology, primarily using borehole data, geophysical data and high-resolution digital elevation models (Sandersen *et al.* 2015). The man-made layers shown in Fig. 2 were mapped using data from boreholes about the thickness and character of infill, and from excavations around subsurface infrastructures. The latter requires detailed information about the age, character and spatial extent of the individual parts of the infrastructure and access to current standards for excavation back-fill (Fig. 3; Pallesen & Jensen 2015).

The digital information about the anthropogenic layer is generally abundant, but also rapidly changing compared with the traditional geological data. Because the elements of the anthropogenic layers change over time, a tool for the modelling of the anthropogenic layers was established in the modelling software GeoScene3D to make a sequential handling of the infrastructure data possible (Pallesen & Jensen 2015).

The need for a high degree of detail is most relevant in the uppermost parts of the 3D model, where the scale of the urban infrastructure typically is counted in metres or tens of metres. Mapping of the man-made layers should therefore be done with a corresponding level of detail. In the deeper parts of the subsurface, the number of boreholes that reach depths of 20 m or more is very limited (Kristensen *et al.* 2015), meaning that the deeper geological succession typically cannot be resolved better than 100 m horizontally (Sandersen *et al.* 2015).

After mapping of the original geological layers and the man-made components the two parts are merged, whereby the latter component replaces the model part of the original geological layers (Fig. 4). In this way, two models are combined into one 3D model. However, due to the above-mentioned scale difference, it is important to choose a common resolution that meets the required need for detail but does not exceed computational capability.

The major part of the geological information in the urban area comes from relatively short boreholes drilled in connection with geotechnical and environmental projects. The geotechnical borehole information is very important, as it provides information about both the original geology and the composition of the man-made fill. Data from many of these boreholes are stored in the national Jupiter database, but its quality is variable because upload of this type of borehole data is not mandatory. In addition, many boreholes have not found their way to the national database at all, because the data were collected by private companies, considering the information their private property. Therefore, the readily available digital geological information does not necessarily reflect all of the existing data, and this problem must be addressed before a 3D model is constructed.

Results

The project resulted in a 3D geological municipality model, and detailed anthropogenic and combined hydrogeological models were made for a chosen site in order to test the modelling in a typical situation. In addition to the models and the model tool in GeoScene3D, descriptions, workflows and recommendations for data acquisition, management and updating procedures were also developed.

In the project, a systematic and comprehensive collation of available data was established within the borders of Odense Municipality. In 2015, the geological model concept provided the 'best so far' foundation for the management of the urban hydrogeology in Odense. The resulting model and its tools were proven to be valuable, as they were quickly taken into use in several new hydrological modelling projects such as modelling of hydrological climate-change effects and detailed infiltration possibilities, as well as the evaluation of the natural protection of drinking-water well fields.

The data and information density proved variable, and therefore information on the data background is important for the municipal decision-making. Detailed studies in Odense showed that in many areas the data coverage is insufficient for the purpose required. Therefore, the geological basis for planning and water management has to be improved, and this requires a dynamic model that can benefit from both existing and new data.

If all additional geological data are to be accessible for future planning, the authorities must ensure that all geological and geotechnical data are reported and available. The investigations in the current project proved that open access to better geotechnical and geological data and modelling would also benefit a wider range of users such as archaeologists, engineers, architects, entrepreneurs and other professionals working with e.g. road and railway construction (Laursen *et al*. 2015). If the 3D model is regularly updated in the future, Odense will also obtain an increasingly robust foundation for the hydrological modelling and management of the urban water cycle. Detailed recommendations and experience from the current project (Mielby *et al*. 2015b), urban data modelling tools in GeoScene3D and data storage facilities for geotechnical information in the Jupiter database (Hansen *et al*. 2015) are available for the benefit of other areas.

Fig. 3. **A**: Large sewer in an excavation to be filled with gravel. Image source: VandCenter Syd. **B**: Anthropogenic model of sewers with other implemented data elements (roads, pipes and buildings).

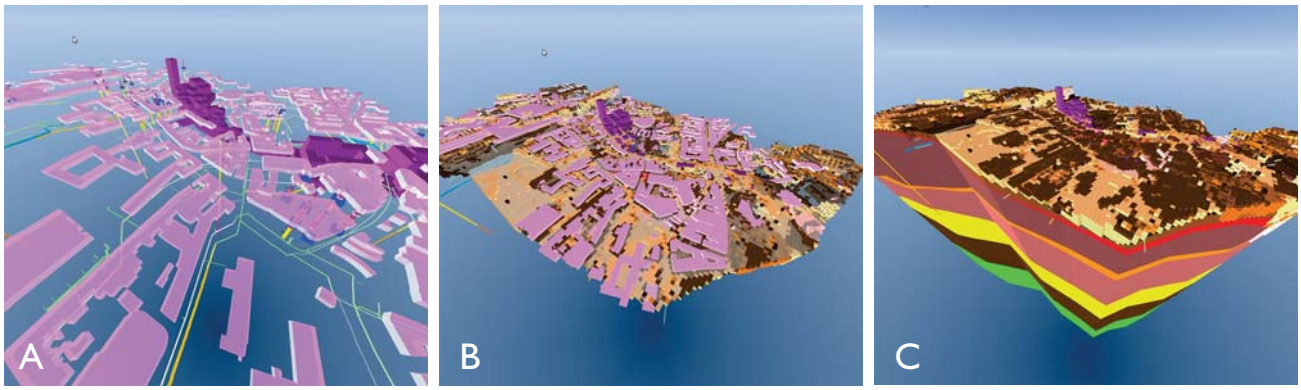

Fig. 4. Elements of the geological modelling. **A**: Buildings and pipes**. B**: Man-made ground with fill. **C**: Combined model showing man-made features and the underlying geological model.

Acknowledgements

The Foundation for Development of Technology in the Danish Water Sector (VTU- Fonden; ans-7497.2012) is thanked for financial support. The project partners Knud Søndergaard and Gert Laursen, Odense Municipality, Christian Ammitsøe and Johan Linderberg, VCS Denmark, Martin Hansen and Margrethe Kristensen, GEUS and Jan Jeppesen, Alectia are acknowledged for fruitful collaboration.

References

COST 2015: *http://www.cost.eu/COST_Actions/tud/Actions/TU1206*. Sub-Urban – A European network to improve understanding and use of the ground beneath our cities.

Hansen, M., Wiese, M.B., Gausby, M. & Mielby, S. 2015: Udvikling af en 3D geologisk/hydrogeologisk model som basis for det urbane vandkredsløb. Delrapport **6** – Teknisk håndtering og lagring af bygeologiske data og modeller, 22 pp. København: De Nationale Geologiske Undersøgelser for Danmark og Grønland.

Jeppesen, J. 2014: Udvikling af en urban-hydrologisk model til simulering af nye innovative LAR-løsninger til lokal håndtering af både regn-vand og grundvand (LARG). Afrapportering af VTU-projekt 29. December 2014.

Jørgensen, F. & Piotrowski, J.A. 2003: Signature of the Baltic Ice Stream on Funen Island, Denmark during the Weichselian glaciation. Boreas **32**, 242–255.

Kristensen, M., Sandersen, P. & Mielby, S. 2015: Udvikling af en 3D geologisk/hydrogeologisk model som basis for det urbane vandkredsløb. Delrapport **2** – Indsamling og vurdering af data, 82 pp. København: De Nationale Geologiske Undersøgelser for Danmark og Grønland.

Laursen, G. & Mielby, S. 2016: Odense. TU1206 COST Sub-Urban WG1 Report.

Laursen, G., Mielby, S. & Kristensen, M. 2015: Udvikling af en 3D geologisk/hydrogeologisk model som basis for det urbane vandkredsløb. Delrapport **3** – Geotekniske data til planlægning og administration, 32 pp. København: De Nationale Geologiske Undersøgelser for Danmark og Grønland.

Mertz, E.L. 1974: Odense og omegns jordbundsforhold: En ingeniørgeologisk beskrivelse. Danmarks Geologiske Undersøgelse Rapport **9**, 37 pp.

Mielby, S., Laursen, G., Linderberg, J., Sandersen, P. & Jeppesen, J. 2015a: Udvikling af en 3D geologisk/hydrogeologisk model som basis for det urbane vandkredsløb. Delrapport **1** – 3D-modellen som basis for håndteringen af det urbane vandkredsløb, 66 pp. København: De Nationale Geologiske Undersøgelser for Danmark og Grønland.

Mielby, S., Jespersen, C.E., Ammitsøe, C., Laursen, G., Jeppesen, J., Linderberg, J., Søndergaard, K., Kristensen, K., Hansen, M., Jensen, N.-P. & Sandersen, P. 2015b: Udvikling af en 3D geologisk/hydrogeologisk model som basis for det urbane vandkredsløb. Synteserapport, 57 pp. København: De Nationale Geologiske Undersøgelser for Danmark og Grønland.

Pallesen, T.M. & Jensen, N.-P. 2015: Udvikling af en 3D geologisk/hydrogeologisk model som basis for det urbane vandkredsløb. Delrapport **5** – Interaktiv modellering af antropogene lag, 58 pp. København: De Nationale Geologiske Undersøgelser for Danmark og Grønland.

Sandersen, P., Kristensen, M. & Mielby, S. 2015: Udvikling af en 3D geologisk/hydrogeologisk model som basis for det urbane vandkredsløb. Delrapport **4** – 3D geologisk/hydrostratigrafisk modellering i Odense, 106 pp. København: De Nationale Geologiske Undersøgelser for Danmark og Grønland.

Authors' addresses

S.M. & P.S., *Geological Survey of Denmark and Greenland, C.F. Møllersvej 8, Building 1110, DK-8000 Aarhus C, Denmark.* E-mail: *smi@geus.dk.*

T.M.P., *I-GIS, Voldbjergvej 14, DK-8240 Risskov, Denmark.*

Monitoring of pesticide leaching from cultivated fields in Denmark

Walter Brüsch, Annette E. Rosenbom, Nora Badawi and Preben Olsen

The Danish Pesticide Leaching Assessment Programme (PLAP) was initiated in 1998 by the Danish Parliament in order to evaluate whether the use of approved pesticides will result in an unacceptable contamination of the groundwater, if applied under field conditions in accordance with current Danish regulation. In this programme, water samples from variably saturated soil and groundwater collected at five cultivated fields are analysed for selected pesticides and their degradation products. The PLAP results are summarised and evaluated in yearly reports and used by the Danish Environmental Protection Agency in the regulation of pesticides in Denmark (Brüsch *et al.* 2015). In order to represent typical farming scenarios in Denmark, the test fields are situated on meltwater and marine sands, and on tile-drained clayey soils in till areas.

Methods

The five cultivated PLAP fields (1.2–2.4 ha), representing different soils and hydrogeological settings, spread across Denmark (Fig. 1) are located at Silstrup, Estrup and Faardrup with tile-drained clayey soils, and at Tylstrup and Jyndevad with sandy soils (Lindhardt *et al.* 2001). The groundwater table is shallow at all fields, which enables a rapid detection of any pesticide leaching to the groundwater (Table 1). The PLAP fields are farmed according to conventional agricultural practice, and pesticides are applied in the maximum permissible doses and as specified in the regulations.

Water samples are collected weekly from drainage at the clayey till fields, and monthly from standard teflon suction cups in the unsaturated zone at the sandy fields, and from horizontal and vertical groundwater monitoring wells at all fields. The wells are installed in buffer zones surrounding the fields in order to avoid artificial transport pathways for pesticides and their degradation products from the surface to the groundwater. The vertical wells are located downstream from the field (Fig. 2), except for one upstream vertical well, which is used to determine the upstream influx to the groundwater beneath the field. The horizontal wells are installed at the clayey till fields at depths of 2–3.5 m under the pesticide-treated areas, and at the sandy fields just beneath the fluctuating groundwater table. Detection of pesticides or their degradation products can be directly related to the specific pesticide application to the PLAP fields by monitoring both the variably and fully saturated soil and accounting for potential upstream influx.

In the drainage from the clayey till fields, the weighted average concentration of pesticides is based on flow-proportional sampling. In the two sandy soils, the weighted average pesticide concentration leached to the suction cups at 1 m depth is estimated from the detected concentrations and estimated percolation on a monthly basis (Brüsch *et al.* 2015).

The analytical programme includes relevant pesticides and their degradation products as well as inorganic compounds such as chloride, nitrate, phosphate and bromide,

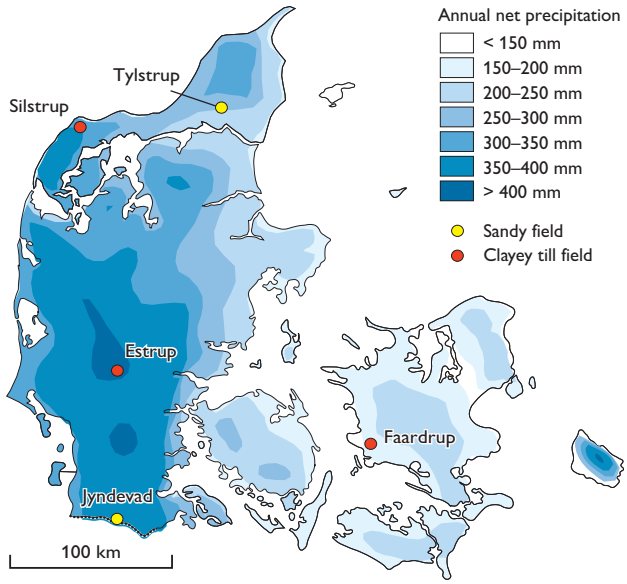

Fig. 1. Annual net-precipitation in Denmark and the location of the five PLAP fields (*http://www2.mst.dk/Udgiv/publikationer/1992/87-503-9581-5/pdf/87-503-9581-5.pdf*; Rosenbom *et al.* 2015). Tylstrup and Jyndevad are located in sandy areas with marine sand and glaciofluvial sand, respectively. Silstrup, Estrup and Faardrup are situated in areas dominated by clayey till, and the three fields are drained. The sediments were deposited during and after the last glaciation.

© 2016 GEUS.

Table 1. Characteristics of the five pesticide leaching assessment fields

	Tylstrup	Jyndevad	Silstrup	Estrup	Faardrup
Precipitation (mm/y)*	668	858	866	862	558
Potential evapotranspiration (mm/y)*	552	555	564	543	585
Area (ha)	1.1	2.4	1.7	1.3	2.3
Tile drain	No	No	Yes	Yes	Yes
Depth to tile drain (m)			1.1	1.1	1.2
Deposited by	Saltwater	Meltwater	Glacier	Glacier	Glacier
Sediment type	Fine sand	Coarse sand	Clay till	Clay till	Clay till
Topsoil classification	Loamy sand	Sand	Sandy clay loam	Sandy loam	Sandy loam

* Based on the period 1961–1990, modified from Lindhardt *et al.* (2001).

which is used as a tracer. The pesticides are generally analysed for two years following application, but the monitoring continues if significant leaching occurs. To evaluate the pesticide leaching, the water balance, including the percolation through the variably saturated soil, is assessed for all five PLAP fields using the numerical model MACRO (Larsbo *et al.* 2005) based on long-term detailed monitoring of climate, crop-growth, soil water content, groundwater table, and if present, drainage flow (Rosenbom *et al.* 2015).

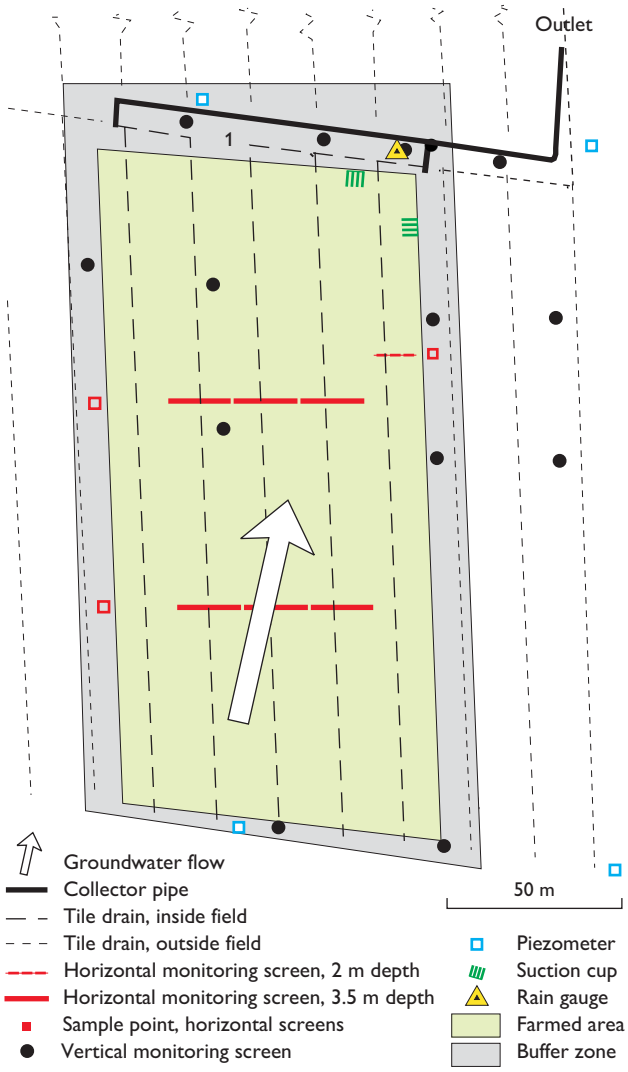

Fig. 2. Overview of the Silstrup field and its technical installations.

Monitoring results

According to the legislation of the European Union, the maximum permissible concentration of any pesticide in groundwater is 0.1 µg/l (Council of the European Union 1994). This limit is not based on health investigations but was the analytical detection limit when the legislation was made in the 1980s, and was chosen to ensure that drinking water did not contain measurable amounts of pesticides. During the latest monitoring period from July 2012 to June 2014, a total of 7378 single analyses of different pesticides or their degradation products were carried out on water samples collected at the five sites. The leaching risk of 22 pesticides and 17 degradation products was evaluated after applying the specific pesticide on specific crops. Of these 39 pesticides and their degradation products, 21 were not detected in any of the water samples.

During the entire monitoring period from May 1999 to June 2014, 51 pesticides and 52 degradation products were analysed. These are listed in the Appendix. The monitoring data showed leaching of 17 of the applied pesticides and their degradation products through the soil to tile drains or suction cups in average concentrations exceeding 0.1 µg/l. These are marked with asterisks in the Appendix.

The results of the monitoring also showed leaching of an additional 17 pesticides, but in low concentrations, marked by † in the Appendix. Although the concentrations exceeded 0.1 µg/l in several water samples collected from suction cups and tile drains at 1 m depth, the average leaching concentrations did not exceed 0.1 µg/l on an annual basis.

In groundwater samples, twenty-one pesticides or their degradation products were only detected at concentrations

Table 2. Total number of pesticides analysed, detected, and detected below 0.1 µg/l in all sample types

		Fine-grained sand	Coarse-grained sand		Clayey till	
		Tylstrup	Jyndevad	Silstrup	Estrup	Faardrup
Pesticides and metabolites	Detections	16	19	39	45	38
	Detections >0.1 µg/l	6	9	22	31	21
	Detections in %	28.1	32.8	59.1	77.6	66.7
	>0.1 µg/l in %	10.5	15.5	33.3	53.4	36.8
Groundwater avg	Nitrate-N	15.5	11.9	3.0	0.4	8.5
	Chloride	49.9	15.6	29.5	11.7	27.1
Drainage avg	Nitrate-N	ns	ns	2.1	3.5	11.2
	Chloride	ns	ns	30.3	26.6	27.5

Samples collected from suction cups, drainage and groundwater in the five PLAP fields between 01 January 2000 and July 2012.
Average nitrate and chloride concentrations from groundwater and drainage in the period January 2011 – July 2012.
Avg: average concentration in mg/l.
ns: no samples.

below 0.1µg/l or not at all. These are marked by § in the Appendix.

At the three clayey till fields, several pesticides were detected in the drainage, whereas the frequency of detection in the groundwater monitoring screens beneath the tile drain system was lower and varied considerably between the three fields. In the two sandy fields, fewer pesticides and degradation products were generally detected, both in the variably saturated soil and in groundwater (Table 2). The different leaching patterns in the sandy and clayey till fields can be attributed to specific hydrological, geological and geochemical conditions. The subsoil C horizon beneath the tile drains at the Estrup field shows low permeability with few macropores (Kjær *et al.* 2005; Rosenbom *et al.* 2015) in contrast to the Faardrup and Silstrup fields, where the clayey till is characterised by fractures and heterogeneity. Hence the fewer records of pesticides and degradation products in the groundwater at Estrup than at Faardrup and Silstrup can be related to the low permeability at the former site.

A comparison between the clayey till fields shows that the number of water samples containing pesticides and degradation products was higher at Silstrup and Estrup (35 and 40%, respectively) than at Faardrup (15%). This can be attributed to different hydro-geochemical conditions and the low net precipitation at Faardrup. The leaching pattern for non-pesticides shows that the average concentration of nitrate-N was much higher in both groundwater and drainage at Faardrup than at the other two fields (Table 2; Ernstsen *et al.* 2015). However, the average chloride content in both drainage and groundwater at Faardrup was higher than at Silstrup (Table 2), due to an up-concentration in the infiltration water caused by the low precipitation at Faardrup. The occurrence of precipitation and subsequent percolation within the first month after application were generally higher at Silstrup and Estrup than at Faardrup (Table 1).

At the clayey till fields, 59–78% of the different applied pesticides and their degradation products were detected in drainage water or groundwater (Table 2), while only 28–33% of them were detected at the sandy fields. High pesticide concentrations dominated at the three clayey till fields, with 33–53% of the detections exceeding 0.1 µg/l, while only 11–16% of the detections at the two sandy fields exceeded the threshold limit. However, the limit of 0.1 µg/l is only relevant for groundwater and not for drainage water.

The average nitrate concentrations were high in the groundwater of the sandy fields and lower at the clayey till fields (Ernstsen *et al.* 2015). However, a high average nitrate concentration was recorded in both the drainage and groundwater from the Faardrup field where the precipitation is low. This is probably because the uppermost part of the till is characterised by high permeability. It is therefore apparent that the pesticide and nitrate concentrations both reflect the geochemical conditions of groundwater and drainage water.

Further details regarding PLAP can be found in Kjær *et al.* (2002, 2003, 2004, 2005, 2007, 2008, 2009, 2011), Rosenbom *et al.* (2010), Brüsch *et al.* (2013a, 2013b, 2015), Ernstsen *et al.* (2015) and Rosenbom *et al.* (2015). For further information please visit: *http://pesticidvarsling.dk/monitor_uk/index.html*.

Conclusions

The results presented here provide an overall picture of the detections of pesticides and their degradation products in soil and groundwater in five monitored cultivated fields representing typical Danish farming activities on clayey and sandy soils in the period from 1999 to 2014. The overall

pesticide leaching detected in the monitoring programme is an outcome of the pesticide selection, hydraulic conditions, type of agriculture and the geochemical conditions such as the redox potential, aerobic conditions and hence the leaching of nitrate-N and potential persistence of individual pesticides. For instance, the leaching of pesticides is more pronounced in fractured clayey soils than in sandy soils due to fast transport in anaerobic fractures in the former soils, in contrast to slower matrix transport in the more aerated sandy soils. This is illustrated by the high number of recorded pesticides in drainage water and groundwater from clayey till soils due to bypassing of the topsoil by rapid leaching through well-connected macropores such as wormholes and fractures (Rosenbom *et al.* 2015). The occurrence of pesticides in samples from the two sandy soils is probably specifically linked to the application of persistent pesticides such as metalaxyl-M applied to potatoes.

References

Brüsch, W., Kjær, J., Rosenbom, A.E., Juhler, R.K., Gudmundsson, L., Plauborg, F., Nielsen, C.B. & Olsen, P. 2013a: The Danish Pesticide Leaching Assessment Programme: Monitoring results May 1999 – June 2011, 108 pp. Copenhagen, Denmark: Geological Survey of Denmark and Greenland.

Brüsch, W., Rosenbom, A.E., Juhler, R.K., Gudmundsson, L., Plauborg, F., Nielsen, C.B. & Olsen, P. 2013b: The Danish Pesticide Leaching Assessment Programme: Monitoring results May 1999 – June 2012, 106 pp. Copenhagen, Denmark: Geological Survey of Denmark and Greenland.

Brüsch, W., Rosenbom, A.E., Badawi, N., v. Platten-Hallermund, F., Gudmundsson, L., Plauborg, F., Nielsen, C.B., Laier, T. & Olsen, P. 2015: The Danish Pesticide Leaching Assessment Programme: Monitoring results May 1999 – June 2013, 110 pp. Copenhagen, Denmark: Geological Survey of Denmark and Greenland.

Council of the European Union 1994: Council Directive 94/43/EC establishing Annex VI to Directive 91/414/EEC concerning the placing of plant protection products on the market. Official Journal of the European Union L227, 1.9.1994, 31–55.

Ernstsen, V., Olsen, P. & Rosenbom, A.E. 2015: Long-term monitoring of nitrate transport to drainage from three agricultural clayey till fields. Hydrology and Earth System Sciences **19**, 3475–3488, *http://dx.doi.org/10.5194/hess-19-3475-2015*.

Kjær, J. *et al.* 2002: The Danish Pesticide Leaching Assessment Programme: Monitoring results May 1999 – June 2001, 150 pp. Copenhagen, Denmark: Geological Survey of Denmark and Greenland.

Kjær, J., Ullum, M., Olsen, P., Sjelborg, P., Helweg, A., Mogensen, B., Plauborg, F., Grant, R., Fomsgaard, I. & Brüsch, W. 2003: The Danish Pesticide Leaching Assessment Programme: Monitoring results May 1999 – June 2002, 158 pp. Copenhagen, Denmark: Geological Survey of Denmark and Greenland.

Kjær, J., Olsen, P., Barlebo, H.C., Juhler, R.K., Plauborg, F., Grant, R., Gudmundsson, L. & Brüsch, W. 2004: The Danish Pesticide Leaching Assessment Programme: Monitoring results May 1999 – June 2003, 146 pp. Copenhagen, Denmark: Geological Survey of Denmark and Greenland.

Kjær, J., Olsen, P., Barlebo, H.C., Juhler, R.K., Henriksen, T., Plauborg, F., Grant, R., Nyegaard P. & Gudmundsson, L. 2005: The Danish Pesticide Leaching Assessment Programme: Monitoring results May 1999 – June 2004, 86 pp. Copenhagen, Denmark: Geological Survey of Denmark and Greenland.

Kjær, J., Olsen, P., Barlebo, H.C., Henriksen T., Plauborg, F., Grant, R., Nyegaard, P., Gudmundsson, L. & Rosenbom, A.E. 2007: The Danish Pesticide Leaching Assessment Programme: Monitoring results May 1999 – June 2006, 99 pp. Copenhagen, Denmark: Geological Survey of Denmark and Greenland.

Kjær, J., Rosenbom, A., Olsen, P., Juhler, R.K., Plauborg, F., Grant, R., Nyegaard, P., Gudmundsson, L. & Brüsch, W. 2008: The Danish Pesticide Leaching Assessment Programme: Monitoring results May 1999 – June 2007, 91 pp. Copenhagen, Denmark: Geological Survey of Denmark and Greenland.

Kjær, J., Rosenbom, A., Olsen, P., Ernstsen, V., Plauborg, F., Grant, R., Nyegaard, P, Gudmundsson, L. & Brüsch, W. 2009: The Danish Pesticide Leaching Assessment Programme: Monitoring results May 1999 – June 2008, 88 pp. Copenhagen, Denmark: Geological Survey of Denmark and Greenland.

Kjær, J., Rosenbom, A.E., Olsen, P., Ernstsen, V., Plauborg, F., Grant, R., Gudmundsson, L. & Brüsch, W. 2011: The Danish Pesticide Leaching Assessment Programme: Monitoring results May 1999 – June 2010, 110 pp. Copenhagen, Denmark: Geological Survey of Denmark and Greenland.

Larsbo, M., Roulier, S., Stenemo, F., Kasteel, R. & Jarvis, N. 2005: An improved dual-permeability model of water flow and solute transport in the vadose zone. Vadose Zone Journal **4**, 398–406.

Lindhardt, B., Abildtrup, C., Vosgerau, H., Olsen, P., Torp, S., Iversen, B.V., Jørgensen, J.O., Plauborg, F., Rasmussen, P. & Gravesen, P. 2001: The Danish Pesticide Leaching Assessment Programme: Site characterization and monitoring design, 73 pp. Copenhagen, Denmark: Geological Survey of Denmark and Greenland.

Rosenbom, A.E., Brüsch, W., Juhler, R.K., Ernstsen, V., Gudmundsson, L., Plauborg, F., Grant, R. & Olsen, P. 2010: The Danish Pesticide Leaching Assessment Programme: Monitoring results May 1999 – June 2009, 102 pp. Copenhagen, Denmark: Geological Survey of Denmark and Greenland.

Rosenbom, A.E., Olsen, P., Plauborg, F., Grant, R., Juhler, R.K., Brusch, W. & Kjaer, J. 2015: Pesticide leaching through sandy and loamy fields – long-term lessons learnt from the Danish Pesticide Leaching Assessment Programme. Environmental Pollution **201**, 75–90.

Authors' addresses

W.B.*, A.E.R. & N.B., *Geological Survey of Denmark and Greenland, Øster Voldgade 10, DK-1350 Copenhagen K, Denmark.*

P.O., *Department of Agroecology, Aarhus University, Blichers Allé 20, DK-8830 Tjele, Denmark.*

*Present address: *Danmarks Naturfredsningsforening, Madsnedøgade 20, DK-2100 Copenhagen Ø, Denmark.* E-mail: *wb@dn.dk*

Appendix. PLAP analyses from May 1999 to June 2014. Part A

Pesticide	Analyte	Tile drain and suction cup					Groundwater				
			Samples	Det.	≥0.1	Max.		Samples	Det.	≥0.1	Max.
Aclonifen	Aclonifen	†	111				§	298			
Amidosulfuron	Amidosulfuron		144	3	1	0.11	§	332			
	Desmethyl-amidosulfuron		24					88			
Aminopyralid	Aminopyralid	†	133				§	261			
Azoxystrobin	Azoxystrobin	*	717	139	16	1.4		1798	3		0.04
	CyPM	*	740	390	144	2.1		1910	69	5	0.19
Bentazone	Bentazone	*	1051	350	43	43		2603	81	8	0.6
	2-amino-N-isopropyl-benzamide		561	4		0.06		1295	1		0.02
Bifenox	Bifenox		303	17	3	0.38		751	7	1	0.1
	Bifenox acid	*	278	55	47	8.6		702	29	23	3.1
	Nitrofen		303	11	4	0.34		751			
Boscalid	Boscalid	†	56				§	111			
Bromoxynil	Bromoxynil		528	5	3	0.6	§	1122			
Chlormequat	Chlormequat	†	95	2		0.017	§	190			
Clomazon	Clomazone		224	1	1	0.28	§	598			
	FMC 65317		216	1	1	0.3		577			
Clopyralid	Clopyralid		219	7	4	4.094	§	520	1		0.026
Cyazofamid	Cyazofamid	†	100				§	262			
Desmedipham	Desmedipham	†	287					580	1		0.033
	EHPC		199					383			
Diflufenican	Diflufenican		109	32	14	0.49		324	1	1	0.47
	AE-B107137	*	121	19	1	0.13		333	1		0.016
	AE-05422291		109					324			
Dimethoate	Dimethoate	†	515	1	1	1.417		1253	1		0.085
Epoxiconazole	Epoxiconazole		330	14	2	0.39		999	1		0.011
Ethofumesate	Ethofumesate	*	519	70	17	12		1095	36	7	1.4
Fenpropimorph	Fenpropimorph	†	657	2		0.038		1531	2		0.029
	Fenpropimorph acid		636	2	1	0.25		1435			
Flamprop-M	Flamprop-M-isopropyl		520	38	1	0.109		1204	1		0.024
	Flamprop		525	23	1	0.35		1212			
Florasulam	Florasulam	†	146					351			
	Florasulam-desmethyl		109					130			
Fluazifop-P-buthyl	Fluazifop-P-butyl		128					232			
	TFMP	*	184	53	24	0.64		555	87	16	0.29
	Fluazifop-P		451	11	4	3.8		1109	7	1	0.17
Fludioxonil	CGA 192155	†	11				§	48			
	CGA 339833		11					48			
Fluroxypyr	Fluroxypyr	*	521	4	3	1.4		1273	2		0.072
Glyphosate	Glyphosate	*	1091	429	136	31		2216	77	5	0.67
	AMPA	*	1092	632	142	5.4		2217	37		0.08
Iodosulfuron-methyl-natrium	Metsulfuron-methyl		332	1		0.054		842			
	Iodosulfuron-methyl	†	60				§	250			
Ioxynil	Ioxynil		527	24	7	0.25		1128	1		0.01
Linuron	Linuron	†	67				§	271			
Mancozeb	ETU		44	7		0.038		200	2		0.024
	EBIS		7					25			
MCPA	MCPA		354	14	3	3.894		916	1		0.019
	2-methyl-4-chlorophenol		354	2	1	0.24		912			
Mesosulfuron-isopropyl	Mesosulfuron-methyl		153	13		0.059	§	411			
	Mesosulfuron		119					119			
Mesotrione	Mesotrione	†	50				§	156			
	AMBA		50					156			
	MNBA		50					156			

Fifty-one pesticides and 52 degradation products analysed in the PLAP programme in the period May 1999 – June 2014. The columns show the number of water samples analysed, number of detections, and detections in concentrations ≥ 0.1µg/l in water samples from the variably-saturated zone (drainage and suction cups), and in groundwater (vertical and horizontal groundwater wells).

Det: number of detections. ≥0.1: number of detections ≥0.1µg/l. Max: maximum concentration in µg/l.

*: Pesticides and their degradation products leached through soil to tile drains or suction cups in average concentrations above 0.1 µg/l.

†: Pesticides not detected or detected only in a few samples above their threshold concentrations at 1 m depth.

§: Pesticides and their degradation products not detected or only detected in a few samples in groundwater.

Appendix. PLAP analyses from May 1999 to June 2014. Part B

Pesticide	Analyte		Tile drain and suction cup				Groundwater			
			Samples	Det.	≥0.1	Max.	Samples	Det.	≥0.1	Max.
Metalaxyl-M	metalaxyl-M		207	15		0.037	592	79	23	1.3
	CGA 108906	*	215	175	69	4.8	593	468	128	2.7
	CGA 62826	*	216	100	25	1.2	593	147	8	0.68
Metamitron	Metamitron	*	515	103	31	26.369	1095	53	7	0.63
	Desamino-metamitron	*	518	129	23	5.549	1094	78	16	1.3
Metrafenone	Metrafenone		136	20		0.072	273	1		0.04
Metribuzin	Metribuzin		97	2		0.024	414	1		0.014
	Diketo-metribuzin		340	256	63	0.69	552	479	336	1.372
	Desamino-diketo-metribuzin	*	255	81	51	2.1	551	256	18	1.831
	Desamino-metribuzin	*	91				392			
Pendimethalin	Pendimethalin		694	89	30	32	1811	1		0.052
Phenmedipham	Phenmedipham		288				580	2		0.025
	MHPC		288	2	1	0.19	580	1		0.053
	3-aminophenol		109				245			
Picolinafen	Picolinafen		117	18		0.07	193			
	CL153815	*	117	31	11	0.5	193			
Pirimicarb	Pirimicarb		887	62		0.077	2120	6		0.035
	Pirimicarb-desmethyl-formamido	*	707	29	13	0.379	1638	2		0.076
	Pirimicarb-desmethyl		780	8		0.053	1911	3		0.042
Propiconazol	Propiconazole		899	32	3	0.862	2084	3		0.035
Propyzamid	Propyzamide	*	257	27	8	1.6	754	10	2	0.14
	RH-24644		257	19		0.051	754	2		0.032
	RH-24580		257	2		0.016	754			
	RH-24655		233	1		0.017	690			
Prosulfocarb	Prosulfocarb		199	6	1	0.18	516	5		0.032
Pyridat	Pyridate		39				116			
	PHCP		125	4	4	2.69	373	14	4	0.309
Rimsulfuron	Rimsulfuron		117				367			
	PPU	*	502	388	74	0.29	1519	432	13	0.23
	PPU-desamino		502	186	6	0.18	1519	107		0.089
Tebuconazole	Tebuconazole	*	289	47	17	2	784	8	2	0.12
	1.2.4-triazol	*					16	7	1	0.17
Terbuthylazine	Terbuthylazine	*	513	213	56	11	1324	88	23	1.9
	Desethyl-terbuthylazine	*	612	365	88	8.3	1664	261	33	0.94
	Desisopropylatrazine		414	156	2	0.44	996	92		0.047
	Hydroxy-terbuthylazine	*	384	136	18	0.99	940	34		0.069
	2-hydroxy-desethyl-terbuthylazine	*	342	128	28	6.3	850	9		0.092
Thiacloprid	Thiacloprid	†	47				§ 100			
	Thiacloprid-amide		47	1		0.012	100			
	M34		55				100			
	Thiacloprid sulfonic acid		56				100			
Thiamethoxam	Thiamethoxam	†	132				§ 359			
	CGA 322704		132				359			
Triasulfuron	Triasulfuron	†	82				§ 301			
	Triazinamin		393				1103	1		0.042
Tribenuron-methyl	Triazinamin-methyl	†	569	2		0.042	§ 1523			
Triflusulfuron-methyl	Triflusulfuron-methyl	†	95				288			
	IN-E7710		95	5		0.014	288			
	IN-M7222		95				288	1		0.052
	IN-D8526		95				288			

Fifty-one pesticides and 52 degradation products analysed in the PLAP programme in the period May 1999 – June 2014. The columns show the number of water samples analysed, number of detections, and detections in concentrations ≥ 0.1µg/l in water samples from the variably-saturated zone (drainage and suction cups), and in groundwater (vertical and horizontal groundwater wells).

Det: number of detections. ≥0.1: number of detections ≥0.1µg/l. Max: maximum concentration in µg/l.

*: Pesticides and their degradation products leached through soil to tile drains or suction cups in average concentrations above 0.1 µg/l.

†: Pesticides not detected or detected only in a few samples above their threshold concentrations at 1 m depth.

§: Pesticides and their degradation products not detected or only detected in a few samples in groundwater.

A WebGIS portal for exploration of deep geothermal energy based on geological and geophysical data

Henrik Vosgerau, Anders Mathiesen, Morten Sparre Andersen, Lars Ole Boldreel, Morten Leth Hjuler, Elina Kamla, Lars Kristensen, Christian Brogaard Pedersen, Bjarni Pjetursson and Lars Henrik Nielsen

The Danish subsurface contains deep geothermal resources which may contribute for hundreds of years to the mixed Danish energy supply (Mathiesen *et al.* 2009). At present only a limited fraction of these resources are utilised in three existing geothermal power plants in Thisted, Margretheholm and Sønderborg (Fig. 1) where warm formation water is pumped to the surface from a production well and, after heat extraction, returned to the subsurface in injection wells (Fig. 2). Deep geothermal energy has the advantage of being a sustainable and environmentally friendly energy source which is furthermore independent of climate and seasonal variations, in contrast to wind and solar energy. The implementation of deep geothermal energy for district heating replacing conventional energy sources, especially coal and oil, may thus lead to a considerable reduction in the emission of greenhouse gases. There are therefore good reasons to include geothermal energy as a central component in Denmark's future supply of energy for district heating. Furthermore, heat-demanding industries may consider the possibility to integrate geothermal energy and energy storage in their production process.

In order to facilitate the use of geothermal energy, a broad majority in the Danish parliament has granted financial support for initiatives within the geothermal field (Energy policy agreement of March 22, 2012). The present paper deals with one of the outcomes of this agreement, namely a WebGIS portal with an overview of existing and

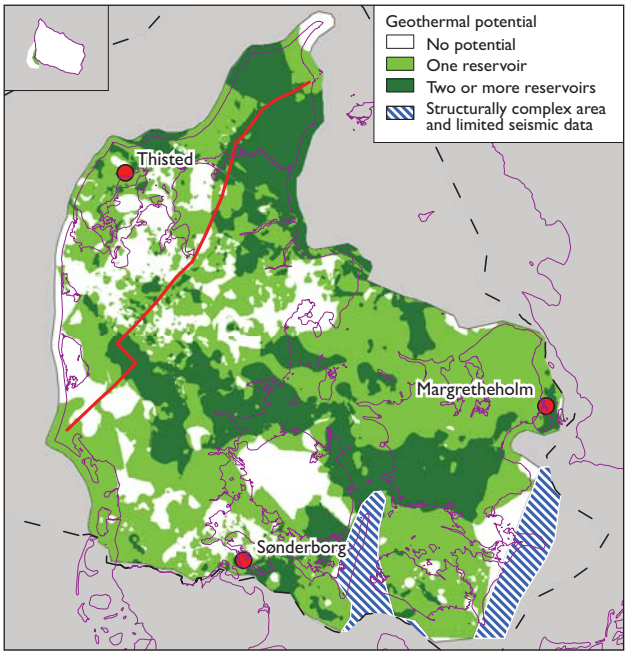

Fig. 1. Distribution of lithostratigraphic units with reservoir properties suitable for geothermal exploration in the geothermal depth zone (800–3000 m), see the main text. The red line indicates the transect covered by the geosection shown in Fig. 5. Positions of the operating geothermal plants are shown.

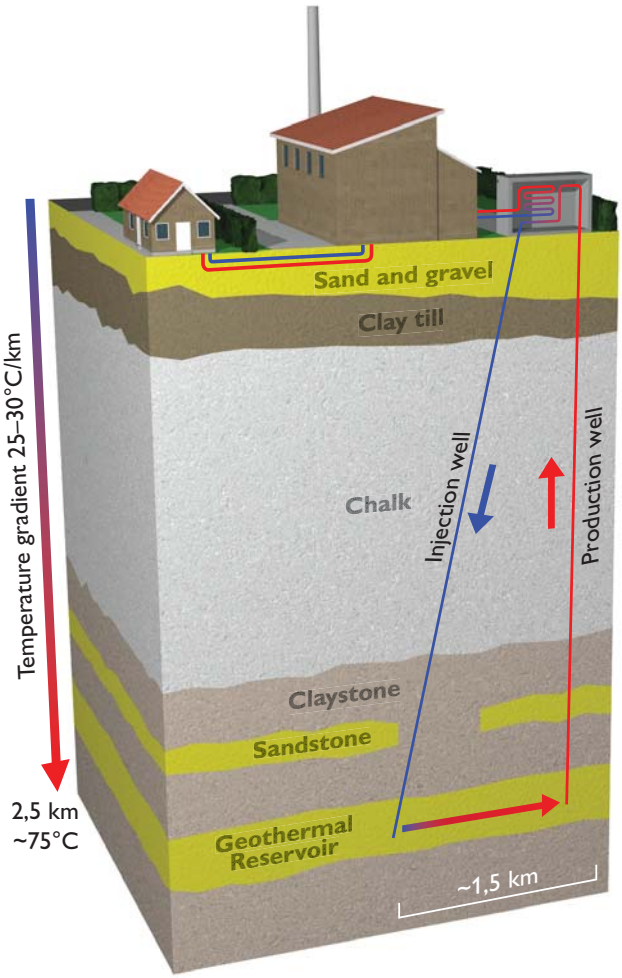

Fig. 2. Principle sketch of a geothermal power plant with production and injection wells to a deep-seated geothermal sandstone reservoir.

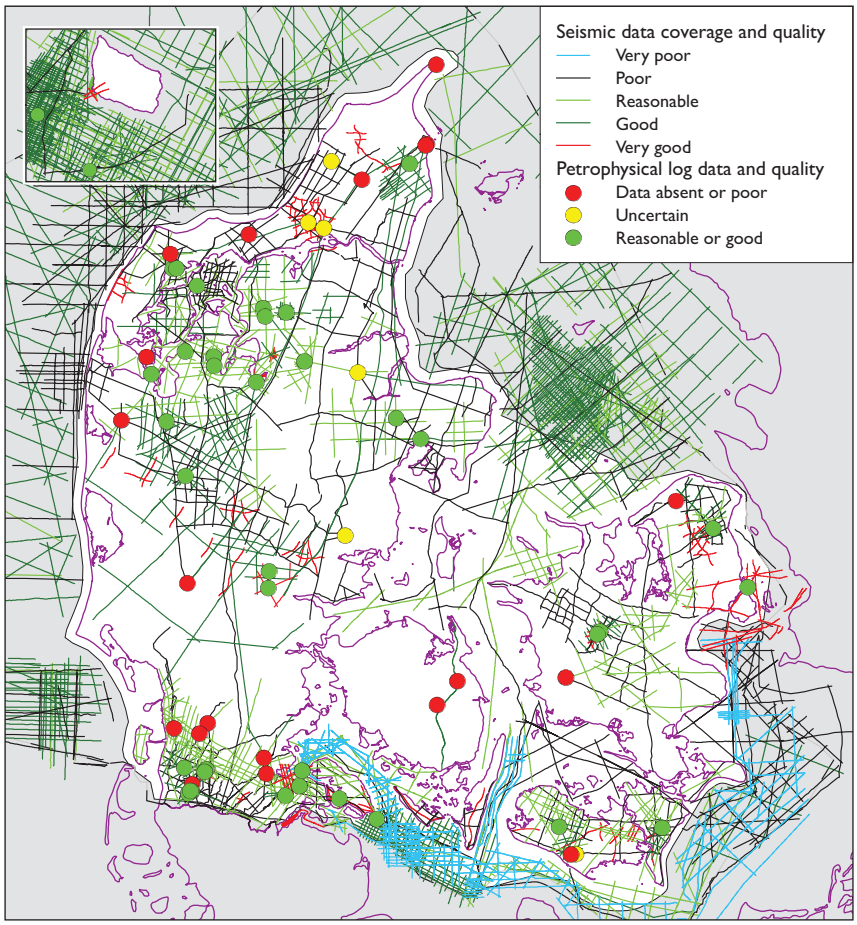

Fig. 3. Coverage and quality of seismic and petrophysical log data from deep wells. The quality indexes reflect to which degree the data can be used to extract information about geothermal relevant lithostratigraphic units in the deep subsurface.

interpreted geological and geophysical data. This will be relevant for all stakeholders in the exploration of deep geothermal resources in the Danish subsurface. The portal focuses on geothermal reservoirs within the 800–3000 m depth interval and provides an overview of the amount and quality of existing geodata, the geological composition of the subsurface, and interpreted thematic products such as geological maps of potential geothermal reservoirs. A comprehensive map from the portal showing onshore and near-offshore locations where the geological conditions are potentially suitable for extraction of deep geothermal energy in Denmark is shown in Fig. 1. Many of the thematic maps are outcomes of the project *The geothermal energy potential in Denmark – reservoir properties, temperature distribution and models for utilization* under the programme *Sustainable Energy and Environment* funded by the Danish Agency for Science, Technology and Innovation.

Geological requirements for geothermal exploitation

In Denmark, successful geothermal exploitation in the deep subsurface requires the presence of thick and laterally coherent sandstone reservoirs with high porosity and permeability, which can ensure effective extraction and re-injection of formation water. A thick and coherent reservoir which is not hydraulically compartmentalised by faults, lateral lithological changes (e.g. grain size) and/or diagenetic features such as compaction and mineralisation implies that a large volume of warm water may be accessible, and that production and injection wells can be placed at appropriate distances from each other while remaining hydraulically connected. A certain distance, e.g. 1,5 km, is needed between the filter screens at reservoir level in order to delay the arrival time of the cool, re-injected water to the vicinity of the production well (Fig. 2). As a rule of thumb this delay should be more than 30 years. On its way to the production well, the cooled water is reheated to some extent by the reservoir matrix and by heat transfer from poorly or non-permeable boundary strata (usually claystone) above and below the reservoir sandstones.

Another important requirement is to find areas where the product of temperature and extractable water volume is large enough to ensure an economically viable geothermal plant. The temperature–depth gradient of 25–30°C/km in the Danish subsurface implies that at depths shallower

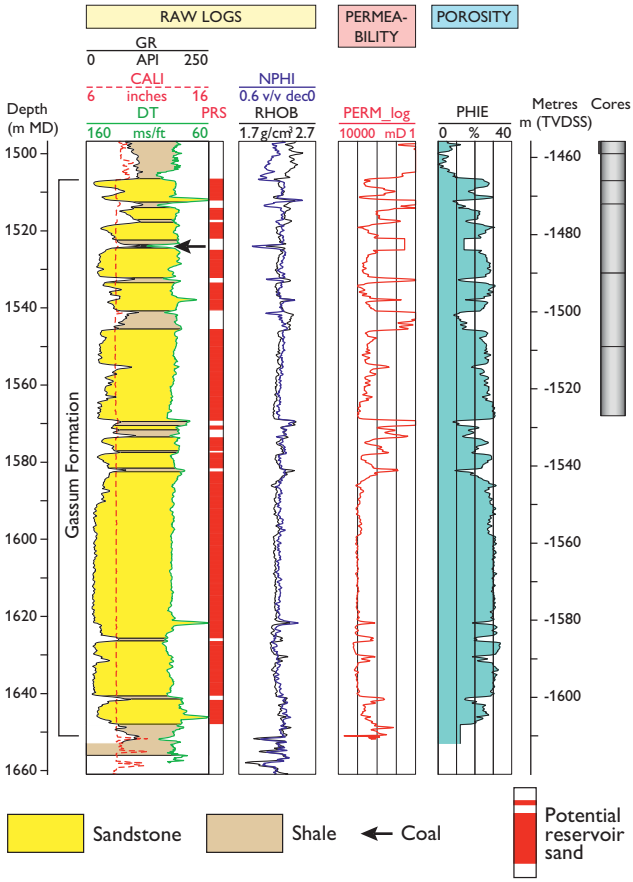

Fig. 4. Petrophysical log evaluation of the Gassum Formation in the Stenlille-1 well including interpretations of lithology, porosity and permeability. **GR**: Gamma-ray log. **API**: Gamma ray radioactivity expressed in accordance with the American Petroleum Institute. **CALI**: Caliper log. **DT**: Sonic log. **PRS**: Potential reservoir sand. **NPHI**: Total porosity log. **RHOB**: Density log. **PERM_log**: Permeability log. **PHIE**: Effective porosity log. **MD**: Measured depth. **TVDSS**: Vertical depth below sea level.

than 800 m the temperature is generally too low, whereas at depths greater than 3000 m, diagenetic alterations related to high pressure–temperature conditions reduce the porosity and permeability of the reservoir sandstones (Poulsen *et al*. 2015; Kristensen *et al*. 2016). Hence, the focus of the portal is the 800–3000 m depth interval.

The geological database

The geological data that provide information about Denmark's deep subsurface mainly consist of information from deep wells and seismic surveys collected over a number of years during oil and gas exploration, and to a lesser extent during studies of potential gas storage and geothermal exploration.

The geographical coverage and quality of the data vary considerably as outlined in Fig. 3. Generally, it is possible to obtain detailed information about the penetrated sedimentary successions from the well data including the depth, thickness and reservoir properties of sandstone reservoirs, e.g. based on core data and petrophysical evaluation of well log data (Fig. 4). The seismic data have been used for large-scale mapping of the depth, thickness and lateral extent of lithostratigraphic units known to contain geothermal reservoir sandstones, as well as for identification and mapping of major faults (Fig. 5). This work involved compilation and integration of the many seismic surveys of different age and quality into a coherent seismic network. Then the network was interpreted in its entirety and used to generate nationwide depth maps to important subsurface horizons, with conversions from seismic-wave travel time to depths below sea level.

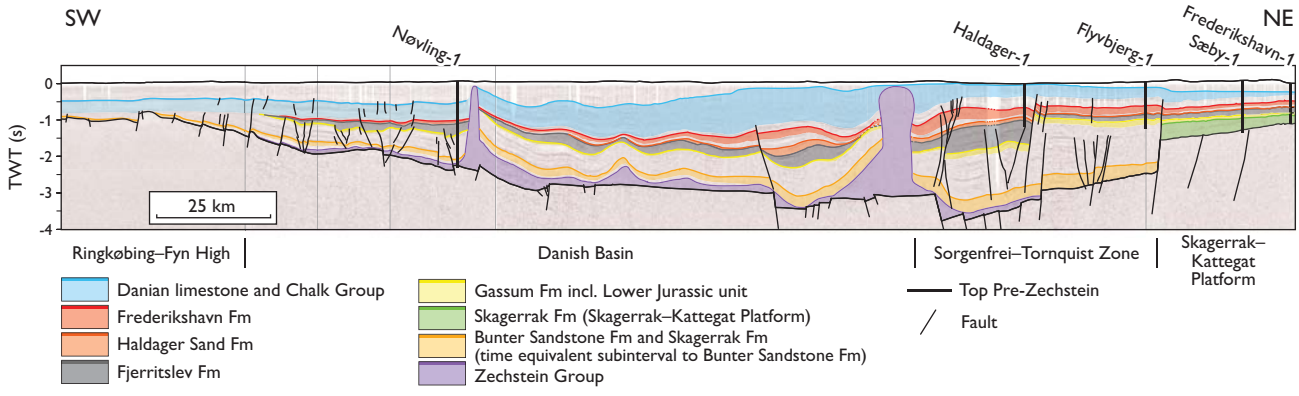

Fig. 5. A regional SW–NE geosection through central and northern Jylland as outlined in Fig. 1. The profile is constructed on the basis of composite seismic profiles shown in the background. Mapped lithostratigraphic units with individual treatment in the portal are highlighted. These include those units which may contain geothermal sandstone reservoirs. In several places the units are truncated by faults, and vertical salt movement from the Zechstein Group has in places uplifted or penetrated the overlying succession. Major structural elements are indicated. Depth is given in seismic two-way travel time (s).

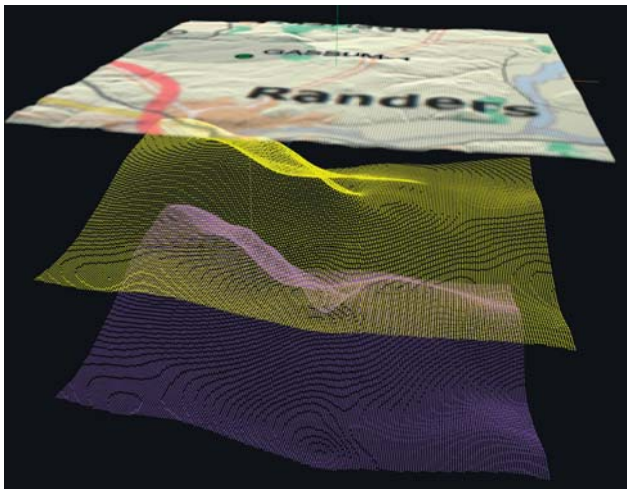

Fig. 6. Interactive 3D tool, available in the WebGIS portal, visualising the variation of subsurface topography of mapped seismic horizons in a given 10 × 10 km area around a selected point.

The depth maps were subsequently used as a base for a new set of maps where constrained reservoir properties such as porosity and temperature were added in relation to depth. In general, the amount of data is too limited for traditional statistical uncertainty analysis. However, based on quality and spatial density analysis and GEUS' general experience, rough uncertainty intervals for the estimated reservoir values are presented for each well in the portal.

The WebGIS portal – content, functionality and perspectives

The first map in the WebGIS portal shows those areas where lithostratigraphic units, containing sandstones with sufficient reservoir properties are considered to be present within the depth interval of 800–3000 m (Fig. 1). The lithostratigraphic units are also treated separately and linked with several relevant theme maps showing e.g. depth, thickness, major faults, reservoir transmissivity and temperature. Additional data, available in the portal, can be added to each of these maps, such as the distribution and quality of seismic data and petrophysical log data from deep wells. The depth maps can also be visualised through an interactive 3D viewer providing an intuitive overview of the subsurface topography of a selection of important horizons (Fig. 6). These maps are to be considered as indicative and are only meant for regional use. This is because the geological data in many areas only provide a rough picture of the subsurface, especially where data are sparse and/or of poor quality. In addition, some of the maps are based on several stages of approximations and generalisations, for instance where largely depth-depending reservoir parameters are paired with depth maps derived from seismic surveys, as briefly described above.

The maps are not final. New well and seismic data can be added and new interpretation tools such as seismic interpolation tools can be included. Refined geological models may also lead to modifications. However, the present maps give a good indication of where in Denmark deep geothermal exploration is relevant, as seen from the geological prerequisites. The use of the maps may thus ensure that new geothermal exploration is directed towards those areas that appear to be most promising based on current knowledge. The various geological map themes also form an important basis for an initial analysis of the geothermal potential at a specific site where the construction of a geothermal plant is considered. In this first step, the maps give an overview of the potential geothermal reservoir intervals (lithostratigraphic units) that may be relevant at the site, and information regarding the type, amount and quality of existing geological data. A more comprehensive estimate of the geothermal potential in a specific area must be based on detailed analysis of the local data and incorporation into local geological models. This work model has been used in an assessment of 28 potential geothermal sites in Denmark in the so-called *Screening project*; another outcome of the above-mentioned policy agreement. The results of this work are also accessible free of charge from the WebGIS portal at *http://DybGeotermi.geus.dk*.

References

Kristensen, L., Hjuler, M.L., Frykman, P., Olivarius, M., Weibel, R., Nielsen, L.H. & Mathiesen, A. 2016: Pre-drilling assessments of average porosity and permeability in the geothermal reservoirs of the Danish area. Geotherm Energy **4:6**, 2–27, *http://dx.doi.org/ 10.1186/ s40517-016-0048-6*

Mathiesen, A., Kristensen, L., Bidstrup, T. & Nielsen, L.H. 2009: Vurdering af det geotermiske potentiale i Danmark. Danmarks og Grønlands Geologiske Undersøgelse Rapport **2009/59**, 30 pp.

Poulsen, S.E., Balling, N. & Nielsen, S.B. 2015: A parametric study of the thermal recharge of low enthalpy geothermal reservoirs. Geothermics **53**, 464–478.

Authors' address

Geological Survey of Denmark and Greenland, Øster Voldgade 20, DK-1350 Copenhagen K, Denmark,. E-mail: *hv@geus.dk*

Towards a national 3D geological model of Denmark

Peter B.E. Sandersen, Thomas Vangkilde-Pedersen, Flemming Jørgensen, Richard Thomsen, Jørgen Tulstrup and Johnny Fredericia

As part of its strategy, the Geological Survey of Denmark and Greenland (GEUS) is to develop a national, digital 3D geological model of Denmark that can act as a publicly accessible database representing the current, overall interpretation of the subsurface geology. A national model should be under constant development, focusing on meeting the current demands from society. The constant improvements in computer capacity and software capabilities have led to a growing demand for advanced geological models and 3D maps that meet the current technical standards (Berg *et al*. 2011). As a consequence, the users expect solutions to still more complicated and sophisticated problems related to the subsurface. GEUS has a long tradition of making 2D maps of subsurface layer boundaries and near-surface geology (Fredericia & Gravesen 2014), but in the change from 2D to 3D and when combining data in new ways, new geological knowledge is gained and new challenges of both technical and organisational character will arise. The purpose of this paper is to present the strategy for the national 3D geological model of Denmark and the planned activities for the years ahead. The paper will also reflect on some of the challenges related to making and maintaining a nationwide 3D model. Initially, the model will only include the Danish onshore areas, with the Danish offshore areas and Greenland to be added later using a similar general setup.

The elements of the national 3D geological model

The national model will be constructed as a 3D geological framework model consisting of a number of surfaces. These surfaces can represent top and bottom of defined geological formations, stratigraphic complexes or other types of spatially recognisable units, as well as erosional surfaces, stratigraphic markers or transgressional surfaces. The surfaces will characterise units defined in a legend of the Danish subsurface compiled in connection with the national 3D geological model project. Interpretation points, lines, polygons, etc. will define the surfaces together with an interpolated or triangulated grid. This framework model is planned to grow continually with the addition of new surfaces. The layered framework model will be supplemented by volumetric cells containing detailed geological information between mapped surfaces (Fig. 1). Lithology and lithofacies or related parameters, such as porosity or resistivity, can be added as attributes to the cells.

The model is intended to contain varying levels of detail and it will be possible to use the model at different scales. The users will be able to download the exact elements they require for a specific modelling purpose within a particu-

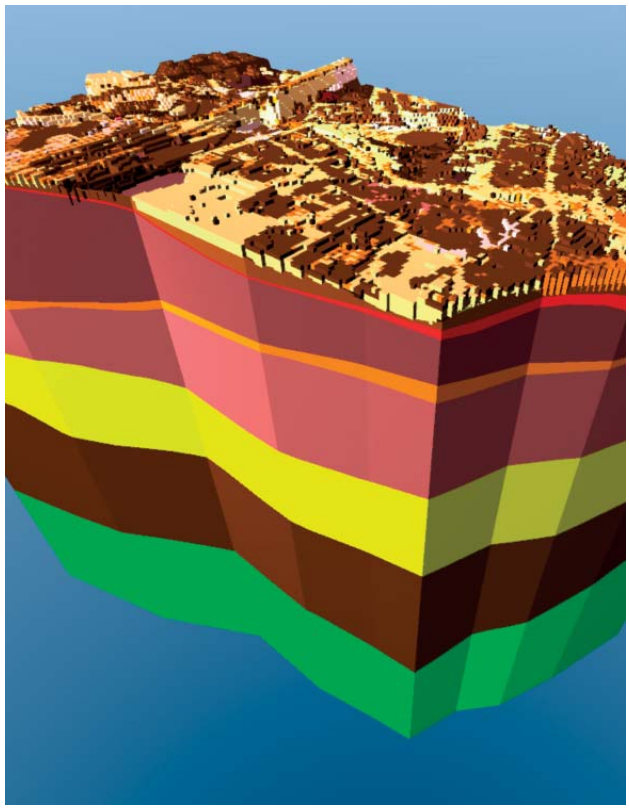

Fig. 1. Model example combining layers and volumetric cells. The man-made layers in the uppermost part of the subsurface are represented as volumetric pixels (voxels), and the deeper parts of the succession as layers. Based on the 3D model of the municipality of Odense (Mielby *et al.* 2015).

© 2016 GEUS.

lar area, i.e. near-surface layers for further hydrogeological modelling in connection with groundwater resource management. This will, of course, require guidance regarding the scale in which the extracted model element can be used. Standards and procedures will be developed for the construction of the model elements as well as for performing quality assurance, quality assessment and model updates. The national model is planned to be platform-independent and by using standardised import and export formats, the construction of model elements will therefore not be restricted to specific modelling software packages.

The model will initially contain a number of key surfaces, but details will continuously be added. At present, a number of surfaces encompassing the deep succession from top pre-Zechstein to the top of the Chalk Group exist in preliminary versions (Table 1). Above this part of the succession, construction of 1–2 major Tertiary surfaces and the top of the pre-Quaternary surface is planned. Modelling of the complex Quaternary geology will be done locally and regionally by using layer boundaries and volumetric cells. Because the amount of dated Quaternary sediments in Denmark is limited these model elements will not necessarily be modelled as specific litho- or chronostratigraphic units, but as units solely defined by lithology.

The model database constitutes an important part of the national 3D geological model containing all the required model elements while at the same time being sufficiently flexible when future elements are added.

Use of existing data and geological models

GEUS hosts a wide range of publicly accessible databases (e.g. Ditlefsen *et al*. 2012; Hansen & Pjetursson 2011; Møller *et al*. 2009a, b; Tulstrup 2004). The most significant databases are the Jupiter well database, the geophysical database GERDA, the oil and gas database FRISBEE and the Geological Models Database. These databases will constitute the main data supply for the national 3D geological model, and therefore their continuous update is very important. The incorporation into the national 3D geological model will ensure that the vast amount of data collected over more than a century is continually used and updated.

In Denmark, 2D and 3D geological mapping and modelling have been performed regionally and locally primarily by GEUS, universities, regional authorities and municipalities, oil companies, the mining industry and consulting companies. Models have typically been made in connection with oil and gas exploration, groundwater and drinking water projects, geothermal projects, raw material and mineral exploration as well as soil and groundwater contamination issues. Especially the intensive groundwater mapping campaign over the past 15 years has produced a large number of publicly available models for the upper parts of the subsurface (Thomsen *et al*. 2013). This has resulted in a patchwork of 2D and 3D models, but because the models have been built in different ways they are difficult to merge. Therefore, in the process of making a new national 3D geological model it is necessary to evaluate and amend the existing models.

The national 3D geological model will be dynamic and regularly updated in order to include new data and interpretations. The modelling will therefore follow strict versioning procedures, with options for displaying the data on which updated interpretations are based.

Model uncertainties, quality assurance and quality control

Handling of model uncertainty has been discussed intensely for many years and many different suggestions have been put forward (e.g. Lark *et al*. 2014; Sandersen 2008; Tacher *et al*. 2006; Wellmann *et al*. 2014). The change from 2D to 3D and the ensuing increased model complexity will create a demand from users for assessment of the inherent uncertainty of the model. This issue is highly complex and the challenges are numerous. The uncertainty of a geological model will be a mixture of the uncertainties of each dataset and the uncertainties of the interpretations of the combined dataset, with the additional challenge of handling both the quantitative and the qualitative aspects.

Table 1. Planned main surfaces in the national 3D geological model

Model element	Surface	Period
Pre-Quaternary succession	Top	Neogene and older
Palaeogene succession	Top	Palaeogene
Chalk Group	Top Bottom	Cretaceous
Frederikshavn Formation	Top Bottom	Cretaceous/Jurassic
Haldager Sand Formation	Top Bottom	Jurassic
Fjerritslev Formation	Top Bottom	Jurassic
Gassum Formation	Top Bottom	Triassic
Bunter Sandstone Formation	Top Bottom	Triassic
Zechstein Group	Top Bottom	Zechstein

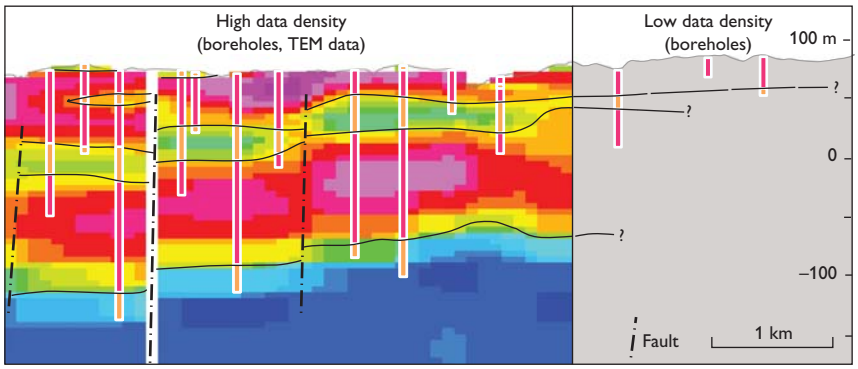

Fig. 2. Cross-section sketch illustrating the challenges of modelling in areas with low data density. Vertical rods represent boreholes with clay (orange) and sand (red). Coloured background in the area with high data density shows measured and gridded sediment resistivity values (**TEM** data; Transient ElectroMagnetic method). Red and purple: high resistivities. Green and blue: low resistivities.

A concept for assessing the uncertainties of the individual model elements will be made specifically for the national 3D geological model to ensure that all model elements are evaluated in the same way. The uncertainty concept will not necessarily be adaptable for use in models other than the national 3D geological model, because it will be tailored specifically to the chosen model setup.

The national 3D geological model will be disseminated to a variety of users and therefore a transparent construction process and a thorough documentation are required. Descriptions of workflows, procedures and guidelines for quality assurance and quality control will be handled by an editorial function in order to keep up a high degree of consistency.

Discussion

In general, varying data coverage and data resolution pose a major challenge for the construction of the national 3D geological model. In the deep parts of the subsurface (below 300–400 m) the data are primarily from boreholes and seismic surveys carried out by the oil and gas industry and with a coverage dictated by the focus of the exploration surveys. In the shallow parts of the subsurface, the data are primarily collected in connection with groundwater investigations, raw material or mineral exploration, soil contamination investigations and geotechnical projects. Data originate from boreholes, seismic surveys, electric and electromagnetic surveys and outcrops. Generally the data density is much higher than in the deeper parts of the subsurface. The shallow part of the Danish subsurface is greatly affected by Pleistocene glaciations. This part is therefore particularly lithologically and structurally complex and requires a large amount of detailed input data.

Even though the data density is rather high in the uppermost parts of the subsurface, the data are in fact often geographically clustered. Therefore, in many areas detailed modelling can only be made within such data clusters. In reality, the result is a patchwork of areas with a high data density in the survey focus areas and a low density in the surrounding areas. This means that the varying data density will be reflected in the geological model interpretations resulting in certain geological elements not being resolved outside the data clusters (Fig. 2). This challenge can be met by constructing a model that can handle different scales with different degrees of detail, but not necessarily with a full geographical coverage of the most detailed interpretations. A model like this will display the actual status of the mapping and show where the geological knowledge is good and where not. In modern 3D modelling software there are no zoom limitations, and if not otherwise stated, the data and the interpreted model can be viewed and evaluated at any scale. It is therefore important to convey the scale-related limitations of the model to the users.

The potential users of the national 3D geological model are numerous (i.e. waterworks, municipalities, governmental agencies, raw-materials and minerals industry, private consultants and educational institutions), and they will have a variety of purposes for their use of the downloaded model elements. To cater for as many of these as possible, the model will be constructed as a multi-purpose tool. This means that the output from the model will require standardised, off-the-shelf products as well as individually tailored elements based on the same framework. An example of a standardised product from the '3D model department store' could be a suite of nation-wide, fixed-scale surfaces to be used in projects dealing with regional or national assessments. A tailored product from the '3D custom shop', on the other hand, could be the delivery of a number of specific surfaces in a selected area supplied with lithological information in volumetric cells to be used in a geographically small-scale project. In this way the 3D model construction procedures can be kept stringent, while the model output can be more flexible in order to meet specific user needs.

Summary and perspectives

The national 3D geological model of Denmark will be constructed from the geological and geophysical data collected during decades of surveying. It will also be based on existing 2D maps and geological models, from which specific elements will be extracted and incorporated. All basic data used in the national 3D geological model are stored in an array of GEUS databases. The model will be dynamic and continuously updated in order to maintain relevance and appeal to the end users. The model will provide a wide range of end users with standardised model downloads as well as with tailor-made products.

Building a national 3D geological model for the country will require a considerable effort over a long period and therefore the model is planned to start with only a limited number of key elements. It will then continue to grow and in the process seek to adapt to the varying demands from society. The short-term strategy is to establish at least 15 key surfaces within the next four years and initiate construction of regional and local geological elements in the shallow parts of the model. The model databases and a beta-version of the web interface will be established and launched. In addition, standards and procedures related to the construction of the 3D model will be described in a series of guidelines. The long-term strategy is to include local and regional surfaces of the main surveyed areas in the national model within the next 10 years, including the Danish offshore areas.

An established dialogue with potential users throughout the process will help target the model contents towards a versatile national model that meets the requirements of the public and at the same time secures the use of the huge amount of valuable data collected over several decades.

Acknowledgements

The authors would like to thank the large number of geologists who have contributed to and participated in the workshops and discussion groups during the initial phases of the work on the national 3D geological model.

References

Berg, R.C., Mathers, S.J., Keefer, D.A. & Kessler, H. (eds) 2011: A synopsis of current three-dimensional geological mapping and modeling in Geological Survey Organizations. Illinois State Geological Survey open file report, Circular **578**, 2011.

Ditlefsen, C., Gausby, M., Salomonsen, J. & Hansen, M. 2012: Vejledning i anvendelse af Modeldatabasen. Geovejledning **9**, GEUS Special publication. 31 pp.

Fredericia, J. & Gravesen, P. 2014: 125 years of geological research for society. Geological Survey of Denmark and Greenland Bulletin **31**, 9–14.

Hansen, M. & Pjetursson, B. 2011: Free, online Danish shallow geological data. Geological Survey of Denmark and Greenland Bulletin **23**, 53–56.

Lark, R.M., Thorpe, S., Kessler, H. & Mathers, S.J. 2014: Interpretative modelling of a geological cross section from boreholes: sources of uncertainty and their quantification. Solid Earth **5**, 1189–1203.

Mielby, S. *et al*. 2015: Udvikling af en 3D geologisk/hydrogeologisk model som basis for det urbane vandkredsløb. Syntese rapport. Geological Survey of Denmark and Greenland Special publication (in Danish only).

Møller, I., Søndergaard, V. H., Jørgensen, F. Auken, E. & Christiansen, A.V. 2009a: Integrated management and utilization of hydrogeophysical data on a national scale. Near Surface Geophysics **7**, 647–659.

Møller, I., Søndergaard, V.H. & Jørgensen, F. 2009b: Geophysical methods and data administration in Danish groundwater mapping. Geological Survey of Denmark and Greenland Bulletin **17**, 41–44.

Sandersen, P.B.E. 2008: Uncertainty assessment of geological models – a qualitative approach. In: Refsgaard, J.C. *et al*. (eds): Calibration and reliability in groundwater modelling: credibility of modelling. International Association of Hydrological Sciences Publication **320**, 345–349.

Tacher, L., Pomian-Srzednicki, I. & Parriaux, A. 2006: Geological uncertainties associated with 3-D subsurface models. Computers & Geosciences **32**, 212–221.

Thomsen, R., Sondergaard, V. & Klee, P. 2013: Greater water security with groundwater – Groundwater mapping and sustainable groundwater management. The Rethink Water network and Danish Water Forum white papers, Copenhagen. Available at *www.rethinkwater.dk*.

Tulstrup, J. 2004: Environmental data and the Internet: openness and digital data management. Geological Survey of Denmark and Greenland Bulletin **4**, 45–48.

Wellmann, F.J., Lindsay, M., Poh, J. & Jessell, M. 2014: Validating 3-D structural models with geological knowledge for improved uncertainty evaluations. Energy Procedia **59**, 374–381.

Authors' address

Geological Survey of Denmark and Greenland, Øster Voldgade 10, DK-1350 Copenhagen K, Denmark; E-mail: psa*@geus.dk*

Pre-Quaternary rocks and sediments with a high level of radioactivity in Denmark

Peter Gravesen and Peter Roll Jakobsen

The pre-Quaternary sediments and rocks in Denmark generally have a low content of radioactive minerals and elements. Uranium, thorium and radium are built into mineral structures or are, for example, adsorbed on the surface of clay minerals, Fe-minerals or organic material.

Radon (^{222}Rn) is a radioactive noble insoluble gas with a half-life of 3.8 days. It belongs to the uranium (^{238}U) decay chain where radon is formed from radium (^{226}Ra).

When Rn is formed by radioactive decay from Ra, the emanation process sends part of the radon produced into the pore spaces of rocks and soils. From here, the radon can enter and accumulate in buildings. The source of the radioactive materials in Danish sediments and rocks is primarily from weathered Precambrian crystalline rocks from Norway, Sweden, Finland and the Danish island of Bornholm. Physical and chemical weathering disintegrates these rocks and rivers transport the material into the Danish–Norwegian and Danish–Polish sedimentary basins.

Several studies have analysed and described the radioactive content of Danish sediments and crystalline rocks (e.g. Damkjær & Korsbech 1985, 1988; Gravesen *et al.* 1996, 1999; Gravesen & Jakobsen 2010) and investigations have demonstrated a relationship between sediments and rocks and Rn levels in Danish buildings (Andersen *et al.* 2001).

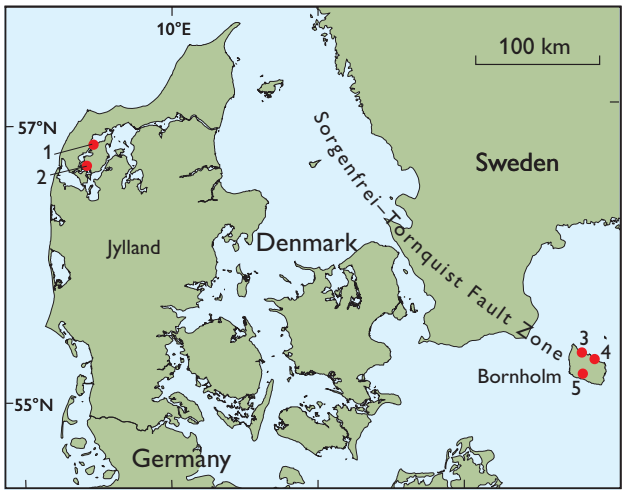

Fig. 1. Map of Denmark with the highest levels of radioactivity measured in surface rocks. **1**: Thisted. **2**: Erslev. **3**: Allinge. **4**: Tejn. **5**: Birkely.

This paper addresses the radioactive content of sediments and rocks with the highest radioactive levels in Denmark and the highest recorded radon emanations: Precambrian crystalline rocks on Bornholm and Late Paleocene clays in north-western Jylland (Fig 1). The data were collected by Gravesen *et al.* (1999) at the Geological Survey of Denmark and Greenland (GEUS) with the aim of characterising and mapping Rn in Danish rocks and sediments.

Methods and data

In Thisted, a 4 m long trench was dug, four shallow boreholes were drilled and older borehole data in GEUS' Jupiter database were studied. The trench was dug to a depth of *c.* 2 m into till deposits and limestone (Fig. 2) and the lithology, structures and macro-pores were described and samples collected. The four 5–6 m deep boreholes were drilled close to the trench. A total of 48 samples of the tills, clay and limestone were described and collected every 30 cm. The samples from the trench each weighed more than 500 g whereas the core samples weighed 300–500 g.

Studies and sampling were carried out at the Bornholm outcrops of granites and diabase at Allinge-Sandvig and Tejn (Fig. 1, loc. 3–4) at the northern end of the island and of the crystalline rocks at Birkely (near the farm of Vallensgård) to the south of Almindingen (Fig. 1, loc. 5). The lithology, structures, weathering, and faults and fractures

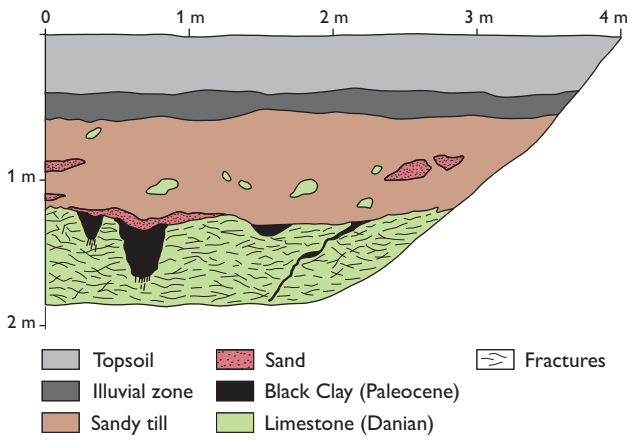

Fig. 2. Geological section in the trench from the eastern part of Thisted.

© 2016 GEUS.

were described. A total of 10 samples of 500–1000 g were collected from the three localities.

The chemical and physical components of the matrix and the petrographical components of the clast material of the samples were analysed. The U concentration was measured by instrumental neutron activation analysis by Activation Laboratories Ltd, Canada. The Ra content was measured with a germanium detector at the National Institute of Radiation Protection, Denmark. The Rn emanation rate was determined using the closed-chamber method using ZnS(Ag) scintillation cells at the Risø National Laboratory, Technical University of Denmark.

Relationship between Danian and Late Paleocene deposits in Thisted

The distribution of Danian – Late Paleocene (65.5–55.8 Ma) deposits in north-western Jylland in the area of Mors and Thisted is related to two salt diapirs, the Erslev salt diapir (Pedersen *et al.* 2013) and the Thisted salt dome (Hansen & Håkansson 1980). Sediment distribution around the two salt structures is similar at the pre-Quaternary surface with Maastrichtian chalk in the middle surrounded by Danian limestone and with Palaeogene clays bordering the limestone. The layers are generally inclined away from the centre of the salt structures.

Different aspects of the radioactive components in the areas were investigated by Damkjær & Korsbech (1985) and Gravesen *et al.* (1996). The Quaternary cover above the Danian limestone is rather thin (0–2 m) in the Thisted area. A topsoil layer overlies Weichselian glacial sandy tills, clayey tills, and just above the limestone is a strongly calcareous till (about 60–80% $CaCO_3$). These tills contain vertical fractures at 5–10 cm intervals.

The Late Danian limestone is partly cemented and can be classified as a calcilutitic or calcarenitic limestone according to grain size. The trenches demonstrated more complex geological structures than expected (Fig. 2). The top surface of the Danian limestone was eroded and brecciated during the Late Paleocene and cut by horizontal and vertical fractures with pronounced karst features and inclined fractures filled with black structureless Paleocene clay which contains Selandian dinoflagellate cysts. The clay also contains limestone clasts and is probably redeposited. At the bottom of the karst structures, several clay-filled fractures reach at least 10–15 cm downwards (Fig. 2). In a few shallow boreholes at Thisted, more than 50 cm of black clay has been encountered indicating non-eroded remnants of the black clay, and black clay material is also enclosed in the till at some locations.

The content of radioactive material in the Thisted sediments is presented in Table 1 (Data from Damkjær & Korsbech 1988 and Gravesen *et al.* 1999). The U, Ra and Rn values for the Danian sediments are comparable with levels for these sediments in other parts of the country (Damkjær & Korsbech 1985) but the high value for the radon emanation of the black clay can only be compared with levels of Paleocene black clay from the Erslev area which has even higher values (Table 1). High levels of radon emanations are also known from Cambrian–Ordovician alum shale: 16 atoms/kg/s, Eocene diatomites: 22 atoms/kg/s, Miocene U-bearing heavy sand: 52 atoms/kg/s, and Miocene black clay: 38.9 atoms/kg/s (Damkjær & Korsbech 1985).

Discussion

Karst in Danish limestone and chalk is found in many areas of northern Jylland but the occurrence in the Thisted trench is noteworthy due to its radioactivity. Karst is formed by acidic water percolating through fractures in the limestone and dissolving parts of it. The erosion of the pre-Quaternary surface started at the inversion and uplift of the Sorgenfrei–Tornquist zone at the end of Cretaceous–Paleocene time followed by Cenozoic sub-areal erosion (Stenestad 2006). The erosion had removed the Late Paleocene clay from most of the Thisted area and redeposited part of the material in the shallow karst holes in the limestone.

In a search for the origin of Rn in buildings Damkjær & Korsbech (1988) investigated sediments from the Erslev area and suggested that redeposited black clay in tills was the source of the high levels of radon. However, the results showed that the high values were in the limestone areas. The later investigation of Andersen *et al.* (2001) demon-

Table 1. Measured radioactive components

Locality	Lithology and age	Uranium ppm	Radium Bq/kg	Radon Atoms/kg/s
Thisted	Weichselian sandy till	0.8–1.9	18.7–24.7	7.5–10.4
	Late Paleocene clay	–	–	42.4
	Danian limestone	< 0.6	2.8–3.3	0.12–0.8
Erslev	Paleocene clay	2.72–26.3	38–300	11.2–130
Allinge	Hammer granite (weathered)	4.2	86.9	–
	Hammer granite	3.0	63.5	–
Tejn	Vang granite	3.8	66.0	–
Birkely	Almindingen granite (weathered)	3.4	41–51	9.6
	Almindingen granite	4.3	50.7	8.8
	Diabase (weathered)	4.2	104.2	39.6
	Clay: weathered diabase	8.5	–	–

strated relatively high levels of Rn in buildings sitting on limestone in Thisted although the radioactivity of limestones at both localities was among the lowest in Danish sediments. The present investigation from Thisted based on the trench and shallow boreholes shows that the high levels of Rn emanation from isolated or redeposited Late Paleocene black clays can probably be the source of the high Rn levels in the buildings in this region. In Sussex, England, high Rn levels in houses are also partly caused by redeposited material on top of low-radioactive chalk (Killip 2004).

Precambrian basement rocks: radioactivity and weathering

Bornholm is situated in the Sorgenfrei–Tornquist Fault Zone south of Sweden (Fig. 1). The Precambrian basement of northern and eastern Bornholm consists of granitic and gneissic rocks which contain abundant leucogranitic bodies, pegmatites and aplites, besides more than 250 mafic dykes that cut these crystalline rocks.

The Kampeløkke Å locality at Allinge consists of medium-grained Hammer granite with a *c.* 20 cm thick crust of weathered granite (Fig. 3). The Hammer granite comprises 41% K-feldspar, 18% plagioclase, 33% quartz, 1% hornblende, 4% biotite, and accessory Ti-magnetite, apatite, epidote, allanite and fluorite (Micheelsen 1961). Large crystals of black gadolinite, a REE-Fe-Be silicate mineral, are found in the area with abundant small red spots of Fe_2O_3 on its crystal surfaces. The granite is cut by vertical and horizontal fractures. The content of radioactive compounds is seen in Table 1. In the Hammer granite the U content is between 3.0 and 4.2 ppm and the Ra content is between 63.5 and 86.9 Bq/kg.

The Møllebæk locality at Tejn consists of coarse-grained Vang granite with very coarse-grained pegmatites covered by 10–20 cm thick weathered granite. The granite contains vertical and horizontal fractures. The Vang granite is composed of 33% K-feldspar, 22% plagioclase, 27% quartz, 5% hornblende, 6% biotite, 3% Ti-magnetite, 1% titanite, 1% apatite and subordinate allanite (Micheelsen 1961). The pegmatites have only a low content of dark minerals (averaging 1%) but 45–60% K-feldspar and 30–40% quartz. The content of radioactive components is comparable to that of the Hammer granite.

The Birkely locality (1½ km north of the farm Vallensgård) is a small quarry with medium-grained Almindingen granite. The mineralogical composition is nearly the same as for the Hammer granite. Figure 4 shows a section with a strongly fractured and faulted part with several partly weathered olivine diabase dykes and weathered granite.

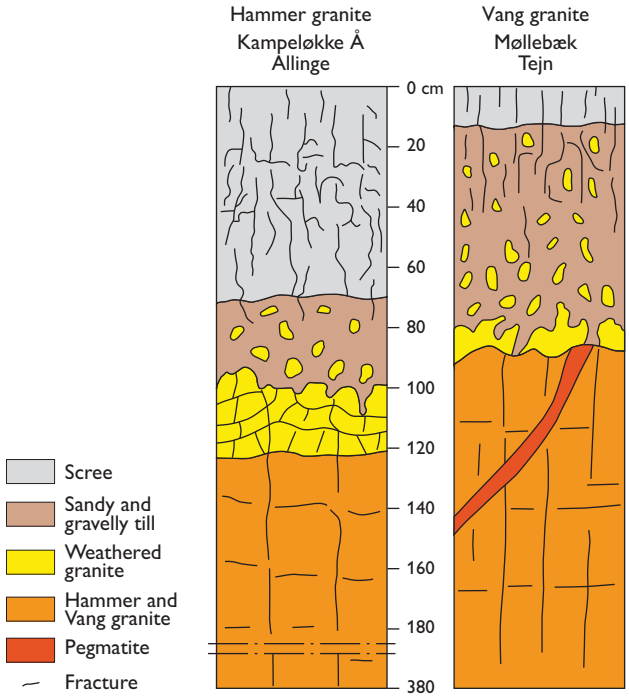

Fig. 3. Geological sections from Allinge and Tejn.

These faults and fractures are orientated WNW–ESE, the same direction as the major fault between the crystalline rocks and the younger sediments (Micheelsen 1961), and the faults have slickensides demonstrating movement.

The diabase dykes mainly contain olivine and pyroxene but biotite, epidote and hornblende also occur (Callisen 1934). Alteration of these minerals produced serpentine, chlorite and calcite. The diabase dykes are orientated NW–SE as are many other diabase dykes and faults in these rocks. Along its contacts with weathered granite, the diabase is altered to green clayey material of chlorite or serpertine (Fig. 4). The rocks in the area are partly weathered and Fe-bearing minerals are oxidised to yellow-brown, clayey iron-rich weathering products on the fracture surfaces. The content of radioactive components is shown in Table 1.

Discussion

In this study, the U content of the Hammer, Almindingen and Vang granites was found to be below 5 ppm, but higher values (6–16 ppm) have previously been recorded (Johansson *et al.* 2016). The olivine diabase dyke yielded a comparable U content, about 4.2 ppm. The granites and diabases have high levels of U, Ra and emanations of Rn, and examples of weathered granites and diabases with higher levels are found. Some of these rocks are among those with the highest radon emanations known in Denmark. The

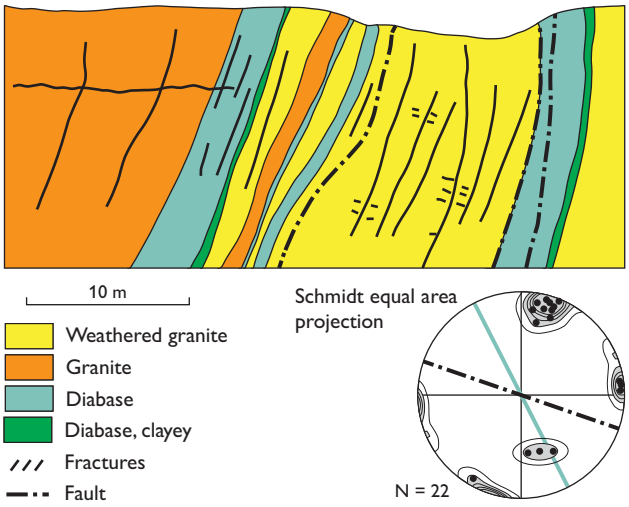

Fig. 4. Geological section from the Birkely quarry, south of Almindingen, Bornholm. The orientation of faults and fractures, and diabase sheets (green) are shown in the diagram.

weathered diabase yields Rn emanation levels comparable to the Paleocene clay from Thisted.

According to leaching investigations of Pliler & Adams (1962), granitic rocks become depleted in U during the first phase of acid chemical weathering, but during the subsequent weathering phases, the top of the weathered rocks become altered and now predominantly consist of resistant U-bearing minerals. The weathering of the ground surface and shallow fractures of the rocks is mainly due to hydrolysis by percolating surface water and fluctuating low temperatures.

The mafic minerals in diabases, such as hornblende, pyroxene and biotite, can be altered to green chlorite or serpentine and eventually form a clayey material hosting the U.

The crystalline rocks are the primary source of radon in buildings on northern Bornholm, and especially where cellar walls consist of unweathered or weathered rocks the Rn concentrations in the buildings can be high (Andersen *et al.* 2001).

Conclusions

The black Paleocene clay on Danian limestone in Thisted and the crystalline rocks on Bornholm are among the Danish deposits with the highest contents of U and Ra, and they also have the highest Rn emanation rates. Other sediments at this emanation level are fine-grained Cambrian–Ordovician alum shale, Eocene diatomites and Miocene black and brown clays and sand. Most of these sediments, like the Thisted clay deposits, have limited distribution and are found below thick Quaternary layers and can be difficult to locate.

Acknowledgements

The Danish Ministry of Health is thanked for financial support.

References

Andersen, C.E., Ulbak, K., Damkjær, A. & Gravesen, P. 2001: Radon i danske boliger. Kortlægning af lands-, amts- og kommuneværdier, 74 pp. Copenhagen: Sundhedsstyrelsen.

Callisen, K. 1934: Das Grundgebirge von Bornholm. Geological Survey of Denmark, II. Række 50, 266 pp.

Damkjær, A. & Korsbech, U. 1985: Measurement of the emanation of radon-222 from Danish soils. The Science of the Total Environment **45**, 343–350.

Damkjær, A. & Korsbech, U. 1988: A search for correlation between local geology and indoor radon concentration. Radiation Protection Dosimetry **24**, 51–54.

Gravesen, P. & Jakobsen, P.R. 2010: Radon content in Danish till deposits: relationship with redox conditions and age. Geological Survey of Denmark and Greenland Bulletin **20**, 39–42.

Gravesen, P., Jakobsen, P.R. & Kelstrup, N. 1996: Radon i danske jordarter II, undersøgelser og konklusioner. Danmarks og Grønlands Geologiske Undersøgelse Rapport **1996/78**, 113 pp.

Gravesen, P., Jakobsen, P.R., Kelstrup, N. & Ernstsen, V. 1999: Kortlægning af radon i danske jordarter 1. Indsamling af grunddata. Danmarks og Grønlands Geologiske Undersøgelse Rapport **1999/81**, 58 pp.

Hansen, J.M. & Håkansson, E. 1980: Thistedstrukturens geologi – et "neotektonisk" skoleeksempel. Dansk geologisk Forening, Årsskrift for **1979**, 1–9.

Johansson, Å., Waight, T. Andersen, T. & Simonsen, S.L. 2016: Geochemistry and petrogenesis of Mesoproterozoic A-type granitoids from the Danish island of Bornholm, southern Fennoscandia. Lithos **244**, 94–108, *http://dx.doi.org/ 10.1016/j.lithos.2015.11.031*

Killip, I.R. 2004: Radon hazard and risk in Sussex, England and the factors affecting radon levels in dwellings in chalk terrain. Radiation Protection Dosimetry **113**, 99–107.

Micheelsen, H.I. 1961: Bornholms grundfjæld. Bulletin Geological Society of Denmark **14**, 308–349.

Pedersen, S.A.S., Jakobsen, P.R., Tougaard, L. & Gravesen, P. 2013: Geological map of Denmark 1:50 000 – map sheet Mors, NW Denmark. Geological Survey of Denmark and Greenland Bulletin **28**, 29–32.

Pliler, R. & Adams, J.A.S. 1962: The distribution of thorium and uranium in a Pennsylvanian weathering profile. Geochimica et Cosmochimica Acta **26**, 1137–1146.

Stenestad, E. 2006: Fluviokarst in the top of the Maastrichtian chalk at Rørdal, northern Jutland, Denmark. Bulletin of the Geological Society of Denmark **53**, 93–110.

Authors' address

Geological Survey of Denmark and Greenland, Øster Voldgade 10, DK-1350 Copenhagen K, Denmark. E-mail: *pg@geus.dk*

Tectonic control on the formation of Roskilde Fjord, central Sjælland, Denmark

Stig A. Schack Pedersen and Peter Gravesen

Roskilde Fjord is a characteristic N–S-trending geomorphological element in north-east Sjælland (Fig. 1). The eastern coastline of the fjord forms a nearly straight, SSE–NNW-trending lineament from the town of Roskilde to the coastal areas at Kattegat. Due to the records from wells, it has long been known that a fault zone has to be present along this lineament (Bondesen 1979). The fault is named after the fjord: the Roskilde Fjord Fault (Fig. 2). However, a detailed analysis of the well data in the Roskilde area has shown that a number of minor faults are present, superposed by various landscape elements. These are the inner fjord and valley distributary at Roskilde, the Kornerup Å valley, the inlet of Lejre Vig and its contributory, and the peninsula of Bognæs (Figs 1, 2).

In this paper we propose a lithostratigraphic division of the Cenozoic deposits and their dynamic development in the Roskilde area. A distribution of the faults with estimated maximum displacements is presented, and their relations to the geomorphological features are outlined. The description is based on several years' studies of the Roskilde Fjord fault complex and presented here due to the recent interest in neotectonics in Denmark and environmental considerations focused on Roskilde Fjord (Gravesen & Pedersen 2005).

Stratigraphy of the Roskilde area

The Palaeogene and Quaternary stratigraphy of the area is briefly outlined here based on well data and a few sand and gravel pit outcrops (Gravesen & Pedersen 2005). The Palaeogene deposits in the area include Danian and Selandian formations (65.5 to 58.7 Ma). The late Danian København Kalk Formation consists of calcisiltitic and calcarenitic yellow-white limestone with some thick chert layers (Thomsen 1995). The overlying, early Selandian deposits were laid down after a period of erosion and often begin with glauconitic conglomerate and greensand of the Lellinge Greensand Formation followed by olive grey glauconitic silty limestone, sand and clay (Clemmensen & Thomsen 2005). The pre-Quaternary unconformity thus truncates Danian as well as Selandian units.

The oldest Quaternary deposits are probably from the late Saalian (150–130 ka BP). The clayey tills and sand layers are found in deep buried valleys down to 80 m below the surface. The deposits are known from wells but are difficult to date precisely. Jacobsen (1985) also suggested that Saalian deposits were the oldest Quaternary deposits in the area. From the early Middle Weichselian thin and fragmented sand layers were deposited in rivers and lakes, and the surficial processes possibly initiated the valley formation *c.* 70–55 ka BP. A Middle Weichselian ice stream from the east, the 55–50 ka BP Old Baltic Ice Stream, deposited the Ristinge Klint Till Formation, characterised by reddish staining of the clayey and sandy tills (Houmark-Nielsen 2010). The Late Weichselian Himmelev Formation consists of cross-bedded meltwater sand and gravel deposited by braided streams from the north (Jacobsen 1985), indicat-

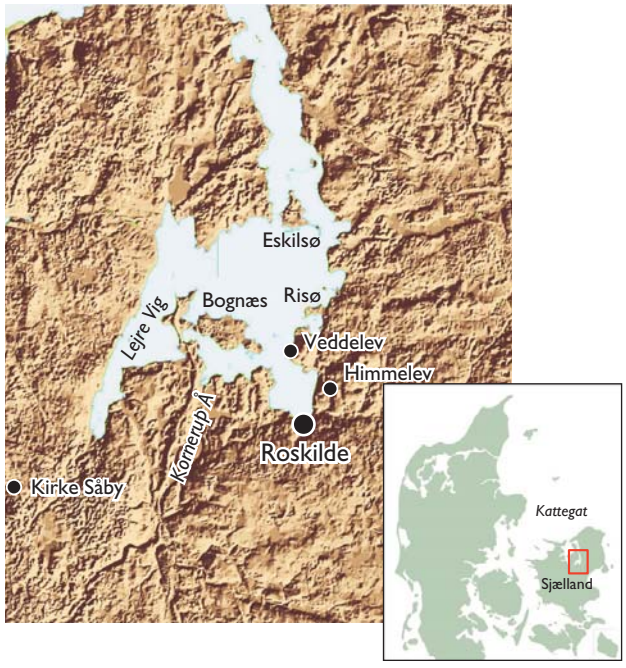

Fig. 1. Terrain model of the Roskilde area and index map of Denmark showing the location of the area in focus. Note the strong S–N-trending lineament including the linear coast lines of Roskilde Fjord.

© 2016 GEUS.

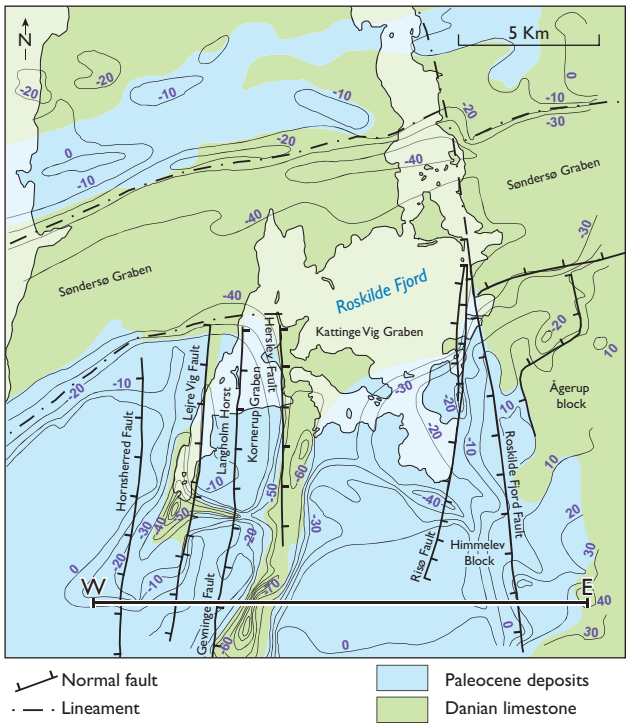

Fig. 2. Geological map of the formations occurring on the pre-Quaternary unconformity surface and location of the cross-section shown in Fig. 4. The contour lines show the depth in metres to the pre-Quaternary unconformity based on well data.

ing deposition at the southern front of the melting Kattegat Ice Stream at *c.* 26 ka BP. This unit is overlain by the grey to brown, massive Mid Danish Till Formation deposited by the ice stream from north-east during the Last Glacial Maximum (Houmark-Nielsen 1987, 2010). The Mid Danish Till Formation is overlain by the Hedeland Formation, which is a very coarse-grained, cross-bedded sand/gravel formation deposited as a proximal sandur and in meltwater channels (Jacobsen 1985). The last ice advance, the Young Baltic Ice Advance, was separated into two. The first, the East Jylland Advance from the south-east and east deposited the East Jylland Till Formation of grey and brown clayey till at 19–18 ka BP (Houmark-Nielsen 2010). In the following period, which was free of ice cover, glaciolacustrine sediments were deposited. The last advance from the east and south-east deposited the brown, clayey Bælthav Till Formation (18–17 ka BP). During the final melting of the last glaciers the Vindinge Formation consisting of fine-grained sand, silt and clay was deposited in a dead ice landscape. Marine Holocene sand and mud deposits are found along the coast of Roskilde Fjord, while freshwater deposits occur along small streams and in lakes.

Method of cross-section construction

The analysis of the subsurface geology in the Roskilde Fjord area was carried out by the construction of a large number of mainly E–W-trending cross-sections perpendicular to the interpreted strike of fault features. The cross-sections were constructed in ArcGIS©, using well data from the Jupiter database along chosen sections with a bandwidth of 1 km. Maps were constructed from a selection of these wells, providing information on the depth to the pre-Quaternary unconformity and the local lithology at the pre-Quaternary surface (Fig. 2). The pre-Quaternary unconfomity map was produced by an integration over the well data points using ArcGIS©.

Depth to the pre-Quaternary unconformity

The map of the depth to the pre-Quaternary unconformity (Fig. 2) shows that the surface forms a high plateau to the east of Roskilde, reaching a level above 30 m a.s.l. Along the drainage creek to the south-eastern arm of Roskilde Fjord and along the eastern coastline, the structural contours of the surface of the pre-Quaternary unconformity are closely spaced and trend N–S, indicating an escarpment parallel to the east coast of the Roskilde Fjord. Below the central part of the southern depression of Roskilde Fjord, where the peninsula of Bognæs is located, the depth to the pre-Quaternary unconformity is more than 40 m b.s.l. Thus, the level change from east to the central part of Roskilde Fjord is almost 80 m.

The south-western corner of the Roskilde Fjord is dominated by two strong lineaments parallel to the geomorphic features Kornerup Å and Lejre Vig, where two buried val-

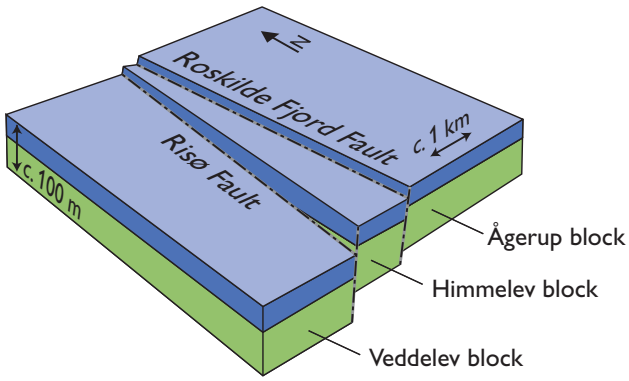

Fig. 3. The block diagram illustrates the relay faults along the east side of Roskilde Fjord.

leys are eroded to a depth of more than 70 m b.s.l. (Fig. 1). Between the lineaments the pre-Quaternary unconformity has an elevation of 0–10 m b.s.l., and farther to the west and south-west at Kirke Såby the surface forms a plateau at about sea level (Fig. 2). To the north the Roskilde Fjord changes from a broad basin to a narrow fjord arm extending northwards. The shift is located to the area around Eskilsø, and the broad basin depression to the south is interpreted as the interference between the Roskild Fjord lineaments and the E–W-trending Søndersø Graben (Fig. 2). This graben system is interpreted as partly tectonically controlled but mainly mirrors a tunnel-valley drainage system to the west related to the Baltic Ice Advance.

Block faulting of Danian limestone and Paleocene limestone and clay

Only two formations are distinguished at the pre-Quaternary unconformity surface: Danian limestone and Paleocene limestone and clay (Fig. 2). Their distribution follows two rules: Danian limestone either appears where a trench has been carved down to a depth below the base of the Paleocene limestone, greensand and clay, or it appears on elevated plateaux above the Paleocene deposits. The latter is the case east of Roskilde, whereas carved trenches are seen below the Kornerup Å valley and the Lejre Vig buried valley (Figs 1, 2). The broad, E–W-trending Søndersø Graben belongs in the first group representing a buried valley sandur.

The faults are relay faults (Korstgård 1996). This means that they have a hinge point where the displacement is negligible, and from where the displacement increases along strike (Fig. 3). A culmination of the displacement occurs about 1–4 km from the hinge point, and then the displacement decreases to another hinge point at the opposite termination of the fault. In the Roskilde fault complex the maximum displacement is calculated to about 60 m, but most faults have displacements only in the range of 10–30 m. The marker horizon used for estimation of the displacement is the boundary between the Danian limestone and the Selandian deposits. This boundary is believed to have been an almost horizontal plane, given that both units are marine successions deposited in the broad shelf environment that dominated the Danish Basin in the Palaeogene.

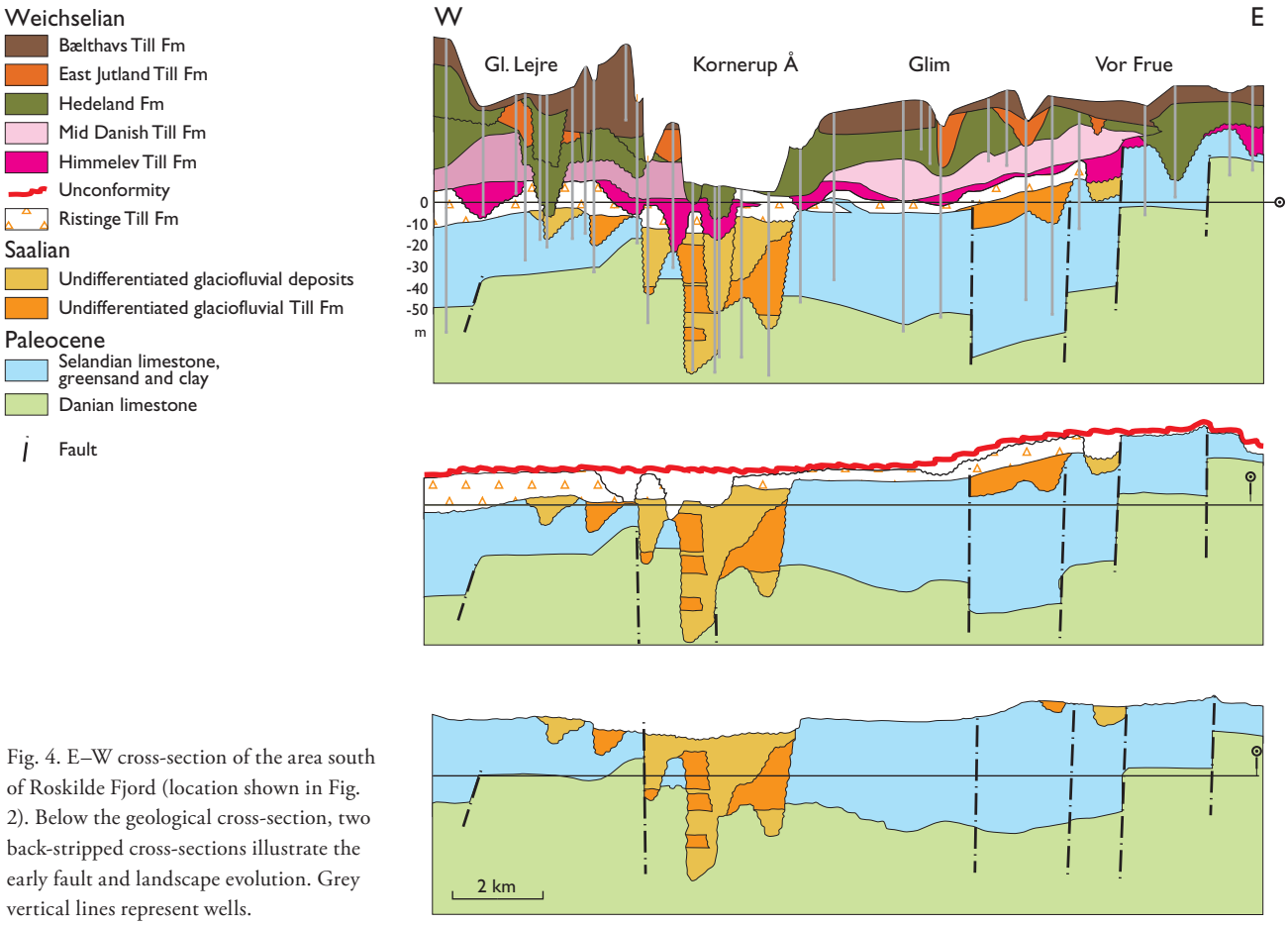

Fig. 4. E–W cross-section of the area south of Roskilde Fjord (location shown in Fig. 2). Below the geological cross-section, two back-stripped cross-sections illustrate the early fault and landscape evolution. Grey vertical lines represent wells.

Glaciodynamic development of the Quaternary succession

The interpretation of the dynamic development includes a palinspastic reconstruction shown in Fig. 4. The interpreted cross-section also illustrates two former structural steps in the development. The first of these goes back to an unconformity that is interpreted as a peneplanation in the main part of the middle-late Weichselian. The second step is a further back-stripping to the supposed Eemian peneplanation after the Saalian glaciation; this scenario illustrates the interpreted faulting of the boundary between the Danian limestone and Selandian unit. Evidently, at this time the Roskilde fault complex had already been active. Furthermore, a deep incised valley along the Kornerup Å lineament was probably initiated in the Neogene prior to the late Pleistocene. We suggest that deep valley erosion in the Elsterian was succeeded by infill into the valley of meltwater sand and tilly material in the Saalian (Fig. 4). During the Middle Weichselian the Ristinge Advance deposited meltwater sand and the Ristinge Till Formation on a succession that had been faulted. In the beginning of the Late Weichselian, the Last Glacial Maximum initiated the Swedish Ice Advance (Pedersen 2012), which resulted in meltwater streams eroding into the surfaces of downthrown blocks. Renewed erosion and deposition took place in the Kornerup Å valley, and new valleys were formed in the blocks to the east and to the west along fault lineaments. After the meltwater sand of the Himmelev Formation had filled the valleys to form a relatively even outwash plane surface, the Mid Danish Till Formation covered the area with a more than 10 m thick clayey basal till.

After the deposition of the Mid Danish Till Formation, a new phase of faulting occurred along the Roskilde Fault. This resulted in a relative uplift of the block to the east and the total vertical displacement by *c.* 60 m. During the Young Baltic Ice Advance in the Late Weichselian the Mid Danish Till Formation and the underlying Himmelev Formation were eroded away from the elevated area to the east, whereas the sequence was preserved in a down-faulted block to the west. The Young Baltic Ice Advance had oscillating advances and retreats including the East Jutland Ice Advance and the Bælthav Ice Advance (Houmark-Nielsen 2010). At this time the main part of eastern Denmark became covered by a huge outwash plane. At Roskilde this resulted in the deposition of the Hedeland Formation which is the main source for gravel exploitation in the Roskilde area (the previous interpretation of the Hedeland Formation by Jacobsen 1985 is now considered redundant). Thin beds of till are commonly present in this meltwater succession, representing the oscillating ice conditions. Before the final erosion of the valleys and fjord arms the Bælthav Till Formation was deposited shaping the present hummocky moraine plateau landscape.

Conclusions

The geomorphology of the Roskilde area mirrors a number of tectonic and depositional elements in the subsurface. The fault zones responsible for several terrain lineaments are relay faults that outline an imperfect en échelon pattern. The fault displacements can be calculated from the position of the boundary between the Danian limestone and the Selandian unit. Neotectonic displacement was active shortly after the deposition of the Mid Danish Till Formation. The deepest buried valleys were probably eroded out during the Elsterian glaciation and filled with sand and till during the Saalian glaciation. These valleys were buried during the Weichselian glaciodynamics.

References

Bondesen, E. 1979: Roskilde, by og landskab – geologi og samfund. In: Birkebæk, F.A. (ed.): 13 bidrag til Roskilde by- og egnshistorie. Roskilde Museums 50 års Jubilæumsskrift, 20–41. Roskilde: Roskilde Museum.

Clemmensen, A. & Thomsen, E. 2005: Palaeoenvironmental changes across the Danian–Selandian boundary in the North Sea Basin. Palaeogeography, Palaeoclimatology, Palaeoecology **219**, 351–394.

Gravesen, P. & Pedersen, S.A.S. 2005: De geologiske forhold ved Risø. Redegørelse udarbejdet på basis af eksisterende data. Danmarks og Grønlands Geologiske Undersøgelse Rapport **2005/30**, 40 pp.

Houmark-Nielsen, M. 1987: Pleistocene stratigraphy and glacial history of the central part of Denmark. Bulletin Geological Society of Denmark, **36**, 189 pp.

Houmark-Nielsen, M. 2010: Extent, age and dynamics of Marine Isotope Stage 3 glaciations in the southwestern Baltic Basin. Boreas **39**, 343–359.

Jacobsen, E.M. 1985: En råstofgeologisk kortlægning omkring Roskilde. Dansk Geologisk Forening, Årsskrift for **1984**, 65–78.

Korstgård, J.A. 1996: Ekstensionsforkastninger. Geologisk Tidsskrift **1**, 1–24.

Pedersen, S.A.S. 2012: Glaciodynamic sequence stratigraphy. In: Huuse, M. *et al.* (eds): Glaciogenic reservoirs and hydrocarbon systems. Geological Society, London, Special Publications **368**, 29–51.

Thomsen, E. 1995: Kalk og kridt i den danske undergrund. In: Nielsen, O.B. (ed.): Danmarks geologi fra Kridt til i dag. Aarhus Universitet Geokompendier **1**, 32–67.

Authors' address

Geological Survey of Denmark and Greenland, Øster Voldgade 10, DK-1350 Copenhagen K, Denmark. E-mail: *sasp@geus.dk*

Middle–Upper Ordovician and Silurian stratigraphy and basin development in southernmost Scandinavia

Niels H. Schovsbo, Arne T. Nielsen and Mikael Erlström

A complete log-stratigraphical breakdown of the Middle Ordovician to lower Silurian shale-dominated succession is presented for the Bornholm–Skåne–Kattegat area in southernmost Scandinavia. A wireline log zonation developed for the onshore Bornholm Palaeozoic shales is extended to include the offshore Palaeozoic shales in the adjacent Rønne Graben. A complete log zonation scheme for the Cyrtograptus shale (late Llandovery–Wenlock) and the lower part of the Colonus shale (Ludlow) is presented including correlation within the Bornholm–Skåne–Kattegat area. The Cyrtograptus shale in the Bornholm area is estimated to be 400 m thick and marks the shift to a rapidly subsiding foreland basin, heralding the Caledonian Orogeny.

The Lower Palaeozoic shales in Denmark and southernmost Sweden are locally very thick (>3 km). The great thickness is mainly due to the presence of expanded Silurian units that formed in an active foreland basin related to the Caledonian Orogeny to the south and west (Michelsen & Nielsen 1991; Vejbæk *et al.* 1994, Eriksson 2012; Calner *et al.* 2013). The thick Silurian succession has only been known from a few deep exploration wells of older date with very limited wireline logging information (cf. Vejbæk *et al.* 1994). However, recent interest in the Scandinavian Lower Palaeozoic shales as a potential shale gas resource has led to a number of new drill holes with modern geological and geophysical logs, considerably increasing our knowledge. In a recent summary, Schovsbo *et al.* (2015) presented a review of the scientific work carried out over the last decade on Bornholm, based on the complete drilling and coring of the onshore Lower Palaeozoic succession. In May 2015, data acquired as part of the exploration programme for shale gas in Skåne by Royal Dutch Shell plc. (Shell) were released by the Swedish authorities, adding to our knowledge on the Lower Palaeozoic shales. These newly released data are integrated here with log data from wells on- and offshore Bornholm as well as older deep wells in western Denmark.

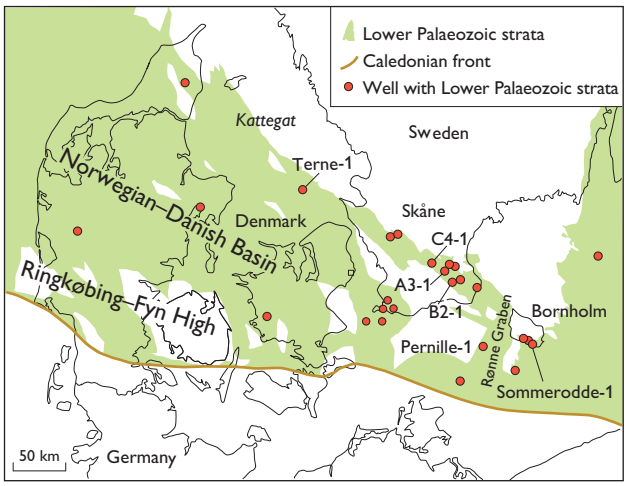

Fig. 1. Distribution of Lower Palaeozoic strata in southernmost Scandinavia with location of wells north of the Caledonian Front that reach the Lower Palaeozoic. Only wells referred to in the paper are named. Wells drilled by Shell in Skåne are Lövestad A3-1, Hedeberga B2-1 and Oderup C4-1.

The Oderup C4-1 well

The exploration programme carried out by Shell in Skåne included drilling of the Lövestad A3-1, Hedeberga B2-1 and Oderup C4-1 wells (Fig. 1) and acquisition of some 80 km of 2D seismic profiles (Calner & Pool 2011; Pool *et al.* 2012). The Oderup C4-1 well drilled in central Skåne has the most complete wireline log suite and is used here as a key well for establishing a Silurian well log stratigraphy (Fig. 2). For all three wells Eriksson (2012) presented a detailed stratigraphic and lithologic evaluation as well as a wireline log-correlation between Skåne and Bornholm. Below a brief description is presented of the drilled sequence in the Oderup C4-1 well, mostly based on Calner & Pool (2011) and Eriksson (2012).

Lower Palaeozoic strata were encountered below a Quaternary cover between 34.5 and 926.9 m terminal depth and the well terminated in the Lower Cambrian Hardeberga Formation. Thin Lower Cambrian Læså (0.3 m) and Gislöv Formations (0.6 m) are overlain disconformably by the Middle Cambrian – Lower Ordovician (Tremadocian) Alum Shale Formation, which is 76.3 m thick

© 2016 GEUS.

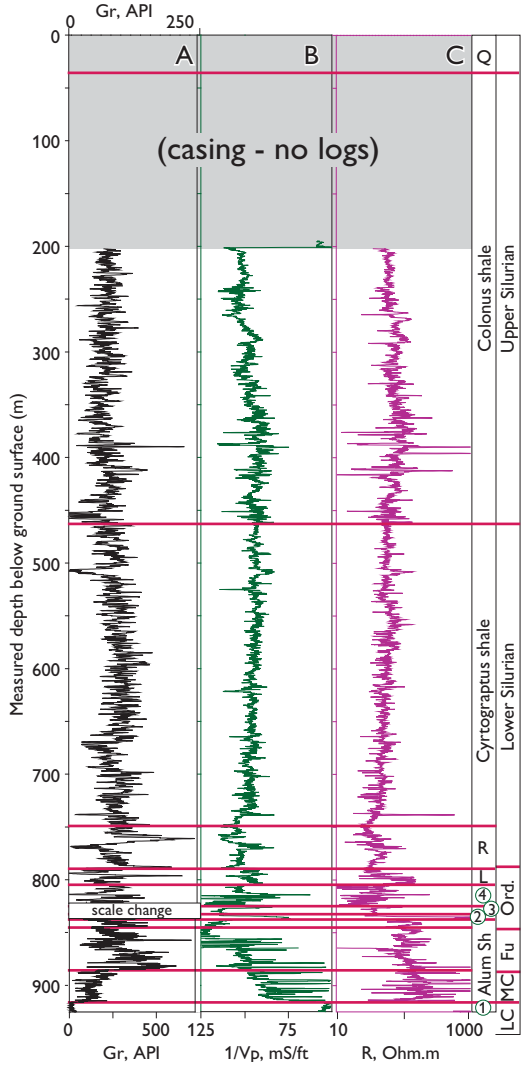

Fig. 2. **A**: Gamma ray curve. **B**: interval transit time velocity. **C**: formation resistivity in the Oderup C4-1 well, Skåne. Note that the definition of the Rastrites shale follows Schovsbo *et al.* (2015). **LC**: Lower Cambrian. **MC**: Middle Cambrian. **Fu**: Furongian. **Ord**: Ordovician. **Q**: Quaternary. **Alum**: Alum Shale Fm. **L**: Lindegård Fm. **R**: Rastrites shale. **1**: Hardeberga, Læså and Gislövs fms. **2**: Komstad Limestone Fm. **3**: Almelund Fm. **4**: Dicellograptus shale (Sularp, Mossen and Fjäcka fms).

(836–912.3 m). The Alum Shale Formation is in turn disconformably overlain by the lower Middle Ordovician Komstad Limestone Formation (832.5–836 m). The Komstad Limestone is in turn overlain by 44 m of Middle and Upper Ordovician shales (788.5–832.5 m) representing the Almelund, Sularp, Mossen, Fjäcka and Lindegård Formations (Fig. 2). The Sularp, Mossen and Fjäcka Formations are here collectively referred to as the Dicellograptus shale.

The base of the Rastrites shale (uppermost Ordovician – lower Silurian) is marked by a change to dark lithologies at 788.5 m, which is also recorded as high gamma ray (Gr) readings (Fig. 2). In the Oderup C4-1 final well report, the top of the Rastrites shale was identified at 733.5 m, where a change from dark to carbonaceous light grey shale occurs. However, adopting the definitions of Schovsbo *et al.* (2015) the top of the Rastrites shale is here defined at a slightly deeper level corresponding to the inflection point of the formation resistivity log at 749 m (Fig. 2). The top of the Cyrtograptus shale is here defined at 460 m where a change from the dark grey Cyrtograptus shale to the light grey Colonus shale occurs. The same horizon has a distinct motif on the Gr log being marked by low readings (Fig. 2). The Colonus shale is dominated by light grey to green-grey, micaceous and slightly calcareous to arenaceous shale with frequent intercalations of grey limestone nodules (Calner *et al.* 2013).

Wireline log-correlations

The log-stratigraphy of Palaeozoic shales on Bornholm, originally defined by Pedersen & Klitten (1990), has recently been redefined and extended to include the complete Rastrites shale (log zones F1–F5) and the onshore part of the Cyrtograptus shale (log zones G1–G5) by Schovsbo *et al.* (2015). The same log zones have been identified in the Oderup C4-1, Terne-1 and Pernille-1 wells (Fig. 3). Correlations between the Terne-1 well and sections on Bornholm and between the Oderup C4-1 well and Bornholm have previously been presented by Michelsen & Nielsen (1991) and Eriksson (2012), respectively, and only minor updates and corrections are made here. In the correlation panels (Fig. 3) additional log zones have been defined in the Cyrtograptus and Colonus shales (new log zones G6–G7 and H1–H2, respectively; see below).

The new log zones of the Cyrtograptus and Colonus shales

The Silurian G5 log zone (see Schovsbo *et al.* 2015) was not completely penetrated by the Sommerodde-1 well onshore Bornholm and the top of the zone is here defined in the Pernille-1, Oderup C4-1 and Terne-1 wells as a characteristic Gr peak co-occurring with a change to slightly higher sonic log velocities (Fig. 3). According to Bjerreskov (1993) and Vejbæk *et al.* (1994), the base of the Pernille-1 well is within the lower Wenlock (uppermost Sheinwoodian), which is slightly older than the Cyrtograptus shale with intercalated tuff-bearing sandstone (Homerian; upper Wenlock) that is exposed at the Sommerodde beach locality onshore Bornholm (Bjerreskov & Jørgensen 1983). This beach section immediately overlies the succession

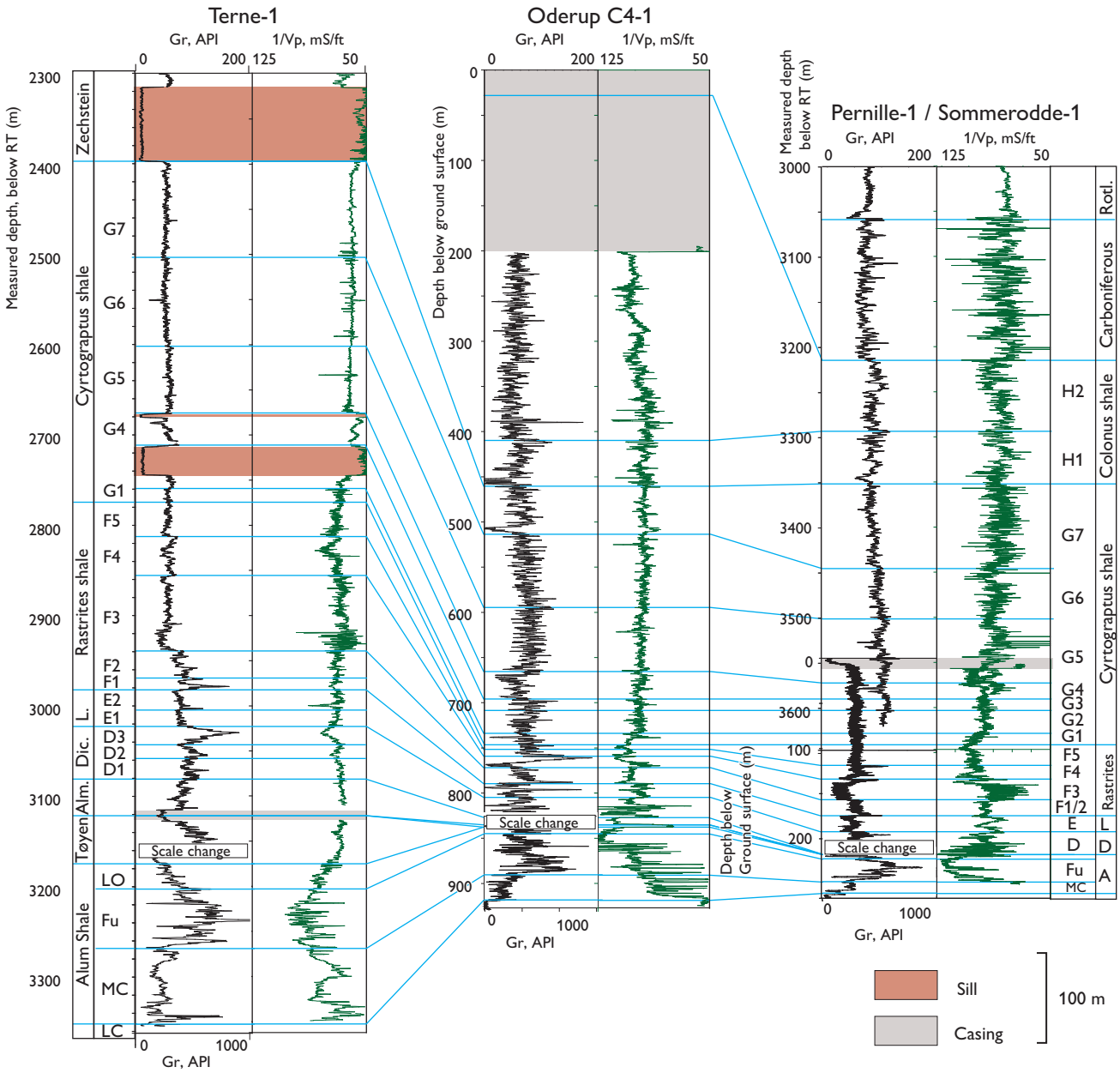

Fig. 3. Well log correlation panel between the Terne-1, Oderup C4-1, Pernille-1 and Sommerodde-1 wells (for location, see Fig. 1). The lower log zonation (D1–D3, F1–F5, G1–G5) is adopted from Schovsbo *et al.* (2015); the G5 (top)–G7 and H1–H2 log zones are new. For simplicity not all log zones are shown including those in the Alum Shale (cf. Schovsbo *et al.* 2015). **Ras. sh**: Rastrites shale. **L**: Lindegård Fm. **D**: Dicellograptus shale. **Alm**: Almelund Shale. **Rotl**: Rotliegendes. **RT**: Rotary table.

penetrated by the nearby Sommerodde-1 well. It is inferred that the tuff-bearing sandstone interval exposed at Sommerodde is seen in the log pattern in the Pernille-1 well as zones with low Gr response and high sonic velocities reflecting cemented sandstone beds (Fig. 3). The G6 log zone is characterised by generally upward-decreasing Gr values and increasing sonic velocities. The top of the zone is defined in the wells by a slight drop in Gr activity. In the Oderup C4-1 well the top occurs just below a distinct low Gr and high sonic velocity bed (Fig. 3). The Gr log continues to show a gradual decrease throughout log zone G7. The top of the zone is defined at an increase in Gr values and a general change to more fluctuating log signatures as seen in the Oderup C4-1 well.

The H1 log zone is distinguished by an increase in Gr values in comparison with the G7 zone. The top is placed at a narrow and significant Gr peak with low sonic velocities that could represent bentonite beds. The H2 log zone

is characterised by a variable log pattern that reflects the more variable lithologies in this unit.

The transition from passive margin to foreland basin

The transition from passive margin to a foreland basin occurred in the early Silurian (Vejbæk *et al.* 1994; Eriksson 2012; Calner *et al.* 2013). In the Kattegat area continuous sedimentation took place throughout this interval whereas Bornholm and Skåne were characterised by temporary local uplifts and condensations (Fig. 3). During most of the Early, Mid and early Late Ordovician, Bornholm was uplifted and no sedimentation occurred apart from the bioclastic early Middle Ordovician Komstad Limestone Fm, whereas Skåne, as exemplified by the Oderup C4-1 well, shows variable degrees of condensation and uplift during the late Early Ordovician to early Silurian. From the onset of deposition of the Cyrtograptus shale, the difference in sedimentation between the areas converges (Fig. 3). This shift was also noted by Eriksson (2012) and Calner *et al.* (2013) and is interpreted to reflect the development of a rapidly subsiding foreland basin. The foregoing uplifts thus heralded the later subsidence and are seen as isostatic adjustments of the margins of Baltica, perhaps including a foreland bulge passage. The uplift first affected Bornholm and later Skåne but apparently did not influence the Kattegat area where continuous subsidence occurred throughout the Ordovician and Silurian.

Conclusions

A complete log-stratigraphical breakdown of the Middle Ordovician to lower Silurian shale-dominated succession is presented for the Bornholm–Skåne–Kattegat area in southernmost Scandinavia. The Cyrtograptus shale (of late Llandovery–Wenlock age) is subdivided into seven log zones and is estimated to be approximately 400 m thick in the Bornholm area based on the Sommerodde-Pernille composite section (Fig. 3). The lower part of the overlying Colonus shale (Ludlow) is divided into two log zones; the total thickness of this shale is unknown. Variable degrees of condensation and uplift occurred in Skåne and on Bornholm during the late Early Ordovician to early Silurian. From the onset of the Cyrtograptus shale deposition, the difference in sedimentation between the areas converges and this shift is interpreted to reflect the development of a rapidly subsiding foreland basin.

Acknowledgements

GeoCenter Denmark is thanked for financial support to the project 'Silurian stratigraphy and Basin development' awarded to NHS and ATN. Comments from reviewers Svend Stouge and Mikael Calner helped improving the final version of the manuscript.

References

Bjerreskov, M. 1993: Pernille-1 well graptolite fauna. GEUS report file 10567. Reported as part of a EFP-89 project. DGU kunderapport 1–5.

Bjerreskov, M. & Jørgensen, K.A. 1983: Late Wenlock graptolite-bearing tuffaceous sandstone from Bornholm, Denmark. Bulletin of the Geological Society of Denmark **31**, 129–149.

Calner, M. & Pool, W. 2011: The first deep wells in the Lower Palaeozoic Colonus Shale Trough, Sorgenfrei-Tornquist tectonic zone, southern Sweden. GFF **133**, 58–59. Stockholm: Geological Society of Sweden.

Calner, M., Erlström, M., Lehnert, O. & Ahlberg, P. 2013: Lower Palaeozoic geology of southern Sweden. In: Calner, M. *et al.* (eds): The Lower Palaeozoic of southern Sweden and the Oslo Region, Norway. Field Guide for the 3rd Annual Meeting of the IGCP project 591. SGU Rapporter och meddelanden **133**, 6–9.

Eriksson, M. 2012: Stratigraphy, facies and depositional history of the Colonus Shale Trough, Skåne, southern Sweden. Dissertations in Geology at Lund University **310**, 37 pp.

Michelsen, O. & Nielsen, L.H. 1991: Well records on the Phanerozoic stratigraphy in the Fennoscandian Border Zone, Denmark: Hans-1, Sæby-1, and Terne-1 wells. Danmarks Geologiske Undersøgelse Serie A **29**, 37 pp.

Pedersen, G.K. & Klitten, K. 1990: Anvendelse af gamma-logs ved korrelation af marine skifre i vandforsyningsboringer på Bornholm. Dansk Geologisk Forening Årsskrift **1987–89**, 21–35.

Pool, W., Geluk, M., Abels, J. & Tiley, G. 2012: Assessment of an unusual European shale gas play: the Cambro-Ordovician Alum Shale, southern Sweden: Proceedings of the Society of Petroleum Engineers/European Association of Geoscientists and Engineers Unconventional Resources Conference, Vienna, Austria, March 20–22, 152339.

Schovsbo, N.H., Nielsen A.T. & Klitten, K. 2015: The Lower Palaeozoic now fully cored and logged on Bornholm. Geological Survey of Denmark and Greenland Bulletin **33**, 9–12.

Vejbæk, O.V., Stouge, S. & Poulsen, K.D. 1994: Palaeozoic tectonic and sedimentary evolution and hydrocarbon prospectivity in the Bornholm area. Danmarks Geologiske Undersøgelser Serie A **34**, 21 pp.

Authors' addresses

N.H.S., *Geological Survey of Denmark and Greenland (GEUS), Øster Voldgade 10, DK-1350 Copenhagen K, Denmark*. E-mail: *nsc@geus.dk*

A.T.N., *Dept. of Geosciences and Natural Resource Management, University of Copenhagen, Øster Voldgade 10, DK-1350 Copenhagen K, Denmark.*

M.E., *Geological Survey of Sweden (SGU), Kiliansgatan 10, SE-223 50 Lund, Sweden*.

Types of formation water and produced water in Danish oil- and gasfields: implications for enhanced oil recovery by injection of 'smart' water

Niels H. Schovsbo, Hanne D. Holmslykke, Claus Kjøller, Kathrine Hedegaard, Lars Kristensen Erik Thomsen and Kim H. Esbensen

Injection of chemically tuned, 'smart' water in oil reservoirs may increase both oil recovery rates and the total recovery (e.g. Morrow & Buckley 2011; Austad 2013; Zeinijahromi *et al*. 2015). This kind of water management has gained increased importance in the Danish North Sea reservoirs due to decreasing sweep efficiency in maturing oilfields. Knowledge about the compatibility of the injected water with local formation waters is, however, a prerequisite for successful implementation. Here, we present a regional overview of formation waters from oil reservoirs in the Danish North Sea, which comprise three main types of formation brine, and one type of modified seawater related to extensive water flooding. The water types show a distinct geographical distribution, which reflects original connate waters that are modified by saline brine being either depleted or enriched in SO_4^{2-}.

Formation water and produced water database

In order to characterise the water types we have selected a total of 33 water analyses, 25 of produced water and six of formation water from North Sea wells (three core samples from the Francisca-1 well and production tests from the Boje-1, Elna-1 and M-9X, wells) and finally two analyses of seawater (North Sea mean water composition and a treated low-sulphate seawater), see Fig. 1. For characterisation, samples analysed for Na, K, Ca^2, Mg^2, Sr^2, Ba^2, Cl^-, and SO_4^{2-} were used. Water density had been measured for most of the samples, however, it was estimated for four samples. The data were collected from Samuelsen *et al*. (2009), Mackay *et al*. (2012), and Undall-Behrend (2012) and from final well reports for the Boje-1, Elna-1, Francisca-1 and M-9X wells.

Water type classification

To classify the water types in our database, Principal Component Analysis (PCA) was applied, whereby a matrix *X* of measured data (*N* samples, *P* variables) is transformed into sets of projection subspaces delineated by Principal Components (each a linear combination of all *P* variables), which display variance-maximised interrelationships between variables (Esbensen 2010, Esbensen *et al*. 2015). PCA *score plots* display groupings, or clusters, of samples based on compositional similarities, as described by the variable correlations (shown in accompanying *loading plots*). They also quantify the proportion of total dataset variance that can be modelled by each component, see Fig. 2. All data analyses in this work are based on auto-scaled data.

The data analysis was performed in two steps. Step one is a PCA analysis of all 33 samples to investigate relationships between seawater and reservoir water (Fig. 2A, B). Based hereon, pure seawater and the samples produced from Skjold, Dan B, Dan F and Halfdan, which represent extensively seawater-flooded reservoirs, were removed

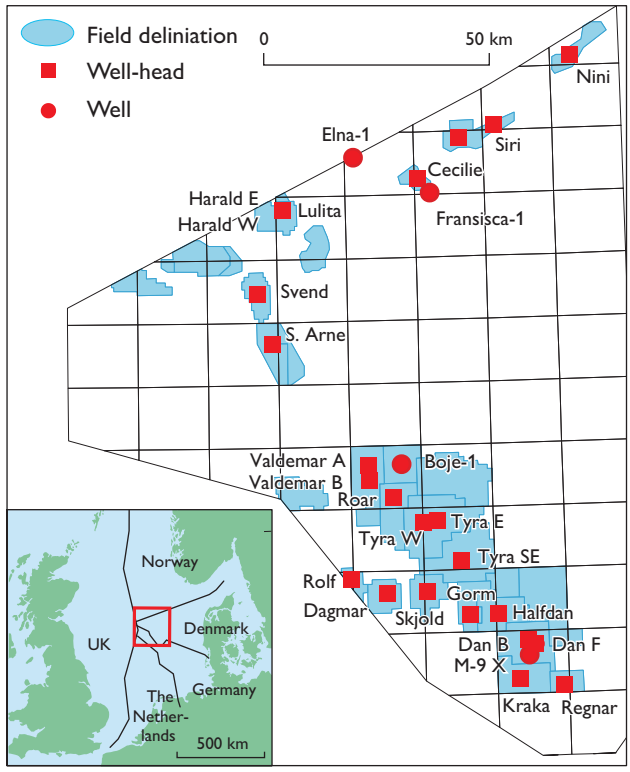

Fig. 1. Location of the wells used for water-type characterisation in the Danish part of the North Sea.

© 2016 GEUS.

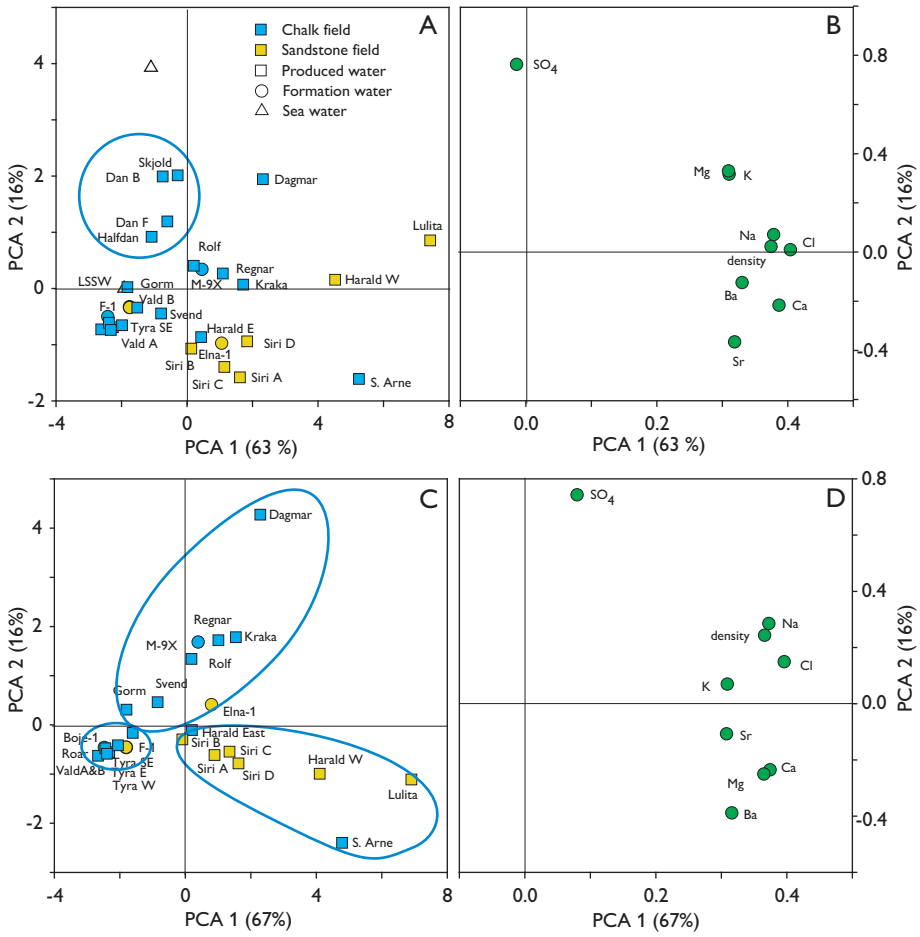

Fig. 2. Principal component analysis, PCA. **A:** Score. **B**: loading plot of PCA on all data. **C**: score. **D**: loading plot of PCA from which seawater from the Dan B, Dan F, Skjold and Halfdan installations and produced waters were excluded. The plot models 79% (A, B) and 83% (C, D) of the total data variance, respectively; variance proportions are shown along each component axis. Water types are classified according to their groupings in A (water type 4) and C (water type 1, 2, 3). **F-1**: Francisca-1. **Vald**: Valdemar. **SW**: seawater. **LSSW**: low SO_4^{2-}-treated seawater.

to examine the relationships between the primary water types, which is done in step 2 of the analysis (Fig. 2C, D). In both PCA models the first two principal component axes resolve 80% of the total data variance, with the main trend expressed on the PCA-1 axis being salinity variation (seen as high positive PCA-1 loadings for Cl, Na and K). The PCA-2 axis displays high positive loadings of SO_4^{2-} and high negative loadings of elements such as Ba, Sr, Mg and Ca.This could indicate that SO_4^{2-} concentrations control the concentration of Ba^{2+}, Sr^{2+}, Mg^{2+} and Ca^{2+} due to the low solubility of e.g. barite ($BaSO_4$) and anhydrite ($CaSO_4$). However, chemical speciation calculations using the numerical code PHREEQC suggest sub-saturation of SO_4^{2-}-bearing minerals except for barite in all water types.

Composition and occurrence of water types

From the PCA analysis, four water types can be identified based on natural groupings in the PCA-2 versus PCA-1 plot (Fig. 2). The most likely cause of the salinity variation is a variable mixing of primary connate waters with brine originating from Permian Zechstein salt, which may or may not be SO_4^{2-}-rich (Warren *et al.* 1994). The characteristics and occurrence of each of the water types are presented below. Water types 1–3 have compositional characteristics similar to types presented in the comprehensive overview paper by Warren *et al.* (1994).

Water type 1 plots within a very narrow group in the third quadrant of the PCA-2– PCA-1 plot (Fig. 2C), characterised by low salinity water with an overall low abundance of all elements (Fig. 3). This water type is found in the Boje-1, Francisca-1, Roar, Tyra E, Tyra SE and Valdemar fields and thus occurs in a broad range of reservoirs from Lower to Upper Cretaceous – Paleocene chalk to Oligocene sandstone. The location borders the greater Tyra–Valdemar area, in geographical areas separated from saline Permian brines (Fig. 4). The water is interpreted to reflect unmodified SO_4^{2-}-depleted formation water.

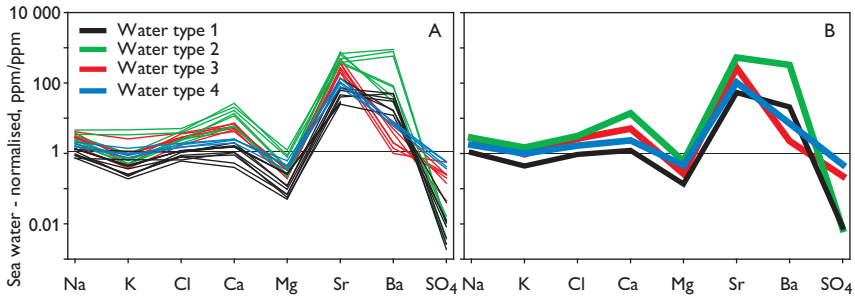

Fig. 3. **A**: Water concentration normalised to seawater composition. **B**: Calculated average compositions of the four water types observed in this study. For display purposes, Ba^{2+} and Sr^{2+} concentrations of 0 ppm in seawater have been increased to 1 ppm.

Water type 2 is characterised by positive PCA-1 and negative PCA-2 scores (Fig. 2C) and can compositionally be characterised by medium to high salinities, no SO_4^{2-}, and high to very high Ca and Ba concentrations (Fig. 3). This water type occurs in the Harald E and W, Lulita, S. Arne, Siri, Nini, Stine and Cecilie fields, all of which are located in the northern part of the Danish North Sea and in the Siri Canyon – i.e. in reservoirs that range in age from Jurassic to Paleocene and both in chalk and sand lithologies. Water type 2 is interpreted to reflect formation water modified by SO_4^{2-} depletion.

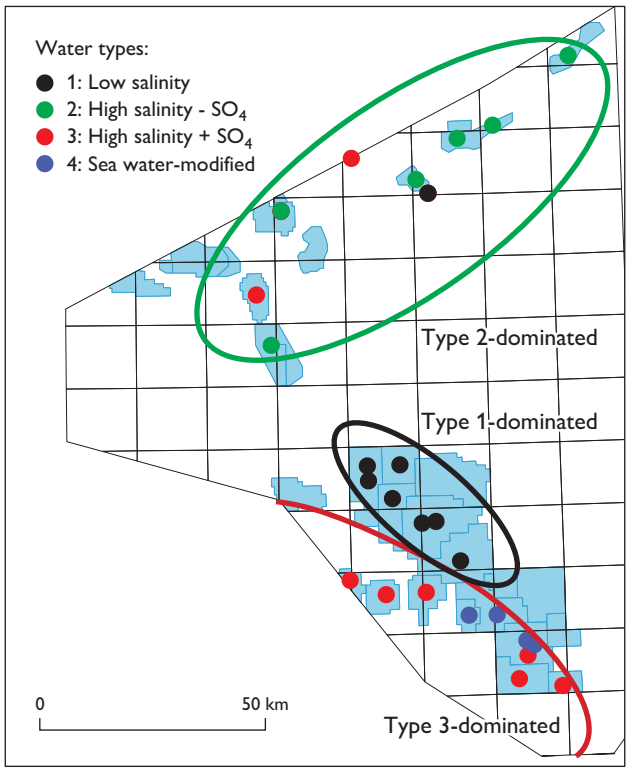

Fig. 4. Occurrence of resolved water types in the Danish oil- and gas-fields. For location names see Fig. 1. The water types are geographically restricted and reflect both structural basin development and reservoir conditions. The seawater modified water type 4 is assumed to have originated as water type 3 based on pre-waterflooding formation water analysis and its structural position within the salt dome province.

Water type 3 plots with generally positive PCA-1 and PCA-2 scores in Fig. 2C, reflecting medium to high salinities and variable, low to high SO_4^{2-} concentrations (Fig. 3). This water type is found in the Dagmar, Elna-1, Gorm, Kraka, M-9X, Regnar, Rolf and Svend fields, most clearly expressed in the intensely fractured Dagmar field sample. This field is situated on top of a salt dome that has reservoir oil in chalk and Zechstein carbonates. Type 3 waters are restricted to chalk reservoirs overlying salt domes in the southern salt dome province, and are interpreted as formation water *enriched* in SO_4^{2-}.

Water type 4 plots close to, or together with seawater with negative PCA-1 and positive PCA-2 scores in Fig. 2A, corresponding to low to medium salinity with high SO_4^{2-} concentrations (Fig. 3). This water type occurs in the Dan, Halfdan and Skjold fields and is interpreted to be the result of decades of extensive water flooding performed by the operator (Energistyrelsen 2013). Analyses of water from the Dan field (the M-9X well; Fig. 2C) prior to flooding suggest that it was originally filled with water type 3.

Implications for enhanced oil recovery by injection of 'smart' water

Water injection is currently applied in several of the Danish oil fields, mainly in order to provide pressure support. However, such injection may also have secondary effects such as increased imbibition, alteration of the reservoir rock wettability or mobilisation of fines with a resulting increase in reservoir sweep. In some cases, the specific chemical composition of the injection water may be important. Thus, it has been suggested that carbonate rocks become more water wet if the injection water contains SO_4^{2-} in combination with excess Ca^{2+} or Mg^{2+} (e.g. Austad 2013). The result is enhanced oil recovery, which is even more pronounced both for chalk and sandstone if the salinity of the injection water is significantly lower than that of the formation water (Morrow & Buckley 2011; Austad 2013).

Although several different mechanistic explanations have been suggested, a supposed change in carbonate rock wettability would involve surface chemical reactions such as ion exchange between SO_4^{2-} and oil molecules (e.g. Austad 2013). Following this argumentation, it is likely that injection of 'smart' SO_4^{2-}-bearing water in chalk reservoirs would have the largest effect in reservoirs with saline formation water depleted in SO_4^{2-} (water type 2). However, the application of SO_4^{2-}-rich water in reservoirs with this type of connate water is not straightforward, as there is a risk of scaling and subsequent clogging of the reservoir if the injected water is mixed with the connate water, due to its high concentrations of Ca^{2+}, Ba^{2+}, and Sr^{2+} (Samuelson *et al*. 2009; Mackay *et al*. 2012). Another risk related to injection of SO_4^{2-}-bearing water in SO_4^{2-}-depleted reservoirs is the possibility of hydrogen sulphide formation due to SO_4^{2-} reducing microbial activity.

For reservoirs already enriched in SO_4^{2-} (water type 3) or with water of relatively low salinity (water type 1), other types of injection water may have greater effects on oil recovery.

In shaly sand reservoirs, injection of low-salinity 'smart' water can also mobilise clay fines, in order to intentionally clog current flow paths and redirect the flow in the reservoir (e.g. Morrow & Buckley 2011; Zeinijahromi *et al*. 2015). In this case, the mobilisation of non-swelling clays is provoked solely by the change in salinity. Therefore, application of this type of water technology seems to be most relevant in reservoirs with connate water of relatively high salinity, such as most of the reservoirs in the Siri Canyon (water type 2).

Conclusions

Four water types are present in the Danish North sea: SO_4^{2-}-bearing, medium- to highly saline water (type 3), SO_4^{2-}-depleted medium to high saline water (type 2), SO_4^{2-}-depleted low saline (type 1), and a seawater-modified manifestation (type 4 water). These water types reflect variable mixing of connate water with deeper brines and are tied in with the known hydrocarbon provinces. Type 2 represents the Siri Canyon and the South Arne – Svend areas. Water type 3 is characteristic of salt dome reservoirs, while water type 1 represents the greater Tyra–Valdemar area. The variable chemistry of the formation water in the Danish North Sea imposes regional differences in production strategies and hence in the designing of 'smart' water for enhanced oil recovery. The classification of water types presented here shows that their composition is predictable and related to geographical domains in the North Sea. This may be useful when designing procedures for optimal water management in the Danish North Sea, e.g. application of low salinity water flooding on mature fields, or in some cases even during the exploration stage.

References

Austad, T. 2013: Water-based EOR in carbonates and sandstones: New chemical understanding of the EOR potential using 'smartwater'. In: Sheng, J.J. (ed.): Enchanced oil recovery field case studies, 301–335. Waltham, MA, USA: Elsevier.

Energistyrelsen, 2013: Danmarks olie- og gasproduktion 2013, 105 pp. København: Energistyrelsen.

Esbensen, K.H. 2010: Multivariate data analysis – in practice. An introduction to multivariate data analysis and experimental design, 5th edition, 598 pp. Oslo: CAMO Software AS.

Esbensen, K., Schovsbo, N.H. & Kristiansen, L. 2015: Down-hole permeability prediction – a chemometric wire-line log feasibility study from a North Sea chalk well. Geological Survey of Denmark and Greenland Bulletin **33**, 13–16.

Mackay, E., Ginty, W.R. & Jones, T.J. 2012: Oilfield scale management in the Siri asset – paradigm shift due to the use of mixed PWRI / seawater injection. 74th EAGE Conference and Exhibition incorporating EUROPEC 2012. Copenhagen, Denmark, 4–7 June 2012. **SPE 154534**, 1–12.

Morrow, N. & Buckley, J. 2011: Improved oil recovery by low-salinity waterflooding. Journal of Petroleum Technology **63**, 106–112.

Samuelsen, E.H., Frederiksen, R.A., Heath, S.M., Thornton, A., Sim, M., Arefjord, A. & McAra, E.K. 2009: Downhole scale control through continuous injection of scale inhibitor in the water injection – a field case. Conference Tekna Geilo paper **240309**, 23 pp.

Undall-Behrend, G. 2012: Produceret vand på Tyra Øst F. Bachelorprojekt Århus Maskinmesterskole, 75 pp.

Warren, E.A., Smalley, C.P. & Howarth, R.J. 1994: Compositional variations of North Sea formation waters, Part 4. Geological Society, London. Memoirs **15**, 119–208.

Zeinijahromi, A., Ahmetgareev, V., Badalyan, A., Khisamov, R. & Bedrikovetsky, P. 2015: Case study of low salinity water injection in Zichebashskoe field. Journal of Petroleum Science Research **4**, 16–31.

Authors' address

Geological Survey of Denmark and Greenland, Øster Voldgade 10, DK-1350 Copenhagen K, Denmark; E-mail: *nsc@geus.dk*

Middle Pleistocene interglacial deposits near Herning, Jylland, Denmark

Bent V. Odgaard, Karen L. Knudsen, Ole Bennike and Henrik J. Granat

Marine interglacial deposits are fairly common and widespread in Denmark, but so far none have been reported from the Herning area in central Jylland. In 2014, the Geological Survey of Denmark and Greenland (GEUS) received samples at one metre intervals from a borehole at 55°59.3′N, 8°56.6′E (elevation 27.56 m above sea level), at Hesselvigvej 7 near Kibæk in central Jylland (Fig. 1). The succession consisted of Miocene and Quaternary deposits. The Quaternary part was dominated by glaciofluvial sand and a single till bed, but it also contained a marine clay unit (16–21 m depth, 6.5–11.5 m a.s.l.). This marine clay contained spines of the sea-urchin *Echinocardium cordatum*, a boreal species known from Eemian and Holocene deposits from Denmark, but unknown from interstadial deposits. A lacustrine unit between 26 and 33 m depth (5.5 m b.s.l. to 1.5 m a.s.l.) consisted of clay, calcareous-rich gyttja and diatomite. Because Quaternary marine deposits are unexpected in this part of Denmark, we report here on analyses of pollen from the lacustrine unit and foraminifera from the marine unit, and we compare these with some interglacial records from Jylland. The analysed samples were treated with standard laboratory methods.

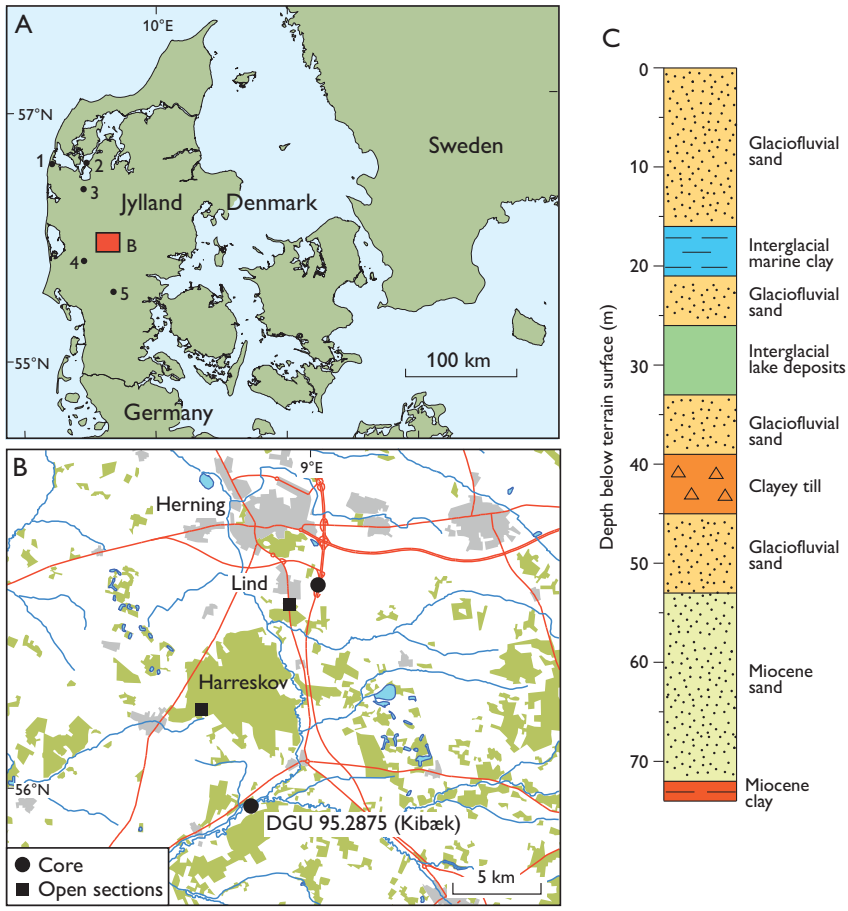

Fig. 1. **A**: Map of Denmark showing the location of the Herning area (red rectangle) and selected interglacial sites. **1**: Harboøre (DGU 43.75), **2**: Kås Hoved (DGU 45.759), **3**: Holstebro Nord (DGU 64.248), **4**: Hoven (DGU 103.1011), **5**: Vorbasse (DGU 123.1217). **B**: Map of the Herning area showing interglacial sites. **C**: Simplified lithological log of the core at Kibæk (DGU 95.2875), with two interglacial units.

© 2016 GEUS.

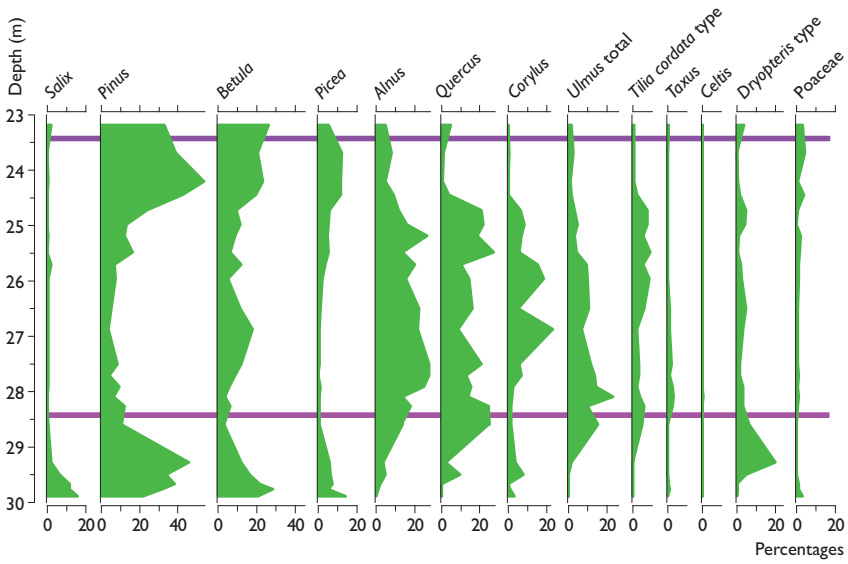

Fig. 2. Simplified percentage pollen diagram from the interglacial deposit at Lind with indication of the stratigraphical correlation of the two pollen samples from Kibæk (DGU 95.2875; purple lines).

The lacustrine unit

Pollen data from two samples (at 31 and 30 m depth) from the organic lacustrine (gyttja) unit clearly show that this is an interglacial deposit with thermophilous taxa such as *Tilia* (lime) and *Buxus* (box). The lack of *Carpinus* (hornbeam) is noteworthy and makes a correlation with the Holstenian or Eemian periods unlikely. In 2003 a core was secured through a thick interglacial deposit at nearby Lind, 14 km north of the Kibæk borehole (Kronborg & Odgaard 2004; Fig. 1). The pollen record of the interglacial part of the Lind core shows a clear correlation to the Harreskovian (Andersen 1965), with absence of *Carpinus*, presence of *Picea* (spruce) throughout the series and traces of *Celtis* (hackberry; Fig. 2). An ordination (principal component analysis, PCA) on the Lind interglacial pollen samples with the Kibæk pollen spectra as supplementary samples shows that the bottom Kibæk sample correlates well with a level of 28.4 m of the Lind core and the upper Kibæk sample with Lind at 23.4 m (Figs 2, 3). This indicates that a full, but thin interglacial lacustrine succession is present at Kibæk. The reason for the thin succession could be that the core site is located near the margin of the former lake basin.

The marine unit

The foraminiferal assemblages from the marine unit (Fig. 4) are dominated by *Elphidium excavatum,* with *Ammonia beccarii* second in abundance. The species composition indicates subtidal, inner-shelf conditions with a gradual shallowing of the water depth and deposition during a full interglacial period. The species *Ammonia beccarii* currently has a northern geographical range limit along southern Norway, and it is not present in interstadial deposits such as the Bølling and Allerød in Denmark. *Ammonia beccarii* immigrated with the marine transgression in the early Holocene.

A principal component analysis (PCA) on selected interglacial foraminiferal stratigraphies from central and north-

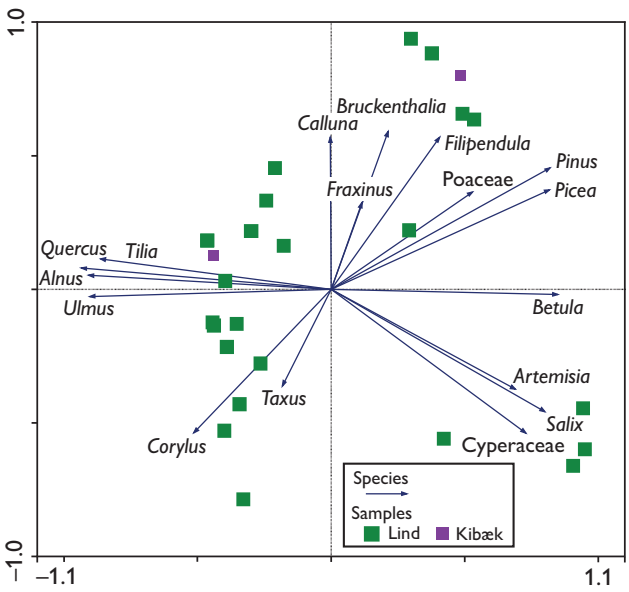

Fig. 3. Principal component analysis (PCA) biplot of the interglacial pollen sequence of Lind with the two Kibæk samples as supplementary samples not influencing the geometry of the plot. The percentage values were log-ratio transformed prior to the analysis. PCA is an ordination technique, which reduces a multidimensional space (here of pollen types) with associated frequencies to fewer dimensions (PCA axes) in such a way that the new dimensions are determined by the directions of largest variation in the original data set. The technique also allows easy comparison between samples of multivariate data such as those derived from microfossil analysis.

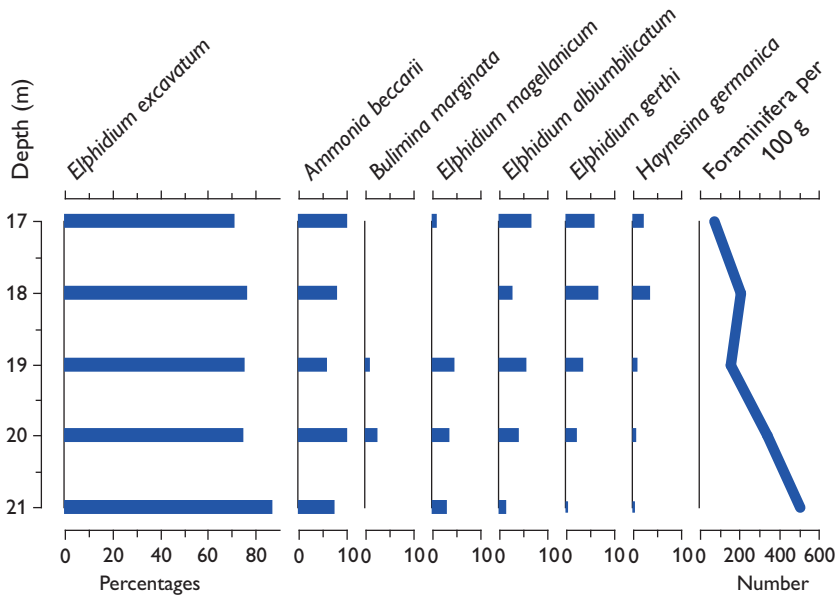

Fig. 4. Percentage distribution of selected foraminifera in the marine unit of the Kibæk core (DGU 95.2875). Note the different scales.

western Jylland shows the Kibæk samples to be intermediate between two long records from Kås Hoved and Holstebro (Fig. 5). This position probably reflects an intermediate facies of the Kibæk deposit between the relatively shallow Kås Hoved facies with *Haynesina orbiculare* as an important species, and the more open marine environment at Holstebro with *Elphidium margaritaceum* as one of the indicators of relatively high salinity. The Kibæk foraminiferal assemblages are closely similar to two samples from Harboøre and Vorbasse, and the species composition found in a sample from an additional nearby interglacial deposit at Hoven (Fig. 1; semi-quantitative data) is also very close to those from Kibæk. *Elphidium excavatum* is dominant and *Ammonia beccarii* is common in all the comparative records.

Age estimate

The unusual presence of a lacustrine, as well as a marine sequence in one Pleistocene series provides a minimum age of the bottom till and a maximum age of the marine deposit. The Danish Harreskovian interglacial pollen record can be correlated to the record at Hunteburg in Germany (Hahne *et al.* 1994). A palaeomagnetic reversal at the base of the Hunteburg series may indicate the presence of the Brunhes–Matuyama boundary, in which case the Hunteburg interglacial series would correspond to marine isotope stage (MIS) 19, almost 800 ka BP. The till at 39–45 m depth at Kibæk would then belong to one of the till units identified in the lower part of the Lind core (Kronborg & Odgaard 2004), deposited during one of the oldest Pleistocene glaciations recorded from Denmark.

The marine unit represents a full interglacial period, but it was not possible to relate it to a specific interglacial. The deposit is, however, older that the Eemian interglacial (MIS 5e), because of the lack of lusitanian elements that char-

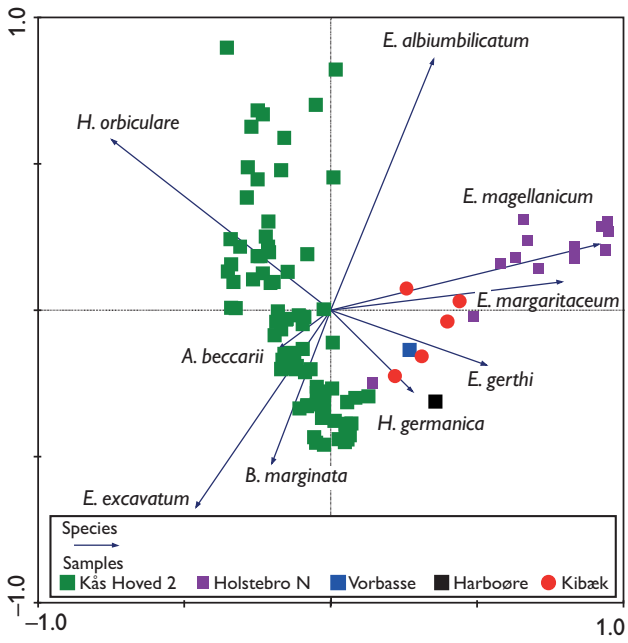

Fig 5. Principal component analysis (PCA) biplot of foraminiferal assemblages from Kås Hoved (Knudsen *et al.* 2014), Holstebro Nord (Kronborg *et al.* 2002), Harboøre (Knudsen 1987), Vorbasse (K.L. Knudsen, unpublished data), and Kibæk (this study). A similar assemblage was also found in a sample from a core near Hoven (DGU 103.1011; semi-quantitative data in GEUS' Jupiter database). For locations see Fig. 1. The percentage values were log-ratio transformed prior to the analysis.

acterise Eemian assemblages in Denmark (e.g. Knudsen 1994). The assemblages from the marine unit are close to those related to Holsteinian interglacial (MIS 11) deposits in Denmark (Fig. 4), but the actual ages of these deposits are also uncertain. A stratigraphical correlation of the interglacial sediments at Kås Hoved with MIS 11 was discussed by Knudsen *et al.* (2014), but further development of optically stimulated luminescence (OSL) dating or other absolute dating methods are needed for more exact age estimates of marine pre-Eemian interglacial records in Denmark. During the late Early and the Middle Pleistocene, foraminiferal assemblages would be expected to be almost identical during similar marine environmental conditions. Some of the Danish records that are traditionally related to the Holsteinian, could thus be from any warm interglacial period with high sea-level during the late Early or Middle Pleistocene. The stratigraphical position of the marine unit in the Kibæk core indicates a Middle Pleistocene age.

It has been suggested that MIS 11 was an exceptionally long and relatively warm interglacial (e.g. Candy *et al.* 2014) and peak global sea level may have reached 8.0–11.5 m higher than today (Chen *et al.* 2014). However, most temperature proxies for MIS 11 give values similar to the Holocene (Candy *et al.* 2014), and according to Bowen (2010) sea levels were close to the present sea level. Because of the orbital similarity between MIS 11 and MIS 1, these are even used as analogues of warm intervals in climatic studies (Berger & Loutre 2003). The temperature indication of interglacial foraminiferal assemblages in Denmark, which is related to the Holsteinian, is also comparable with the Holocene and present day temperatures in the region.

It is remarkable that the Middle Pleistocene marine interglacial records at Kibæk, Vorbasse and Hoven in central Jylland are found several metres above sea level, whereas the Harboøre and Holstebro records in north-western Jylland are found at more than 30 m b.s.l. A comparison of the core sites with the pre-Quaternary surface map of Denmark (Binzer & Stockmarr 1994) shows that Kibæk, Vorbasse and Hoven are located in areas with a high-lying pre-Quaternary surface, whereas Harboøre and Holstebro represent an area with a low-lying pre-Quaternary surface. Although glacial tectonics may have displaced some of the interglacial marine records the general elevational pattern of these sediments indicates that the central part of Jylland may have experienced a tectonic uplift during the Quaternary.

References

Andersen, S.T. 1965: Interglacialer og interstadialer i Danmarks kvartær. Meddelelser fra Dansk Geologisk Forening **15**, 486–506.

Berger, A. & Loutre, M.-F. 2003: Climate 400,000 years ago, a key to the future? American Geophysical Union Geophysical Monograph **137**, 17–26.

Binzer, K. & Stockmarr, J. 1994: Geologisk kort over Danmark. 1:500 000. Prækvartæroverfladens højdeforhold. Danmarks Geologiske Undersøgelse Kortserie **44**.

Bowen, D.Q. 2010: Sea level ~400 000 years ago (MIS 11): analogue for present and future sea level? Climate of the Past **6**, 19–29.

Candy, I., Schreve, D.C., Sherriff, J & Tye, G.J. 2014: Marine Isotope Stage 11: palaeoclimate, palaeoenvironments and its role as an analogue for the current interglacial. Earth-Science Reviews **128**, 18–51.

Chen, F., Friedman, S., Gertler, C.G., Looney, J., O'Connell, N., Sierks, K. & Mitrovica, J.X. 2014: Refining estimates of polar ice volumes during the MIS 11 interglacial using sea level records from South Africa. Journal of Climate **27**, 8740–8746.

Hahne, J., Mengeling, H., Merkt, J. & Gramann, F. 1994: Die Hunteburg-Warmzeit ("Cromer-Komplex") und Ablagerungen der Elster-, Saale- und Weichsel-Kaltzeit in der Forschungsbohrung Hunteburg GE 58 bei Osnabrück. Geologisches Jahrbuch **A134**, 117–166.

Knudsen, K.L. 1987: Elsterian-Holsteinian foraminiferal stratigraphy in the North Jutland and Kattegat areas, Denmark. Boreas **16**, 359–368.

Knudsen, K.L. 1994: The marine Quaternary in Denmark: a review of new evidence from glacial-interglacial studies. Bulletin of the Geological Society of Denmark **41**, 203–218.

Knudsen, K.L., Ditlefsen, C., Penney, D.N., Kristensen, P., Kronborg, C. & Eiríksson, J. 2014: Elsterian-Holsteinian deposits at Kås Hoved, northern Denmark: sediments, foraminifera, ostracods and stable isotopes. Boreas **43,** 251–271.

Kronborg, C. & Odgaard, B.V. 2004. Nyt om Danmarks ældste kvartære aflejringer. DGF kvartærgeologisk møde november 2004. Geologisk Tidsskrift **2004(2)**, 23–24.

Kronborg, C., Nielsen, O.B., Sørensen, J. & Kragelund, A. 2002: Ringkøbing Amt, Holstebro Nord, boring DGU Nr. 64.1248. Geologisk Institut, Aarhus Universitet, Report **02RK–01,** 39 pp.

Authors' addresses

B.V.O. & K.L.K., *Department of Geoscience, Aarhus University, Høegh-Guldbergs Gade 2, DK-8000 Aarhus C, Denmark*. E-mail: *bvo@geo.au.dk*

O.B. & H.J.G., *Geological Survey of Denmark and Greenland, Øster Voldgade 10, DK-1350 Copenhagen K, Denmark.*

Geochemistry of the Maastrichtian Rørdal Member, Jylland, Denmark: Ce anomaly as a palaeo-redox proxy

Christian Knudsen and Bodil W. Lauridsen

The chemical composition of chalk and marl reflects the mixture of carbonate particles and clastic input deposited on the seabed together with growth of authigenic minerals and diagenesis. The Rørdal quarry in Jylland (Fig. 1) is known for its alternating chalk–marl succession (Surlyk *et al.* 2010) and the aim of this article is to investigate how this cyclicity is reflected in the geochemical signature of the sequence and test if this has implications for the interpretation of the depositional environment as well as the chemostratigraphy in the chalk.

The observed variation in the benthic fauna and the cyclic character of the chalk–marl succession may reflect an environmental response to orbital forcing. The benthic fauna shows higher species diversity and density in the chalk than the marl layers, suggesting more favourable living conditions in the former (Lauridsen & Surlyk 2008), whereas no differences in environmental stress between the two environments could be derived from a study of the trace fossils (Lauridsen *et al.* 2011).

The *c.* 10 m thick Rørdal Member was established as a lithostratigraphic unit by Surlyk *et al.* (2010) and recognised as an expression of a late Maastrichtian cooling event. X-ray diffraction (XRD) analysis indicates that the marly layers represent a relative increase in smectite clays and illite together with some quartz and analcime. The inorganic geochemical evolution in Maastrichtian chalk was investigated by Jørgensen (1986) who noted changes in Sr/Ca and Mn/Ca ratios towards the end of the Maastrichtian in the North Sea Central Graben, leading to the conclusion that geochemistry is a "conceivable tool in basin analysis in the lithologically rather monotonous chalk sequence" (p. 267). However, a systematic geochemical analysis of the chalk has never been undertaken and this work is an attempt to look into the potential of understanding the geology of the chalk by analysing a wide range of elements in chalk and marl.

Chemical variability related to clay content

Sixty-three samples from the Rørdal quarry were ground, digested in aqua regia and analysed for 66 elements using the Elan 6100 Quadrupole ICP-MS at the Geological Survey of Denmark and Greenland (GEUS). The data reduction was based on TotalQuant software with emphasis on the trace element analysis. The analytical procedure follows Larsen *et al.* (2009).

The cyclicity and the alternation between chalk and marl are easily recognised in the geochemical profile (Fig. 2) with an increase in the concentration of major and minor elements such as Al, Si, Fe, Mg and K in the marly layers caused by the presence of clay. The eight peaks in Fig. 2 can be correlated to the eight peaks in the marly layers of the Rørdal Member which can be identified in the gamma log in a nearby well (Surlyk *et al.* 2010). The gamma-radiation in the well log can be explained by the increased content of K in the marl (Fig. 2A). Iron is the element after Al with the highest increase in concentration in the marly layers indicating that the clay minerals are rich in Fe. Magnesium also shows an increase in the marly layers (Fig. 2A), and the combined clay minerals in the marl – which according to Surlyk *et al.* (2010) consist of smectite and illite – must be rich in Fe, K and Mg. The content of Al, Fe and K is about three times higher in the marl than in the chalk.

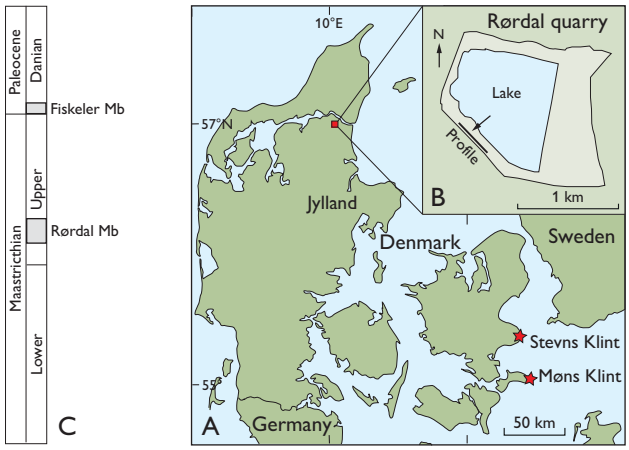

Fig. 1. **A**: Location of the Rørdal quarry, Stevns Klint and Møns Klint in Denmark. **B**: Map of the Rørdal quarry with the profile where the samples were collected. **C**: Stratigraphic section with Rørdal and Fiskeler members.

© 2016 GEUS.

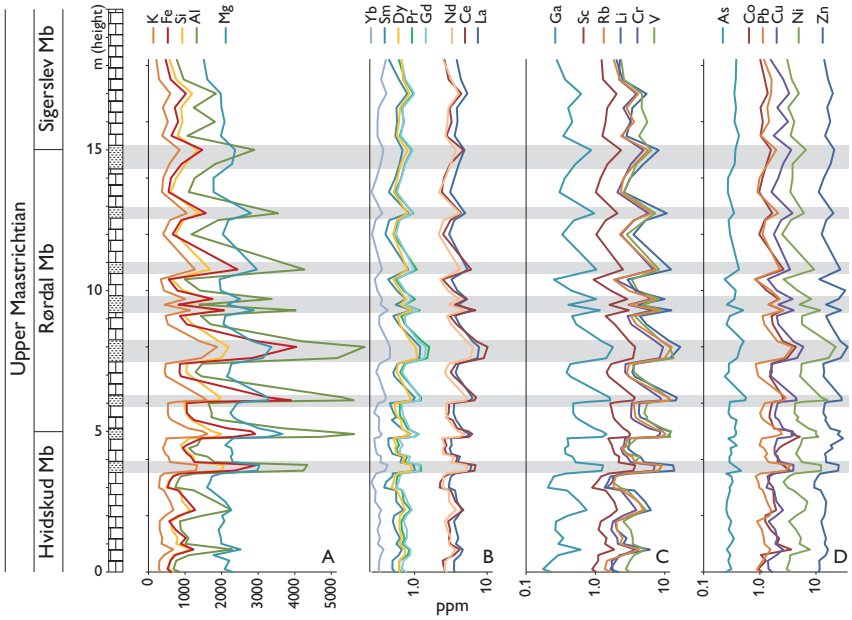

Fig. 2. Chemical profiles through the Rørdal Member including the uppermost part of the Hvidskud Member and the lowermost part of the Sigerslev Member. Marly layers are shown as grey shaded bands. **A**: Major and minor elements. **B**: REE; logarithmic scale. **C**: Lithophile trace elements; logarithmic scale. **D**: Chalcophile elements with Ni and Co; logarithmic scale. Stratigraphy from Surlyk *et al.* (2013).

The concentration of many trace elements, including the rare-earth elements (REE), is also elevated in the marly layers (Fig. 2B). If all REE were located in clay the increase would be three times higher, as is the case with Al, K and Fe, but the content of REE in the marl is 'only' 1.5 times higher than in the chalk. This suggests that although the REE concentration is higher in the clay than in the chalk a substantial fraction of the REEs is located in the carbonate component of both chalk and marl. Lanthanum and Nd follow parallel tracks (Fig. 2B), whereas Ce crosses both tracks with relatively high Ce in the marl. Light REE (La, Ce, Pr, Nd and Sm) are more abundant than heavy REE (Er, Tm, Yb and Lu) in the marl compared to the chalk, which can also be seen as higher La/Lu ratios (Figs 3E, 4).

Lithophile elements such as Th, Cs, Rb, Be, Cr, Sc and Li increase in concentrations in the marl (of which Rb and Li are shown in Figure 2C) and are *c.* 2.5 to 3 times higher in the marl than in the chalk, similar to the behaviour of Al and K. This suggests that these elements are almost entirely located in the clay. Chalcophile elements such as Pb, As, Zn and Cu (Fig. 2D) are *c.* 1.5 times higher in the marl than in the chalk similar to the REE mentioned above.

The content of most elements in the succession varies with the clay content. However, this is not the case for Nb, Zr, Mn and Ti (Fig. 3A). Mica and clay commonly contain some Ti, Zr and Nb, elements that also occur in mafic volcanic material. These elements are difficult to leach out of minerals and generally follow clay and mica in sedimentary environments. If the clay was clastic or volcanogenic one would expect that the content of elements such as Ti, Zr and Nb would be elevated in the marl. However, this is not the case, suggesting that a fraction of the clay may be of authigenic origin.

Manganese is probably hosted in the carbonate and its concentration is relatively stable throughout the analysed section. There is a decrease in the Ba content in the Rørdal Member (Fig. 3B) relative to the underlying Hvidskud Member with the lowest contents in its middle part. There is an increase in Sr content in the overlying Sigerslev Member. Jørgensen (1986) observed a similar increase in the Sr content in chalk from the North Sea Basin and this may be regional.

Ce anomaly as a proxy for redox potential

The REE commonly occur as cations with a valency of three and the different REE have similar geochemical behaviour in the sedimentary environment. However, one of the elements, Ce, can also occur as Ce^{4+} with a very low solubility in marine environments as compared to Ce^{3+}. Where no fractionation of Ce relative to the other REE has occurred, the distribution would be seen as a straight line on Fig. 3D. To quantify the fractionation of Ce, the term Ce anomaly (Ce/Ce*) has been introduced; Ce is the measured cerium concentration and Ce* is what the Ce content would have been without fractionation, based on the contents of La and Nd. The Ce anomaly is calculated: $Ce/Ce^* = 3Ce^N/(2La^N + Nd^N)$ where REE^N is the measured concentration normalised relative to chondrite (Boynton 1984). In this paper a Ce anomaly is referred to as negative when Ce is depleted relative to the other REE and as positive if Ce is enriched relative to the other REE. In

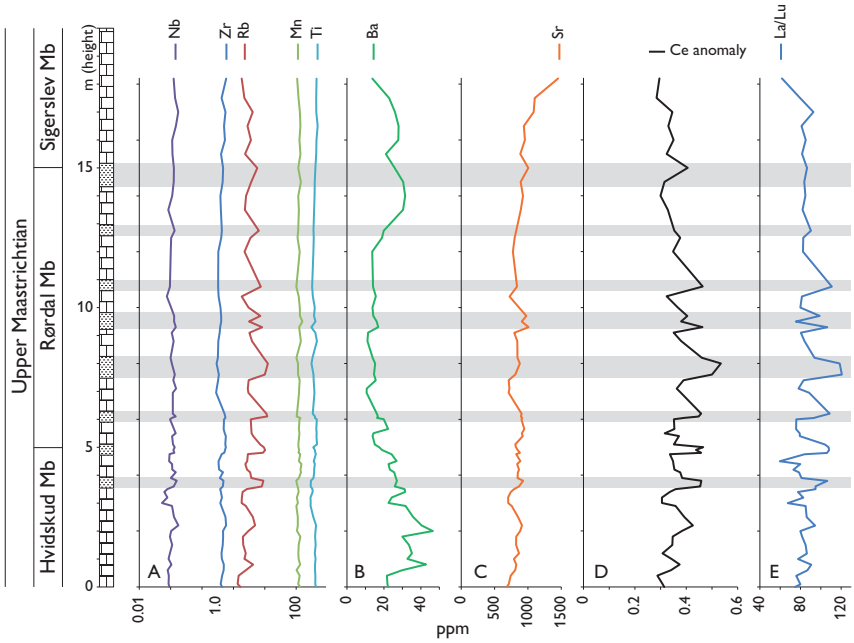

Fig. 3. Chemical profiles in the Rørdal Member. Same stratigraphy as Fig. 1. Marly layers are shown as grey shaded bands. **A**: Nb, Zr, Rb, Mn and Ti; logarithmic scale. **B**: Ba. **C**: Sr. **D**: Ce anomaly. **E**: La/Lu ratio; logarithmic scale.

the modern marine environment, a negative Ce anomaly is indicative of oxic conditions (German & Elderfield 1990) which, in turn, is caused by the low solubility of Ce^{4+} and low availability of Ce. This feature offers the possibility to look into variations in the redox conditions during deposition of the chalk (Jeans *et al.* 2015). In Fig. 4 it can be seen that there is a negative Ce anomaly both in the chalk and in the marl in the Rørdal quarry as well as in the chalk and the fish-clay at Stevns. There is also a negative Eu anomaly which is probably caused by the source of the REE being slightly depleted in Eu (Frei & Frei 2002). The negative Ce anomaly in the chalk at Stevns is more pronounced than in the chalk at Rørdal (Fig. 4) suggesting that the environment during deposition of the chalk at Stevns was more oxic than at Rørdal. The chalk at Stevns has a higher stratigraphic position (in the Sigerslev Member) and the change in the Ce anomaly with time could suggest that the oxygen availability in the chalk sea increased with time during the late Maastrichtian. Alternatively, this could suggest that the chalk at Stevns was deposited in a shallower sea.

The Ce concentration at Rørdal changes with lithology and stratigraphic position in the section (Fig. 3D); it is lower in the chalk than in the marl, indicating that the environment was more oxic in the chalk than in the marl. The REE (including Ce) are located in the carbonate component as well as in the clay as mentioned above. Accordingly, the Ce anomaly reflects the combined effect of the composition of the seawater where the coccoliths and where the clay were formed. Surlyk *et al.* (2010) suggested that the clay in the Rørdal Member is derived from volcanic eruptions. Such clay, derived from alteration of volcanic glass, is likely to have an overall resemblance to the REE distribution in the source. However, the transformation from glass to clay in the marine environment could be the cause of the negative Ce anomaly found in the marl. The fish-clay at Stevns also has this negative Ce anomaly which is indicative of formation of clay in a marine environment (Kastner *et al.* 1984; Frei & Frei 2002). The question is then whether the clay was (trans)formed from volcanic glass in the free water masses or in the seabed. The seabed is likely to have been less oxic than the free water mass, and formation of the clay in the seabed would explain the difference in the redox potential compared to the chalk formed in the free water mass. Finally, the composition of the clay minerals could have been modfied during diagenesis in the presence of organic material affecting the Ce anomaly.

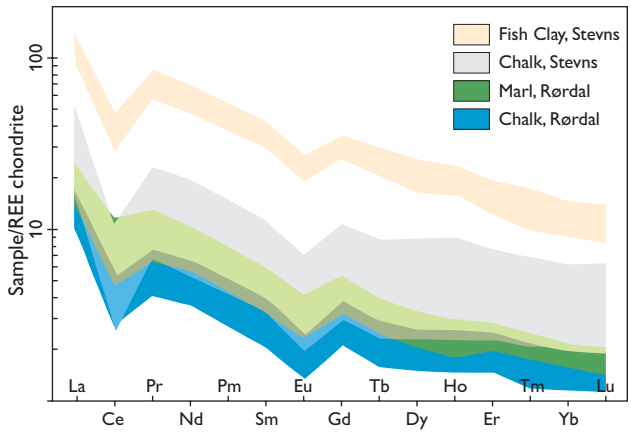

Fig. 4. Chondrite-normalised REE distribution patterns for the Rørdal samples compared with REE data from Stevns Klint (Frei & Frei 2002).

Summary and outlook

The chemical composition of the chalk–marl sequence at Rørdal in Jylland reflects the varying proportions of carbonate and clay. The content of major and minor elements such as Si, Al, Fe and K is proportional to the clay content, with a threefold increase in the marly layers relative to the chalk layers. It is suggested that these elements are located in clay minerals together with lithophile trace elements such as Li, Ga, Rb, Cs and Th which likewise increase threefold in the clay relative to the chalk. Other elements such as Pb, As, Zn and Cu and the REE are found in *c.* 1.5 times higher concentrations in the marl, and these elements are located both in the clay and the carbonate component of the succession. The clay has a light REE enrichment compared to the chalk.

Formation of the clay as authigenic minerals may explain why large ion lithophile elements such as Zr and Nb, as well as Ti, are not incorporated in the clay. The content of Ba in the Rørdal Member is low relative to the under- and overlying strata, and the deposition of Ba could be tested as a chemo-stratigraphic marker and environmental proxy.

The REE distribution shows a negative Ce anomaly both in the chalk and in the marl, suggesting that the environment was oxic throughout the deposition, and as the Ce anomaly is more pronounced in the chalk, the environment was more oxic where the carbonate was formed than in the clay. This observation matches the observation that there is higher species diversity and density in the chalk than in the marl (Lauridsen & Surlyk 2008). If the clay and the carbonate were formed in the same water mass, the observed alternating redox level would be indicative of changing conditions in the sea. However, if the main part of the clay was formed in the seabed as authigenic minerals or was affected by diagenesis, then the alternating redox levels indicated by the Ce anomaly reflects changes in redox conditions at or in the seabed. The Ce anomaly in chalk from Stevns is larger than in chalk from Rørdal, suggesting that the environment was more oxic in the chalk sea towards the end of the Maastrichtian. These differences could be related to changes in temperature over time. A recent study by Thibault *et al.* (2016) suggests a global cooling with superimposed cool/warm fluctuations in the last 8 Ma of the Maastrichtian including e.g. the Rørdal and Sigerslev Members. It is suggested that the Ce anomaly can be used as a palaeo-redox indicator or proxy to compare environments across chalk basins. In this context it is interesting to analyse both carbonate and clay components from the marl.

Acknowledgement

We wish to thank Lars Stemmerik for constructive comments on earlier versions of the manuscript.

References

Boynton, W.V. 1984: Cosmochemistry of the rare earth elements: meteorite studies. In: Henderson, P. (ed.): Rare earth element geochemistry, 63–114. Amsterdam: Elsevier.

Frei, R. & Frei, K.M. 2002: A multi-isotopic and trace element investigation of the Cretaceous–Tertiary boundary layer at Stevens Klint, Denmark – inferences for the origin and nature of siderophile and lithophile element geochemical anomalies. Earth and Planetary Science Letters **203**, 691–708.

German, C.R & Elderfield , H. 1990: Application of the Ce anomaly as a paleoredox indicator: the ground rules. Paleoceanography **5**, 823–833.

Jeans, C.V., Wray, D.S. & Williams, C.T. 2015: Redox conditions in the Late Cretaceous Chalk Sea: the possible use of cerium anomalies as palaeoredox indicators in the Cenomanian and Turonian chalk of England. Acta Geologica Polonica **65**, 345–366.

Jørgensen, N.O. 1986: Geochemistry, diagenesis and nannofacies of chalk in the North Sea Central Graben. Sedimentary Geology **48**, 267–294.

Kastner, M., Asaro, F., Michel, H.V., Alvarez, W. & Alvarez, L.W. 1984: The precursor of the Cretaceous–Tertiary boundary clays at Stevns Klint, Denmark, and DSDP Hole 465A. Science **226** (4671), 137–143.

Larsen, L M., Heaman, L.M., Creaser, R.A., Duncan, R.A., Frei, R. & Hutchinson, M. 2009: Tectonomagmatic events during stretching and basin formation in the Labrador Sea and the Davis Strait: evidence from age and composition of Mesozoic to Palaeogene dyke swarms in West Greenland, Journal of the Geologicla Society (London) **166**, 999–1012.

Lauridsen, B.W. & Surlyk, F. 2008: Benthic faunal response to late Maastrichtian chalk–marl cyclicity at Rørdal, Denmark. Palaeogeography, Palaeoclimatology, Palaeoecology **269**, 38–53.

Lauridsen, B.W., Surlyk, F. & Bromley, R.G. 2011: Trace fossils of a cyclic chalk–marl succession; the upper Maastrichtian Rørdal Member, Denmark. Cretaceous Research **32**, 194–202.

Surlyk, F., Stemmerik, L., Ahlborn, M., Harlou, R., Lauridsen, B.W., Rasmussen, S.L., Schovsbo, N., Sheldon, E. & Thibault, N.R. 2010: The cyclic Rørdal Member – a new lithostratigraphic unit of chronostratigraphic and palaeoclimatic importance in the upper Maastrichtian of Denmark. Bulletin of the Geological Society of Denmark **58**, 89–98.

Surlyk, F., Rasmussen, S.L., Boussaha, M., Schiøler, P., Schovsbo, N.H., Sheldon, E., Stemmerik, L. & Thibault, N.R. 2013: Upper Campanian–Maastrichtian holostratigraphy of the eastern Danish Basin. Cretaceous Research **46**, 232–256.

Thibault, N., Harlou, R., Schovsbo, N.H., Stemmerik, L., Surlyk, F. 2016: Late Cretaceous (late Campanian–Maastrichtian) sea surface temperature record of the Boreal Chalk Sea. Climate of the Past **12**, 429–438.

Authors' address

Geological Survey of Denmark and Greenland, Øster Voldgade 10, DK-1350 Copenhagen K, Denmark, E-mail: *ckn@geus.dk*

New zircon U-Pb and Hf isotopic constraints on the crustal evolution of the Skjoldungen region, South-East Greenland

Thomas F. Kokfelt, Tomas Næraa, Kristine Thrane and Leon Bagas

We report new zircon U-Pb and Hf isotopic data from the Skjoldungen region between *c.* 62°30′ and 63°40′N in South-East Greenland. The work was carried out under the South-East Greenland Mineral Endowment Task (SEGMENT); a joint project between the Geological Survey of Denmark and Greenland (GEUS) and the Ministry of Mineral Resources (MMR) in Greenland to assess the mineral endowment and update the geological knowledge of the region using modern petrological, geochemical and geochronological tools. This paper presents new zircon U-Pb and Hf isotopic data from a range of different Archaean rocks in the Skjoldungen region, which greatly improve the understanding of the history of crustal growth.

Regional geology

The Skjoldungen region in South-East Greenland as defined here covers the ice-free area between Mogens Heinesen Fjord in the south and Bernstorff Isfjord in the north (Fig. 1). The region exposes a mid- to lower-crustal section of the Archaean North Atlantic craton (Kolb *et al.* 2013 and references therein). The dominant rock type is granodiorite with lesser amounts of monzogranite and rare tonalite, commonly with nebulitic to agmatitic textures, and with abundant mafic and ultramafic inclusions. The northern part of the region includes grey orthogneiss that is interleaved with the agmatitic gneiss. The southern part is structurally highly complex containing abundant migmatitic rocks, generally recording lower crustal conditions. Remnants of older supracrustal rocks forming kilometre-sized lensoidal belts of mafic granulite, ultramafic rocks and paragneiss are found in the northern and southernmost parts of the region (Fig. 1). These rocks are commonly invaded by felsic partial melts, dismembering their border zones into smaller units that also account for the agmatitic texture of the surrounding gneiss.

Kolb *et al.* (2013) and Bagas *et al.* (2013) proposed that the region was deformed during both the > *c.* 2800 Ma Timmiarmiut and the *c.* 2790–2700 Ma Skjoldungen orogenies. The Timmiarmiut orogeny is only weakly defined based on deformation events in the southern part of the area that are overprinted by the Skjoldungen orogeny. Skjoldungen island and its surroundings reached granulite facies peak conditions at *c.* 2760–2740 Ma. Subsequent orogenic collapse characterised by fast exhumation rates (Berger *et al.*

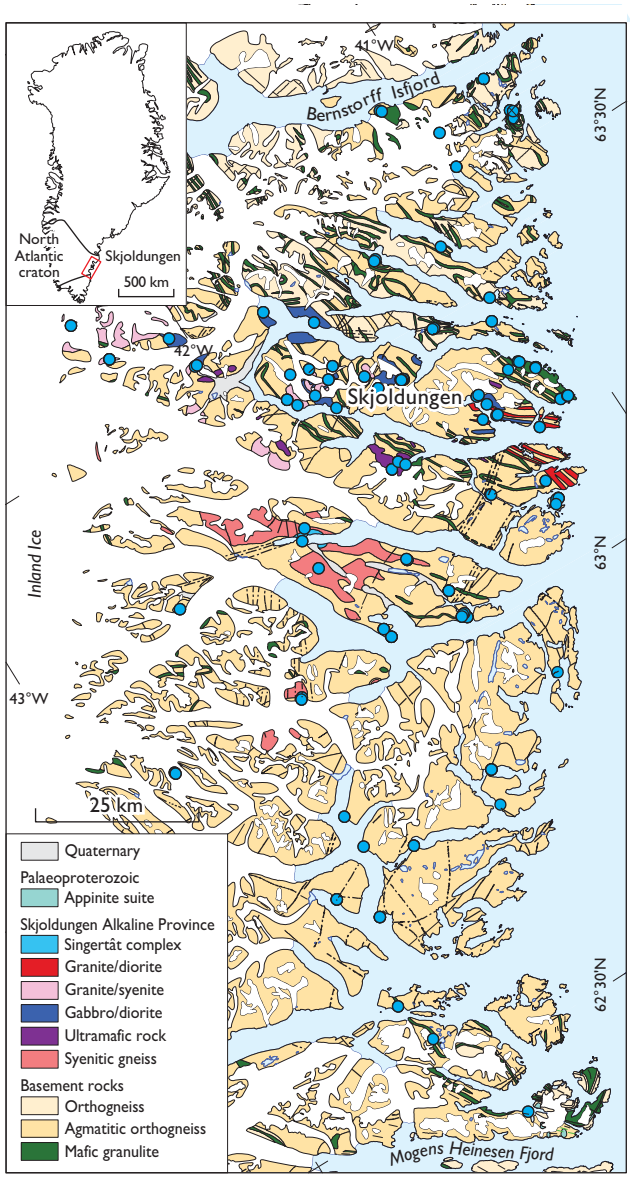

Fig. 1. Geological map of the Skjoldungen region, South-East Greenland, showing locations of samples (blue circles) selected for zircon U-Pb geochronology and zircon Hf isotope analysis.

© 2016 GEUS.

2014) resulted in extensive crustal remelting and continued emplacement of mildly alkaline plutons forming the Skjoldungen Alkaline Province, which constitutes a globally rare occurrence of Archaean alkaline magmatism (Blichert-Toft *et al.* 1996). The province comprises a large number of mafic and ultramafic to differentiated intrusions within a large area of *c.* 2400 km^2 centered at the WNW-trending Skjoldungen island (Blichert-Toft *et al.* 1995). The magmatism comprises a slightly alkaline, *c.* 2750–2690 Ma, stage followed by a highly alkaline, *c.* 2680-2664 Ma Singertât stage, which includes nephelinitic and carbonatitic rocks (Nielsen & Rosing 1990; Nutman & Rosing 1994; Kolb *et al.* 2013).

Samples and methods

A total of 109 samples of orthogneiss, migmatite, granitic rocks, pegmatite and aplite were collected for U-Pb zircon geochronology. As seen in Fig. 1 the geographical sample distribution is uneven, with most samples collected in the northern part of the region. Similarly, coastal areas are more densely sampled than remote and less accessible areas near the ice sheet.

Most U-Pb data were acquired using laser ablation-single collector-magnetic sector field-inductively coupled plasma-mass spectrometry (LA-SF-ICP-MS) at GEUS, employing a Thermo Finnigan Element2 mass spectrometer coupled to a New Wave Research UP213 frequency-quintupled solid state Nd:YAG laser system. The analytical procedures followed Frei & Gerdes (2009) and Dziggel *et al.* (2014). A few samples were analysed at the Nordsim facility at the Natural History Museum in Stockholm using standard procedures in Whitehouse *et al.* (1999), and at the SHRIMP facility at Curtin University using standard procedures in Compston *et al.* (1984). Different textural domains of the zircon grains such as cores and rims were documented using scanning electron microscopy and targeted during analysis. Hf isotope data by LA-ICPMS were obtained on a subset of samples, targeting the same textural domains as were analysed for U-Pb. The Hf isotope data were analysed at the University of Frankfurt following the methods in Gerdes & Zeh (2006).

Results: *U-Pb data*

More than 7000 analytical spots on zircon grains from the 109 samples resulted in 178 interpreted U-Pb ages, reflecting that some samples contained more than one age population. Intrusion ages were calculated from analyses that were 90–110% concordant, or from upper concordia intercepts. Single spot ages interpreted as inherited should be treated as minimum ages due to potential ancient Pb-loss. The U-Pb age data are summarised in a density distribution diagram (Fig. 2A) where the data define two age groups: a group (shown in red) of granitic veins, sheets and plutons, pegmatite and aplite dykes contemporaneous with the Skjoldungen orogeny, and a group (shown in blue) of pre-Skjoldungen ages related to both grey orthogneiss samples and inherited zircon grains. Grains that are older than the main intrusive age are interpreted as inherited. In the southern area such grains are thought to represent older, reworked gneiss protoliths. In the Skjoldungen Alkaline Province inherited zircons are likely to reflect crustal contamination of juvenile melts. Overall, the dataset spans about 1.3 Ga of Earth history from *c.* 3880 to 2600 Ma, but with the overwhelming majority of ages between *c.* 3250 and 2690 Ma. A major age peak between *c.* 2750 and 2690 Ma reflects that about one third of the analysed samples were collected from the Skjoldungen Alkaline Province. At closer inspection, this relatively narrow age range may be divided into several distinct age peaks at *c.* 2750, 2740, 2710 and 2695 Ma (Fig. 2A).

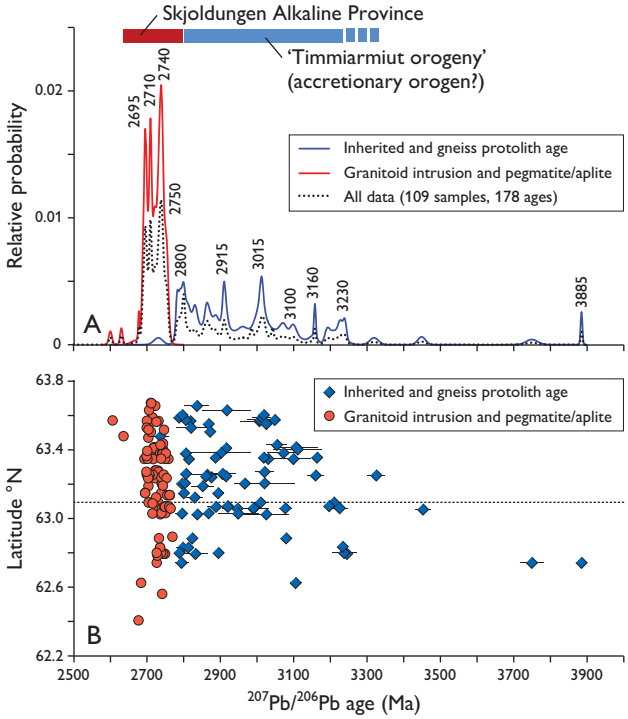

Fig. 2. **A**: $^{207}Pb/^{206}Pb$ age distribution diagram for the Skjoldungen region, based on 109 samples that provide 178 distinct ages. The black dashed curve indicates the relative probability of all age data. **B**: $^{207}Pb/^{206}Pb$ ages plotted against geographical latitude. The rare, detected oldest age components are restricted to the southern part of the region, whereas the dominant ≤3100 Ma age components are equally distributed.

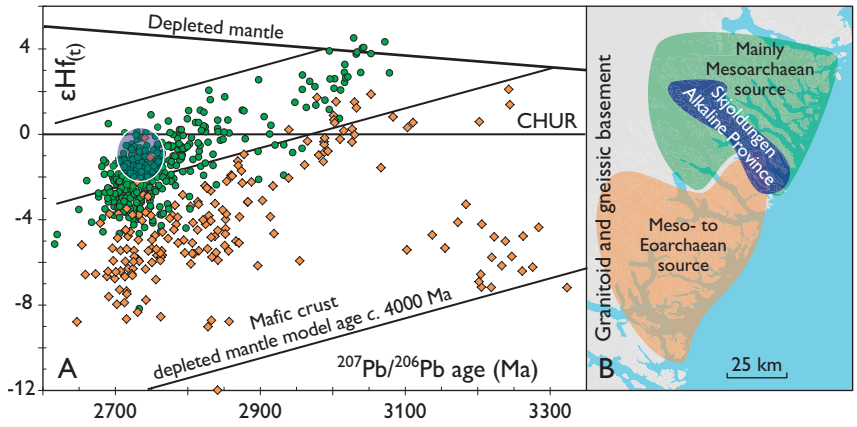

Fig. 3. Geographical distribution of zircon analytical data. **A**: Zircon εHf plotted against $^{207}Pb/^{206}Pb$ ages. Samples collected north and south of 63°10′ shown in green and brown. The compositional range of the Skjoldungen Alkaline Province (blue field; Næraa *et al.* 2015) corresponds to a near-chondritic signature and overlaps with the data from the northern part of the region. **CHUR**: Chondritic uniform reservoir. **B**: Division of the Skjoldungen region into geographical areas based on zircon Hf isotopic compositions. The northern part is derived from a mainly Mesoarchaean source (2950–3100 Ma), and the southern part from a mainly Meso- and Eoarchaean source (≥3200 Ma).

The zircon ages are plotted against geographical latitude in Fig. 2B. The diagram displays a systematic difference in the age distribution of inherited zircons north and south of 63°10′N, despite the above-mentioned uneven sampling density. The southern and northern areas share a significant inherited population with ages spanning from *c.* 3100 to 2800 Ma, but whereas the northern area has few zircon grains older than *c.* 3100 Ma, the southern area contains several inherited grains with ages between *c.* 3880 and 3100 Ma. The diagram also arguably reveals a broad trend of northwards decreasing maximum ages. A similar, albeit less pronounced and more local, trend is seen for the younger intrusions of Skjoldungen Alkaline Province, where the oldest ages of *c.* 2750 Ma are found in the south (syenitic gneiss in the Skirner Bjerge and Kassertoq areas), and the ages decrease down to *c.* 2720 Ma in the north (Figs 1, 2B). These age trends reflect regional differences in the crust at depth and have implications for the interpretation of the regional geodynamic evolution.

Results: *Hf isotope data*

Combined U-Pb and Hf zircon isotope data have been obtained from 29 samples (Fig. 3). The data in Fig. 3A are displayed in Fig. 3B by assigning individual samples to either the northern or southern area by combining intrusive and inherited ages for each area for simplicity. The northern area is characterised by relatively higher initial εHf values and is interpreted as being more juvenile, with a depleted mantle model age of *c.* 3100 Ma. The southern area has somewhat lower initial εHf values and has older model ages of *c.* 4000–3300 Ma (assuming a linear depleted mantle model from εHf = 0 at 4500 Ma to +17 at present), and is interpreted as less juvenile. Although both areas also share an age distribution between 3100 and 2700 Ma, the Hf isotope data indicate that the melts in the northern and southern areas were sourced from different regions, with the northern area tapping a relatively more juvenile and younger crustal reservoir than the southern area.

Discussion and summary

The comprehensive new U-Pb and Hf isotope dataset from the Skjoldungen region sheds new light on the tectono-magmatic evolution of the North Atlantic craton. As illustrated in Figs 2B and 3, the Skjoldungen region can be divided into two crustal terranes with distinct Hf isotopic signatures, albeit with partially overlapping age profiles. Both terranes include U-Pb zircon ages between 3100 and 2700 Ma, but the southern terrane also contains a noticeable component of inherited grains between *c.* 3880 and 3200 Ma (Figs 2, 3). Traces of such old crustal remnants have rarely been found in South-East Greenland but have been recorded from local stream sediments (Thrane & Keulen 2015).

Although the basement throughout the Skjoldungen region records a similar age distribution from *c.* 3100 Ma onwards, the zircon Hf isotopic data define two distinct crustal source terranes, where the zircon Hf isotope data in these rocks display higher initial εHf values in the north than in the south (Fig. 3).

The few inherited zircon ages from *c.* 3880 to 3100 Ma leave the geodynamic setting responsible for the earliest magmatic activity unclear. Still, the U-Pb-Hf isotope data suggest long-lived growth of a terrane or crustal block that includes very old (>4000 Ma) crustal source components. The subsequent period from *c.* 3100 to 2800 Ma records semi-continuous magmatic activity throughout the entire Skjoldungen region with contemporaneous development of rocks of the northern and southern terranes and diminishing juvenile input over time, as reflected by the steady decrease in Hf isotope compositions (Fig. 3A). These signatures could reflect that the northern terrane formed in

an accretionary orogeny that was building out from south to north. In this model, south-verging subduction along the northern boundary of the southern terrane would have proceeded for several hundreds of millions of years with progressive accretion of arc systems to form the northern juvenile terrane. Alternatively, the northern terrane with its distinct and younger Hf source signature could have developed as a separate entity prior to the Skjoldungen orogeny, in which case the broad overlap in ages between the southern and northern terranes would be coincidental. The prolonged period of accretion-related magmatism diminished at *c.* 2800 Ma, where the prelude to the Skjoldungen orogeny represents a shift in tectonic setting to that of a continent–continent collision orogeny (Bagas *et al.* 2013; Kolb *et al.* 2013). The orogeny was associated with renewed, intensified magmatism and the development of the Skjoldungen Alkaline Province (Blichert-Toft *et al.* 1995).

The new zircon data from the main magmatic stage of the Skjoldungen Alkaline Province are consistent with formation in a protracted time period from *c.* 2750 to 2690 Ma, overlapping with the late stage of the Skjoldungen orogeny. Whole rock Hf isotope data from mafic intrusions in the province plot with near-primitive mantle signatures (εHf from 0 to –2) and overlap with the Hf zircon isotope composition of the northern area (Næraa *et al.* 2015). The slightly negative Hf isotope values are consistent with derivation from a slightly enriched mantle source, probably coupled with an enrichment in incompatible elements arising from the preceding subduction processes, and by assimilation of crustal material. The new age data from the province also suggest distinct magmatic events at *c.* 2750, 2740, 2710 and 2695 Ma. The reason for such episodic magmatism is currently not understood but might be tectonically controlled.

The new U-Pb-Hf isotopic data dramatically widen the insight into the crustal development of South-East Greenland. The new data indicate that the study region consists of two different domains, a southern one containing source components older than c. 3200 Ma (up to *c.* 4000 Ma), and a northern one entirely younger than *c.* 3100 Ma. These systematics might either be explained by the existence of two distinct crustal terranes that were amalgamated at *c.* 2800 Ma, or as one continuous terrane that was built out by progressive accretion from south to north between *c.* 3100 and 2800 Ma.

References

Bagas, L., Næraa, T., Kolb, J., Reno, B.L. & Fiorentini, M.L. 2013: Partial melting of the Archaean Thrym Complex of southeastern Greenland. Lithos **160–161**, 164–182.

Berger, A., Kokfelt, T.F. & Kolb, J. 2014: Exhumation rates in the Archean from pressure–time paths: Example from the Skjoldungen Orogen (SE Greenland). Precambrian Research **255**, 774–790.

Blichert-Toft, J., Rosing, M.T., Lesher, C.E. & Chauvel, C. 1995: Geochemical Constraints on the Origin of the Late Archaean Skjoldungen Alkaline Igneous Province, SE Greenland. Journal of Petrology **36**, 515–561.

Blichert-Toft, J., Arndt, N.T. & Ludden, J.N. 1996: Precambrian alkaline magmatism. Lithos **37**, 97–111.

Compston W., Williams I. & Meyer C. 1984: U-Pb geochronology of zircons from lunar breccia 73217 using a sensitive high mass-resolution ion microprobe. Journal of Geophysical Research: Solid Earth (1978–2012) **89**, B525–B534.

Dziggel, A., Diener, J.F.A., Kolb, J. & Kokfelt, T.F. 2014: Metamorphic record of accretionary processes during the Neoarchaean: The Nuuk region, southern West Greenland. Precambrian Research **242**, 22–38.

Frei, D. & Gerdes, A. 2009: Precise and accurate in situ U–Pb dating of zircon with high sample throughput by automated LA-SF-ICP-MS. Chemical Geology **261**, 261–270.

Gerdes, A. & Zeh, A. 2006: Combined U–Pb and Hf isotope LA-(MC-) ICP-MS analyses of detrital zircons: comparison with SHRIMP and new constraints for the provenance and age of an Armorican metasediment in Central Germany. Earth and Planetary Science Letters **249**, 47–61.

Kolb, J., Thrane, K. & Bagas, L. 2013: Field relationship of high-grade Neo- to Mesoarchaean rocks of South-East Greenland: Tectonometamorphic and magmatic evolution. Gondwana Research **23**, 471–492.

Nielsen, T.F.D. & Rosing, M.T. 1990: The Archaean Skjoldungen Alkaline Province, South-East Greenland. Rapport Grønlands Geologiske Undersøgelse **148**, 93–100.

Nutman, A & Rosing, M.T. 1994: SHRIMP U-Pb zircon geochronology of the Archaean Ruinnæsset syenite, Skjoldungen alkaline province, South-East Greenland. Geochimica et Cosmochimica Acta **58**, 3515–3518.

Næraa, T., Bagas, L., Tusch, J., Kokfelt, T.F. & Münker, C. 2015: Pro- and retrograde igneous activity during the Neoarchaean Skjoldungen orogeny in the SE Greenland. Goldschmidt Abstracts **2248**.

Thrane, K. & Keulen, N. 2015: Provenance of sediments in the Faroe–Shetland Basin: Characterisation of possible source components in Southeast Greenland. In: 5th Faroe Islands Exploration Conference: Proceedings of the 4th Conference, 7–25. Annales Societatis Scientiarum Færoensis Supplementum LXIV.

Whitehouse, M.J., Kamber, B.S. & Moorbath, S. 1999: Age significance of U–Th–Pb zircon data from early Archean rocks of west Greenland – a reassessment based on combined ion-microprobe and imaging studies. Chemical Geology **160**, 210–224.

Authors' addresses

T.F.K. & K.T., *Geological Survey of Denmark and Greenland, Øster Voldgade 10, DK-1350 Copenhagen K, Denmark.* E-mail: *TFK@geus.dk*

T.N., *Department of Geology, Lund University, Sölvegatan 12, SE-223 62 Lund, Sweden.*

L.B., *School of Earth and Environment, University of Western Australia, 35 Stirling Highway, Crawley WA 6009, Australia.*

In situ fractionation and inward migration of the solidification front in the Skaergaard intrusion, East Greenland

Troels F.D. Nielsen

For more than 80 years the Skaergaard intrusion, 68°N in southern East Greenland, has been a foremost natural laboratory for the study of the crystallisation and fractionation of basaltic magma. This process has been of prime importance in the evolution of the Earth and other stony planets. Models that have been developed and refined during numerous studies of this particular intrusion have been part of the foundation for petrogenetic modelling for decades. In later years, vast amounts of new data have been added, due to systematic sampling in the field and from analysis of exploration drill cores. Methods for the study on grain-size scale have advanced, and the quest for a well-supported genetic model for the PGE-Au mineralisation of the intrusion has intensified. The new data and insight question the applicability of conventional petrogenetic modelling, and as a consequence, increasing importance is placed on *in situ* crystallisation and fractionation in mush zones at the roof, walls and floor of the intrusion.

The Skaergaard intrusion

The Skaergaard intrusion (Wager & Brown 1968) is a comparatively small but well-preserved and well-exposed layered gabbro intrusion (Fig. 1A). It is 56 Ma old (Wotzlaw *et al.* 2012) and was emplaced during the opening of the North Atlantic. It is 7 × 11 km in surface exposure, has a total structural height of *c.* 4 km, and, dependent on the chosen modelling paradigm, has a box-like (Nielsen 2004) or ellipsoid shape (Irvine *et al.* 1998, Svennevig & Guarnieri 2012) and a volume of *c.* 300 km^3. The intrusion crystallised concentrically inward from the margins (Fig. 1B) with the Layered Series (LS, LZ, MZ and UZ) in the bowl-shaped floor, the Marginal Border Series (MBS) on the walls, and Upper Border Series (UBS) below the roof. The UBS and LS meet at the Sandwich horizon (SH). All three series are subdivided on the basis of a parallel evolution in liquidus parageneses (Salmonsen & Tegner 2013 and references therein).

New research initiatives

Petrogenetic modelling of the Skaergaard gabbros and the evolution of the melt in the intrusion have traditionally rested on the textural interpretation of the gabbros as rocks composed of liquidus crystals, continued growth of these

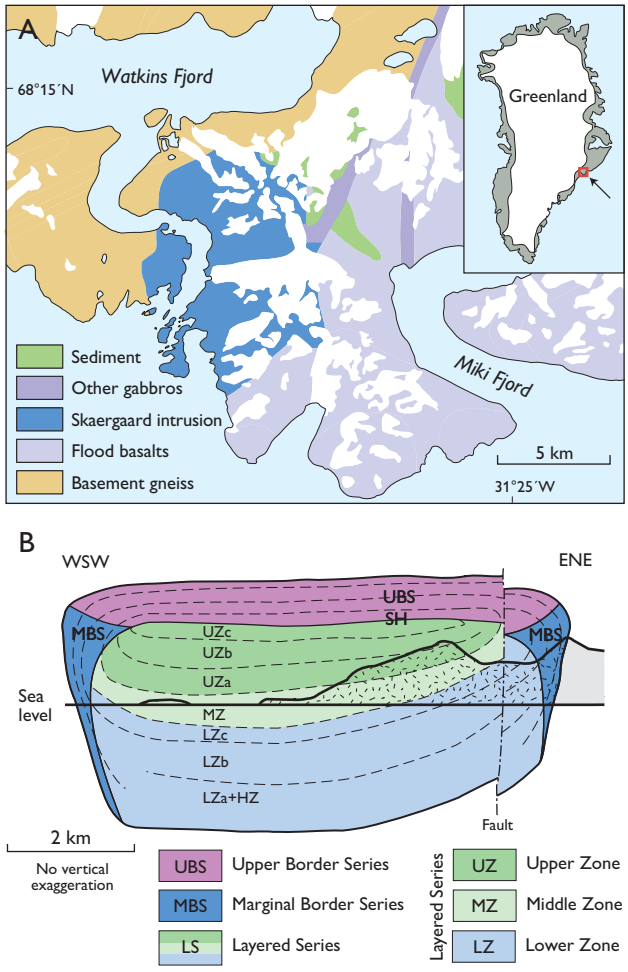

Fig. 1. **A**: Geological setting of the Skaergaard intrusion between basement gneisses, sediments, other gabbros and flood basalts. Location in Greenland in insert. **B**: Reconstructed cross-section (Nielsen *et al.* 2015). The Upper and Lower Zones of the Layered Series are subdivided on the basis of liquidus paragenesis (see text). Sea level and present topography are shown in black lines.

© 2016 GEUS.

crystals in equilibrium with the bulk liquid (adcumulus growth), and crystallisation of solids from trapped liquids. Sorting of crystals on the magma chamber floor has been likened to processes established for clastic sediments, including stratification of crystal mushes in matrix-supported mass flows. Despite challenges these models have remained robust, and most researchers are faithful to this classic cumulus paradigm and the modelling tools developed therefrom.

Research initiatives in the later decades of the 20th century (McBirney 1996 and references therein) provided much new information and were accompanied by investigations facilitated by the exploration of PGE-Au mineralisation in the intrusion (e.g. Bird *et al.* 1991). Notable outcomes of this research include the development of double diffusive convection models (McBirney & Noyes 1979), evaluation of the petrogenetic importance of immiscibility between Fe-rich and Si-rich silicate melts (Jakobsen *et al.* 2011 and references therein), as well as evidence for isotopic disequilibrium and tight age controls on the emplacement and solidification of the intrusion (see Wotzlaw *et al.* 2012, and references therein).

The studies of the Skaergaard intrusion surged in 2000 with access to assay data and up to 1200 m long drill cores. The data in the public domain allowed calibration of structural models for the interior of the intrusion (Nielsen 2004), erection of compaction models (Tegner *et al.* 2009; McKenzie 2011), and studies of the mineralisation (Nielsen *et al.* 2005, 2015; Andersen 2006; Rudashevsky *et al.* 2015 and references therein; Holwell *et al.* 2015; Keays & Tegner 2015). Petrographic studies focused, e.g. on compositional variations in plagioclase (Namur *et al.* 2014) and on clinopyroxene-filled dihedral angles between plagioclase crystals (e.g. Holness 2015 and references therein). Changes in dihedral angles give indications for, e.g. the arrival of new phases on the liquidus of the silicate melts and changes in permeability, and thus for the controls on the mobility of elements of economic interest.

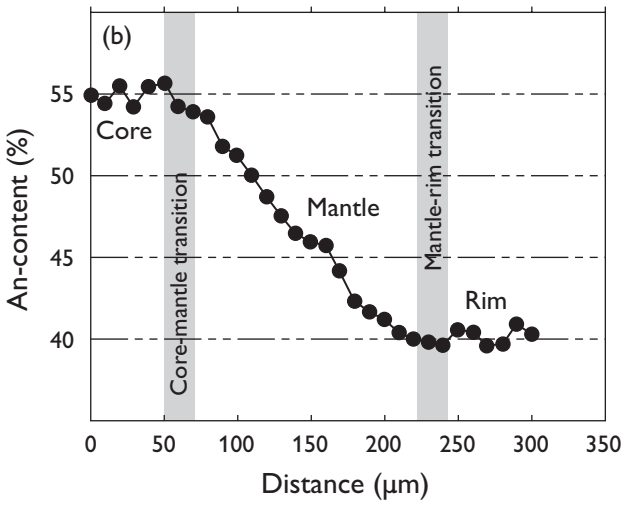

Fig. 2. Compositional variation in LZb plagioclase crystal with small core (liquidus) and broad mantle crystallised during *in situ* fractionation involving mush melt, and rim crystallised during buffered crystallisation (after Namur *et al.* 2014).

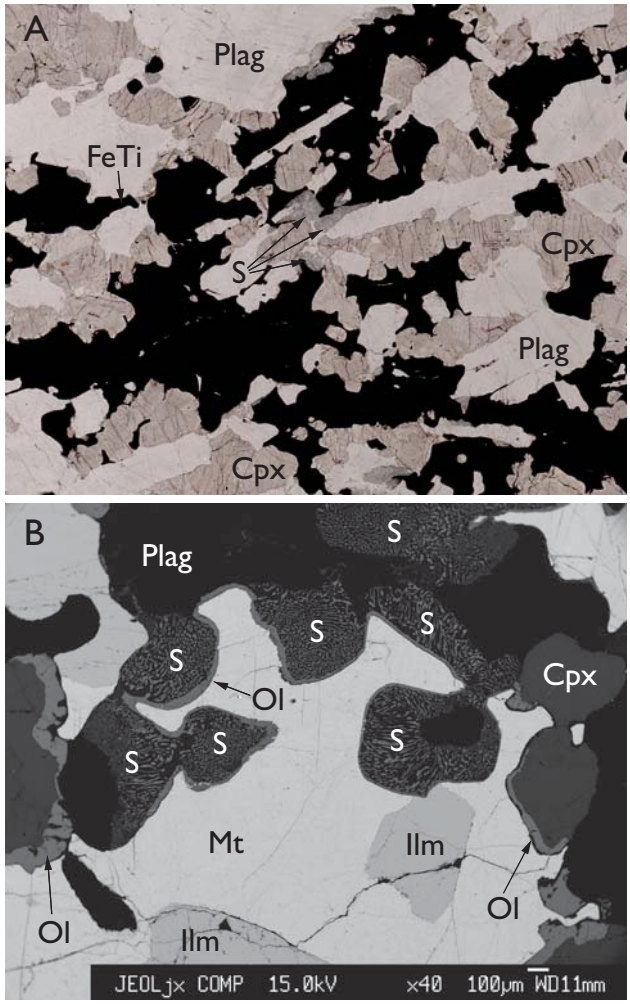

Fig. 3. **A**: Transmitted light image (*c.* 13 × 9 mm) showing interconnected magnetite and ilmenite that crystallised from interstitial mush melt. **B**: Electron microprobe backscatter image (see Nielsen *et al.* 2015). Symplectites (**S**) formed by reaction between plagioclase and reactive Fe-rich mush melt that crystallised most of the magnetite and ilmenite in the view. **Cpx**: clinopyroxene (with exsolutions in Fig. 3B). **FeTi**: Fe-Ti-oxides. **Ilm**: ilmenite. **Mt**: magnetite. **Plag**: plagioclase. **Ol**: olivine. **S**: symplectitic intergrowths. Scale at base of the image.

The importance of *in situ* fractionation

Modelling based on the classic cumulate paradigm suggests that the proportion of trapped liquid decreased from 30–50 per cent to only a few per cent during the solidification of the intrusion (Tegner *et al.* 2009). This is, however, in conflict with reactions between liquidus minerals and Fe-rich silicate melts (Holness *et al.* 2011) and the occurrence of immiscible melt droplets throughout much of the floor cumulates (Jakobsen *et al.* 2011 and references therein). They are supposed to result from extended *in situ* crystallisation and fractionation (Langmuir 1989) in crystal mush, long residence time, and ineffective compaction. This is supported by the very common zonation in plagioclase (an example is shown in Fig. 2, Namur *et al.* 2014) and the distribution of magnetite crystallised from interstitial melt (Fig. 3A; Nielsen *et al.* 2015).

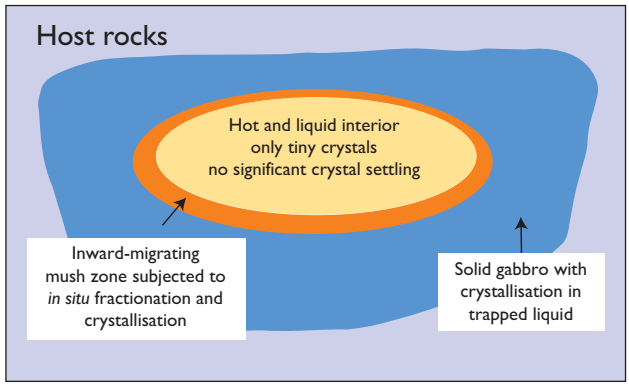

Fig. 4. Principles of the proposed model of inward migration of mush zone and liquidus front. The inward-migrating mush zone is shown in orange. The residual bulk liquid in the centre has only small and suspended crystals of liquidus phases. The remaining bulk melt is always at liquidus due to feedback from the mush zone (see Nielsen *et al.* 2015 for details of model).

Toward a new solidification model

A magma chamber will always be hot in the middle and crystallisation will always occur in the crystal mush between solidified gabbro and the remaining melt, unless the system is affected by vigorous convection. In the Skaergaard intrusion this seems unlikely due to the concentric solidification (Nielsen 2004). All gabbro samples have recorded a temperature interval on the line of liquid descent and all have witnessed the inward migration of the crystallisation front, fronts with new phases on the liquidus of the mush liquid, and the solidification front. The mushy layer is a sub-chamber of crystal mush migrating inwards, and the samples we collect reflect only processes within the mush itself and the bulk composition of the liquid that was processed in the mush (Fig. 4).

Any sample of the gabbros is composed of minerals left behind by the inward-migrating mush layer. In broad terms, the composition of the floor gabbro is equal to bulk liquid minus what rose out of the floor, e.g., low density melt, and that of the roof gabbro is equal to what remained under the roof, e.g. low density minerals and melt (Salmonsen & Tegner 2013; Nielsen *et al.* 2015). Roof and floor series are complementary, and neither series represents the evolution of the bulk magma, but their weighted average does. The modelling of the evolution of layered intrusions is commonly only based on exposed floor cumulates, and the common neglect of complementary successions in the lost roof of the intrusions may therefore lead to erroneous petrogenetic conclusions.

Undoubtedly, future research in the Skaergaard intrusion and its mineralisation will focus on very detailed petrography, mineralogy, *in situ* mineral chemistry and isotope geochemistry, and on unravelling of the complexities of the solidification processes. Petrogenetic modelling on the basis of bulk rock chemistry without detailed petrographic information is prone to lead to significant oversimplification and unwarranted confirmation of the chosen models.

References

Andersen, J.C.Ø. 2006: Postmagmatic sulphur loss in the Skaergaard Intrusion: Implications for the formation of the Platinova Reef. Lithos **92**, 198–221.

Bird, D.K., Brooks, C.K., Gannicott, R.A. & Turner, P.A. 1991: A gold-bearing horizon in the Skaergaard Intrusion, East Greenland. Economic Geology **86**, 1083–1092.

Holness, M.B. 2015: Plagioclase growth rates control three-grain junction geometry in dolerites and gabbros. Journal of Petrology **56**(11), 2117–2144.

Holness, M.B., Stripp, G., Humphreys, M.C.S., Veksler, I.V., Nielsen, T.F.D. & Tegner, C. 2011: Silicate liquid immiscibility within the crystal mush: late-stage magmatic microstructures in the Skaergaard intrusion, East Greenland. Journal of Petrology **52**, 175–222.

Holwell D.A., Keays, R.R., McDonald, I. & Williams, M.R. 2015: Extreme enrichment of Se, Te, PGE and Au in Cu sulfide microdroplets: evidence from LA-ICP-MS analysis of sulfides in the Skaergaard Intrusion, east Greenland. Contributions to Mineralogy and Petrology **170:53**, *http://dx.doi.org/10.1007/s00410-015-1203-y*

Irvine, T.N., Andersen, J.C.Ø. & Brooks, C.K. 1998: Included blocks (and blocks within blocks) in the Skaergaard Intrusion: geological relations and the origins of rhythmic modally graded layers. Geological Society of America Bulletin **110**, 1398–1447.

Jakobsen, J.K., Veksler, I.V., Tegner, C. & Brooks, C.K. 2011: Crystallization of the Skaergaard intrusion from an emulsion of immiscible iron- and silica-rich liquids: Evidence from melt inclusions in plagioclase. Journal of Petrology **52**, 345–373.

Keays, R.R. & Tegner, C. 2015: Magma chamber processes in the formation of the low-sulphide magmatic Au–PGE mineralization of the

Platinova Reef in the Skaergaard intrusion, East Greenland. Journal of Petrology **56**, 2319–2340.

Langmuir, C. H. 1989: Geochemical consequences of *in situ* crystallization. Nature **340**, 199–205.

McBirney, A.R. 1996: The Skaergaard Intrusion. In: Cawthorn, R.G. (ed.): Layered Intrusions, 147–180. Amsterdam: Elsevier.

McBirney,A,R. & Noyes, R.M. 1979: Crystallization and layering of the Skaergaard Intrusion. Journal of Petrololgy **20**(3), 487–554.

McKenzie, D. 2011: Compaction and crystallization in magma chambers: towards a model of the Skaergaard Intrusion. Journal of Petrology **52**(5), 905–930.

Namur, O., Humphreys, M.C.S. & Holness, M.B. 2014: Crystallization of interstitial liquid and latent heat buffering in solidifying gabbros: Skaergaard intrusion, Greenland. Journal of Petrology **55**(7), 1389–1427.

Nielsen, T.F.D. 2004: The shape and volume of the Skaergaard Intrusion, Greenland: implications for mass balance and bulk composition. Journal of Petrology **45**(3), 507–530.

Nielsen, T.F.D., Andersen, J.C.Ø. & Brooks, C.K. 2005: The Platinova Reef of the Skaergaard intrusion. In: Mungall, J.E. (ed.): Exploration for platinum-group element deposits, 431–455. MAC Short Course **35**. Ottawa: Mineralogical Association of Canada.

Nielsen T.F.D., Andersen J.C.Ø., Holness, M.B., Keiding, J.K., Rudashevsky, N.S., Rudashevsky, V.N., Salmonsen, L.P., Tegner, C. &. Veksler, I.V. 2015: The Skaergaard PGE and gold deposit: the result of *in situ* fractionation, sulphide saturation, and magma chamber-scale precious metal redistribution by immiscible Fe-rich melt. Journal of Petrology **56**(8), 1643–1676.

Rudashevsky, N.S., Rudashevsky, V.N. & Nielsen, T.F.D. 2015: Intermetallic compounds, copper and palladium alloys in Au–Pd ore of the Skaergaard pluton, Greenland. Geology of Ore Deposits **57**(8), 674–690.

Salmonsen, L.P. & Tegner, C. 2013: Crystallization sequence of the Upper Border Series of the Skaergaard intrusion: revised subdivision and implications for chamber-scale magma homogeneity. Contributions to Mineralogy and Petrology **165**, 1155–1171.

Svennevig, K. & Guarnieri, P. 2012: From 3D mapping to 3D modelling: a case study from the Skaergaard intrusion, southern East Greenland. Geological Survey of Denmark and Greenland Bulletin **26**, 57–60.

Tegner, C., Thy, P., Holness, M.B., Jakobsen, J.K. & Lesher, C.E. 2009: Differentiation and compaction in the Skaergaard Intrusion. Journal of Petrology **50**(5), 813–840.

Wager, L.R. & Brown, G.M. 1968: Layered igneous rocks. Edinburgh and London: Oliver & Boyd, 588 pp.

Wotzlaw, J.-F., Bindeman, I.N., Schaltegger, U., Brooks, C.K. & Naslund, H.R. 2012: High-resolution insights into episodes of crystallization, hydrothermal alteration and remelting in the Skaergaard intrusive complex. Earth and Planetary Science Letters **355–356**, 199–212.

Author's address

Geological Survey of Denmark and Greenland, Øster Voldgade 10, DK-1350 Copenhagen K, Denmark; E-mail: *tfn@geus.dk*

Palaeovalleys at the basal unconformity of the Palaeoproterozoic Karrat Group, West Greenland

Pierpaolo Guarnieri, Camille A. Partin and Diogo Rosa

In the Rinkian belt of West Greenland, reworked Archaean gneisses are overlain by supracrustal successions of the Palaeoproterozoic Karrat Group, defined by Henderson & Pulvertaft (1967) as comprising two formations: the Qeqertarssuaq Formation and the Nûkavsak Formation. The group was later extended to include the Mârmorilik Formation (Henderson & Pulvertaft 1987) originally considered to be of Archaean age (Henderson & Pulvertaft 1967) but later shown to be Palaeoproterozoic, resting with a depositional unconformity on Archaean gneiss (Garde 1978). Henderson & Pulvertaft (1987) suggested that the carbonate-dominated Mârmorilik Formation in the south was laterally equivalent to the siliciclastic-dominated Qeqertarssuaq Formation in the north, the two subbasins being separated by a basement topographic high.

The Karrat Group and the Archaean basement were metamorphosed and folded during the Rinkian orogeny (Henderson & Pulvertaft 1987; Grocott & Pulvertaft 1990). During ship- and helicopter-supported fieldwork in 2015, the Kangerluarsuk–Maarmorilik area (Fig. 1) was visited to sample the Zn-Pb-mineralised horizons found by RTZ Mining and Exploration Ltd. (Coppard *et al.* 1992) along the basement-cover boundary and to obtain oblique photographs of the contact that was described as faults on the Mârmorilik geological map sheet (scale 1:100 000, Henderson & Pulvertaft 1987). The aim of this paper is to show preliminary new results on the geometry and type of unconformity between the Palaeoproterozoic Karrat Group and the underlying gneisses, and to describe a new stratigraphic unit representing here the lowermost sedimentary sequence above the unconformity. This unit is of particular relevance as it controls the distribution of the Zn-Pb mineralisation.

Palaeoproterozoic palaeovalleys as a result of unconformity

One of the best localities to characterise the basal unconformity of the Palaeoproterozoic Karrat Group is along a cliff face of Qaarsukassak at the head of Kangerluarsuk (Fig. 1). The more than 1800 m high cliff face exposes Archaean basement rocks (Umanak gneiss) and greywackes of the Nûkavsak Formation (Henderson & Pulvertaft 1987). The contact between the Archaean basement and the Karrat Group was originally mapped as a series of faults, probably based on binocular observations from a boat in the 1960s, and from the black and white aerial photographs that were available at that time. The detail of our new oblique photographs clearly shows that this contact corresponds to a nonconformity with incised valleys into Archaean basement gneiss filled by Palaeoproterozoic siliciclastic rocks of the Karrat Group (Figs 2, 3).

The palaeotopography that is preserved below the Palaeoproterozoic sedimentary cover appears deeply excavated with highs and lows representing an ancient palaeodrainage system with a topographic relief of 300–400 m (Fig. 3). Qaarsukassak represents one of the domal structures described by Henderson & Pulvertaft (1987), and the palaeotopography is accentuated by this fold structure. The south-eastern and north-western limbs of this wide upright anticline were visited and the basal unit was sampled (Fig. 2).

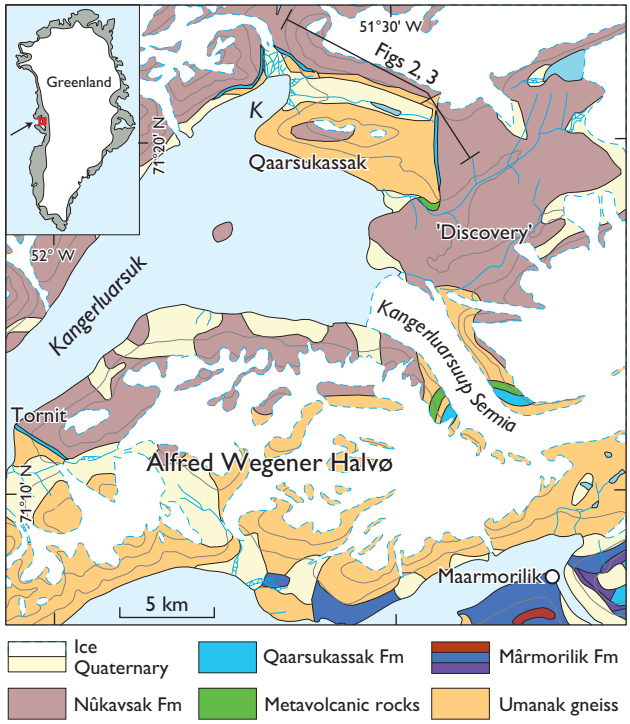

Fig. 1. Simplified geological map of the central Karrat Group area (modified from Escher & Pulvertaft 1995). **K**: Kangerlussuakassak.

© 2016 GEUS.

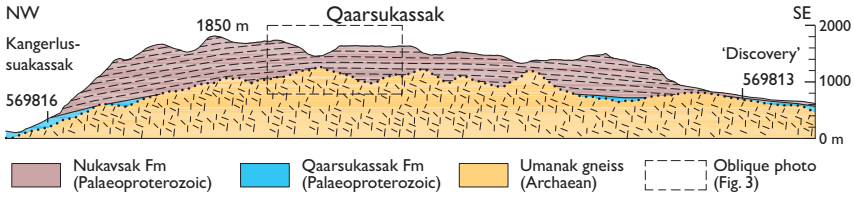

Fig. 2. Geological cross-section of Qaarsukasak showing the Palaeoproterozoic unconformity with the incised palaeovalleys into the Archaean Umanak gneiss infilled by the Qaarsukassaq Formation at the bottom and the Nûkavsak Formation on top. The locations along the cross-section of two analysed samples (Fig. 5) are also shown.

The overall geometry of the Archaean–Palaeoproterozoic unconformity displays important regional differences. In the Maarmorilik sector to the south the palaeosurface appears to be a peneplain covered by the basal quartzites of the Mârmorilik Formation described by Garde (1978); in the central Kangerluarsuk sector described here, it is represented by well-developed incisions filled with a new stratigraphic unit and local occurrences of lava flows. To the north of the studied area, in the Karrat Isfjord sector, the unconformity is represented by an undulated palaeosurface covered by thick metavolcanic rocks that were also noted by Henderson & Pulvertaft (1987).

Qaarsukassak Formation

Here we describe a new stratigraphic unit in the Karrat Group, informally named the Qaarsukassak Formation, which occurs locally below the Nûkavsak Formation in the Kangerluarsuk fjord area (Fig. 1). This sequence was previously described at the so-called 'Discovery' showing by Coppard *et al.* (1992). The report describes a 30–66 m thick quartzite-carbonate succession with a mineralised zone occurring dominantly in calcite-bearing dolostone, and bounded by the Archaean basement gneiss and the Nûkavsak Formation. The measured section from the base to the inferred stratigraphic top (Fig. 4) reveals that its stratigraphic thickness prior to structural repetition is less than 20 m.

The lower contact with the Archaean basement gneiss is a planar to undulating erosional surface that preserves a depositional contact. Laminated to massive quartzite fines upward into fine-grained metamorphosed sandstones and sandy mudstones, including calcite-cemented and graphitic quartzites (Unit 1). These siliciclastic rocks are overlain in sharp contact by light grey to white metacarbonate rocks with pods of massive tremolite and in some horizons, minor graphite (Unit 2). This is succeeded by another quartzite unit (Unit 3), followed by dark grey, laminated metacarbonate rocks with possible slump folds and minor tremolite veining (Unit 4). The overlying, rusty weathering metasedimentary rocks including graphitic, metamorphosed mudstones and siliciclastic rocks represent the ore zone (Unit 5). The upper contact of the Qaarsukassak Formation with the Nûkavsak Formation is not well-exposed. Also of note is a thin re-sedimented calcitic marble horizon within the basal part of the Nûkavsak Formation, which might be derived from contemporaneous erosion of the Qaarsukassak Formation.

All metacarbonate rocks in the Qaarsukassak Formation at the 'Discovery' section described here are calcitic. The Mârmorilik Formation, by contrast, contains both calcitic and dolomitic marble (Garde 1978). The primary occurrence of calcitic marble in the upper Mârmorilik Formation suggests possible correlation with the Qaarsukassak Formation. The presence of tremolite in some outcrops of

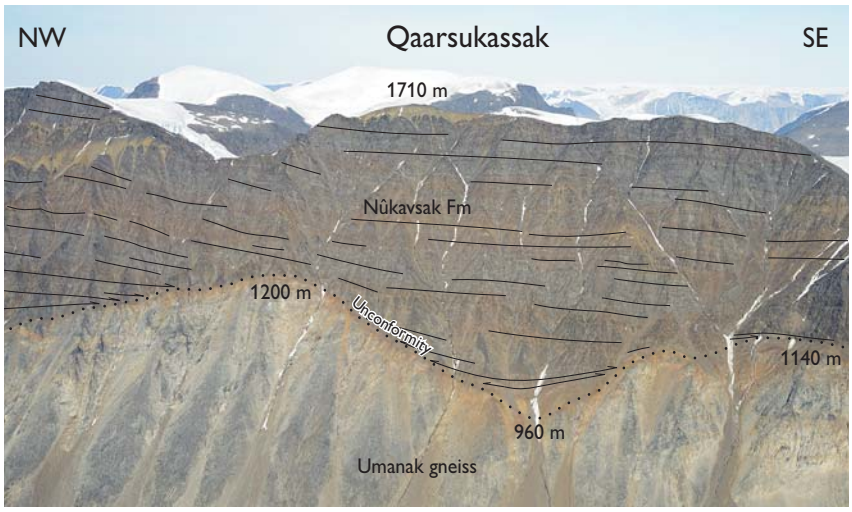

Fig. 3. The geometry of valleys and onlap of Palaeoproterozoic greywackes of the Nûkavsak Formation at Qaarsukassak, photographed from a helicopter. The difference between bottom and top of the palaeorelief is about 240 m. Position of image shown on Fig. 2.

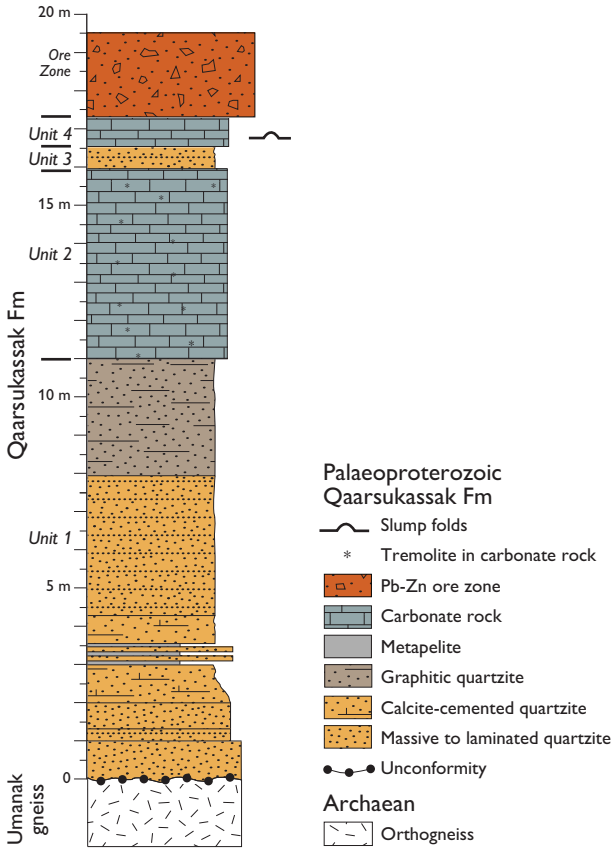

Fig. 4. Stratigraphic section of the Qaarsukassak Formation at the type locality of Qaarsukassak at head of Kangerluarsuk (Fig. 2 for location).

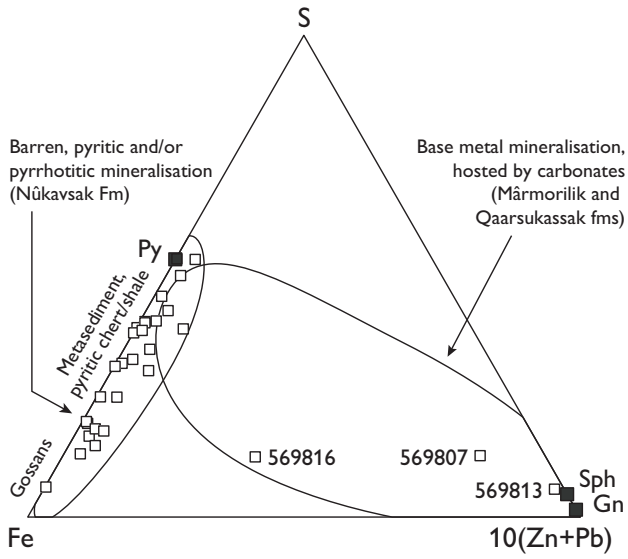

Fig. 5. Fe–S–10(Zn+Pb) ternary diagram with discriminant compositional areas of base-metal mineralisation hosted by carbonates of the Mârmorilik and Qaarsukassak formations (right) and the rusty-weathering zones hosted by the Nûkavsak Formation (left). **Py**: Pyrite. **Gn**: Galena. **Sph**: Sphalerite.

the Qaarsukassak Formation, though, suggests the former presence of dolomite or high-Mg calcite. Unit 1 of the Qaarsukassak Formation could represent a fluvial environment, but outcrops lack the sedimentary structures to confirm this. Instead, the Qaarsukassak Formation was likely deposited in a shallow marine environment. The Qaarsukassak Formation shows minor thickness variations along strike, suggesting that its deposition infilled pre-existing topographical lows in the Archaean basement gneiss. In addition to the main section in the 'Discovery' area, similar rocks also occur at two other localities, namely at Tornit on the south side of Kangerluarsuk and along Kangerluarsuup Sermia (Fig. 1), although exposures are not laterally continuous. At Tornit the orientation of the Qaarsukassak Formation is vertical and forms part of the overturned limb of the Kigarsima Nappe (Henderson & Pulvertaft 1987). At this outcrop the formation occurs between a thin amphibolite unit and the Nûkavsak Formation as a *c.* 10 m thick section comprised of calcitic marble and rusty metasedimentary rocks, with quartzite, a possible quartz-pebble conglomerate and siliceous marble. The section might be repeated by folding and therefore only less than 10 m thick. At Kangerluarsuup Sermia an overturned 30–40 m section of dark grey, tremolite-bearing dolomitic marble with black layers of metamudstone occurs structurally below Archaean basement gneiss, which is thrust over the marble. The Qaarsukassak Formation extends to the north-west side of the section shown in Fig. 2 on the north-western limb of the wide anticline at Kangerlussuakassak.

Mineralisation

Carbonate-hosted Zn-Pb mineralisation is common in the calcitic marble of the upper Mârmorilik Formation and was exploited at the Black Angel mine between 1973 and 1990 (Thomassen 1991). Additionally, Coppard *et al.* (1992) identified intermittent stratabound Zn-Pb mineralisation of the 'Discovery' and Kangerluarsuup Sermia occurrences, hosted within a carbonate and siliciclastic sequence. This sequence was considered to be the basal sequence of the Mârmorilik Formation by Coppard *et al.* (1992). Here, we allocate this succession to the Qaarsukassak Formation, since it is not in contact with the Mârmorilik Formation and the two units are separated by the basement topographic high. The recognition and understanding of the distribution of this formation are important as the formation controls the distribution of the regional Zn-Pb mineralisation, which should be distinguished from rusty-

weathering, pyritic or pyrrhotitic, but barren horizons located in the Nûkavsak Formation.

A ternary diagram (Fig. 5) discriminates the signatures of the base-metal mineralisation hosted by carbonate rocks of the Mârmorilik or Qaarsukassak formations, and of the rusty-weathering horizons hosted by the Nûkavsak Formation. The latter are dominated by pyrite or pyrrhotite and lack significant amounts of base metals (Fig. 5). Due to the effects of weathering, resulting in gossanous horizons, compositions of the sulphides in exposed rocks can depart from pyrite and become enriched in iron and depleted in sulphur. The former have variable amounts of iron sulphide, but can also have significant sphalerite or galena contents. The two samples closest to the metal corner were collected at the previously established 'Discovery' and 'South Lakes Glacier' occurrences, samples 569813 and 569807, respectively. A third sample (569816, Fig. 5) was collected *c.* 10 km to the north-west (Fig. 2) where mineralisation was not previously seen. Although the absolute base-metal content of this sample is not high, it is elevated relative to sulphur (akin to the tenor concept in nickel exploration). Its presence supports potential correlation with the Mârmorilik Formation and the proposed continuation of the Qaarsukassak Formation, hosting base-metal mineralisation, to the north-western limb of the wide anticline of the cross section shown in Fig. 2.

Discussion and conclusion

Henderson & Pulvertaft (1987) proposed a Palaeoproterozoic structural high of Archaean basement gneiss exposed on Alfred Wegener Halvø, bounding the carbonate-dominated Mârmorilik basin to the south and separating it from the Qeqertarssuaq and Nûkavsak formations in the north. Our new observations show that such Archaean basement gneiss in the Kangerluarsuk area is heavily incised, and that Palaeoproterozoic palaeovalleys were filled in with siliciclastic and carbonate rocks of the Qaarsukassak Formation (new informal unit) that correlates well with the Mârmorilik Formation and is conformably overlain by the Nûkavsak Formation. Its intermediary, mixed siliciclastic-carbonate sedimentation could have been marginal marine and transitional into sedimentation of the turbiditic greywackes of the Nûkavsak Formation.

The palaeovalleys observed at Qaarsukassak seem to reflect an erosional event prior to the deposition of a sedimentary cycle represented by a carbonate-rich basin in the Maarmorilik area and an area rich in volcanic components in the north, separated by a continental shelf area. The erosion may have been related to a re-organisation of the basin structure, where uplift in some areas created the observed palaeotopography beneath the Nûkavsak Formation.

The observations in the Kangerluarsuk area described here, coupled with new observations from the Qeqertarssuaq Formation in the north which will be described elsewhere, may suggest that the Karrat Group comprises more than one sedimentary cycle separated by erosion and possibly deformation. An ongoing geochronological study of detrital zircon from different units within the Karrat Group is expected to yield new information about the depositional ages of its individual formations.

Acknowledgments

This work was carried out within the framework of an ongoing project financed by the Geological Survey of Denmark and Greenland (GEUS) and the Ministry of Mineral Resources of Greenland (MMR).

References

Coppard, J., Swatton, S. & Harris, C.J. 1992: Karrat exclusive exploration licence. 1992 year-end report, 19 pp. Unpublished report, RTZ Mining and Exploration Limited (in archives of the Geological Survey of Denmark and Greenland, GEUS Report File 21297).

Escher, J.C. & Pulvertaft, T.C.R. 1995: Geological map of Greenland, 1:2 500 000. Copenhagen: Geological Survey of Greenland.

Garde, A.A. 1978: The Lower Proterozoic Marmorilik Formation, east of Mârmorilik, West Greenland. Meddelelser om Grønland **200**(**3**), 71 pp.

Grocott, J. & Pulvertaft, T.C.R. 1990: The Early Proterozoic Rinkian belt of central West Greenland. In: Lewry, J.F. & Stauffer, M.R. (eds) The Early Proterozoic Trans-Hudson Orogen of North America. Geological Association of Canada Special Paper **37**, 443–463.

Henderson, G. & Pulvertaft, T.C.R. 1967: The stratigraphy and structure of the Precambrian rocks of the Umanak area, West Greenland. Meddelelser fra Dansk Geologisk Forening **17**, 1–22.

Henderson, G. & Pulvertaft, T.C.R. 1987: Geological map of Greenland, 1:100 000. Mârmorilik 71 V.2 Syd, Nûgâtsiaq 71 V.2 Nord, Pangnertôq 72 V.2 Syd. Lithostratigraphy and structure of a Lower Proterozoic dome and nappe complex. Descriptive text. 72 pp. Copenhagen: Geological Survey of Greenland.

Thomassen, B. 1991: The Black Angel lead-zinc mine 1973–90. Rapport Grønlands Geologiske Undersøgelse **152**, 46–50.

Authors' addresses

P.G. & D.R., *Geological Survey of Denmark and Greenland, Øster Voldgade 10, DK-1350 Copenhagen K, Denmark.* Email: *pgua@geus.dk*

C.A.P., *Department of Geological Sciences, University of Saskatchewan, 114 Science Place, Saskatoon, SK S7N 5E2, Canada.*

Investigations of past climate and sea-ice variability in the fjord area by Station Nord, eastern North Greenland

Niels Nørgaard-Pedersen, Sofia Ribeiro, Naja Mikkelsen, Audrey Limoges and Marit-Solveig Seidenkrantz

The marine record of the Independence–Danmark fjord system extending out to the Wandel Hav in eastern North Greenland (Fig. 1A) is little known due to the almost perennial sea-ice cover, which makes the region inaccessible for research vessels (Nørgaard-Pedersen *et al.* 2008), and only a few depth measurements have been conducted in the area. In 2015, the Villum Research Station, a new logistic base for scientific investigations, was opened at Station Nord. In contrast to the early exploration of the region, it is now possible to observe and track the seasonal character and changes of ice in the fjord system and the Arctic Ocean through remote sensing by satellite radar systems. Satellite data going back to the early 1980s show that the outer part of the Independence–Danmark fjord system is characterised by perennial sea ice whereas both the southern part of the fjord system and an area 20–30 km west of Station Nord are partly ice free during late summer (Fig. 1B). Hence, marine-orientated field work can be conducted from the sea ice using snow mobiles, and by drilling through the ice to reach the underlying water and sea bottom.

Earlier studies have shown that the last deglaciation of the region occurred in the early Holocene (Funder 1989; Nørgaard-Pedersen *et al.* 2008) and the sea subsequently inundated the fjord system. Based on onshore evidence from eastern North Greenland, beach ridges and frequent deposition of drift wood during the Holocene Thermal Maximum at about 8000–5000 years BP indicate a period of open water and a mean summer temperature higher than today (Funder *et al.* 2011).

During the first field season in 2015 at the new station, a number of field-based research projects were carried out coordinated by the Arctic Science Partnership (ASP, http://www.asp-net.org/) and the Arctic Research Centre (ARC) at Aarhus University, Denmark. The Geological Survey of Denmark and Greenland (GEUS) and ARC carried out the fjord sediment coring project described here. The main objective of the marine geoscience field work was to collect sediment cores, which can be used to reconstruct past sea-ice variability through recent centuries and millennia. A major aspect was also the impact of sea ice on primary production, mainly diatoms and dinoflagellates and on biogeochemical cycles and the Arctic ecosystem.

This paper presents preliminary results of the sediment coring work and also new information on the bathymetry in the fjord area up to 50 km from Station Nord. A time-series of satellite radar images of sea-ice types in the fjord system provided by the Danish Meteorological Institute (DMI) for the last decade is discussed to better understand the recent sea-ice dynamics in the area. An introduction to the ongoing laboratory work and data processing is also included.

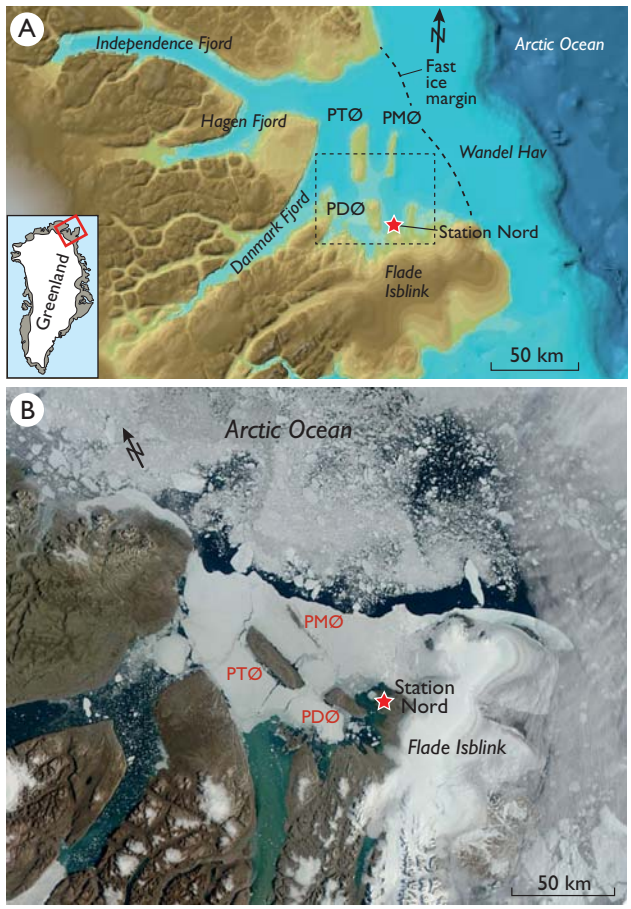

Fig. 1. **A**: Study area (framed area) near Station Nord and Villum Research Station (red star), eastern North Greenland. The average position of the fast-ice edge toward the Arctic Ocean pack-ice drift is indicated. Map source: IBCAO vers. 3.0 (Jakobsson *et al.* 2012). **B**: Satellite image (DMI AQUA) of the area from 15 August 2015. **PDØ**: Prinsesse Dagmar Ø. **PTØ**: Prinsesse Thyra Ø. **PMØ**: Prinsesse Margrethe Ø.

© 2016 GEUS.

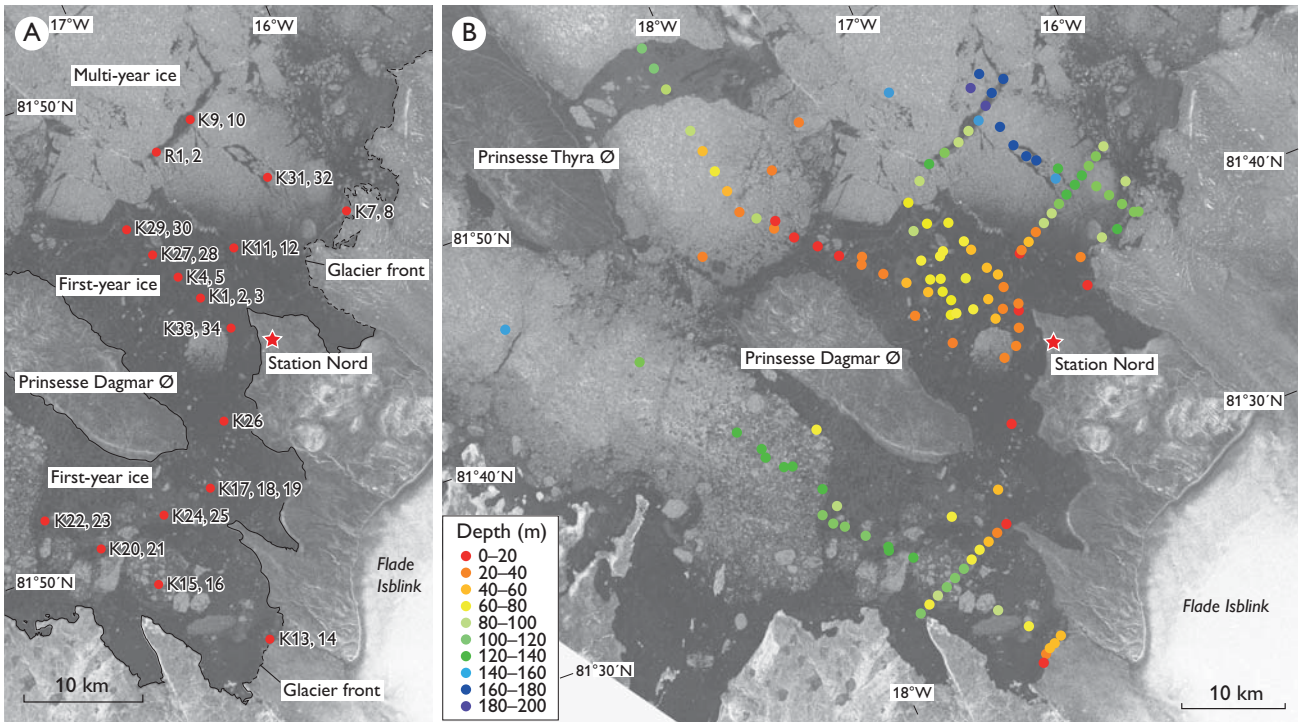

Fig. 2. **A**: Radar satellite image of the study area (SAR Sentinel-1 from 29.01.15), showing areas of seasonal (dark grey) and multi-year ice (light grey). There is no open water. High resolution SAR image (courtesy of Leif Toudal, Danish Meteorological Institute). Red dots: core sites. **K**: Kajak core. **R**: Rumohr core. Stippled lines: marine-terminating margins of Flade Isblink. **B**: Bathymetry data points with colour code for 20 m depth intervals overlain on SAR satellite image. Depth data sources are from the 2015 ASP field season (echo soundings and CTD based data) supplemented by data collected in 2006 by Naja Mikkelsen (GEUS), Yngve Kristoffersen (University of Bergen, Norway), and René Forsberg (DTU Space, Denmark).

Ice conditions

Satellite data show that the northern hemisphere has experienced a significant decrease in sea ice during the past *c.* 35 years, with a late summer sea-ice net loss in excess of 10% per decade, in addition to decreases seen in ice extent, thickness and age (Perovich & Richter-Menge 2015). Older (>4 years) and thicker sea ice is now only dominant in northern Arctic Canada and off northern Greenland. The large Independence–Danmark fjord system in eastern North Greenland is characterised by a semi-permanent fast-ice cover (Wadhams 1986) in the outer part and in the inner more southern part by a seasonal ice cover, which breaks up and partly melts during August–September (Fig. 1A). A coastal open water lead (polynya) is often observed between the northern margin of the fast ice and the drifting Arctic pack ice. The fast ice in the outer fjord system is protected by three large islands (the 'Prinsesse islands'; Figs 1, 2), which make it stable for a number of years before parts of it break up (Wadhams 1986 and available satellite data). Very thick and old ice of the 'sikkussak' type has, therefore, been observed earlier at the mouth of the fjord system (Wadhams 1986). During exceptionally warm summers the outer fast-ice cover has broken up, for example as observed in mid-August 2003 (Rasmussen 2004). The 2003 event coincided with break-up of the thick fast ice off the large NE Greenland ice stream in 2002 and 2003.

While planning our field work we used synthetic aperture radar (SAR) and visible band images (AQUA, TERRA) captured over the last decade from DMI (http://ocean.dmi.dk/arctic/nord.uk.php) in order to characterise the multi-year ice dynamics of the fjord system and to select the sampling sites. Sea-ice radar reflectivity is sensitive to the roughness of the ice and the presence of saltwater droplets within newer ice. Thus, older and more deformed multi-year ice appears white or light grey (more reflection), whereas younger, first-year ice appears dark grey or black (less reflection). Hence, it is possible to identify areas characterised by first-year ice and distinguish these from multi-year ice covered areas (Fig. 2). Moreover, by examining the ice-cover character on SAR images from DMI from 2009 onwards, it is possible to date different patches of fast-ice cover. Ice tongues of glacier ice and icebergs debouching out to the sea from the ice cap of Flade Isblink can be identified north-east and south-west of Station Nord (Fig. 2).

The SAR and visible band image record for the past decade reveals that the oldest fast ice in the study area is found

in the Wandel Hav. This ice appears to be at least 6 years old and may date back to 2004 following the total break-up in 2003. A similar area of older ice patches is situated between the Prinsesse Thyra Ø and Prinsesse Margrethe Ø (Fig. 2). In mid-August 2012, the fast-ice cover at the mouth of the Independence Fjord and Danmark Fjord broke up, creating a wide-open connection to the Arctic Ocean in the area north-west of Prinsesse Thyra Ø. Freeze-up later in 2012 created the constellation of multi-year ice coverage persisting until today. Only the outer rim of the old fast-ice cover may occasionally be eroded by loss of ice fragments, which drift away with the Arctic pack-ice drift.

The Flade Isblink ice cap is mainly drained by two outlets along its western margin. A comparison of earlier maps (Higgins 1991) and 2015 satellite-derived data indicates that the outlet immediately north of Station Nord has retreated about 13 km southwards between 1991 and 2015. Higgins (1991) estimated the average flow speed of the outlet glacier to be of a few hundred metres per year. Satellite radar data from the last decade confirm this estimate, but also indicate that the outlet glaciers have been surging (Joughin *et al.* 2010).

Field work

We collected sediment cores from 11 April to 2 May 2015 in the ice-covered fjord area (Figs 2, 3). Sampling took place up to about 30 km from the station along several transects determined according to ice conditions and existing knowledge of bathymetry. We used two snow mobiles with sledges (3–4-person team) for transport. We selected sampling sites based on a geo-referenced high-resolution radar satellite image (Sentinel-1 SAR from 31.01.2015) revealing areas of first and multi-year ice as well as glacier-front positions and larger icebergs (Fig. 2). Whenever possible, we targeted sites with thin first-year ice (about 1.0–1.2 m) and avoided sites covered by thick (>3 m) multi-year ice, which was very arduous to drill through.

At each core site, we first removed the snow cover, which was usually at least 1 m thick, and used a 9 inch ice-auger to drill two or more overlapping holes in the ice, sufficiently large for the coring devices (Fig. 3). At most locations, we measured water depths with an echo sounder, but at oceanographic stations we used CTD data (conductivity, temperature and depth). We sampled sediment with a Kajak Sediment Corer (25–75 cm long tube, 45 mm inner diameter), a Rumohr Lot Corer (50–100 cm long tube, 75 mm inner diameter), and at a few stations, with a Van Veen Grab Sampler (top 10 cm surface sediment). We used a tripod with a top-mounted hydraulic winch (Pot Hauler) connected to a petrol-driven power pack to retrieve the *c.* 60 kg Rumohr Corer, whereas Kajak cores were retrieved with a hand winch (Fig. 3). Drilling large holes through 1–3 m of sea ice was time-consuming, and we found that Kajak coring was the most efficient approach. We collected duplicate or triplicate Kajak cores at most coring sites and one Kajak core from each site was subsampled at 1 cm intervals at the Villum Research Station. Sea-ice cores were collected using a Kovacs Ice Corer System for biochemical and taxonomic studies of the sea-ice algal communities.

Fig. 3. Recovering a Kajak core with seabed sediments. Photograph: Jesper Hoffmann.

Bathymetrical data

Apart from a single study of short sediment cores and water-depth measurements south-west and north-west of Prinsesse Dagmar Ø close to Station Nord (Nørgaard-Pedersen *et al.* 2008) very little is known about the bathymetry and sedimentation record of this remote area. Bathymetrical datasets from the limited earlier field projects in the area have, for this study, been updated by new data from the 2015 ASP field season. Earlier data consist of echo soundings carried out in 2006 and reconnaissance data. The 2015 field season dataset consists of echo sounding data and CTD-derived bathymetry data. As the CTD data are corrected for water-column velocity differences (due to water masses with different salinities and temperatures), these may be considered the most accurate. Water depths increase from *c.* 20 m near Station Nord to >150 m 20–30 km northwards (Fig. 2B). In front of the glacier outlet margin 10–15 km north-east of Station Nord, a trough is found with depths up to 100–150 m right up to the glacier margin at 81°40′N. There is a shallow area between Prinsesse Dagmar Ø and Prinsesse Thyra Ø with water depths between 20 and 30 m, but the depth increases

to >100 m towards the north. South of Prinsesse Dagmar Ø, a trough possibly connected to the mouth of the Danmark Fjord shows depths in the range of 130–150 m. The trough axis rises to about 115 m *c.* 10 km from the glacier outlet margin and reaches depths of maximum 50 m at the glacier margin.

Preliminary results and outlook

A total of 37 sediment cores were retrieved from 17 sites along transects up to *c.* 30 km from Station Nord (Fig. 2A). Many of the Kajak cores are only a few decimetres long. However, we recovered cores exceeding 0.5 m from more water-rich mud close to glacier margins and at the few Rumohr core sites.

A spatial study of sea-ice and productivity proxies including dinoflagellate cysts, diatoms, foraminifera, biomarker IP25 (a proxy for sea ice) and biogenic silica is currently being conducted for the 17 sampling sites, to establish a baseline of recent conditions that will serve as modern analogues for reconstructions of sea-ice variability and changes in oceanographic conditions during earlier time periods.

Selected sediment cores are being analysed for ^{210}Pb and ^{137}Cs content to estimate sedimentation rates at the study sites and establish a chronology for the topmost part of the cores. The first dating results show sedimentation rates in the order of 0.04–0.06 cm/y. Preliminary investigations of the microfossil content of the sediments revealed calcareous benthic foraminifera and a few ostracods, particularly at the deeper sites, which allows for the possibility to use ^{14}C dating to establish a robust chronology for the sediment records. Furthermore, studies of the sites located north of Station Nord show a stronger marine influence, whereas the sites towards the north-west and south have a clear signal of freshwater or glacial influence. Complementary to the climate proxy work, a characterisation of the protist communities is being undertaken by germination, growth tests, and molecular analyses (DNA) targeting the two main groups of primary producers: diatoms and dinoflagellates. Investigations of the sampled sea-ice cores showed that during the early part of the season's field work the sea ice was barren of algae. This is attributed to light attenuation by the snow (average snow thickness of 1 m). *In situ* light measurements, and fluorescence measurements on 25 sea-ice core samples (bottom 5 cm) using a phytoplankton analyser showed no detectable photosynthetic activity (information from the Phytobiology Team, Aarhus University).

The field work provided us with some first insights into an ice-covered, very remote and large fjord system of eastern North Greenland. The preliminary data confirm presence of biogenic remains and sedimentary signatures which can be used as proxies for palaeo-environmental reconstructions and deciphering of the younger part of the Holocene climate history in this region.

Acknowledgements

We thank Kunuk Lennert, Jesper Hoffman, Egon Frandsen and the late John Lau for logistic support. We thank Leif Toudal (DMI) for making geo-referenced satellite SAR images of the study area available. ASP 2015 oceanographers Igor Dmitrenko and Sergei Kirilov are also acknowledged for sharing CTD depth data. We thank the Station Nord military personnel for their great hospitality and help. The field work was partly financed by the Villum Foundation (grant no. VKR023454 to Sofia Ribeiro) and by the Arctic Research Centre, Aarhus University.

References

Funder, S. (ed.) 1989: Quaternary geology of the ice-free areas and adjacent shelves of Greenland. In: Fulton, R.J. (ed.): Quaternary geology of Canada and Greenland. The Geology of North America **K-1,** 741–792. Boulder, Colorado: Geological Society of America.

Funder, S., Kjeldsen, K.K., Kjær, K.H. & Ó Cofaigh, C. 2011: The Greenland Ice Sheet during the past 300,000 years: a review. In: Ehlers, J., Gibbard, P.L. & Hughes, P.D. (eds): Quaternary glaciations – extent and chronology – a closer look. Developments in Quaternary Sciences **15**, 699–714. Amsterdam: Elsevier.

Higgins, A.K. 1991: North Greenland glacier velocities and calf ice production. Polarforschung **60**, 1–23.

Jakobsson, M. *et al.* 2012: The international bathymetric chart of the Arctic Ocean (IBCAO) Version 3.0. Geophysical Research Letters 39, L12609, *http://dx.doi.org/10.1029/2012GL052219.*

Joughin, I., Smith, B.E., Howat, I.M., Scambos, T. & Moon, T. 2010: Greenland flow variability from ice-sheet-wide velocity mapping. Journal of Glaciology **56** (197), 415–430.

Nørgaard-Pedersen, N., Mikkelsen, N. & Kristoffersen, Y. 2008: Late glacial and Holocene marine records from the Independence Fjord and Wandel Sea regions, North Greenland. Polar Research **27**, 209–221.

Perovich, D.K. & Richter-Menge, J.A. 2015*:* Regional variability in sea ice melt in a changing Arctic. Philosophical Transactions of the Royal Society **A373**, 2045, *http://dx.doi.org/10.1098/rsta.2014.0165*.

Rasmussen, L. 2004: Set fra oven: Et hjørne af Grønland. Vejret **100**, 17–20.

Wadhams, P. 1986: The ice cover. In: Hurdle, B.G. (ed.): The Nordic Seas, 21–78. New York: Springer-Verlag.

Authors' addresses

N.N.-P., S.R., N.M. & A.L., *Geological Survey of Denmark and Greenland, Øster Voldgade 10, DK-1350 Copenhagen K, Denmark.* E-mail: *nnp@geus.dk*

M.-S. S., *Department of Geoscience, Aarhus University, Høegh-Guldbergs Gade 2, DK-8000 Aarhus C, Denmark.*

Placing Greenland ice sheet ablation measurements in a multi-decadal context

Dirk van As, Robert S. Fausto, John Cappelen, Roderik S.W. van de Wal, Roger J. Braithwaite, Horst Machguth and the PROMICE project team*

In recent years, the Greenland ice sheet has been losing mass at an average rate of 262 ± 21 Gt yr^{-1} (2007–2011; Andersen *et al.* 2015). Part of this mass loss was due to increases in melt, reducing the surface mass budget (Enderlin *et al.* 2014). Also, the acceleration of many marine-terminating outlet glaciers increased the dynamic mass loss (Rignot *et al.* 2008). Both mass-loss mechanisms are linked to recent increases in atmospheric and oceanic temperatures (Dutton *et al.* 2015). For instance, in summer 2012 Greenland experienced exceptionally warm atmospheric conditions, causing nearly the entire ice-sheet surface to melt for two periods of several days (Nghiem *et al.* 2012) and contributing to the largest annual ice-sheet mass loss on record (Khan *et al.* 2015). This is in contrast to a return to more average conditions in 2015 (Tedesco *et al.* in press).

In 2007 the Programme for Monitoring of the Greenland Ice Sheet (PROMICE) was initiated to monitor both the surface mass budget and dynamic contributions to mass change. For the monitoring, *c.* 20 automatic weather stations were distributed over eight regions of the Greenland ice sheet (Fig. 1), primarily in the ablation area where surface melting is most prominent (Van As *et al.* 2011). These stations record a suite of meteorological and radiative variables that allow for surface-energy budget closure, and reveal the relative importance of the different energy fluxes contributing to melting. Each station also monitors ablation by sonic height rangers, pressure transducers and ablation stakes (Fausto *et al.* 2012).

Table 1 shows that the 2015 melt season yielded ablation totals below the PROMICE average (i.e. reduced surface mass loss) in all regions except the two northernmost ones: KPC and THU. Along the south-western ice sheet margin the 2015 ablation anomalies appear to be one third below average. However, what has to be accounted for in the interpretation is that the PROMICE observational period contained several warm years and summers. Figure 2 illustrates that there have been considerable fluctuations in atmospheric temperatures at Greenland coastal sites with continuous records dating back to the 19th century. The PROMICE observational period distinctly classifies as one with above-average temperatures, both in the relatively warm south and colder north (Fig. 2). This is also likely to imply above-average ablation, and thus biased PROMICE ablation anomalies. It is therefore more insightful to evaluate recent ablation measurements in the context of a more representative

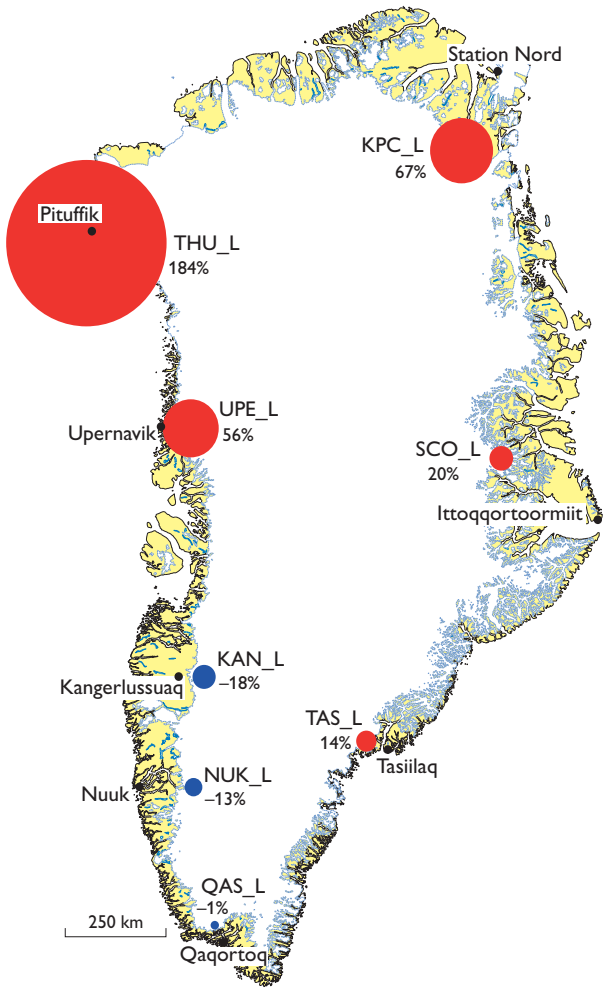

Fig. 1. Map of Greenland with 2015 ablation anomaly values referenced to the 1961–1990 period at the lower (suffix **L**) PROMICE weather station sites. Black dots indicate DMI weather stations selected for this study.

* Charalampos Charalampidis, Jason E. Box, Anne M. Solgaard, Andreas P. Ahlstrøm, Konstanze Haubner, Michele Citterio and Signe B. Andersen

© 2016 GEUS.

Table 1. Temperature and ablation statistics for the PROMICE weather station sites

	KPC_L	SCO_L	TAS_L	QAS_L	NUK_L	KAN_L	UPE_L	THU_L
Temperature JJA 1961–1990 (°C)	1.7	2.7	5.5	6.5	5.5	9.2	4.1	3.9
Temperature JJA 2008–2015 (°C)	2.8	5.0	6.7	7.3	7.5	10.5	6.3	5.3
Annual net ablation PROMICE (m ice eq.)	2.2	3.2	3.6	6.4	5.5	3.8	2.6	1.8
2015 ablation anomaly ref. to the PROMICE average (%)	7	–1	–14	–20	–31	–34	–12	30
Annual net ablation 1961–1990 (m ice eq.)	1.4	2.7	2.7	5.1	4.4	3.1	1.5	0.8
Temperature sensitivity (line slope) (m ice eq. °C^{-1})	0.71	0.25	0.79	1.23	0.64	0.63	0.55	0.89
Correlation of linear fit (r)	0.59	0.50	0.60	0.75	0.83	0.71	0.81	0.94
RMSD* of linear fit (m ice eq.)	0.5	0.3	0.6	0.9	0.6	0.5	0.3	0.2
Uncertainty ablation calculation (m ice eq.)	0.6	0.4	0.7	0.9	0.6	0.6	0.5	0.4
2015 ablation anomaly referenced to 1961–1990 (%)	67 ± 40	20 ± 15	14 ± 25	–1 ± 18	–13 ± 15	–18 ± 19	56 ± 31	184 ± 43

* RMSD: root mean squared differences

climate. Greenland studies often use the 1961–1990 period, during which the ice sheet is assumed to have been in near-steady state (e.g. Braithwaite *et al.* 1992; Rignot *et al.* 2008). The main aim of this study is to reference PROMICE-measured ablation to this 1961–1990 'climate normal'.

Present-day temperatures in a multi-decadal perspective

In order to determine the 1961–1990 reference climate, we need observational records spanning that period and recent years. The only continuous and (on these time scales) relevant Greenland data series that exist have been recorded in coastal areas, by weather stations of the Danish Meteorological Institute (DMI). For this study we selected those DMI time series that were gathered closest to the PROMICE weather station sites and were initiated before 1961 (Fig. 1). The earliest measurements (primarily of air temperature) were taken in the 1700s; several continuous records date back to the mid to late 1800s (Fig. 2).

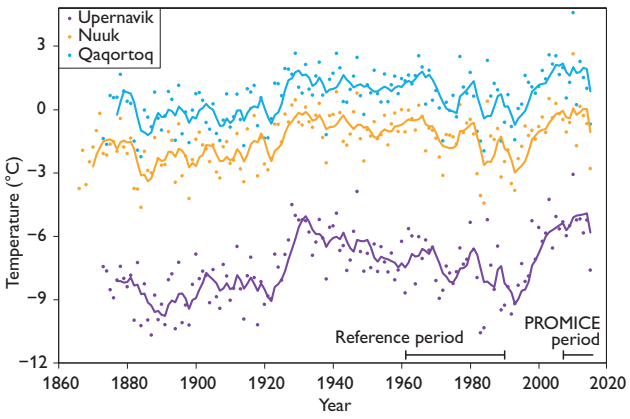

Fig. 2. Annual (dots) and five-year (lines) running-mean temperatures at the three longest-running DMI measurement sites used in this study. Arrows indicate the 1961–1990 reference period and the PROMICE period (2007–present).

Ice sheet surface melting occurs predominantly in summer, so for the purpose of this study we calculated the average June–July–August (JJA) temperature for each year, following e.g. Braithwaite *et al.* (1992). Temperature anomalies were calculated by subtracting the 1961–1990 JJA average. We obtained monthly average data from the DMI technical report 15-04 (Cappelen 2015) and supplemented these with 2015 data.

Table 1 shows that at all selected DMI sites the JJA temperature during the PROMICE observational period is higher than in the reference period. The smallest difference is found at Qaqortoq in South Greenland (0.8°C), and the largest at Ittoqqortoormiit in the east (2.4°C). For the years with PROMICE annual ablation values (2008–2015), only three out of a total of 64 station years (5%) had negative JJA temperature anomalies indicative of conditions colder than during the reference period, emphasising the need for a well-defined context.

Measurements of ice ablation along the ice-sheet margin

The first PROMICE weather stations were established in 2007 (Van As *et al.* 2011), thus providing annual net-ablation values since 2008 (i.e. end of melt season 2007 until end of melt season 2008). At any given site five to eight years' worth of ablation data exist. In this study we only make use of the eight weather stations that are located closest to the ice-sheet margin (all with suffix 'L' for 'lower'). At these elevations, summer ablation is much larger than winter accumulation, resulting in stronger correlations between net ablation and atmospheric temperature anomalies than higher on the ice sheet where ablation becomes an increasingly small contributor to the surface-mass budget. Selecting the 'lower' PROMICE stations provides us with a total of 56 ablation years.

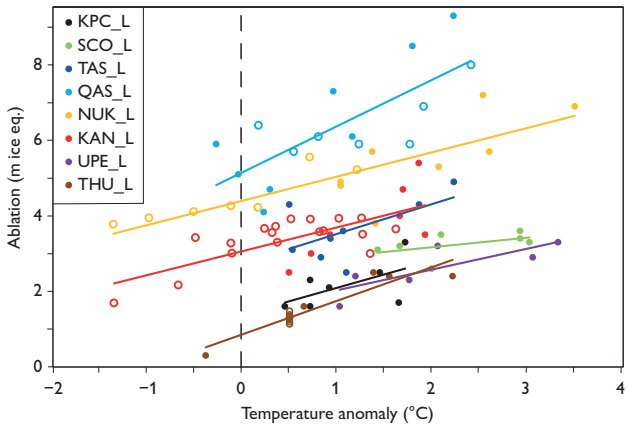

Fig. 3. Measured annual net ablation from PROMICE (dots) and other projects (circles) plotted against the regional temperature anomaly referenced to the 1961–1990 period. Lines illustrate linear least-squares fits.

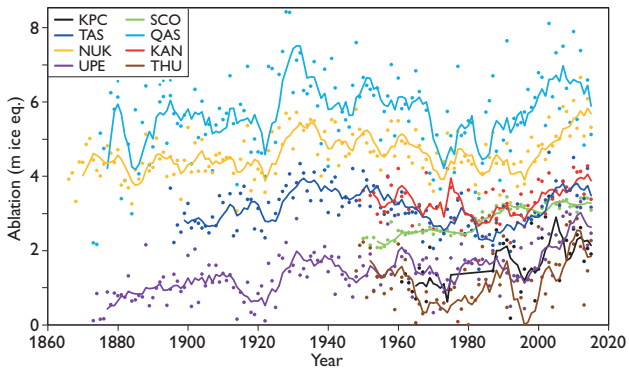

Fig. 4. Estimated yearly (dots) and five-yearly (lines) net ablation for sites currently instrumented by PROMICE.

We supplement the PROMICE data with older ablation observations gathered in close proximity to the current station locations, at identical elevations, and covering the entire 'hydrological' year, i.e. referenced to the end of the melt season. At four station sites, such measurements from before 2008 exist, namely at QAS_L for 2001–2007 (e.g. Podlech *et al.* 2004), at NUK_L for 1981–1987 (e.g. Braithwaite *et al.* 1992), at KAN_L since 1991 (Van de Wal *et al.* 2012) and at THU_L in 1954 (Schytt 1955). These 40 historical measurements bring our grand total to 96 ablation years.

Present-day ablation in a multi-decadal perspective

In this study we relate annual net-ablation values to JJA temperatures following e.g. Braithwaite *et al.* (1992), but without precipitation due to lacking DMI data. Besides, differences in precipitation at the DMI and PROMICE sites can be large due to spatial heterogeneity. In Fig. 3 we plotted the annual net-ablation values against the temperature anomalies calculated from DMI weather stations in the region. At all sites, the ablation totals typically increase with temperature, as indicated by the linear least-squares fit lines. The slopes of these lines are the regional temperature sensitivities, which is relatively low at the SCO_L site with 0.25 m ice equivalent (eq.) $°C^{-1}$, and high for QAS_L where roughly an additional 1.2 m of ice would ablate for every degree JJA temperature increase (Table 1). We find an average temperature sensitivity of the ice-marginal area of 0.71 ± 0.28 m ice eq. $°C^{-1}$ (standard deviation given), rather similar to the value of 0.5 m water eq. $°C^{-1}$ mentioned in e.g. Braithwaite *et al.* (1992).

A key element in this study is the ablation value at which the fitted lines intercept the 0°C temperature anomaly line, which for some sites requires extrapolation. The intercept values represent net ablation in the reference climate. Most PROMICE ablation values exceed the intercept values specific to their sites: ablation is larger in recent years than in the reference period. Table 1 shows that the largest relative increase is found at THU_L, where we estimate annual net ablation to have increased by *c.* 120%. The reference period adjustment for PROMICE ablation values is substantial at all sites (0.6–1.2 m ice eq., Table 1).

We need to be cautious in the interpretation of these results as the number of data points is still rather small. Furthermore, one cannot expect a perfect correlation between ablation and temperature because: (1) melt is the result of a surplus in energy at the ice-sheet surface, of which only part is provided by atmospheric heat content, (2) the horizontal and vertical distances between the DMI and PROMICE observation sites are considerable, and (3) winter accumulation is part of the net ablation signal but not a function of JJA temperatures. As a measure of uncertainty of reference-period ablation due to the above, we calculate the root mean squared differences (RMSD) between the measured and calculated values. These range from 0.2 to 0.9 m ice eq. (Table 1). To this we add a conservatively chosen measurement uncertainty in the annual net-ablation values of 0.3 m ice eq. (Fausto *et al.* 2012), resulting in total uncertainties ranging from 0.4 to 0.9 m ice eq. The largest uncertainty is found for QAS_L, likely due to interannual variability in winter accumulation and the station's positioning in an irregular, crevassed terrain prior to its 1.5 km relocation in 2009.

Through the above re-referencing procedure the 2015, ablation anomalies become considerably larger (Table 1, Fig. 1). After reference adjustment, we find positive

2015 anomalies for all sites except QAS_L, NUK_L and KAN_L, though these do not exceed their uncertainty ranges. The largest anomaly still occurs at THU_L, but is 184 ± 43% when referenced to the 1961–1990 climate, six times larger than the 30% value when referenced to the PROMICE average.

Approximating past ablation

The relations found between JJA temperature and annual net ablation in Fig. 3 can be used to estimate ablation from temperature in any year. In Fig. 4 we used these functions for all summers for which DMI temperature data are available – though some of the earlier data were discarded to maintain continuity. We assume the uncertainties listed in Table 1 to apply for these calculations as well, although it should be noted that the derived functions are less well constrained in the range with negative temperature anomalies (Fig. 3).

We conclude that at our study sites annual net ablation is likely to be larger in recent years than during any previous period in the instrumental era, covering up to 150 years. Especially at the more northern locations we find that ablation increases in recent years are large. Yet Fig. 4 suggests that in southern Greenland ablation peaked significantly around 1930. While most of Greenland underwent relatively warm (summer) conditions in the 1930s (Cappelen 2015), this was most notable at the more southern locations, resulting in amplified ablation values according to our estimates. JJA temperatures were higher in 1928 and 1929 than in any other year of the Qaqortoq record, both attaining values of 9.2°C. This suggests that ablation in those years may have exceeded the largest net ablation measured on the Greenland ice sheet (9.3 m ice eq. at QAS_L in 2010), although this is not beyond the uncertainty that accounts for important factors such as winter accumulation.

Acknowledgements

This is a publication in the framework of the DANCEA-funded Programme for Monitoring of the Greenland Ice Sheet (PROMICE), in collaboration with several other projects. The KAN stations are funded by the Greenland Analogue Project (GAP). Stake measurements by Utrecht University are funded through the NWO polar programme.

References

Andersen, M.L. *et al.* 2015: Basin-scale partitioning of Greenland ice sheet mass balance components (2007–2011). Earth and Planetary Science Letters **409**, 89–95.

Braithwaite, R.J., Olesen O.B. & Thomsen H.H. 1992: Calculated variations of annual ice ablation at the margin of the Greenland ice sheet, West Greenland, 1961–1990. Journal of Glaciology **38** (129), 266–272.

Cappelen, J. (ed.) 2015: Greenland – DMI historical climate data collection 1784–2014. Danish Meteorological Institute Technical Report **15–04**, 97 pp.

Dutton, A., Carlson, A.E., Long, A.J., Milne, G.A., Clark, P.U., DeConto, R., Horton, B.P., Rahmstorf, S. & Raymo, M.E. 2015: Sea-level rise due to polar ice-sheet mass loss during past warm periods. Science **349** (6244) aaa4019.

Enderlin, E.M., Howat, I.M., Jeong, S., Noh, M.-J., Van Angelen, J.H. & Van den Broeke, M.R. 2014: An improved mass budget for the Greenland ice sheet. Geophysical Research Letters **41** (3), 866–872.

Fausto, R.S., Van As, D., Ahlstrøm, A.P. & Citterio, M. 2012: Assessing the accuracy of Greenland ice sheet surface ablation measurements by pressure transducer. Journal of Glaciology **58** (212), 1144–1150.

Khan, S.A., Aschwanden, A., Bjørk, A.A.,Wahr, J., Kjeldsen, K.K. & Kjær, K.H. 2015: Greenland ice sheet mass balance: a review. Reports on Progress in Physics **78**, 046801.

Nghiem, S.V. *et al.* 2012: The extreme melt across the Greenland ice sheet in 2012. Geophysical Research Letters **39**, L20502.

Podlech, S., Mayer, C. & Bøggild, C.E. 2004: Glacier retreat, mass-balance and thinning: Sermilik Glacier, South Greenland. Geografiska Annaler **86A**, 305–317.

Rignot, E., Box, J.E., Burgess, E. & Hanna E. 2008: Mass balance of the Greenland ice sheet from 1958 to 2007. Geophysical Research Letters **35**, L20502.

Schytt, V. 1955: Glaciological investigations in the Thule Ramp area. Report Snow, Ice, and Permafrost Research Establishment **28**, 88 pp. Corps of Engineers, U.S. Army.

Tedesco, M. *et al.* in press: Greenland ice sheet [in 'State of the Climate in 2015']. Bulletin of the American Meteorological Society **97**(7).

Van As, D., Fausto, R.S. & PROMICE Project Team 2011: Programme for Monitoring of the Greenland Ice Sheet (PROMICE): first temperature and ablation records. Geological Survey of Denmark and Greenland Bulletin **23**, 73–76.

Van de Wal, R.S.W., Boot, W., Smeets, C.J.P.P., Snellen, H., Van den Broeke, M.R. & Oerlemans, J. 2012: Twenty-one years of mass balance observations along the K-transect, West Greenland. Earth Systems Science Data **4**, 31–35.

Authors' addresses

D.v.A., R.S.F., H.M., C.C., J.E.B., A.M.S., A.P.A., K.H., M.C. & S.B.A., *Geological Survey of Denmark and Greenland, Øster Voldgade 10, DK-1350 Copenhagen K, Denmark*. E-mail: *dva@geus.dk*

H.M. also at *Department of Geography, University of Zurich, Winterthurerstrasse 190, 8057 Zürich, Switzerland.*

K.H. also at *Natural History Museum, Copenhagen University, Øster Voldgade 5, DK-1350 Copenhagen K, Denmark.*

J.C., *Danish Meteorological Institute, Lyngbyvej 100, DK-2100 Copenhagen Ø, Denmark.*

R.S.W.v.d.W., *Institute for Marine and Atmospheric Research, Utrecht University, Princetonplein 5, 3584 CC Utrecht, The Netherlands.*

R.J.B., *School of Environment, University of Manchester, Oxford Road, Manchester M13 9PL, UK.*

Regional climate-model performance in Greenland firn derived from *in situ* observations

Charalampos Charalampidis, Dirk van As, Peter L. Langen, Robert S. Fausto, Baptiste Vandecrux and Jason E. Box

Recent record-warm summers in Greenland (Khan *et al.* 2015) have started affecting the higher regions of the ice sheet (i.e. the accumulation area), where increased melt has altered the properties of firn (i.e. multi-year snow). At high altitudes, meltwater percolates in the porous snow and firn, where it refreezes. The result is mass conservation, as the refrozen meltwater is essentially stored (Harper *et al.* 2012). However, in some regions increased meltwater refreezing in shallow firn has created thick ice layers. These ice layers act as a lid, and can inhibit meltwater percolation to greater depths, causing it to run off instead (Machguth *et al.* 2016). Meltwater at the surface also results in more absorbed sunlight, and hence increased melt in the accumulation area (Charalampidis *et al.* 2015). These relatively poorly understood processes are important for ice-sheet mass-budget projections.

Regional climate models (RCMs) simulate energy fluxes and mass transfer between the atmosphere and the ice-sheet surface. Their accuracy depends on model physics and numerical sophistication, as well as on the atmospheric forcing implemented at their boundaries based on global weather reanalyses or general circulation models (see below). Ice-sheet mass-budget calculations using RCMs therefore need to be validated against observations. In this study, we evaluate the performance of the subsurface scheme of the HIRHAM5 RCM (Christensen *et al.* 2006) by comparing it with firn temperatures measured at the KAN_U weather station from April 2009 to September 2013 (Charalampidis *et al.* 2016). We determine the reasons for temperature biases by comparing HIRHAM5 with a validated surface energy balance (SEB) model over the same period (Charalampidis *et al.* 2015).

Firn temperature measurements

Situated 1840 m above sea level (a.s.l.), KAN_U is the uppermost automatic weather station at an elevation transect of meteorological and mass-budget monitoring sites in the south-western part of the Greenland ice sheet (Charalampidis *et al.* 2015; 67°0′N, 47°1′W). The long-term equilibrium line altitude, where summer ablation balances winter accumulation, is 1553 m a.s.l. (Van de Wal *et al.* 2012). KAN_U is located above that, and thus monitors melt, percolation and refreezing in firn. Established in April 2009, the KAN_U record includes the high melt seasons of 2010, 2011 and 2012 (Charalampidis *et al.* 2015).

The subsurface temperature analysis by Charalampidis *et al.* (2016) revealed that in the 2010 and 2011 high melt summers, meltwater occupied the pore volume between 2 and 3 m below the surface (Fig. 1A). The continued refreezing of this temporarily retained, near-surface liquid water until after the end of both the 2010 and 2011 melt seasons contributed to the merging of superimposed annual ice layers. These ice layers were observed at depths between 2.5 and 5.5 m in May 2012 (Machguth *et al.* 2016). Subsequently, meltwater by the end of August 2012 was confined in the upper 2.5 m relative to the May 2012 surface, with subsequent runoff in response to the intense surface lowering. By September 2012, after the onset of cold atmospheric conditions, refreezing occurred below 2.5 m by meltwater percolation to the limited available pore volume between the ice layers. The latent heat release by refreezing at depth in autumn 2012 resulted in a high December–January–February average firn temperature of –6.1°C between 2 and 5 m depth (Charalampidis *et al.* 2016), while the accumulating snow cover provided thermal insulation from the cold winter atmosphere.

The HIRHAM5 regional climate model

We use HIRHAM5 at 5 × 5 km horizontal resolution, which has demonstrated good results for the climate of the Greenland ice-sheet margin (e.g. Langen *et al.* 2015). It uses 31 vertical atmospheric levels and a time step of 90 seconds. At the lateral boundaries, the model is forced at 6-hour intervals with wind, temperature, specific humidity and atmospheric pressure from the ERA-Interim weather reanalysis (Dee *et al.* 2011). The model computes processes in the atmosphere, including clouds, solar radiation attenuation, longwave radiation emission and precipitation. These variables then determine the energy balance and mass budget at the surface. Daily-smoothed, MODIS-derived surface albedo regulates solar radiation absorption (Box *et al.* 2012).

© 2016 GEUS.

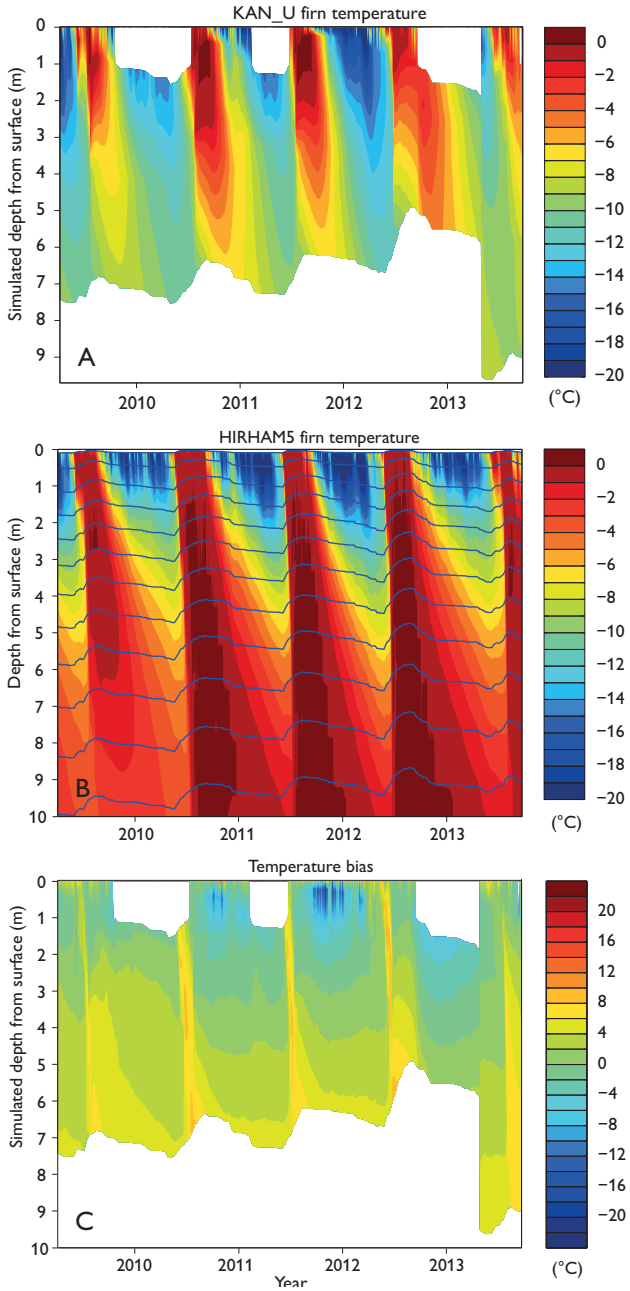

Fig. 1. **A**: Firn temperatures observed at KAN_U (Charalampidis *et al.* 2016). **B**: HIRHAM5-simulated firn temperatures at the location of KAN_U, with the blue lines indicating the simulated depth of the mid-point of each layer. **C**: The difference between the two (B minus A).

The subsurface scheme (version 7.11) uses 25 layers with a total depth of 70 m water equivalent (*c.* 78 m physical distance at KAN_U). It accounts for heat diffusion, vertical water transport and refreezing, as well as temperature, and pressure-dependent densification of snow and firn after Vionnet *et al.* (2012). Each layer can hold liquid water corresponding to 2% of the snow pore volume and excess water percolates downward to the next layer. Water is assumed to run off when it encounters a layer of pore close-off density (i.e. 830 kg/m^3; Herron & Langway 1980). Before runoff occurs, the water is available for superimposed ice formation onto the ice layer.

Simulated versus observed firn temperatures

The HIRHAM5-simulated firn temperature evolution at KAN_U is shown in Fig. 1B. A seasonality following surface forcing is evident: 0°C from summer melting and about –20°C near the surface in winter. During the melt season, the simulation shows maximum firn temperature at depths *c.* 2 m in 2009 and *c.* 9 m in 2010, and even deeper in the following years. Accordingly, the extent of the simulated temperate layer (i.e. temperatures between –1 and 0°C) increases from 6 m in summer 2009 to more than 10 m in 2010 and the following melt seasons. The propagation of the temperate conditions at depth suggests concurrent meltwater percolation, refreezing and latent heat release. However, the observed temperate layer did not extend below 3 m at any point (Fig. 1A).

The firn temperature bias (simulated minus observed) is shown in Fig. 1C by comparing the interpolated HIRHAM5 values at observational depths with the observed ones. The model bias is mostly positive and increases with depth. Typical differences for the deepest measurements range between +6 and +12°C. Negative differences occur during winter at depths less than 2 m in all years except 2012. In winter 2012, the RCM underestimates firn temperatures as deep as 3 m.

Table 1 shows the average summer and winter HIRHAM5 firn temperatures at specific depths, and the biases. The summer difference averaged over all available depths is +5.7°C. Better agreement between HIRHAM5 and observations is found for winter with an average difference of +3.2°C. In winter 2012, HIRHAM5 agreement is best, and is the only instance in the comparison when model bias at any of the listed depths was negative. This agreement is indicative of the abnormally warm conditions that persisted in the top 2–5 m firn after the extreme 2012 melt season, but also of the efficiency of the HIRHAM5 simulation of surface-heat transfer into firn.

Explaining the bias

Subsurface differences between RCM and the observations can be due to differences in surface melt, quantity and depth of meltwater percolation and the timing of refreezing.

Table 1. Average HIRHAM5 firn temperatures, linearly interpolated to specific depths (left columns) and biases (right columns) at KAN_U (Charalampidis *et al.* 2016)

Depth	2009		2010		2011		2012		2013	
Summer temperatures (°C; June–July–August)										
2 m	–2.9	+3.1	–0.4	+4.3	–1.9	+3.5	–0.3	+5.3	–4.2	+3.5
3 m	–3.6	+4.7	–1.0	+5.5	–2.3	+4.7	–1.1	+5.9	–4.4	+4.5
4 m	–3.6	+6.1	–1.5	+6.5	–2.3	+6.0	–1.4	+6.9	–4.1	+5.1
5 m	–3.6	+6.3	–1.7	+7.1	–2.1	+6.8	–1.3	–	–3.6	+5.7
6 m	–3.4	+6.7	–1.8	+7.9	–1.7	+7.7	–1.2	–	–3.0	+6.4
Following winter temperatures (°C; December–January–February)										
2 m	–9.5	+3.2	–8.9	+0.7	–12.2	+0.3	–8.7	–2.0	–	–
3 m	–6.5	+4.6	–5.9	+1.7	–8.4	+2.2	–6.0	+0.1	–	–
4 m	–4.6	+5.1	–3.8	+3.2	–5.5	+4.1	–4.0	+1.9	–	–
5 m	–3.4	+5.9	–2.3	+4.7	–3.3	+5.7	–2.6	+3.2	–	–
6 m	–2.7	+6.4	–1.2	+5.8	–1.9	+6.4	–1.6	–	–	–

The comparison of HIRHAM5 with a validated SEB model forced by *in situ* observation data (Charalampidis *et al.* 2015) shows good agreement in simulated melt estimates (Fig. 2A). HIRHAM5 slightly underestimates melt in all years (differences less than 31 MJ/m^2) except 2011 (excess of 7 MJ/m^2). The cumulative difference in melt energy between the two models over the course of five melt seasons amounts to 68 MJ/m^2, approximately equal to the total melt in July 2013. This suggests that the positive firn temperature biases are not due to exaggerated melt.

HIRHAM5 substantially underestimates refreezing (Fig. 2B). The differences are less than 15% in all years except 2012, when the difference is 44% and approximately equal to total refreezing in 2013 (380 kg/m^2). With well-simulated melt and underestimated refreezing by HIRHAM5, the firn temperature bias is due to prolonged wintertime refreezing at great depth. As a result of the overestimated latent heat release at depth during every year, HIRHAM5 wintertime low temperature extremes remain at depths no greater than *c.* 3 m (Fig. 1B).

Both HIRHAM5 and Charalampidis *et al.* (2015) overestimate the percolation depth. As analysed by Charalampidis (2016), the SEB model captures the thermal evolution of firn well. The model was initialised on 4 April 2009 based on firn temperature observations, and height-corrected 2012 firn densities, thus calculating realistic cold content (i.e. the required energy to raise firn temperature at 0°C) and heat diffusion estimates throughout the 4.5-year simulation. The SEB model does not calculate liquid water retention, thus all percolating meltwater is refrozen at every time step, which is incorrect close to the surface (2–3 m depth; Fig. 1A). However, no refreezing (i.e. no latent heat release) after the melt season at depth results in more realistic wintertime cooling of deep firn.

HIRHAM5 was initiated more than two decades before 2009. Additionally, the current subsurface scheme of HIRHAM5 cannot reproduce ice layers. This inability results in unrealistic representation of firn stratigraphy, and thus estimation of cold content, which is dependent on firn temperature and density. On 4 April 2009, the thermal state of the subsurface in HIRHAM5 is the integrated result of all previous simulation years, and is already on average 4.6°C too warm in the upper 10 m of firn (Fig. 1C). The associated cold content integrated over the first 10 m is 72 MJ/m^2. By

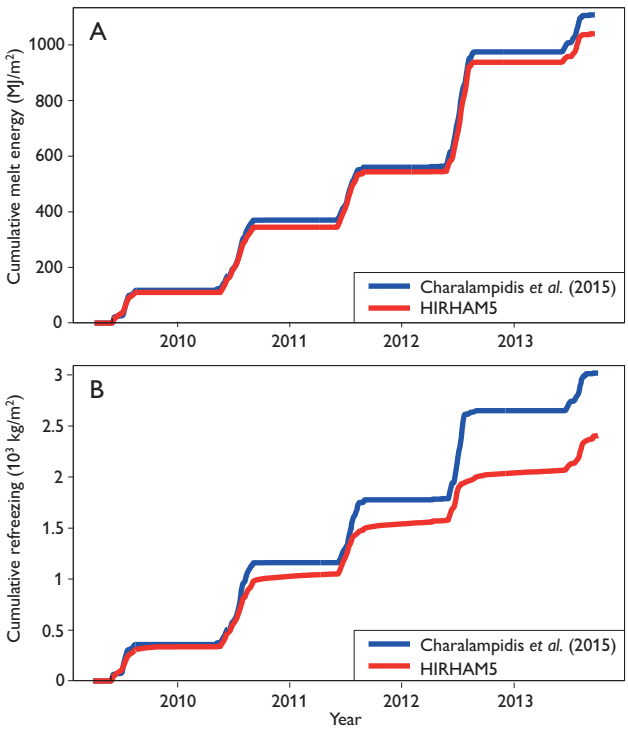

Fig. 2. Cumulative melt energy (**A**) and total refreezing (**B**) at KAN_U by HIRHAM5 and Charalampidis *et al.* (2015).

comparison, the cold content on the same day in Charalampidis *et al.* (2015) is 151 MJ/m^2. One third of the difference in cold content is due to differences in firn density.

Near-complete cold content depletion (i.e. firn temperature at 0°C) of the first 10 m of firn is simulated by HIRHAM5 for 2010. Thereafter, this temperate firn retains liquid water, which refreezes during winter under the influence of subfreezing conditions diffused from the surface. This results in wintertime latent heat release at depth that in 2010 to 2012 is sustained until the beginning of the following melt season (Fig. 2B). Eventually, this premature depletion of cold content leads to overestimation of the percolation depth, liquid water retention and heat in firn.

Concluding remarks

Judging from the simulation of wintertime firn temperatures in the period April 2009 to September 2013, HIRHAM5 is able to realistically reproduce subsurface processes when heat conduction dominates. Yet the comparison of HIRHAM5 with observations and SEB model output reveals an overestimation of the percolation depth, liquid water retention and heat input from refreezing.

For April 2009, HIRHAM5 calculates less than half of the cold content estimate based on observations in the first 10 m of firn. This is the result of the 1989 initialisation of HIRHAM5 and thus the cumulative effect of the imprecise determination of heat diffusion, as HIRHAM5 is unable to adequately represent ice-layer formation in firn. A HIRHAM5 subsurface scheme with improved accounting of shallow firn stratigraphy would greatly improve heat diffusion estimates over long simulation periods, and thus provide more reliable simulations.

Acknowledgements

The KAN_U weather station is funded by the Greenland Analogue Project, with contributions from the Programme for Monitoring of the Greenland Ice Sheet (PROMICE). This is a PROMICE publication and contribution number 76 of the Nordic Centre of Excellence SVALI, 'Stability and Variations of Arctic Land Ice', funded by the Nordic Top-level Research Initiative (TRI). The study has been supported by the Danish Council for Independent research (DFF) project 4002-00234 'Understanding and predicting non-linear change in the permeability of Greenland firn'.

References

Box, J.E., Fettweis, X., Stroeve, J.C., Tedesco, M., Hall, D.K. & Steffen, K. 2012: Greenland ice sheet albedo feedback: thermodynamics and atmospheric drivers. The Cryosphere **6**, 821–839.

Charalampidis, C. 2016: Climatology and firn processes in the lower accumulation area of the Greenland ice sheet. Digital comprehensive summaries of Uppsala Dissertations from the Faculty of Science and Technology **1372**, 81 pp. Acta Universitatis Upsaliensis, Uppsala, Sweden.

Charalampidis, C., van As, D., Box, J.E., van den Broeke, M.R., Colgan, W.T., Doyle, S.H., Hubbard, A.L., MacFerrin, M., Machguth, H. & Smeets, C.J. 2015: Changing surface–atmosphere energy exchange and refreezing capacity of the lower accumulation area, West Greenland. The Cryosphere **9**, 2163–2181.

Charalampidis, C., van As, D., Colgan, W.T., Fausto, R.S., Macferrin, M. & Machguth, H. 2016: Thermal tracing of retained meltwater in the lower accumulation area of the southwestern Greenland ice sheet. Annals of Glaciology, available on CJO2016, *http://dx.doi.org/10.1017/aog.2016.2*

Christensen, O.B., Drews, M., Christensen, J.H., Dethloff, K., Ketelsen, K., Hebestadt, I. & Rinke, A. 2006: The HIRHAM regional climate model version 5. Danish Meteorological Institute Technical Report **06–17**, 22 pp. Copenhagen: Danish Meteorological Institute.

Dee, D.P. *et al.* 2011: The ERA-Interim reanalysis: configuration and performance of the data assimilation system. Quarterly Journal of the Royal Meteorological Society **137**, 553–597.

Harper, J., Humphrey, N., Pfeffer, W.T., Brown, J. & Fettweis, X. 2012: Greenland ice-sheet contribution to sea-level rise buffered by meltwater storage in firn. Nature **491**, 240–243.

Herron, M.M. & Langway, C.C. 1980: Firn densification: an empirical model. Journal of Glaciology **25**(93), 373–385.

Khan, S.A., Aschwanden, A., Bjørk, A.A., Wahr, J., Kjeldsen, K. & Kjær, K. 2015: Greenland ice sheet mass balance: a review. Reports on Progress in Physics **78**(4), 046801.

Langen, P.L. *et al.* 2015: Quantifying energy and mass fluxes controlling Godthåbsfjord freshwater input in a 5-km simulation (1991–2012). Journal of Climate **28**, 3694–3713.

Machguth, H., MacFerrin, M., van As, D., Box, J.E., Charalampidis, C., Colgan, W., Fausto, R.S., Meijer, H.A.J., Mosley-Thompson, E. & van de Wal, R.S.W. 2016: Greenland meltwater storage in firn limited by near-surface ice formation. Nature Climate Change **6**, 390–393.

Van de Wal, R.S.W., Boot, W., Smeets, C.J.P.P., Snellen, H., van den Broecke, M.R. & Oerlemans, J. 2012: Twenty-one years of mass balance observations along the K-transect, West Greenland. Earth System Science Data **4**, 31–35.

Vionnet, V., Brun, E., Morin, S., Boone, A., Faroux, S., Le Moigne, P., Martin, E. & Willemet, J.-M. 2012: The detailed snowpack scheme Crocus and its implementation in SURFEX v7.2. Geoscientific Model Development **5**, 773–791.

Authors' addresses

C.C., D.v.A., R.S.F., B.V. & J.E.B., *Geological Survey of Denmark and Greenland, Øster Voldgade 10, DK-1350 Copenhagen K.* E-mail: *cc@geus.dk*

P.L.L., *Climate and Arctic Research, Danish Meteorological Institute, Lyngbyvej 100, DK-2100 Copenhagen Ø, Denmark.*

C.C., also at: *Department of Earth Sciences, Uppsala University, Villavägen 16, SE-752 36 Uppsala, Sweden.*

B.V., also at: *Arctic Technology Centre (ARTEK), Technical University of Denmark, Brovej, byg. 118, DK-2800 Kgs. Lyngby, Denmark.*

Crustal structure over the Nagssugtoqidian deformation front in West Greenland: Receiver Function analysis

Trine Dahl-Jensen, Peter H. Voss and Tine B. Larsen

A marked change in crustal thickness is seen at the deformation boundary between the undisturbed Archaean core in the south and reworked Archaean gneiss in the foreland of the Nagssugtoqidian orogen in West Greenland. In addition, intra-crustal boundaries can be tentatively interpreted. This is the first information on crustal structure in the area, which is known for kimberlite, carbonatite and ultramafic lamprophyre occurrences, and diamond exploration.

The information is based on two summer seasons of passive seismological data – earthquakes – recorded on five broadband seismological stations placed on an almost 200 km long profile crossing the deformation boundary. The stations were installed in the remote area with solar panels and batteries. Between 11 and 27 distant earthquakes were recorded on each of the five stations used for the Receiver Function analysis.

Geological background

The Receiver Function profile (Fig. 1) is located on Precambrian rocks in Central West Greenland. It crosses over a deformation front marking the southern Nagssugtioqidian front defined by the transition from undeformed, discordant dykes in the south to extensively deformed dykes in the southern Nagssugtoqidian orogen in the north. Between the Inland Ice and Sukkertoppen ice cap this front is marked by a sharp change in aeromagnetic signatures (van Gool *et al.* 2002). The structural front coincides with a metamorphic transition and marks the southernmost boundary of penetrative Palaeoproterozoic reworking at amphibolite facies. There is a continuity of lithologies across the southern Nagssugtoqidian front, and reverse, south-directed thrusting shows that the southern Nagssugtoqidian orogen is a parautochthonous foreland belt (van Gool *et al.* 2002).

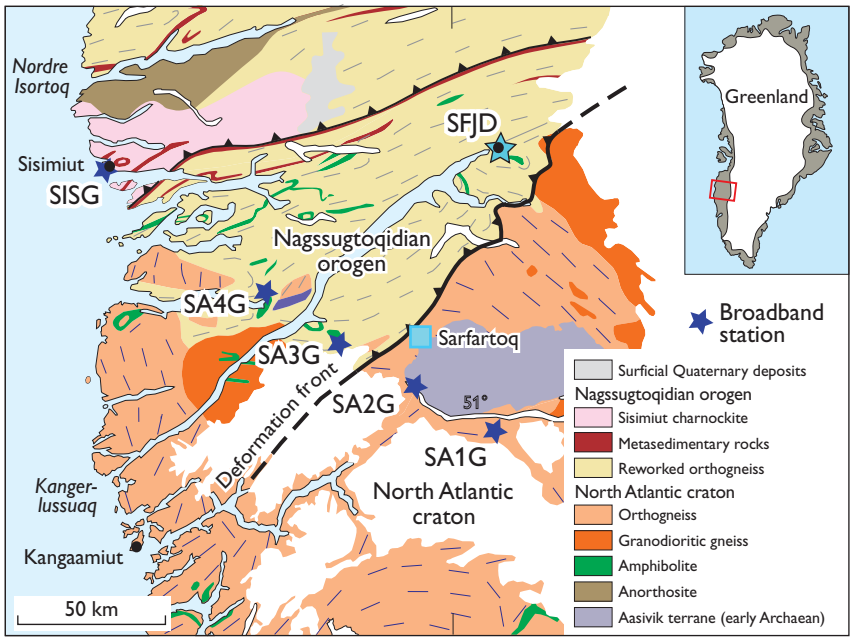

Fig. 1. Geological map of the area (Henriksen *et al.* 2009). The location of the deformation front is based on aeromagnetic data (Rasmussen & van Gool 2000). The stations used are indicated by a blue star. The station SFJD was not used.

Fig. 2. The seismic stations. The almost 100 % exposure of bedrock allows for all stations to be placed on hard rock. **A**: SA1G. The completed installation in 2006 with solar panels facing south, the sensor placed on bedrock and insulated, and just as the datalogger, protected against the elements. Photo: K.K Sand. **B**: SA2G was installed in 2006. Photo: P.H.Voss. **C**: SA4G packed in 2007 for return. Photo: H. Rasmussen. **D**: From SA3G. The seismic stations were deployed and returned by an Air Greenland AS350. Photo: H. Rasmussen.

Data and method

Receiver Function (RF) analysis relies on recording naturally occurring earthquakes followed by the isolation of S-waves generated locally at geological boundaries under the recording station from incoming P-waves from distant earthquakes (Ammon 1991).

Data acquisition

To acquire data, five seismometer stations were installed along a profile with *c.* 34 km distance (Fig. 1). Four of the stations where located in the wilderness (Fig. 2), and one in the town of Sisimiut. The stations were equipped with Güralp-3T broadband 3-component sensors and 24 bit SAM data loggers, recording data locally. The stations recorded data from June 2006 to early September 2007. Power was supplied by batteries, charged by solar panels. Consequently the stations did not record in November, December and January when the lack of sunlight prohibited charging the batteries. For each station, teleseismic events were selected in several steps. Lists of events over magnitude 5.0 were generated from international earthquake catalogues (USGS 2015), and useable events were selected by individual inspection of the recorded waveforms. The noise conditions varied from station to station.. In total, 41 individual earthquakes (Fig. 3) were accepted for analysis on one or more of the five stations, resulting in 95 earthquake records for RF analysis. The number of accepted records varied from 11 to 27 on the individual stations. The events range from magnitude 5.3 to 8.3 and cover a large azimuth and distance range around Sarfartoq.

Method

For each of the records the RF was calculated (Kind *et al.* 1995; Yuan *et al.* 1997). First, a bandpass filter of 2–50 sec (0.5–0.02 Hz) was applied. Then the P phases were rotated in three dimensions to minimise early energy on the radial and transverse components. This procedure aligns one component (L) with the incoming P energy, one (Q) with the SV energy and one (T) with SH energy. The energy from the P-S converted phases should then be isolated on the Q component, and the T component should not contain any energy if the structure beneath the station is horizontally stratified. The obtained inclination and azimuth were compared to the theoretical values calculated using the IASP91 model (Kennett & Engdahl 1991), and events discarded if the inclination differed by more than around 5° and azimuth by more than 10–15°. The Q component was then deconvolved with the L component (Ammon 1991) to produce the 95 receiver functions (RFs). The final step is to depth-convert and back-trace each RF in 3D in the earth and project the data onto a profile following the method described in (Yuan *et al.* 1997).

Results

Figure 4 shows the back-traced receiver functions from each station along the profile. The RFs overlap more and more with depth, providing a complete cover at *c.* 50 km depth for the four inland stations where the distance between stations is *c.* 34 km. The Mohorovicic discontinuity (Moho) is clearly seen, as well as some indications of intra-crustal boundaries. The frequency content of the RF is low (0.5–0.02 Hz) so we cannot expect to resolve structural details. The depth to Moho varies from just under 40 km at the SE (inland) end of the profile to just under 50 km at the NW end, which lies offshore. The change of depth to Moho appears as a slope dipping 18° towards NW in the plane of the profile, starting at the location where the profile crosses the deformation front, and thus at the sharp boundary seen on the aeromagnetic data (Rasmussen & van Gool 2000; van Gool *et al.* 2002). The crustal thickness at Kangerlussuaq (SFJD, Fig. 1) is 47 km (Dahl-Jensen *et al.* 2003), correlating well with the thickness along the profile NW of the deformation zone. South of the deformation front, the shallower Moho also is in agreement with thinner crust reported in the Archaean block in South Greenland (Dahl-Jensen *et al.* 2003). The slope on Moho starts directly underneath the location of the deformation front on the surface, indicating that the deformation front is fairly steep. The intra-crustal boundaries are poorly defined, due to the relatively large distance between the stations, but all indicate a dip towards NW, mimicking the slope on the Moho. To the SE of the deformation front the intracrustal converters seem weaker, possibly indicating the more undisturbed Archaean rocks of the North Atlantic craton.

Fig. 3. In all, 41 events were selected for RF analysis recorded on one or several of the five stations on the profile (green triangle). The events (red dots) are scaled by magnitude, ranging from 5.3 to 8.3.

Evaluation and outlook

This study illustrates that recording distant earthquakes over a period of several months, along a profile of seismological sensors can be utilised to image local, large-scale structures, which are valuable in areas where active source seismic acquisition is very costly. The profiles obtained can provide information on crustal thickness and intra-crustal structure. Higher resolution images than available in this study can be obtained if station spacing is smaller. RFs also

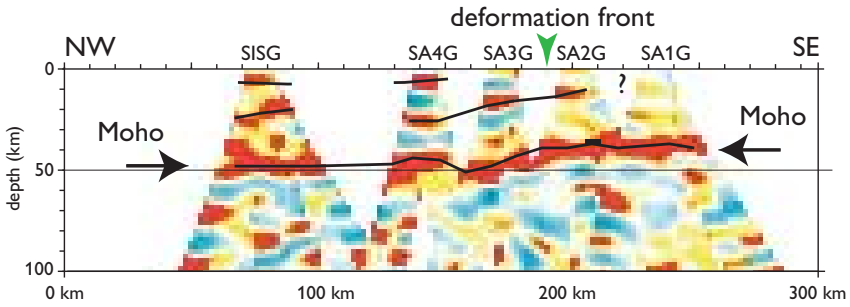

Fig. 4. The profile is scaled 1:1 horizontally and vertically; no vertical exaggeration. Red colour marks a conversion at an interface with higher impedance below the boundary (increasing velocity and density with depth). Under each station the backtraced traces from the individual RF derived from different earthquakes can be seen as a cone, overlapping more with depth. The interpretation of Moho and intra-crustal converters are marked with a thin black line.

allow mapping of deeper structures in the mantle. The study area is an exploration area for diamonds (Tappe *et al.* 2011), and information on the lithosphere will contribute to the understanding of the generation of diamond-bearing formations. A next step will be to look for converted phases from the base of the lithosphere. These are expected to have a negative polarity as the velocities are expected to drop at the transition from the lithosphere into the asthenosphere. For example, in East Greenland a similar profile outlined a fossil subduction zone (Schiffer *et al.* 2014).

Acknowledgements

SeisUK at University of Leicester lent us the instruments for data collection. The Ministry of Mineral Resources, Greenland, provided the funds for the installation, operation and recovery of the stations in Greenland.

References

Ammon, C.J. 1991: The isolation of receiver effects from teleseismic P-waveforms. Bulletin of the Seismological Society of America **81**(6), 2504-2510.

Dahl-Jensen, T., Larsen, T.B., Woelbern, I., Bach, T., Hanka, W., Kind, R., Gregersen, S., Mosegaard, K., Voss, P. & Gudmundson, O. 2003: Depth to Moho in Greenland: receiver-function analysis suggests two Proterozoic blocks in Greenland. Earth and Planetary Science Letters **205**(3-4), 379–393.

Henriksen, N., Higgins, A.K., Kalsbeek, F. & Pulvertaft, T.C.R. 2009: Greenland from Archaean to Quaternary. Descriptive text to the 1995 Geological map of Greenland, 1:2 500 000. 2nd edition. Geological Survey of Denmark and Greenland Bulletin **18**, 126 pp.

Kennett, B.L.N. & Engdahl, E.R. 1991: Traveltimes for global earthquake location and phase identification. Geophysical Journal International **105**(2), 429–465.

Kind, R., Kosarev, G.L. & Petersen, N.V. 1995: Receiver functions at the stations of the German Regional Seismic Network (GRSN). Geophysical Journal International **121**(1), 191–202.

Rasmussen, T.M. & van Gool, J.A. 2000: Aeromagnetic survey in southern West Greenland: project Aeromag 1999. In: Dawes, P.R. & Higgins, A.K. (eds): Review of Greenland activities 1999. Geology of Greenland Survey Bulletin **186**, 73–77.

Schiffer, C., Balling, N., Jacobsen, B.H., Stephenson, R.A. & Nielsen, S.B. 2014: Seismological evidence for a fossil subduction zone in the East Greenland Caledonides. Geology **42**(4), 311–314.

Tappe, S., Pearson, D.G., Nowell, G., Nielsen, T., Milstead, P. & Muehlenbachs, K. 2011: A fresh isotopic look at Greenland kimberlites: Cratonic mantle lithosphere imprint on deep source signal. Earth and Planetary Science Letters **305**(1–2), 235–248.

USGS 2015: National Earthquake Information Center - NEIC. *http://earthquake.usgs.gov/earthquakes/?source=sitenav*: United States Geological Survey.

van Gool, J.A.M., Connelly, J.N., Marker, M. & Mengel, F.C. 2002: The Nagssugtoqidian Orogen of West Greenland: tectonic evolution and regional correlations from a West Greenland perspective. Canadian Journal of Earth Sciences **39**, 665–686.

Yuan, X., Ni, J., Kind, R., Mechie, J. & Sandvol, E. 1997: Lithospheric and upper mantle structure of southern Tibet from a seismological passive source experiment. Journal of Geophysical Research **102**(B12), 27491–27500.

Authors' address

Geological Survey of Denmark and Greenland, Øster Voldgade 10, DK-1350 Copenhagen K, Denmark; E-mail: *tdj@geus.dk*

New geophysical and geological mapping of the eastern Baffin Bay region, offshore West Greenland

Ulrik Gregersen, Paul C. Knutz and John R. Hopper

The Geological Survey of Denmark and Greenland has carried out a detailed mapping project in the eastern Baffin Bay region covering *c.* 200 000 km^2 (Fig. 1). The purpose of the study was to update the previous mapping by using the most recent data and provide an improved basis for evaluation of the geological development and hydrocarbon potential of the region. After licensing rounds in 2007–2008 and 2010 considerable new geophysical and geological data were acquired in the region, and the extensive database now includes more than 100 000 km 2D seismic data and a number of wells (Fig. 1). The results of the work are summarised below and suggest deep basins and large ridges with complex structures.

Geological setting

In areas along the West Greenland continental margin, a number of basins with Proterozoic, Cretaceous and Cenozoic sedimentary successions have been identified (e.g., Dawes 1997; Dam *et al.* 2009; Rolle 1985). A number of rifted basins with large structural highs are interpreted to have developed in the east Baffin Bay region (Whittaker *et al.* 1997; Gregersen *et al.* 2013). During the Paleocene and Eocene, oceanic crust developed in central Baffin Bay and the Cretaceous rifted continental margin of West Greenland was separated from eastern Canada (Oakey & Chalmers 2012). The large-scale movements between Greenland and Canada generated new structures during the Palaeogene and reactivated faults within Cretaceous basins.

Results

The study included seven sub-projects: (1) seismic interpretation and mapping; (2) well correlation; (3) biostratigraphy; (4) seismic facies analysis and seismic inversion; (5) overview of source rocks; (6) maturity modelling; and (7) structural development. This paper describes some key results from the seismic interpretation and structural development. Interpretation of horizons and units were carried out with Schlumberger Petrel© software and included data from wells, seismic surveys, gravity surveys and magnetic surveys. Additional data from seabed sampling and outcrops in the region were used for geological interpretation and as analogues. A robust framework was established with fourteen seismic stratigraphic horizons (A1–Hx) and eleven mega-units (A–H). Seismic cross-sections show deep, rifted basins separated by large structural highs (Fig. 2). The lateral extends and topography of the basins and structures are outlined in depth-structure maps (Fig. 3).

In the Kap York Basin (Fig. 4), the upper part of mega-unit H can be correlated to parts of a 4.6 km/sec. TWT velocity zone from refraction seismic lines of Reid & Jackson (1997). They interpreted this zone to include Thule Supergroup sedimentary rocks, which crop out north of the study area (Dawes 1997). Thus the upper part of mega-unit H below horizon H1 (Fig. 2) probably includes sedimentary rocks with some analogues to the Thule Supergroup. Seismic interpretation suggests that some of the

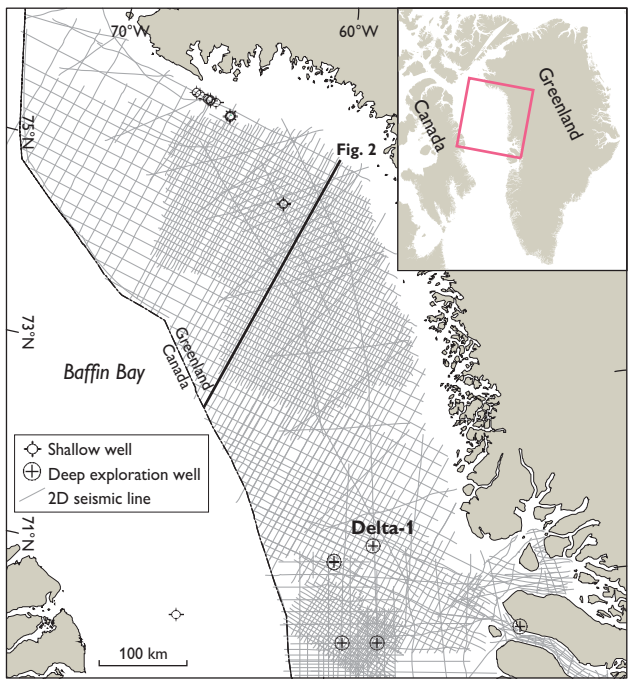

Fig. 1. Map of the study area in eastern Baffin Bay with 2D seismic data used and the location of shallow and deep exploration wells. Location of the seismic line of Fig. 2 is also shown.

© 2016 GEUS.

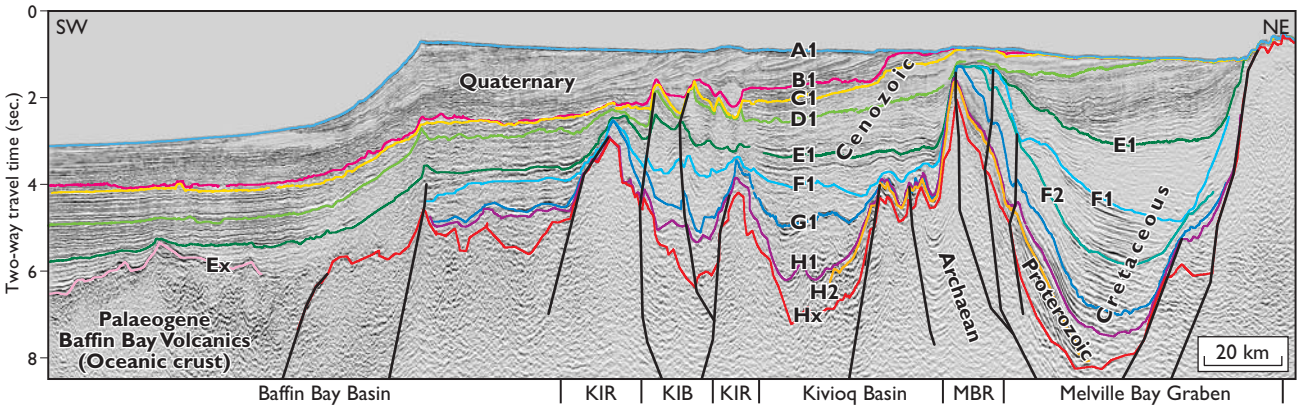

Fig. 2. Seismic line NE–SW across the eastern Baffin Bay region showing deep basins and large structures. The horizon boundaries of the seismic mega-units A–H are shown by coloured horizons from A1 to Hx and likely ages are shown. Note that some of the major deep-seated faults continue nearly vertically upwards through parts of the Cenozoic section indicating late compressional faulting. The names of the main structural elements are shown below the line and are from SW to NE: Baffin Bay Basin. **KIR**: Kivioq Ridge. **KIB**: Kivioq Basin. **MBR**: Melville Bay Ridge. Melville Bay Graben (Fig. 4). The seismic line is courtesy of TGS-NOPEC Geophysical Company ASA. Location of the seismic line is shown in Fig. 1.

wedge-shaped units in mega-unit H (Fig. 2) were probably formed by extension during the Proterozoic.

Sedimentary successions in the Baffin Bay may also resemble those from the Nuussuaq Basin, where Cretaceous nearshore to deltaic sandy deposits were documented (Dam *et al.* 2009). Seismic interpretation below horizon F1 (mega-unit F) shows prograding-aggrading clinoforms and troughs or channels possibly from deltaic systems (Gregersen *et al.* 2013).

During parts of the Late Cretaceous, relative tectonic quiescence prevailed and thick uniform units were deposited in the basins. Marine mudstone deposits with suggested source-rock intervals and oil seeps were recovered from both West Greenland (Bojesen-Koefoed *et al.* 1999) and northern East Canadian islands (MacLean & Williams 1983; Brent *et al.* 2013). Within the mapped basins, these marine mudstones may be analogous to deposits in mega-units E and F, between horizons E1 and G1 (Fig. 2). Extensional faulting occurred during the Late Cretaceous to earliest Paleocene by local rifting in the Nuussuaq Basin (Dam *et al.* 2009) and locally in a few other places in the region.

In north-eastern Baffin Bay, major Cretaceous rift basins trend SE–NW and are located east of the Kivioq Ridge (Fig. 4). West of the Kivioq Ridge, extensive volcanic areas have been mapped primarily from seismic reflection and magnetic anomaly data (Fig. 4). Studies with refraction seismic data (Damm 2010; Suckro *et al.* 2012; Altenbernd *et al.* 2014) showed oceanic crust in the eastern part of the Baffin Bay Basin. Seismic facies analyses combined with interpretation of magnetic data in the present study and in Gregersen *et al.* (2013) outline the eastern boundary of the oceanic crust (also named Baffin Bay Volcanics) at nearly the same location (Figs 2, 4). The oceanic crust developed as Greenland and its rifted margin separated from Canada during the Paleocene and Eocene (Oakey & Chalmers 2012). The north-east and northward movements of Greenland's rifted basins caused compression-related

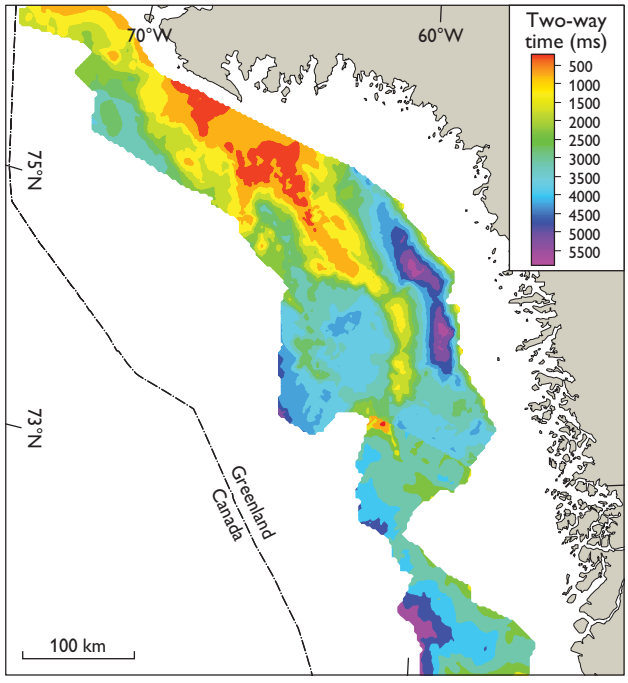

Fig. 3. Depth-structure map of horizon F1 with two-way travel time. This level is not drilled in the region but interpretation suggests that the horizon may be of a Late Cretaceous (Campanian?) age. The map illustrates the outline of large structures and basins of eastern Baffin Bay.

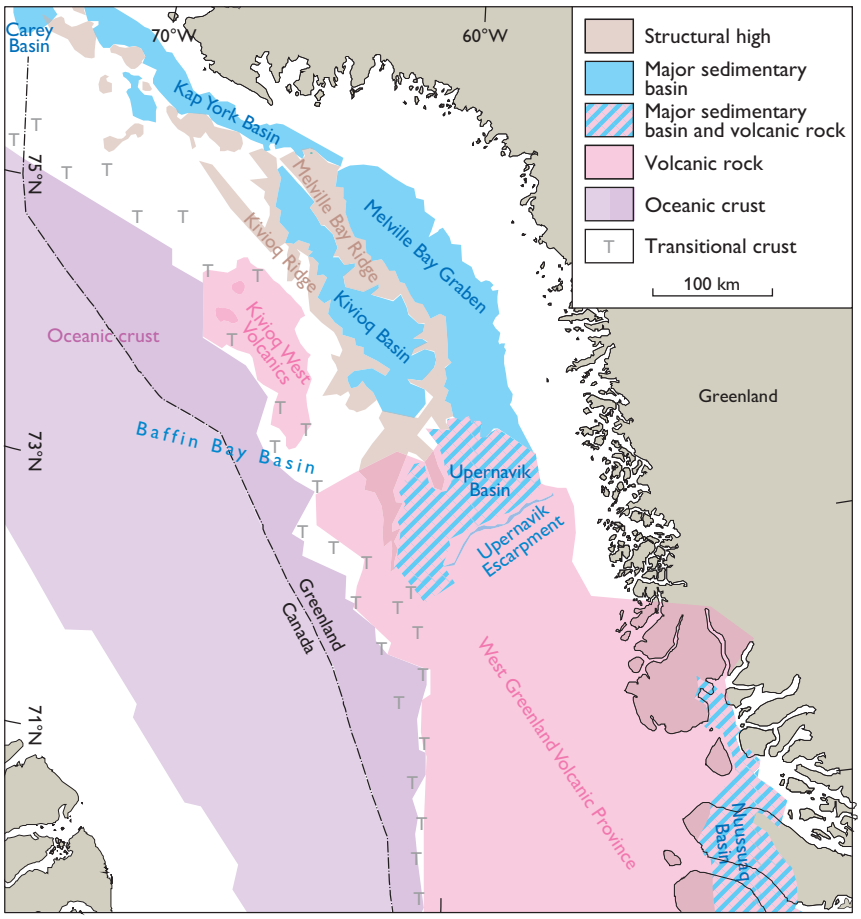

Fig. 4. Structural elements map of eastern Baffin Bay. The extent of the Canadian part of the Baffin Bay oceanic crust is from Oakey & Chalmers (2012).

tectonism with inversion, transtension and thrust faults developing (Fig. 2). The Palaeogene compression-related faulting in eastern Baffin Bay was probably a consequence of the same overall plate movements which also caused the Eurekan tectonic phase in North Greenland and Ellesmere Island. Portions of the large ridge structures likely contain block-faulted and post-rift Cretaceous sedimentary rocks later compressed into ridges such as the Melville Bay Ridge and the Kivioq Ridge (Figs 2–4). During the Palaeogene, flood basalts and other volcanic rocks developed in the West Greenland Volcanic Province and probably also in the Kivioq West volcanic area (Fig. 4). Paleocene–Eocene volcanic rocks cover parts of the Cretaceous basins such as in the Nuussuaq Basin (Dam *et al.* 2009; Larsen *et al.* 2015). Samples of flood basalt from the Delta-1 well offshore central West Greenland (Fig. 1) were dated to *c.* 50–56 Ma (Nelson *et al.* 2015). Sedimentary geometries suggesting basin-floor fan deposits were formed during the late Eocene to Oligocene in mega-unit D, above horizon E1 (Fig. 2), presumably related to the Eurekan compressive phase. This was followed by more passive infilling of the remnant rift basins lasting until middle Miocene (horizon D1; Fig. 2). During the late Miocene to Pliocene, large contourite drift- and mass-transport systems (e.g. mega-slides) developed in Baffin Bay within mega-units B and C (between horizons B1 and D1; Fig. 2) (Knutz *et al.* 2015). The final phase of basin development is characterised by major progradation of the West Greenland shelf towards southwest (mega-unit A between A1 and B1; Fig. 2) mainly as a result of trough-mouth fans formed by late Pliocene–Pleistocene glaciations (Knutz *et al.* 2015).

Interpretation of seismic facies and attributes has identified a number of amplitude anomalies (bright events) and vertical disturbances (chimney structures) on seismic data over structural highs in the Cenozoic section. Some of the features could relate to upwards migration of fluids and possible active petroleum systems. Some of the source rocks that produce oil seeps in the Nuussuaq Basin and equivalent sources in west Baffin Bay could occur in basins of eastern Baffin Bay (Bojesen-Koefoed 2011). Large structural crests within Cretaceous sections occur close to deep basins (Fig. 2), and some of the structures may include potential traps for hydrocarbons, given the right conditions.

The updated mapping and new interterpretation in this study have improved the large-scale mapping of the structures and basins of the eastern Baffin Bay region, outlining a prospectivity potential and also pointing to uncertainties and risks that require future clarification.

Acknowledgements

The study was co-financed by the Ministry of Mineral Resources (Government of Greenland) and GEUS. The constructive comments and improvements of the manuscript from referees Lynn Dafoe and Christopher Harrison are appreciated and acknowledged. TGS-NOPEC Geophysical Company ASA is acknowledged for permission to publish the seismic section.

References

Altenbernd, T., Jokat, W., Heyde, I. & Damm, V. 2014: A crustal model for northern Melville Bay, Baffin Bay. Journal of Geophysical Research–Solid Earth **119**, 8610–8632.

Bojesen-Koefoed, J.A. 2011: West Greenland petroleum systems. An overview of source rocks and oil seepages and their implications for offshore petroleum exploration. Danmarks og Grønlands Geologiske Undersøgelse Rapport **2011/42**, 49 pp.

Bojesen-Koefoed, J.A., Christiansen, F.G., Nytoft, H.P. & Pedersen, A.K. 1999: Oil seepage onshore West Greenland: evidence of multiple source rocks and oil mixing. In: Fleet, A.J. & Boldy, S.A.R. (eds): Petroleum geology of Northwest Europe: Proceedings of the 5th conference. Geological Society, London, 305–314.

Brent, T.A., Chen, Z., Currie, L.D. & Osadetz, K. 2013: Assessment of the conventional petroleum resource potential of Mesozoic and younger structural plays within the proposed National Marine Conservation Area, Lancaster Sound, Nunavut. Geological Survey of Canada, Open File **6954**, 40 pp.

Dam, G., Pedersen, G.K., Sønderholm, M., Midtgaard, H., Larsen, L.M., Nøhr-Hansen, H. & Pedersen, A.K. 2009: Lithostratigraphy of the Cretaceous–Paleocene Nuussuaq Group, Nuussuaq Basin, West Greenland. Geological Survey of Denmark and Greenland Bulletin **19**, 171 pp.

Damm, V. 2010: The expedition of the research vessel "Polarstern" to the Arctic in 2010 (ARK-XXV/3). Berichte zur Polar- und Meeresforschung (Reports on Polar and Marine Research) **621**, 234 pp. Alfred Wegener Institut für Polar- und Meeresforschung, Germany, *http://hdl.handle.net/10013/epic.36297*.

Dawes, P.R. 1997: The Proterozoic Thule Supergroup, Greenland and Canada: history, lithostratigraphy and development. Geology of Greenland Survey Bulletin **174**, 150 pp.

Gregersen, U., Hopper, J.R. & Knutz, P.C. 2013: Basin seismic stratigraphy and aspects of prospectivity in the NE Baffin Bay, Northwest Greenland. Marine and Petroleum Geology **46**, 1–18.

Knutz, P.C., Hopper, J.R., Gregersen, U., Nielsen, T. & Japsen, P. 2015: A contourite drift system on the Baffin Bay–West Greenland margin linking Pliocene Arctic warming to poleward ocean circulation. Geology **43**, 907–910.

Larsen, L.M., Pedersen, A.K., Tegner, C., Duncan, R.A., Hald, N. & Larsen, J.G. 2015: Age of Tertiary volcanic rocks on the West Greenland continental margin: volcanic evolution and event correlation to other parts of the North Atlantic Igneous Province. Geological Magazine **153**(3), 487511, *http://dx.doi.org/10.1017/S0016756815000515*.

MacLean, B. & Williams, G.L. 1983: Geological investigations of Baffin Island Shelf in 1982. In: Current Research, Part B, Geological Survey of Canada, Paper **83-1B**, 309–315.

Nelson, C.E., Jerram, D.A., Clayburn, J.A.P., Halton, A.M. & Roberge, J. 2015: Eocene volcanism in offshore southern Baffin Bay. Marine and Petroleum Geology **67**, 678–691.

Oakey, G.N. & Chalmers, J.A. 2012: A new model for the Paleogene motion of Greenland relative to North America: Plate reconstructions of the Davis Strait and Nares Strait regions between Canada and Greenland. Journal of Geophysical Research **117**, 1–28.

Reid, I. & Jackson, H.R. 1997: Crustal structure of northern Baffin Bay: Seismic refraction results and tectonic implications. Journal of Geophysical Research **102**, 523–542.

Rolle, F. 1985: Late Cretaceous – Tertiary sediments offshore central West Greenland: lithostratigraphy, sedimentary evolution, and petroleum potential. Canadian Journal of Earth Sciences **22**, 1001–1019.

Suckro, S.K., Gohl, K., Funck, T., Heyde, I., Ehrhardt, A., Schreckenberger, B., Gerlings, J., Damm, V. & Jokat, W. 2012: The crustal structure of southern Baffin Bay: implications from a seismic refraction experiment. Geophysical Journal International **190**, 37–58.

Whittaker, R.C., Hamann, N.E. & Pulvertaft, T.C.R. 1997: A new frontier province offshore northwest Greenland: structure, basin development, and petroleum potential of the Melville Bay area. American Association of Petroleum Geologists Bulletin **81**, 978–998.

Authors' address

Geological Survey of Denmark and Greenland, Øster Voldgade 10, DK-1350 Copenhagen K, Denmark; E-mail: *ug@geus.dk*

Mapping of the CO_2 storage potential in the Nordic region

Karen Lyng Anthonsen, Peter Frykman and Carsten Møller Nielsen

The concept of utilising available pore space in deep saline sandstone aquifers for storage of CO_2 was recognised in the late 1980s. In 1996, the first commercial CO_2 storage project began with injection into sandstones of the Utsira Formation in Norway. The formation is located above the Sleipner Formation from where the Sleipner field produces natural gas. The project was initiated due to a high CO_2 content of the natural gas, which was subjected to a Norwegian offshore carbon tax. The natural gas is produced on the Sleipner platform where the CO_2 is separated, captured and reinjected from a neighbouring platform. The potential for using the technology to reduce CO_2 emissions from large stationary point sources initiated many research projects aimed at mapping areas with potential CO_2 storage capacity around the world.

In 2008, the Nordic countries decided to set up a special venture for climate, energy and the environment by launching the *Top-Level Research Initiative* promoting research within six sub-programmes, including one on *Carbon, Capture and Storage* (CCS). With this background the Nordic CCS Competence Centre (NORDICCS) was initiated in 2011, involving major Nordic CCS research institutes, industry and stakeholders. One of the main outcomes of the project, which terminated in 2015, is a web-based Nordic CO_2 Storage Atlas (data.geus.dk/nordiccs/map.xhtml), which aims to make CCS-related data and interpretations available to decision makers and the public.

The newly released atlas combines data from previous CO_2 storage screening and mapping projects (GESTCO, EU GeoCapacity and the Norwegian CO_2 Storage Atlas) with new data for areas not previously covered. The atlas gives an overview of storage options and the associated reservoir properties in Denmark, Norway, Sweden and Iceland.

CO_2 storage site screening in the Nordic region

The project focused on CO_2 storage (1) in sandstone aquifers, (2) by chemical reaction in basalts and (3) in depleted hydrocarbon fields. Large-scale geological storage of CO_2 in sandstone aquifers requires the presence of a porous and permeable subsurface layer, a burial depth of minimum 800 m to keep the CO_2 as a dense phase, and an adequate top seal preventing the buoyant CO_2 from migrating to the surface. Areas with the largest storage potential are associated with sedimentary basins containing widespread sandstone layers. Sedimentary basins with storage potential are situated as a marginal belt around the Scandinavian peninsula from the Baltic Sea, through Denmark and along the Norwegian coast, whereas the shallow sedimentary basins in Finland are not considered appropriate for CO_2 storage (Teir *et al.* 2010). In Iceland, the storage potential is not related to sedimentary basins, but to injection of CO_2-saturated water into porous basalts (Fig. 1). The dissolved CO_2 reacts with divalent cations in the basalt-forming stable carbonate minerals such as calcite, dolomite, magnesite, siderite, and Mg-Fe carbonate solid solutions (Gislason *et al.* 2010).

Compared to storage in saline aquifers, the CO_2 storage capacity in hydrocarbon fields is in general minor, but late-

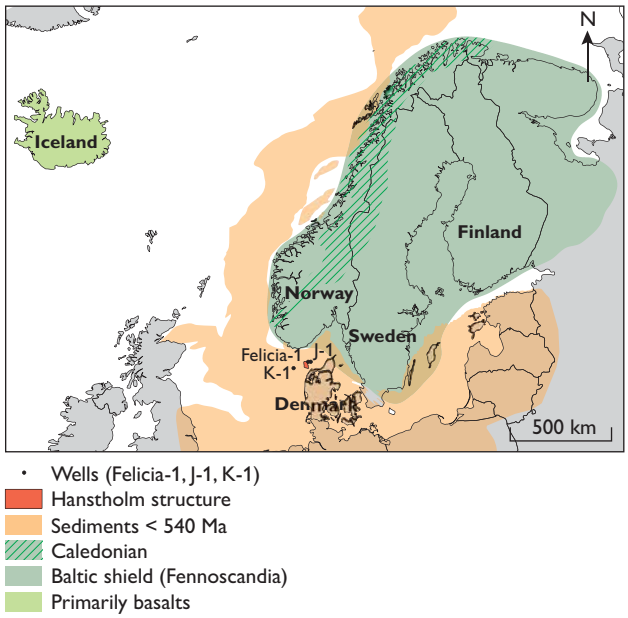

Fig. 1. Generalised geological overview of the Precambrian Baltic shield and the sedimentary basins.

© 2016 GEUS.

stage oil production may profit from enhanced oil recovery (EOR) by injection of CO_2. Thus the highest potential for industrial-scale storage is obtained when EOR is used in connection with the CO_2 storage. The geological and engineering knowledge accumulated from producing oil and gas fields is also more detailed than for aquifer storage sites.

The data compiled in the web-based atlas include an approximate outline of storage formations and aquifers with information for each unit on depth, thickness, lithology, proportion of sand, age and reservoir type, based on well data and seismic interpretations. Furthermore, reservoir properties such as porosity, permeability, salinity, CO_2 density, storage efficiency factor and estimated storage capacity are listed. In order to illustrate the geological complexity, major faults are included in the atlas. Likewise, an outline of the sealing formations is included in order to indicate storage integrity.

The compiled data were used to characterise and rank storage formations and traps and to calculate CO_2 storage capacities. The ranking criteria were grouped into four main categories: reservoir properties, seal properties, safety/risk and maturity/data coverage. This resulted in a selection of the most prospective Nordic storage areas, based on available geological knowledge up to 2014 (Anthonsen *et al.* 2014). The ranking revealed that the most prospective storage areas are found in the Norwegian North Sea. This is basically a result of the knowledge from the intensive oil and gas exploration making the Norwegian areas more mature for exploitation of storage capacity. It has to be stressed that there are large uncertainties in many of the evaluated parameters and that more data and further data analysis are required before any of the sites are ready for CO_2 injection.

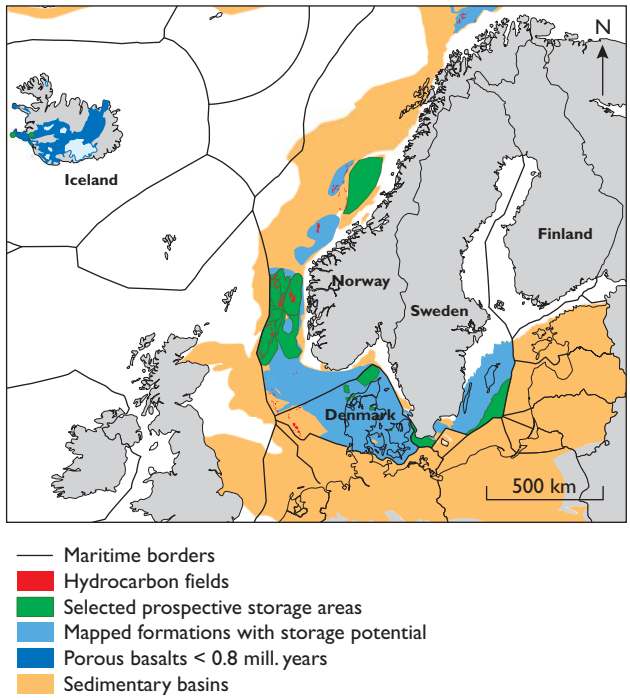

Fig. 2. All mapped Nordic CO_2 storage formations (blue) and the selected most prospective areas in green. The dark blue area in Iceland is the highly porous basalt areas considered most promising for CO_2 injection.

Mapped CO_2 storage capacity

The storage capacity estimates make use of the same methodology as the EU GeoCapacity project; see Vangkilde-Pedersen *et al.* (2009). The total mapped CO_2 storage capacity for Denmark, Norway and Sweden is 134 000 megaton (Mt). The storage capacity related to saline aquifers is 120 000 Mt, with 22 000 Mt in Denmark, 94 600 Mt in Norway (hereof 72 800 Mt in the North Sea) and 3 400 Mt in Sweden. The total number includes 14 000 Mt in hydrocarbon fields, with 2 000 Mt in Denmark and 12 000 Mt in Norway (Røkke *et al.* in press; Fig. 2).

It should be emphasised that the presented storage capacities are regarded as simple estimates based on volumetric calculations of the available pore space and multiplied with a storage efficiency factor. Improved geological data and reservoir modelling work will be necessary to narrow the specific uncertainties for the storage capacity estimates. Storage capacity estimates for porous basalts are based on a different methodology, and for onshore Iceland the calculated capacity ranges between 21 000 and 400 000 Mt depending on the calculation approach (Snæbjörnsdóttir *et al.* 2014).

The storage capacity has to be seen in relation to the CO_2 emission, which was 152.8 Mt in 2011 for all large stationary point sources (emission >70 Kt) in the five Nordic countries, with 25.8 Mt in Denmark, 55.6 Mt in Finland, 1.6 Mt in Iceland, 23.1 Mt in Norway and 46.6 Mt in Sweden. On a European scale the total emission from stationary point sources mapped in the EU GeoCapacity project was 2 000 Mt (Anthonsen *et al.* 2011), implying that theoretically all CO_2 emissions for 70 years from these sources in Europe could be stored in the Nordic region.

Modelling CO_2 storage capacity in Denmark

The procedure for the estimation of storage capacity is illustrated by a case study of the Hanstholm structure, using simple, static calculations supplemented with dynamic simulations. The dynamic simulation has the advantage that both reservoir properties such as heterogeneity and

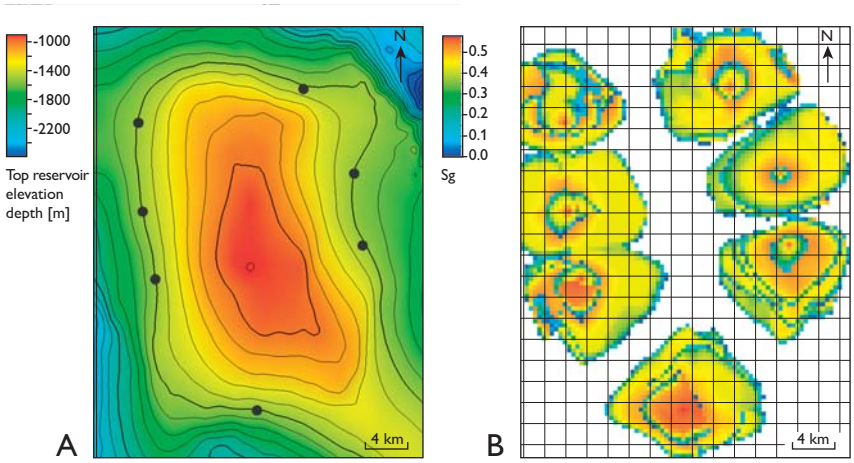

Fig. 3. **A**: Maps with depth contours for the top reservoir level and the position of the seven injection wells. The seven wells were positioned by iteration to effectively fill most of the structure. **B**: An optimum filling simulation of the Hanstholm structure. Injection period is 40 years.

operational conditions can be accounted for, leading to a more realistic capacity number. The dynamic assessment requires that a 3D reservoir model is constructed, as it involves flow and pressure calculations over the time span of the operational period. The background for constructing this model is briefly described here.

The informal name Hanstholm structure is used for an offshore domal closure covering 603 km², situated offshore *c.* 40 km north-west of the city of Hanstholm (Fig. 1). The water depth at the site is *c.* 30 m. The target for storage is Upper Triassic – Lower Jurassic sandstones of the Gassum Formation. This formation consists of fine- to medium-grained, locally coarse-grained sandstones interbedded with heteroliths, claystones and locally thin coal beds (Michelsen *et al.* 2003; Nielsen 2003). The sandstones were deposited by repeated progradation of shoreface and deltaic units forming laterally continuous sheet sandstones separated by offshore marine claystones. Fluvial sandstones dominate in the lower part of the formation as in most of the Fennoscandian Border Zone. The structure is situated close to the edge of the Fjerritslev Fault of the Sorgenfrei-Tornquist zone, and is formed by uplift due to post-depositional salt tectonics. The structure is interpreted from the depth structure map of the 'Top Triassic' as defined by Japsen & Langtofte (1991), and has been used as a template for defining top and bottom of a reservoir with uniform thickness.

The depth to top reservoir is approximately 890 m below mean sea level, and the deepest closing contour is at approximately 1330 m (Fig. 3A). The theoretical spill point is situated at the south-eastern flank of the structure spilling into the Thisted domal structure.

The structure has not been drilled and data for the reservoir have to be extrapolated from information from the nearby Felicia-1, J-1 and K-1 wells (Fig. 1). It should be noted, however, that Felicia-1 is drilled at the crest of a rotated fault block, and is believed to show an extraordinarily large thickness of the Gassum Formation with a thick mudstone in the middle part, reflecting topographic influence from the nearby salt pillow during deposition. This may result in marked differences in reservoir properties between this well and the undrilled structure. The well J-1 some 30–40 km to the north-east has therefore been used as a template for the sand-shale sequence in the reservoir model. The claystones of the Fjerritslev Formation form the top seal of the aquifer. The Fjerritslev Formation is expected to be *c.* 500 m thick above the Hanstholm aquifer.

The reservoir model was used for a capacity study by simulating seven injection wells around the perimeter of the flank, and their positions were optimised by iteration to give the most complete filling pattern on the structure (Fig. 3B). CO_2 was injected at a constant rate of 4.2 Mt per well per year. The dynamic simulations account for an injection period of 40 years and with a preconditioned safety

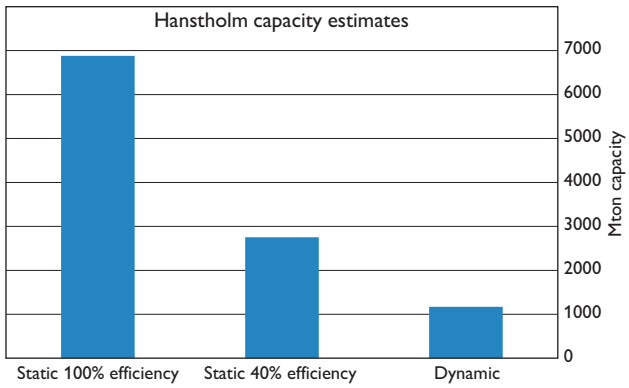

Fig. 4. Comparison of different capacity estimates including values from the dynamic simulation of optimum filling of the Hanstholm structure in Denmark. The previous estimate was based on static calculations and an assumed effieciency factor of 40%.

margin of the allowed pressure increase set to maximum 85% of the lithostatic pressure below the cap rock in order to avoid any fracture propagation in the cap rock. The resultant storage capacity was 1170 Mt CO_2, but a change of the safety margin will naturally influence the storage capacity. The derived dynamic capacity for the Hanstholm structure can be compared to previous estimates of 2753 Mt based on the static model characteristics and an assumed efficiency factor; in this case 40% efficiency (Fig. 4) as described by Larsen *et al.* (2003).

Summary

Mapping of sandstone units (aquifers) and their associated reservoir properties have resulted in a web-based CO_2 storage atlas. The reservoir data and properties were used to characterise and rank the potential storage areas and sites in an attempt to point out the most prospective ones based on currently available geological knowledge (Fig. 2). It is essential for the development of a CO_2 storage site to know how much capacity is available. In the initial screening phase static theoretical estimates are used, but dynamic modelling of CO_2 injection is very important in order to narrow the uncertainties of the storage capacities. The reduction in total storage capacity from previously published static calculations to the modelled dynamic calculations is one of the key conclusions from the CO_2 injection simulation. However, even if a reduction of the static capacity estimates is taken into account, it is clear that the Nordic region has substantial storage capacity in saline aquifers (Anthonsen *et al.* 2014; Lothe *et al.* 2015).

Acknowledgements

This article has been produced with support from NORDICCS, under the *Top-level Research Initiative CO_2 Capture and Storage* programme, and Nordic Innovation. The authors acknowledge the following partners for their contributions: Statoil, Gassco, Norcem, Reykjavik Energy, CO_2 Technology Centre Mongstad, Vattenfall and the *Top-level Research Initiative* (Project number 11029).

References

Anthonsen, K.L., Frykman, P. & Nielsen, L.H. 2011: The potential for geological storage of CO_2 in Denmark is very promising. In: Sønderberg Petersen, L. & Larsen H. (eds): Energy systems and technologies for the coming century. Risø International Energy Conference 2011, May 10–12. Proceedings, 48–55.

Anthonsen, K.L., Aagaard, P., Bergmo, P.E.S., Gislason, S.R., Lothe, A.E., Mortensen, G.M. & Snæbjörnsdottir, S.Ó. 2014: Characterisation and selection of the most prospective CO_2 storage sites in the Nordic region. Energy Procedia **63**, 4884–4896.

Gislason, S.R., Wolff-Boenisch, D., Stefansson, A., Oelkers, E.H., Gunnlaugsson, E., Sigurdardottir, H. & Sigfussson, B. 2010: Mineral sequestration of carbon dioxide in basalt: A pre-injection overview of the CarbFix project. International Journal of Greenhouse Gas Control **4**(3), 537–545.

Japsen, P. & Langtofte, C. 1991: Geological map of Denmark 1:400 000. The Danish Basin: 'Top Trias' and the Jurassic – Lower Cretaceous. Danmarks Geologiske Undersøgelse Map Series **30**.

Larsen M., Bidstrup T. & Dalhoff, F. 2003: Mapping of deep saline aquifers in Denmark with potential for future CO_2 storage. A GESTCO contribution. Danmarks og Grønlands Geologiske Undersøgelse Rapport **2003/39**, 83 pp.

Lothe, A.E., Emmel, B., Bergmo, P.E., Mortensen, G.M. & Frykman, P. 2015: Updated estimate of storage capacity and evaluation of seal for selected aquifers (D26). NORDICCS Technical report **D 6.3.1401**, 80 pp.

Michelsen, O., Nielsen, L.H., Johannessen, P.N., Andsbjerg, J. & Surlyk, F. 2003: Jurassic lithostratigraphy and stratigraphic development onshore and offshore Denmark. In: Ineson, J.R. & Surlyk, F. (eds): The Jurassic of Denmark and Greenland. Geological Survey of Denmark and Greenland Bulletin **1**, 147–216.

Nielsen, L.H. 2003: Late Triassic – Jurassic development of the Danish Basin and the Fennoscandian Border Zone, southern Scandinavia. In: Ineson, J.R. & Surlyk, F. (eds): The Jurassic of Denmark and Greenland. Geological Survey of Denmark and Greenland Bulletin **1**, 459–526.

Røkke, N.A., Aarlien, R., Mazzetti, M., Kielland Haug, J.J., Skagestad, R., Onaeheim, K., Lund, H., Kjärstad, J. & Anthonsen, K.L. in press: Final Report. NORDICCS, Nordic CCS Competence Centre. Nordic Innovation Publication.

Snæbjörnsdóttir, S.Ó., Wiese, F., Fridriksson, T., Ármannsson, H., Einarsson, G.M. & Gislason, S.R. 2014: CO_2 storage potential of basaltic rocks in Iceland and the oceanic ridges. Energy Procedia **63**, 4585–4600.

Teir, S. *et al.* 2010: Potential for carbon capture and storage (CCS) in the Nordic region. VTT Tiedotteita – Research Notes **2556**, 53–73.

Vangkilde-Pedersen, T. *et al.* 2009: Assessing European capacity for geological storage of carbon dioxide – the EU GeoCapacity project. Energy Procedia **1**, 2663–2670.

Authors' address

Geological Survey of Denmark and Greenland (GEUS), Øster Voldgade 10, DK-1350 Copenhagen K, Denmark. E-mail: *kla@geus.dk*

Burial and exhumation history of the Labrador-Newfoundland margin: first observations

Peter Japsen, Paul F. Green, Johan M. Bonow, Alana M. Hinchey and Derek H.C. Wilton

The continental shelf of Labrador and Newfoundland has a long history of hydrocarbon exploration, and the accumulated oil production from the northern Grand Banks exceeds one billion barrels (Fig.1). The Canada-Newfoundland & Labrador Offshore Petroleum Board (*www.cnlopb.ca*) awarded several new licenses on the northern Grand Banks in 2015 and announced licensing rounds for the Labrador Sea region in the coming years.

Vertical motion along passive continental margins such as the Atlantic margin of Canada, plays an essential role in shaping these margins and their petroleum systems; in particular by removing sedimentary strata (Japsen *et al.* 2012; Green *et al.* 2013). It is thus a fundamental question whether a hiatus in the stratigraphic record represents an episode of stability and non-deposition or an event involving deposition followed by removal of rocks. In this context, a hiatus represents not only a gap in the stratigraphic record, but also a gap in our understanding of the geological history.

In terms of hydrocarbon systems, failure to account for greater depths of burial prior to exhumation can lead to serious underestimation of the maturity of petroleum resources. Similarly, the effects of exhumation on the timing of hydrocarbon generation, on changes in migration routes and on any reservoir hydrocarbons also require assessment (Doré *et al.* 2002). Insights into the uplift history of a margin are also important for understanding the source-to-sink system of sediment input into offshore basins.

In broader terms of geological development, understanding the history of vertical movements along a passive continental margin is important for investigating whether the elevated regions along these margins, such as the Torngat Mountains in northern Labrador (Fig. 1), are either (a) the eroded remnants of ancient orogens (McGregor *et al.* 2013), (b) rift shoulders related to processes during rifting and break-up (Weissel & Karner 1989) or (c) the results of post-breakup episodes of burial and exhumation driven by plate-tectonic forces (Japsen *et al.* 2006, 2012; Green *et al.* 2013).

Studies of the burial and exhumation history both onshore and offshore of Labrador and Newfoundland are, however, scarce, but several observations – that we review in the following – indicate that a number of uplift episodes followed by denudation, both pre- and post-breakup, shaped the present-day structure of the margin.

Evidence for episodes of burial and exhumation of the margin

The Atlantic margin of Canada has many features in common with passive continental margins in other parts of the world (Japsen *et al.* 2012; Green *et al.* 2013), such as elevated plateaux (i.e. regional high-level landscapes of low, relative relief) at 1 to 2 km or more above sea level (a.s.l.) cut by deeply incised valleys and commonly separated from an adjacent coastal plain by one or more escarpments. The Torngat Mountains with peaks reaching 1.7 km a.s.l. in northern Labrador, slope much more steeply towards the Labrador Sea than they do towards the hinterland farther

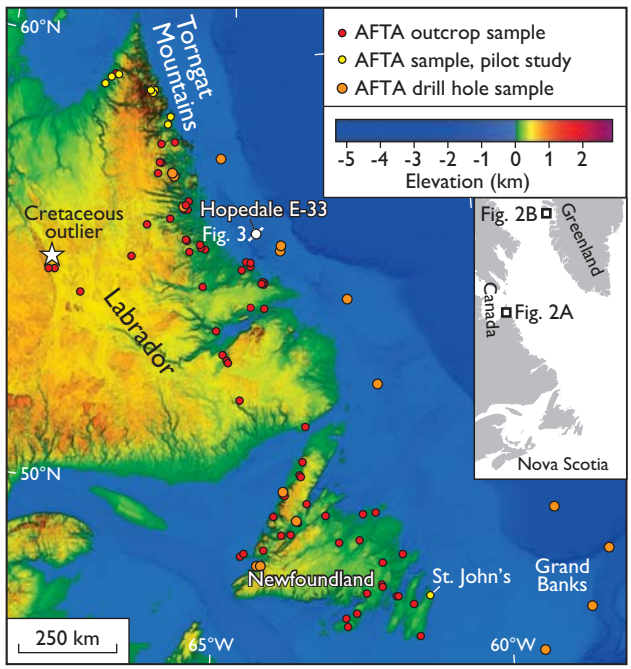

Fig. 1. Outline of the study area, *c.* 1500 km along the Labrador-Newfoundland margin between 46 and 60.5°N. Yellow star: Cretaceous outlier at Schefferville (Dorf 1967). **AFTA**: Apatite fission-track analysis.

© 2016 GEUS.

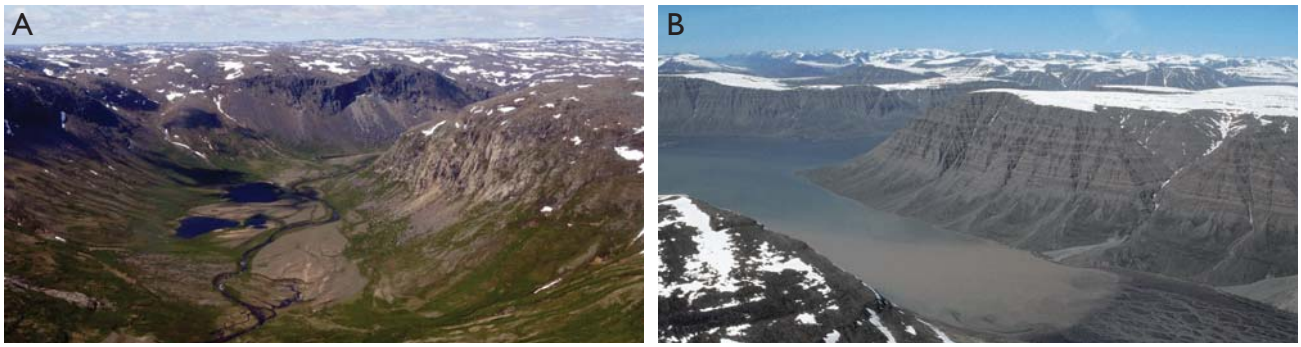

Fig. 2. Similar landscapes on the conjugate margins across the Labrador Sea. **A**: Elevated plain (*c.* 800 m a.s.l.) across Precambrian basement cut by a deep valley, Torngat Mountains, Labrador. **B**: Elevated plain (*c.* 900 m a.s.l.) across Paleocene basalts cut by a deep valley, Disko island, West Greenland. The study will investigate whether the elevated plain is a Cenozoic erosion surface as it is the case for the conjugate margin in West Greenland (Bonow *et al.* 2006; Japsen *et al.* 2006). Photo locations in Fig. 1.

west in interior Labrador, and their overall shape is thus similar to that of the coastal mountains in Greenland (Fig. 2). However, farther south (e.g. on Newfoundland) elevations do not reach 1 km a.s.l. As along other passive margins, Mesozoic–Cenozoic rift systems parallel the Labrador-Newfoundland margin with a transition from continental to oceanic crust farther offshore. Here breakup occurred in the Early Cretaceous east of Newfoundland and in the Paleocene east of Labrador. The syn- and post-rift sediments at the landward margin of these rifts dip towards the rifts and are truncated by one or more shallow unconformities or by the seabed (Fig. 3). In particular, the margin of Labrador shares the characteristics listed above with the conjugate margin of West Greenland where the geological record documents that the present-day high mountains are not remnants of the rifting process but the result of much later uplift which partially removed thick, post-rift deposits (Japsen *et al.* 2006).

Evidence from the offshore domain

Dickie *et al.* (2011) noted that the Tertiary sediments along Labrador are tilted seaward and truncated (Fig. 3), and that late Oligocene as well as younger (possibly Miocene) unconformities might correspond to phases of uplift of the Labrador margin as proposed by McMillan (1973). According to Dickie *et al.* (2011), the sedimentary record along the Labrador margin is difficult to interpret because of the limited dating of the younger, post-Oligocene section, and the many phases of channelling and erosion that are exhibited. Subsequently, Ainsworth *et al.* (2014) studied the Cretaceous–Tertiary stratigraphy of the Labrador Shelf and provided improved constraints on several unconformities; in particular they documented the presence of a regional Miocene hiatus. Figure 4 shows evidence that the pre-Pliocene sequences along Labrador have been more deeply buried in the past, most likely prior to the removal of Miocene strata. Also on the Grand Banks, uplift and exhumation were important processes for the shaping of petroleum systems (Sinclair *et al.* 1994; Avery 2001).

Evidence from the onshore domain

Precambrian rocks dominate Labrador and Newfoundland, but Phanerozoic cover rocks are present across the region, for example in the Palaeozoic basins of western Newfoundland (Cooper *et al.* 2001). Hendriks *et al.* (1993) interpreted apatite fission-track data from western Newfoundland to indicate major episodes of late Carboniferous and Jurassic exhumation, which agree with evidence from thermal maturity of Palaeozoic rocks that they had been more deeply buried below a cover up to 3 km thick (Wil-

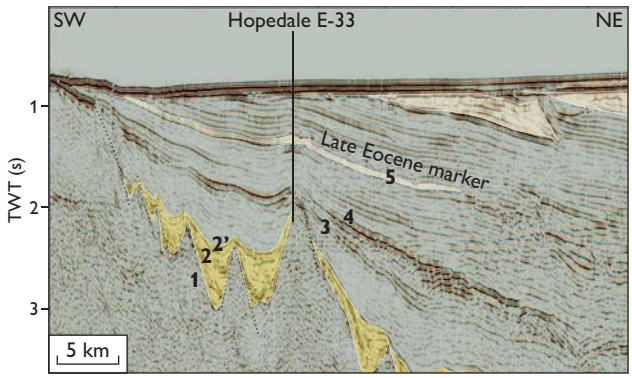

Fig. 3. Seismic profile off Labrador illustrating post-Eocene tilting and truncation of the sedimentary sequences (after Dickie *et al.* 2011). Unconformities: **5**: late Eocene. **4**: base Eocene. **3**: mid-Paleocene. **2'**: Late Cretaceous. **2**: mid-Cretaceous. **1**: top basement. Sand-prone units: Gold and yellow colours. Location on Fig. 1. **TWT**: two-way travel time.

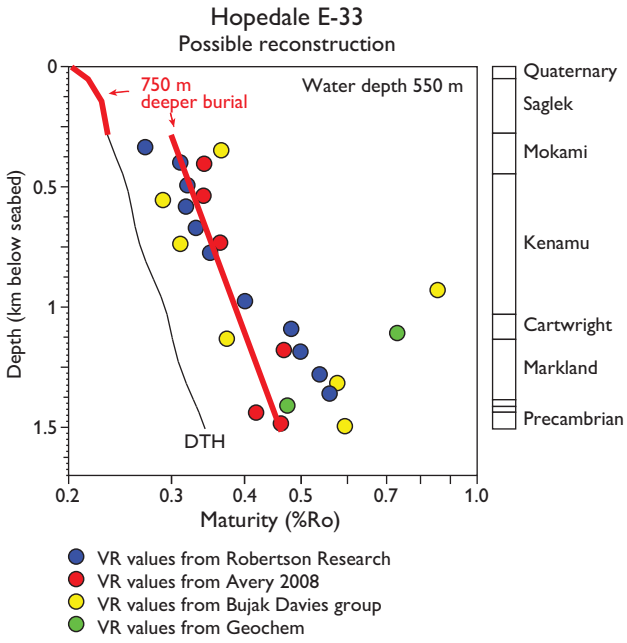

Fig. 4. Scattered vitrinite reflectance (VR) data from various labs for the Hopedale E-33 well (source: Canada Basin Database; *http://basin.gdr.nrcan.gc.ca/index_e.php*; location in Figs 1, 3). The solid black line shows the profile predicted if all units in the well are currently at their maximum post-depositional temperatures (default thermal history, DTH). All values plot consistently above the black line, suggesting that units below the Plio-Pleistocene Saglek Formation have been hotter in the past, although a detailed interpretation of these data is not possible because of the scatter in the data and differences between datasets. The red profile shows the prediction from a history in which the pre-Saglek section has been buried more deeply by 750 m prior to exhumation.

liams *et al.* 1998). Pe-Piper & MacKay (2006) presented evidence for Early Cretaceous drainage from western Newfoundland to areas onshore and offshore Nova Scotia.

An outlier of Cretaceous sediments on central Labrador around Schefferville (Dorf 1967) constrains the construction of a relative denudation chronology based on stratigraphic landscape analysis and for thermochronological modelling by documenting when basement rocks were exhumed to the surface. White *et al.* (2000) included the Schefferville outlier in their evidence for an Albian connection between the Labrador Sea and the Cretaceous Western Interior Seaway of North America.

Grist & Zentilli (2003) reported evidence for post-Jurassic exhumation with as much as 30°C of post-Paleocene cooling of the southern portion of the Canadian Atlantic margin, based on fission-track data from e.g. Nova Scotia. They also reported high vitrinite reflectance values for Jurassic strata in the Fundy Basin, offshore Nova Scotia, in agreement with 2 km of post-Jurassic erosion inferred from seismic data.

Integrated investigation of the vertical movements along the margin

The observations reviewed above demonstrate that episodes of burial and exhumation have affected the Atlantic margin of Canada both prior to and after break-up. The available evidence does not, however, allow further definition of the timing and magnitude of the vertical movements that shaped the present-day margin. In particular, it is not possible to define when the mountains along the margin reached their present elevation. We have therefore initiated a research project aimed at defining the main events of burial and exhumation along the margin onshore and offshore Labrador and Newfoundland (Fig. 1). The study has three components:

(1) A thermochronological study based on samples from outcrops and from onshore and offshore boreholes with associated thermal history interpretations (Green *et al.* 2013). A pilot study comprising apatite fission-track analysis (AFTA) data in 12 samples (Fig. 1) revealed a long history of Phanerozoic cooling and exhumation episodes, notably a regional Triassic event during which a sample of latest Neoproterozoic sandstone collected in St. John's cooled below 110°C, corresponding to the onset of removal of a kilometre-thick cover of Palaeozoic–Triassic rocks.

(2) A stratigraphic landform analysis of the study area based on digital elevation data and stratigraphic information to map exposed denudation surfaces. This analysis provides evidence of both uplift and subsidence using cross-cutting relationships between palaeosurfaces (onshore unconformities expressed as large-scale, low-relief surfaces produced by erosion to base level) and stratigraphic constraints. We intend to use this analysis to construct a relative chronology for surface formation and tectonic events (Green *et al.* 2013).

(3) An integrated interpretation of the geological, geomorphological and thermochronological data. We will combine the relative denudation chronology from the stratigraphic landscape analysis with the absolute timing of cooling events determined from the AFTA data in order to estimate the timing and magnitude of uplift and exhumation along the margins of Labrador and Newfoundland.

Studying uplift/exhumation with just one technique in isolation provides only part of the story. Without the AFTA data, the landform analysis will only yield a relative event chronology. Without the landform analysis, it will not be possible to conclude whether surface uplift accompanied exhumation as recorded by the AFTA data.

Summary

The stratigraphic record along the continental margin of Labrador and Newfoundland provides ample evidence for

vertical movements both prior to and after break-up; on the island of Newfoundland, late Carboniferous and Jurassic phases of exhumation removed kilometre-thick covers over Palaeozoic basins (Hendriks *et al.* 1993; Williams *et al.* 1998), and in Labrador, Cretaceous sediments rest on Precambrian basement (Dorf 1967). In the offshore domain, several major hiatuses punctuate the stratigraphic record; e.g. along Labrador between the Palaeozoic sediments and Precambrian basement and between Lower Cretaceous volcanics and underlying Palaeozoic sediments, intra-Cretaceous and base-Tertiary unconformities and several intra-Tertiary unconformities (mid-Paleocene, late Eocene, mid-Oligocene and Miocene; Ainsworth *et al.* 2014). It is our ambition to combine the evidence from the stratigraphic record with results from stratigraphic landscape analysis and thermochronology to provide a coherent model of the timing and magnitude of the vertical movements along the margin both prior to and after break-up.

Acknowledgements

We thank sponsoring oil companies for financial support and the Geological Survey of Newfoundland and Labrador for funding the AFTA pilot study.

References

Ainsworth, N.R., Riley, L., Bailey, H.W. & Gueinn, K.J. 2014: Cretaceous–Tertiary stratigraphy of the Labrador Shelf, Riley Geoscience Ltd., commissioned by Nalcor Energy, *http://www.nalcorenergy.com/OILGAS/labrador-biostratigraphy.asp*

Avery, M.P. 2001: Vitrinite reflectance (Ro) of dispersed organic matter from Husky/Bow Valley *et al.* Golconda C-64. GSC Open File Report **4013**, 14 pp., *http://basin.gdr.nrcan.gc.ca/wells/single_maturation_e.php?well=D302*

Bonow, J.M., Japsen, P., Lidmar-Bergström, K., Chalmers, J.A. & Pedersen, A.K. 2006: Cenozoic uplift of Nuussuaq and Disko, West Greenland – elevated erosion surfaces as uplift markers of a passive margin. Geomorphology **80**, 325–337.

Cooper, M., Weissenberger, J., Knight, I., Hostad, D., Gillespie, D., Williams, H., Burden, E., Porter-Chaudhry, J., Rae, D. & Clark, E. 2001: Basin evolution in western Newfoundland: New insights from hydrocarbon exploration. AAPG Bulletin **85**, 393–418.

Dickie, K., Keen, C.E., Williams, G.L. & Dehler, S.A. 2011: Tectonostratigraphic evolution of the Labrador margin, Atlantic Canada. Marine and Petroleum Geology **28**, 1663–1675.

Doré, A.G., Cartwright, J.A., Stoker, M.S., Turner, J.P. & White, N. (eds) 2002: Exhumation of the North Atlantic margin: timing, mechanisms and implications for petroleum exploration. Geological Society, London, Special Publications **196**, 494 pp.

Dorf, E. 1967: Cretaceous insects from Labrador I. Geologic Occurrence. Psyche **74**, 267–269.

Green, P.F., Lidmar-Bergström, K., Japsen, P., Bonow, J.M. & Chalmers, J.A. 2013: Stratigraphic landscape analysis, thermochronology and the episodic development of elevated passive continental margins. Geological Survey of Denmark and Greenland Bulletin **30**, 150 pp.

Grist, A. & Zentilli, M. 2003: Post-Paleocene cooling in the southern Canadian Atlantic region: evidence from apatite fission track models. Canadian Journal of Earth Sciences **40**, 1279–1297.

Hendriks, M., Jamieson, R.A., Willett, S.D. & Zentilli, M. 1993: Burial and exhumation of the Long Range inlier and its surroundings, western Newfoundland: results of an apatite fission-track study. Canadian Journal of Earth Sciences **30**, 1594–1606.

Japsen, P., Bonow, J.M., Green, P.F., Chalmers, J.A. & Lidmar-Bergström, K. 2006: Elevated, passive continental margins: Long-term highs or Neogene uplifts? New evidence from West Greenland. Earth and Planetary Science Letters **248**, 315–324.

Japsen, P., Chalmers, J.A., Green, P.F. & Bonow, J.M. 2012: Elevated, passive continental margins: Not rift shoulders, but expressions of episodic, post-rift burial and exhumation. Global and Planetary Change **90–91**, 73–86.

McGregor, E.D., Nielsen, S.B., Stephenson, R., Petersen, K.D. & Macdonald, D.I.M. 2013: Long-term exhumation of a Palaeoproterozoic orogen and the role of pre-existing heterogeneous thermal crustal properties: a fission-track study of SE Baffin Island. Journal of the Geological Society, London **170**, 877–891.

McMillan, N.J. 1973: Shelves of Labrador Sea and Baffin Bay, Canada. In: McCrossan, R.G. (ed.): Future petroleum provinces of Canada, their geology and potential. Canadian Society of Petroleum Geology, Memoir **1**, 473–517.

Pe-Piper, G. & Mackay, R.M. 2006: Provenance of Lower Cretaceous sandstones onshore and offshore Nova Scotia from electron microprobe geochronology and chemical variation of detrital monazite. Bulletin of Canadian Petroleum Geology **54**, 366–379.

Sinclair, I.K., Shannon, P.M., Williams, B.P.J., Harker, S.D. & Moore, J.G. 1994: Tectonic control on sedimentary evolution of three North Atlantic borderland Mesozoic basins. Basin Research **6**, 193–217.

Weissel, J.K. & Karner, G.D. 1989: Flexural uplift of rift flanks due to mechanical unloading of the lithosphere during extension. Journal of Geophysical Research – Solid Earth **94**, 13919–13950.

White, T.S., Witzke, B.J. & Ludvigson, G.A. 2000: Evidence for an Albian Hudson arm connection between the Cretaceous Western Interior Seaway of North America and the Labrador Sea. Geological Society of America Bulletin **112**, 1342–1355.

Williams, S.H., Burden, E.T. & Mukhopadhyay, P.K. 1998: Thermal maturity and burial history of Paleozoic rocks in western Newfoundland. Canadian Journal of Earth Sciences **35**, 1307–1322.

Authors' addresses

P.J., *Geological Survey of Denmark and Greenland (GEUS), Øster Voldgade 10, DK-1350 Copenhagen K, Denmark.* E-mail: *pj@geus.dk*

P.F.G., *Geotrack International, 37 Melville Road, Brunswick West, Victoria 3055, Australia.*

J.M.B., *Geovisiona AB, Högbyvägen 168, SE-17554 Järfälla, Sweden and Mid Sweden University, Kunskapens väg 1, SE-831 25 Östersund, Sweden.*

A.M.H., *Geological Survey, Department of Natural Resources, Government of Newfoundland and Labrador, P.O. Box 8700, St. John's, Canada NL A1B 4J6.*

D.H.C.W., *Memorial University of Newfoundland, P.O. Box 4200, St. John's, Canada NL A1C 5S7.*

The Greenland Mineral Resources Portal – another step forward

Mikael Pedersen, Martin Hansen, Bjørn H. Heincke and Leif Thorning

In April 2015, the Geological Survey of Denmark and Greenland (GEUS) together with the Ministry of Mineral Resources in Greenland (MMR) made further progress in the development of web-based facilities to present and disseminate geoscientific information and data. This was presented in a new version of the Greenland Mineral Resources Portal. The portal now provides the users with access to a wealth of geological, geophysical and geochemical data – mostly free of charge (Fig. 1). The primary goal of the portal is to facilitate data searches for exploration companies, but the benefits from the easy access to geoscience data are also open to academic researchers. It is the plan to add several new functionalities to the portal in 2016, and interested users are invited to visit the portal at www.greenmin.gl on a regular basis to follow progress.

Geoscience data – from archive to internet

GEUS, and its forerunner in Greenland (GGU), had as its core activity the production of geological maps. In the early days, observations and data were documented in field notes and on paper maps, but since the 1980s more and more field data have been recorded digitally. Old archive data are still valuable because in Greenland data acquisition is expensive. Therefore GEUS has worked on digitising and securing historic data and integrating them into modern databases with access through the internet.

GEUS has placed geological data from Greenland on the internet since 2005, when the Greenland Mineral Occurrence Map database (GMOM) was first opened to the public (Thorning *et al.* 2004). Initially, the GMOM portal expanded geographically year by year, providing access to mineral occurrence data extracted by GEUS from released company reports. In 2011, a new, more ambitious programme was launched as a collaborative project between GEUS and the Bureau of Minerals and Petroleum in Greenland (BMP), the forerunner of MMR. The objective was to compile data and maps from the whole of Greenland into a modern web-platform – the Greenland Mineral Resources Portal – with access to large amounts of

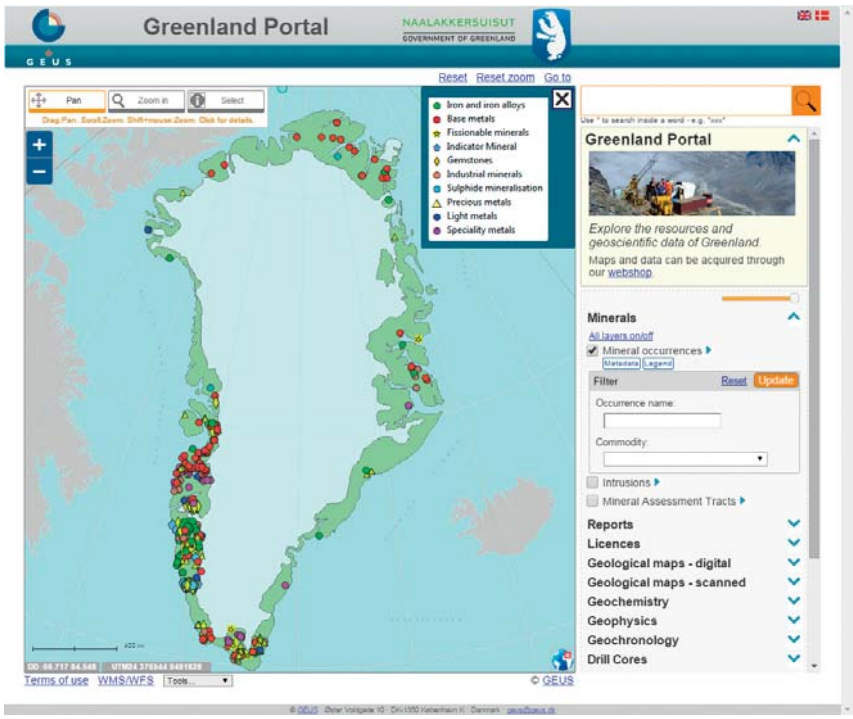

Fig. 1. The interactive map of the Greenland Mineral Resources Portal showing the mineral occurrence layer.

© 2016 GEUS.

Fig. 2. Northernmost Greenland as it appears in the interactive geological map of Greenland on a scale of 1:500 000.

geoscientific metadata, including full texts of reports made for companies from the DODEX database (Riisager *et al.* 2011). The first version of this portal was released in the beginning of 2012, and mainly provided information about the existence of data in different areas, but only to a limited degree the data themselves. However, the need for easy data access for industry was obvious and increasingly the actual data from the large range of GEUS geological databases were added. In 2015 new content and functions were launched to give the users access to download or purchase geochemical and geophysical data and a range of other data types such as geological maps and sample data.

High-quality data

Geological data are essential for development in the mining sector. Factors such as data quality and access to databases are therefore important parameters when rating a country's attraction to investors as expressed by, for example, the annual survey of mining companies undertaken by the Fraser Institute (Jackson & Green 2016). In its capacity as a national geological data and knowledge centre, it has for many years been GEUS' fundamental task to develop databases securing valuable data assets. High-quality databases, however, rely not only on skilled developers, but also very much on geoscientific personnel that can continuously ensure the quality of the content. All data have been quality controlled in the central, authoritative databases before being stored and made available in the Greenland Mineral Resources Portal. A few of the data types are described below.

Geophysical data. Geophysical data are in great demand for mineral exploration and the integration of such data into the portal has therefore been a high priority. During the past two decades, GEUS and BMP/MMR have jointly acquired airborne geophysical data in Greenland within the AEM Greenland and Aeromag projects (Rasmussen *et al.* 2013). Geophysical data are regularly reported by exploration companies to the Greenland authorities as part of their licensing conditions and these are released to the public after a confidentiality period of five years. Prior to 2011, these surveys were handled file by file, but an important achievement of the portal project has been to develop a relational database for the geophysical metadata and data files to make them identifiable for purchase or download via the portal. This work is ongoing, and at present a total of 35 geophysical surveys are available.

Geochemical data. Stream sediment samples have been collected in Greenland since 1971 and geochemical mapping by means of systematically collected and analysed stream sediment samples has been undertaken by GGU/GEUS since 1975. A geochemical atlas of West and South Greenland was published in 2001 (Steenfelt 2001a) based on 7122 samples analysed for 43 chemical elements. A major task in the preparation of the atlas was the elimination of bias in the analytical data as a prerequisite for the production of the element distribution maps (Steenfelt 1999, 2001b). In 2011, a similar exercise was performed on five elements determined in 2644 stream sediment samples from North Greenland as part of an assessment of the zinc

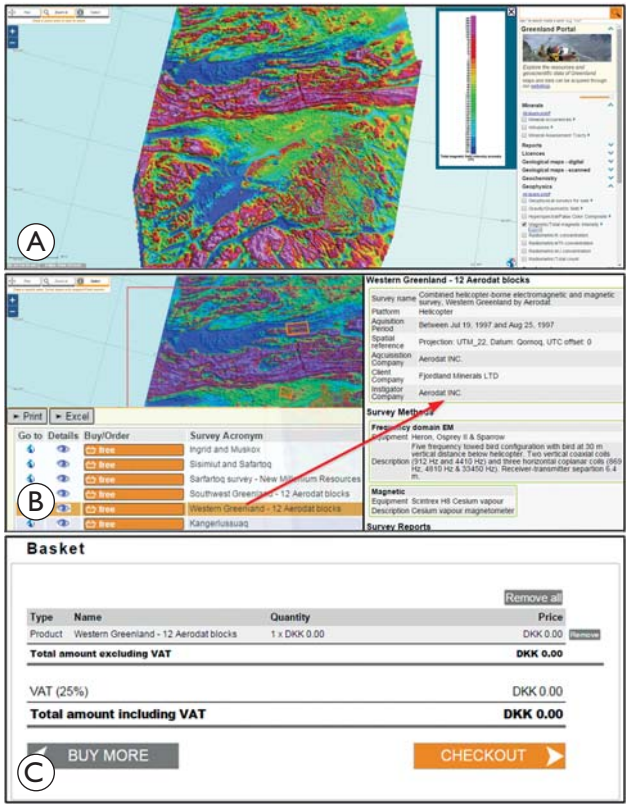

Fig. 3. **A**: The *Total magnetic intensity* layer shows where airborne magnetic data are available. **B**: The layer of *Geophysical surveys for sale* provides information on the individual geophysical surveys. Intuitive interaction between search results and the map makes it easy to see what geographical areas are part of the individual surveys. Based on metadata and the access to survey reports the user can assess the surveys before purchase or download. **C**: Individual surveys can be added to the online shopping basket and checked out through the webshop.

potential (Thrane *et al.* 2011). All geochemical data from these two projects are available in the Greenland Mineral Resources Portal – via the interactive map interface and as free download from the associated webshop. An important part of the ongoing project is the quality control of all geochemical analyses from more than 15 000 raw (non-calibrated) stream and scree sediment samples as well as from soil samples and heavy mineral concentrates – all of which are part of the portal.

Geological maps. Geological mapping of Greenland has led to a series of published maps at standard scales. The maps were traditionally produced using engraving techniques, but in 1998 GEUS turned to digital production of paper maps. In recent years the old paper maps have been digitised and made into seamless, geographically referenced products with homogeneous legends, suitable for web applications. A seamless 1:100 000 scale map with a homogenised legend covering 10 map sheets in southern West and South-West Greenland was finalised in 2010 (Keulen *et al.* 2010), and in 2013 GEUS launched a 1:500 000 scale compilation covering the whole of the ice-free area of Greenland (Pedersen *et al.* 2013; Fig. 2). Both map layers form important base maps in the Greenland Mineral Resources Portal. The GIS data from the 1:500 000 scale map are available for free download from the webshop.

Targeting the end users

The development of digitised facilities has been going on for many years during which valuable experience has been gathered. The development has always been demand-driven, but even though exploration companies are a quite well-defined user group, various requirements need to be addressed. The focus is not only to provide access to as much reliable data as possible, but also to create online facilities for screening and evaluating the data. Therefore, the development of the portal is based on cases that describe scenarios for a specific user (e.g. a small-scale miner) expecting a certain result. A couple of scenarios are given in the following to demonstrate the flexibility and potential of the Greenland Mineral Resources Portal.

Scenario 1: Discovery and download of geophysical data in a given area. Many exploration geologists are interested in geophysical data from a specific area. In the interactive map of the Greenland Mineral Resources Portal it is easy to zoom in on an area and see the available aeromagnetic data by switching on the *Total magnetic intensity* layer (Fig. 3A).

By adding the *Geophysical surveys for sale* layer to the map, information about the individual geophysical surveys available in the area, including metadata and reports, can be inspected (Fig. 3B).

The user buys data by adding the relevant surveys to the shopping basket, after which they can be checked out from the webshop (Fig. 3C). Many geophysical datasets are available free of charge, and others can be paid by credit card and subsequently downloaded.

Scenario 2: Search for stream sediment samples with high gold content. In the interactive map users can search through each of the geochemical datasets for samples with an element content larger than a value defined by the user. This makes it possible for the user to easily assess areas of interest

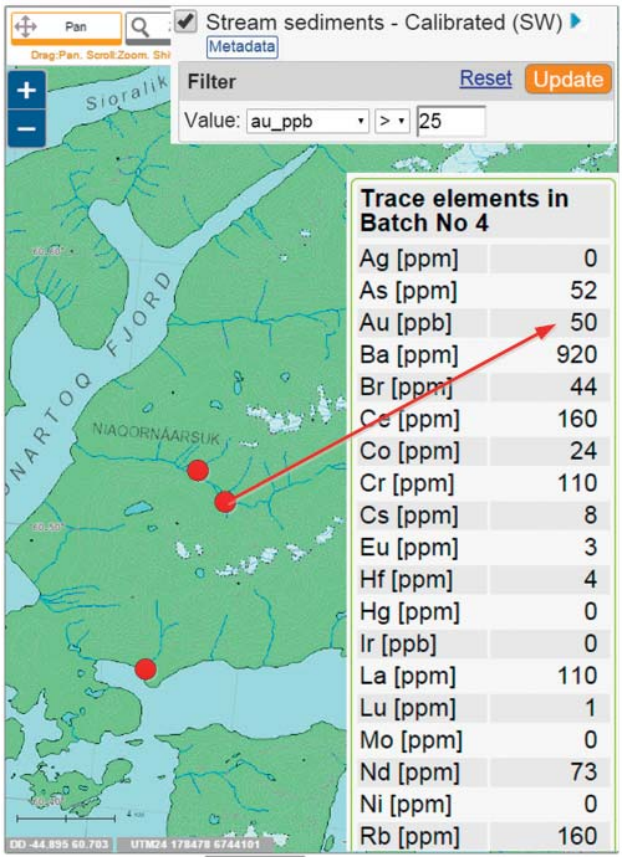

Fig. 4. A search for samples with more than 25 ppb gold in the calibrated stream sediment dataset from South-West Greenland. All analytical results for a given sample can be seen on the screen, and the entire (or geographic subsets) of the dataset can be downloaded from the webshop.

without advanced GIS software. In Fig. 4 the result of a search for samples with more than 25 ppb gold is shown for an area in South-West Greenland. The locations of stream sediment samples that fulfil that criterion are displayed on a map, and more information about the samples can be seen by clicking the red dots.

More advanced users can download all of the geochemical datasets (or geographic subsets) free of charge from the webshop for further analyses using their own software.

Looking ahead

The development of the Greenland Mineral Resources Portal is ongoing. More and more data types are added, and the existing datasets are continuously supplemented. In 2016, it is the plan to add a geochronological database and a drill-core directory and future plans include integration of satellite imagery, additional aerial photographic collections, more geochemical and geophysical data and digital elevation models. The user-friendly functions of the portal interface will be further improved and refined along the way, and users are always encouraged to give feed-back to GEUS and the Ministry of Mineral Resources for continuous improvements.

Acknowledgements

The Ministry of Mineral Resources under the Government of Greenland is thanked for financial support for the development of the Greenland Mineral Resources Portal. The authors also wish to thank the team from the Department of Petrology and Economic Geology as well as the Geological Datacentre at GEUS, who have actively worked to make the Greenland Mineral Resources Portal a success.

References

Jackson, T. & Green, K.P. 2016: Fraser Institute annual survey of mining companies 2015, 86 pp. Vancouver: Fraser Institute.

Keulen, N.T., Kokfelt, T.F. & Scherstén, A. 2010: Notes on the common legend to the 1:100 000 digital geological map of southern West and South-West Greenland, 61º 30´–64ºN. Danmarks og Grønlands Geologiske Undersøgelse Rapport **2010/119**, 41 pp.

Pedersen, M., Weng, W.L., Keulen, N.T. & Kokfelt, T.F. 2013: A new seamless digital 1:500 000 geological map of Greenland. Geological Survey of Denmark and Greenland Bulletin **28**, 65–68.

Rasmussen, T.M., Thorning, L., Riisager, P. & Tukiainen, T. 2013: Airborne geophysical data from Greenland. Geology and Ore, Exploration and Mining in Greenland **22**, 12 pp.

Riisager, P., Pedersen, M., Jørgensen, M.S., Schjøth, F. & Thorning, L. 2011: DODEX – Geoscience documents and data for exploration in Greenland. Geological Survey of Denmark and Greenland Bulletin **23**, 77–80.

Steenfelt, A. 1999: Compilation of data sets for a geochemical atlas of West and South Greenland based on stream sediment surveys 1977 to1997. Danmarks og Grønlands Geologiske Undersøgelse Rapport **1999/41**, 33 pp.

Steenfelt, A. 2001a: Geochemical atlas of Greenland – West and South Greenland. Danmarks og Grønlands Geologiske Undersøgelse Rapport **2001/46**, 39 pp.

Steenfelt, A. 2001b: Calibration of stream sediment data from West and South Greenland. A supplement to GEUS Report 1999/41. Danmarks og Grønlands Geologiske Undersøgelse Rapport **2001/47**, 43 pp.

Thorning, L., Christensen, L., Schjøth, F. & Stendal, H. 2004: Greenland Mineral Occurrence Map. Status report for the development of a prototype for the Internet, January 2004. Danmarks og Grønlands Geologiske Undersøgelse Rapport **2004/28**, 52 pp.

Thrane, K., Steenfelt, A. & Kalvig, P. 2011: Zinc potential in North Greenland. Danmarks og Grønlands Geologiske Undersøgelse Rapport **2011/143**, 64 pp.

Authors' address

Geological Survey of Denmark and Greenland), Øster Voldgade 10, DK-1350 Copenhagen K, Denmark, E-mail: *mp@geus.dk*

aFieldWork – an Android app for offline recording of geological information and data display

Martin Hansen, Matti Nelleman Petersen, Thomas F. Kokfelt and Bo Møller Stensgaard

Since 2008 the Geological Survey of Denmark and Greenland (GEUS) has used handheld devices (Personal Digital Assistents PDAs) for collecting field data in a digital format. Since PDAs are becoming obsolete and new device technology with improved functionality is available, it was decided to develop an Android-based application (app) that can be used by many mobile telephones and to test this on different devices during field work in Greenland.

The main objectives of the system are to provide field geologists working in remote areas without internet access with a quick and efficient way of: (1) recording information on a geological locality in digital format, (2) displaying existing digital geodata on maps, (3) securing a consistent way of reporting data and (4) transferring data quickly and efficiently to the central databases and GIS environments once the field teams return from their field work.

With the handheld device and the app (the system) the user collects data much in the same way as it was previously done using the modified GanFeld software with the PDAs (Schlatter *et al.* 2010), but with improved functions and a more user-friendly interface. The development of the system was guided by the following prerequisites:

- the device has to be relatively robust, lightweight, small and easy to handle,
- the device has to be easily replaceable and relatively cheap,
- the device includes an internal GPS and camera of sufficient quality with low power consumption; recharging must be with solar panels, or a mobile generator,
- the device must have backup, both internal (SD memory card) and external (laptop) during field work,
  the app must be independent of mobile networks and must work offline,
- the app must store data in a well-structured format allowing for easy transfer to other GIS environments,
- the system should allow for both data collection and display in the field, and editing of data in the field camp,
- new data as well as existing geodata and maps (topographic data, geological maps, geochemical, geophysical, etc.) should be displayed together, and easily imported into the app,
- the system should have a simple, intuitive, user-friendly interface that is easy to operate in the field under difficult conditions.

The decision to develop an app for the Android platform was based on (1) the wide variety of relatively cheap Android devices available in many different sizes (including several robust versions), (2) the Java development language runs on a Windows platform, the main development platform used at GEUS, and (3) the possibility to store data on a SD removable memory card that can easily be transferred to a laptop or PC in the field camps.

The aFieldWork app

The app was designed to require as little typing as possible. This was done to make digital capture of field data as easy and efficient as possible. The app is database-driven meaning that data have to be entered in a structured and consistent fashion. Although some of the data entry is compulsory and is entered via scrollable, drop-down lists of pre-defined and fixed content, other information is optional and includes free-text entry. The mandatory entry points and the predefinition of selection lists also induce the field geologists to describe and classify localities and geological features in a consistent way.

The first version of the app was a prototype allowing for sufficient collection of information about localities, lithology, samples, structures and photographs. The system was further developed and refined based on field tests of the prototype in Greenland.

Online and offline maps

Two different map types are implemented in the app. The user can choose to use (1) online maps from OpenStreetMap (if connected to the internet), or (2) pre-loaded OpenStreetMap or a series of pre-loaded maps stored in a database. The last option is by far the most advanced and requires considerable preparation, but provides the most flexibility including custom-drawn maps at different zoom levels (scales) as well as various overlays of other data types (Fig. 1).

© 2016 GEUS.

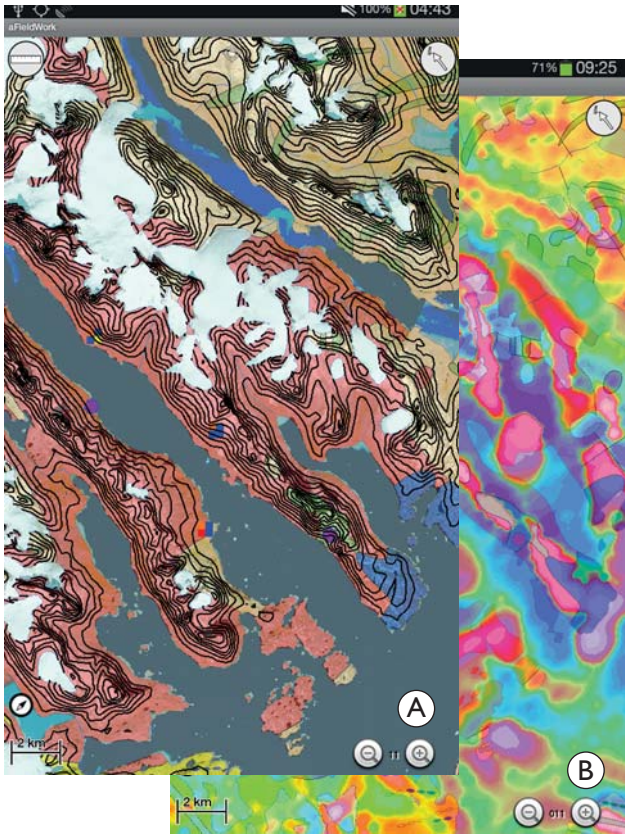

Fig. 1. **A**: Geological (1:500 000) map with layers of topographic contours and various locality point symbols. **B**: The same geographical area with an overlay of the analytical signal of the total magnetic intensity on top of the geological map.

All map types show and create geological localities as symbols. As long as the GPS is on, a colour-coded indicator shows each locality and the type of information which is attached to the locality. The user can make drawings and queries about spatial data, such as contours, trend lines and former localities. From the map a click on any locality or point will display attached information which can then be edited. While the map is displayed on the screen the user's position and walking direction will be shown. It is also possible to create points on the map that are not related to geological observations, a function useful for planning reconnaissance missions or drop-offs in the field by helicopter or boat. The user can make distance measurements on the maps and quickly obtain the coordinates of any point.

How to enter data

All data entries are geo-referenced via geographical co-ordinates taken from an internal GPS in the Android device together with information about its accuracy. The sample numbering follows GEUS' sample numbering system.
The user may prompt manual text entries, for e.g. longer descriptions of localities, rocks and samples. For example, the data entry point, or menu, for samples will not appear before the user selects the 'sample button'. This ensures a smooth and efficient data entry without interference of unnecessary information and menus. The selection lists are in many cases designed so that the most frequently used entries are listed first and can be tailor-made before field use for special requirements.

'Localities'. A locality is created by tapping the 'New Locality' button on the start-up screen of the aFieldWork app (Fig. 2). The user is then prompted for a description of the locality (not mandatory). The co-ordinates are displayed as decimal degree, degree decimal minutes or converted to UTM coordinates, along with their GPS accuracy and time of creation. The locality is automatically stored and provided with a unique locality ID which is composed of the year, the unique GEUS initials of the geologist and the number of the locality, e.g. 14smw003 for the third locality of the geologist smw in the year 2014.

From the locality screen it is possible to add free text notes or to open entry points for 'Earth Materials', 'Samples', 'Structure' or 'Photos'. Each entry point has been colour-coded to facilitate identification (Fig. 2).

'Earth Materials' (lithology). The entry point 'Earth Materials' (Fig. 3) refers to information about the lithologies found at a given locality. This information is entered from a predefined, hierarchical system of 'Rock Class', 'Rock Type' and subsequently 'Rock Name' allowing a narrowing down to a few items with a few taps on the screen. The classification of the 'Earth Materials' (the rocks) follows classification schemes suggested by the International Union of Geological Sciences (IUGS). It is possible to omit a rock name at 'Earth Materials'. Extra information, such as colour, metamorphic grade, mineralogy (as 'common', 'alterations' and 'ore' minerals) and fossils can be entered. This information is mostly entered via predefined selection lists. Once the 'Earth Materials' data are entered it can be saved, not only to the locality, but also to a Quick list ('quiklst'). This makes it easy to add information from this Quick list to additional localities with the same 'Earth Material' information.

'Samples'. At the entry point 'Sample' the user can number and register information on particular rock samples collected in the field. The rock samples must be connected to an

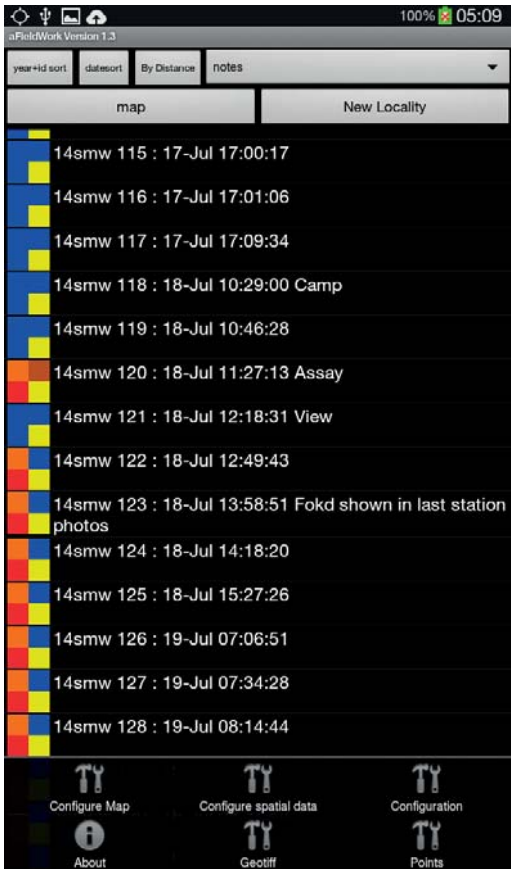

Fig. 2. The main screen of the app showing a list of localities with colour code added for easy reference: 'Earth Materials' (lithology), 'Samples', 'Structure' measurements or 'Photos'.

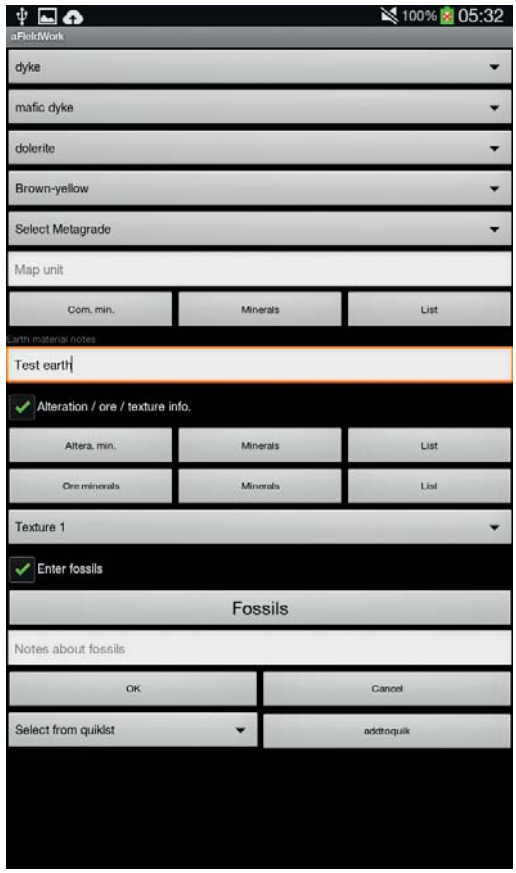

Fig. 3. The 'Earth Material' (lithology) data entry screen.

'Earth Material' entry and cannot be saved without this critical information. The 'Earth Material' entry can either be an existing one or can be created when the 'Sample' entry point is selected. The sample is automatically assigned a sample number (by default one increment above the previous sample number). A sample type and a sample purpose can be selected from drop-down lists and a free text can also be entered.

Structural measurements. At the entry point 'Structure' the user can digitally capture information on a structural measurement. Like rock samples, structural observations must be connected to an 'Earth Material'.

Structural class (linear or planar), type (e.g. fault, shear zone for a planar class) and detail (e.g. generation for a foliation) can be selected from drop-down lists. Measurements made by a hand-held compass can be entered as numbers using a keyboard or by two sliding bars.

'Photos'. Photographs can be taken with the internal camera, in which case there is no need for data entry besides an optional free text description of the photograph. If an external camera is used, the user can enter the first and last number of the photographs taken at a given locality. It is also possible to enter free text for the photograph taken with an external camera. Sketches and annotations can be added to the photographs taken by the internal camera. They will be saved as separate files leaving the original photograph intact.

Behind the screen

All data are stored in an SQLite database used in most small digital devices. It is a relatively advanced database system supporting foreign keys, triggers and (with an extension) spatial data. The back-end database structure ensures well-structured, compatible data and facilitates data transfer to

other databases. Because the predefined selection lists in aFieldWork app are based on the database queries it is easy to extend the system or to configure it to suit the geological requirements of specific areas.

Part of the application (app) is based on open source software. The database handling is based on the Android SQLite Manger (aSQLiteManger), the map is based on the Mapsforge library (Mapsforge) and the spatial functions on the SpatiaLite library (SpatiaLite).

Future development

A future update of the app could be improved by adding a number of new features:

- import of points from Google Earth,
- built in documentation of all 'Earth materials' and 'Structure' classes,
- an easy overview of all structural data by symbols,
- the possibility to choose a location on the map and be guided there,
- easy export of data for analysis and planning of field work in field camps,
- use of air-pressure sensors to improve altitude determinations,
- new information fields for registering the type of locality, e.g. geological locality, field camp, archaeological sites, emergency pick-up site, etc.,
- display of the paths taken during field work,
- display geo-referenced raster images (e.g. images of geophysical, geochemical and remote sensing data) which will most likely be based on the RasterLite library (RasterLite).

Future versions of the app will enable the user to handle other sample types, e.g. stream sediments. It will be possible to develop and add new modules and functions including improved tools for importing and extracting data and maps.

Conclusions

Compared to the previous PDA-based system, data entry in aFieldWork app is much easier and faster with the new Android system. The design is simpler and more intuitive. The presence of a real database system and look-up tables on the devices ensures data integrity. It also allows swift transfer of data to central databases after field work. The SQLite databases are binary and compatible between different platforms so an SQLite database generated on an Android device can simply be moved to a Windows computer and used from this without any conversion.

The Android system is easy to configure and the large open-source community makes a lot of free software available.

GEUS has successfully used small digital handheld devices and software for digital data capture and observations on localities, rocks, samples, etc. in Greenland for a number of years. With the development of the new aFieldWork app, GEUS has modernised and improved this important field work tool for the geologist.

Acknowledgements

The Android system was tested during field work in South-East Greenland by participants in the SEGMENT 2012. The participants in these field parties provided valuable input and comments to the system which are greatly appreciated. Thanks to the two referees, Thorsten Nagel and Denis M. Schlatter, who contributed with valuable suggestions which greatly improved the manuscript.

References

Schlatter, D.M., Buller, G., Larsen, U. & Stensgaard, B.M. 2010: Digital field data capture: the Geological Survey of Denmark and Greenland experiences in Greenland. The Association of Applied Geochemistry, Explore **147**, 2–14.

aSQLiteManger, RasterLite, SpatiaLite *http://www.gaia-gis.it/gaia-sins/spatialite-sql-4.4.0.html*

Mapsforge *https://github.com/mapsforge/mapsforge*

Authors' address

Geological Survey of Denmark and Greenland, Øster Voldgade 10, DK-1350 Copenhagen, Denmark, E-mail *mh@geus.dk*

jAgeDisplay: software for evaluation of data distributions in U-Th-Pb geochronology

Tonny B. Thomsen, Tjerk Heijboer and Pierpaolo Guarnieri

During the past 10–15 years, analytical innovations in geochronology have greatly enhanced the application of geochronological data to geological problems. The advances are mainly driven by developments in laser ablation inductively coupled plasma mass spectrometry (LA-ICPMS) which allows for rapid determination of U-Th-Pb ages of mineral grains in large sample sets. LA-ICPMS has now become the most common tool in the application of zircon geochronology to a host of different geological problems.

One of the most regularly used approaches to evaluate complex U-Th-Pb geochronological data populations is to use a diagram that combines a binned frequency histogram and a probability density distribution plot (PDP), as described by Sircombe (2004) and Ludwig (2003). This type of diagram is particularly common in sedimentary provenance studies using large sets of age data (Morton *et al.* 1996; Pell *et al.* 1997; Rainbird *et al.* 1997; Sircombe 1999; Fergusson *et al.* 2001). It is also useful for the analysis of complex age patterns in metamorphic and igneous rocks. The Microsoft Excel workbook AgeDisplay (Sircombe 2004) has often been used to produce these diagrams but it is not supported by versions of Excel that are newer than 2003. Stand-alone software for PC written in Java was therefore developed by the Geological Survey of Denmark and Greenland (GEUS). It is based on the same formulae as described in Sircombe (2004), thus the name jAgeDisplay (with j for Java), and has additional features and graphic improvements. Here we present the setup, operation and capability of the software with examples from single-grain U/Pb age data obtained by LA-ICPMS spot analysis.

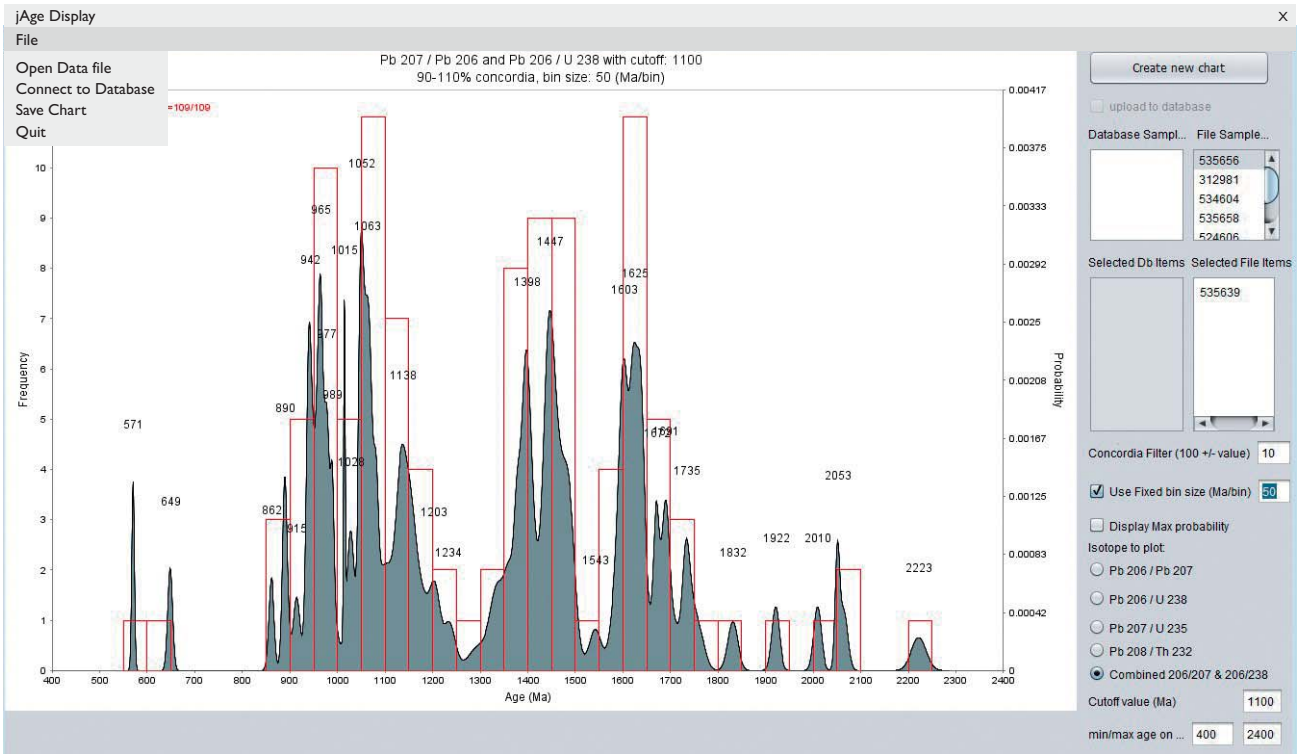

Fig.1. Combined 400–2400 Ma histogram and PDP chart with calculated maximum probability ages for distinct distribution peaks of zircon populations from a single sample, using coupled $^{206}Pb/^{238}U$ and $^{207}Pb/^{206}Pb$ age pairs. A crossover age of 1100 Ma is used, where $^{206}Pb/^{238}U$ ages and $^{207}Pb/^{206}Pb$ ages are used below and above this age, respectively. A *Fixed bin size* of 50 Ma/bin and a *Concordia Filter* of ±10% were used.

© 2016 GEUS.

Setup and operation of jAgeDisplay

The jAgeDisplay package (current version 1.0) for PC includes an executable Jar file, a Java MS DOS batch file, a HTML readme file, a brief manual and a folder with test data files. The application is available as shareware from the corresponding author, and it is installed by copying the files you receive to any PC with Java.

jAgeDisplay supports both comma-separated (CSV) and tab-delimited (TAB) input text files, with the same table headers and data types as in AgeDisplay, Iolite (Paton *et al*. 2011), and GEUS' in-house Zirchron software and database. The input file can include age data from one or more samples, which are loaded from the *File* menu in the main window (Fig. 1) using the *Open Data file* option. The input file includes four commonly used radiogenic U-Th-Pb age pairs, viz. $^{206}Pb/^{238}U$, $^{207}Pb/^{235}U$, $^{207}Pb/^{206}Pb$ and $^{208}Pb/^{232}Th$, together with the sample identification, the name or number of individual analyses, the name of the analytical sequence and information about correction for common lead content. Output charts can be saved in PDF or PNG file format through the *Save Chart* option in the *File* menu.

The main window consists of a chart area to the left and the selected sample parameters to the right. When an input file has been loaded, the samples available for plotting are found in the *File Samples* field or, if loaded from a database, in the *Database Samples* field. To plot one or more of the loaded samples, they are dragged and dropped in their respective *Selected File Items* or *Selected Db Items* fields. The parameters to be used for the chart are selected, and the *Create new chart* button is pressed.

Combined histograms and probability–density plots for each radiogenic age pair ($^{206}Pb/^{238}U$, $^{207}Pb/^{235}U$, $^{207}Pb/^{206}Pb$, $^{208}Pb/^{232}Th$) can be produced. In addition, charts combining the $^{206}Pb/^{238}U$ and $^{207}Pb/^{206}Pb$ age pairs can be made by manually setting a specific age (denoted *Cutoff value*) that controls the change from using $^{206}Pb/^{238}U$ ages for the younger age range to $^{207}Pb/^{206}Pb$ ages for the older age range of the chart (Fig. 1). The frequency in terms of number of analyses for each bin in the histogram is shown on the left y-axis, and the calculated probability distribution of zircon ages for the data set on the right y-axis. Thus, the probability–density distribution provides an estimate of the true mineral-age distribution for a given rock sample.

The plots can be adjusted by the following parameters:

- *Concordia Filter* is the maximum allowed discordance (in per cent) for analyses to be considered as concordant, and is determined as 100 ± Set#Value. This separates the age data used for the plot into two different fields representing 'concordant' and 'discordant' data. In detrital zircon provenance studies a value of ±10% is often used, where this threshold is used as a measure of the quality of the calculated ages. In contrast to AgeDisplay, the complete data set including the 'discordant' data is not shown behind the 'concordant' data, but separately using the same axis as for the concordant data.

- *Use Fixed bin size (Ma/bin)* allows a histogram of filtered ages to be plotted (based on the concordant data obtained via the *Concordia Filter*), where the bin size in million years (Ma) is manually chosen. If this checkbox is deselected, a calculated value for the bin size is used, based on the formulae in Doane (1985).

- *Display Max Probability* (checkbox) shows the ages of the calculated probability peaks for the 'concordant' data set.

- *Min/Max age* controls the age range to be shown in the chart.

Additional parameters can be set through right-clicking on the produced chart, where the title, chart title, axis range, appearance and colours can be modified.

jAgeDisplay can display a single chart for one data set or stacked charts of several data sets (Fig. 2). Stacked charts are useful for comparison of data sets sampled, e.g. at different geographical, stratigraphical or lithological locations in order to identify trends or differences in the age distributions. The stacking follows the order chosen in the *Selected File Items* (or *Selected DB Items*) window at the right, and can be rearranged as appropriate. As the purpose of stacking is to compare, the stacked data sets are displayed for the same age range as set by the *Min/Max age* control.

Use of jAgeDisplay in sedimentary provenance and petrological studies

Detrital studies typically aim to characterise the age population(s) from a sample by means of a large number of single grain analyses, e.g. obtained by LA-ICPMS. In statistical terms the goal of such studies is to estimate the so-called probability density function that gives the relative *likelihood* of the different ages in the population (Vermeesch 2012). Zircon is the most common mineral used for detrital studies, but other mineral phases like rutile and titanite are increasingly being employed in order to obtain supplementary information (e.g. Zack *et al*. 2004; Stendal *et al*. 2006; Meinhold *et al*. 2008; Thomsen *et al*. 2015;

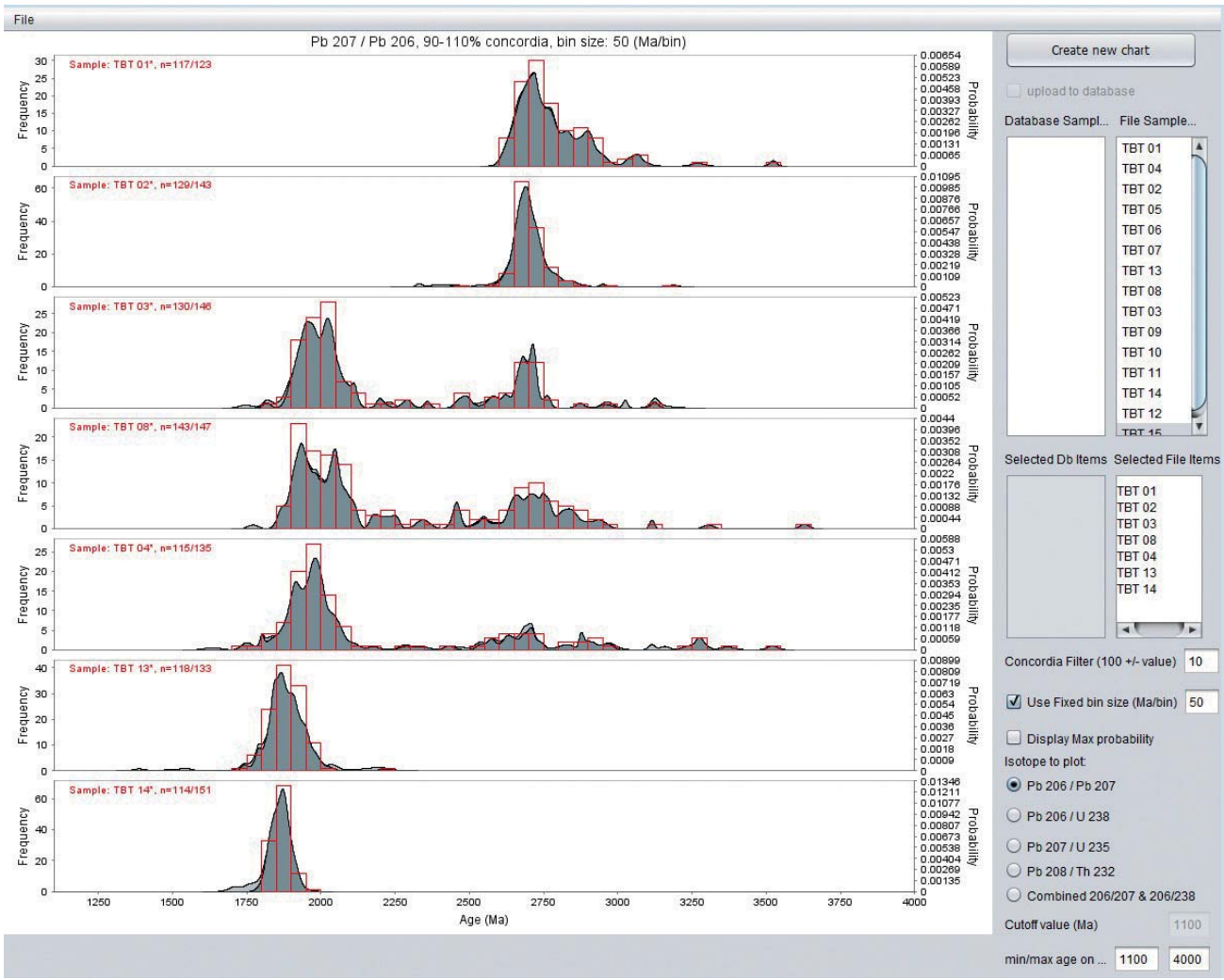

Fig. 2. Stacked chart of combined histograms and PDP charts from 1100 to 4000 Ma of zircons from seven samples using $^{207}Pb/^{206}Pb$ ages, a *Fixed bin size* of 50 Ma/bin and a *Concordia Filter* of ±10%.

Bruand *et al*. 2016). Signatures of sediment sources not represented in the zircon data set may be present in detrital titanite, rutile or apatite populations. In addition, age data on these minerals may provide further chronological and petrogenetic insight into the tectono-thermal history of their source regions (e.g. McAteer *et al*. 2010, 2014; Knudsen *et al*. 2015; Thomsen *et al*. 2015). Similarily, in metamorphic and magmatic petrology, complex zoning patterns that correspond to distinct geological events can be recorded in zircon, baddeleyite, titanite, rutile, apatite, monazite, xenotime, allanite or any other accessory mineral phase for which the age can be determined by U-Th/Pb methods and can be assessed in probability density plots diagrams through the jAgeDisplay software.

Future options in jAgeDisplay

Although PDPs constitute the most widespread method used today for displaying detrital age distributions, they lack a firm theoretical basis as probability density estimators, and this may produce counter-intuitive results when the number of analyses and/or their quality (precision) is high (Vermeesch 2012). Accordingly, an alternative and robust standard statistical technique, the Kernel Density Estimation (KDE) as described in Vermeesch (2012), will be included in jAgeDisplay, so that users can compare the two methods. We also expect to include a more versatile option for age distribution plots, where any two isotopic pairs can be used in a PDP or KDE diagram, in a similar way as the built-in option for combined $^{206}Pb/^{238}U$ and $^{207}Pb/^{206}Pb$ age distributions.

Detailed statistics reporting information on the calculated maximum probability peaks can be useful for improved age differentiation of, e.g. magmatic or metamorphic episodes. At present, this information is only indirectly reported through the plot axis. We expect to include this information in pop-up windows for single peaks and as a print-out option including the statistics of all peaks or a chosen age section of the plot.

Finally, the jAgeDisplay software offers an option to load input files from a database through a local server connection (*File => Connect to Database*). At present, this option only allows reading of certain data types from GEUS' Oracle server. It is our intention to expand this and thus provide users with access to data from a local server repository.

Additional remark

In this presentation only U/Pb geochronological data obtained by LA-ICPMS analysis on zircon are used. jAgeDisplay can of course also evaluate U-Th-Pb data acquired by other instrumentation and complex age distribution patterns measured from other accessory phases such as titanite, rutile, apatite, monazite, allanite, perovskite, xenotime or other minerals that can incorporate U or Th into their crystal structure.

References

Bruand, E., Storey, C. & Fowler, M. 2016: An apatite for progress: Inclusions in zircon and titanite constrain petrogenesis and provenance. Geology **44**(2), 91–94, *http://dx.doi.org/10.1130/G37301.1*

Doane, D.P. 1985: Aesthetic frequency classifications. The American Statistician **30**, 181–183.

Fergusson, C.L., Fanning, C.M. & Green, T.J. 2001: Proterozoic–Cambrian detrital zircon and monazite ages from the Anakie Inlier, central Queensland: Grenville and Pacific-Gondwana signatures. Australian Journal of Earth Sciences **48**(6), 857–866.

Knudsen C., Thomsen T.B. & Hinchey, A. 2015: Detrital zircon, rutile and titanite investigations from present-day Labrador river drainages: fingerprinting the Grenvillean front. Goldschmidt Conference, Prague, 16–21 August 2015. Abstract 1627 only.

Ludwig, K. 2003: User's Manual for Isoplot 3.00: A geochronological toolkit for Microsoft Excel. Berkeley Geochronology Center Special Publication **4**, 74 pp.

McAteer, C.A., Daly, J.S., Flowerdew, M.J., Connelly, J.N., Housh, T.B. & Whitehouse, M.J. 2010: Detrital zircon, detrital titanite and igneous clast U–Pb geochronology and basement–cover relationships of the Colonsay Group, SW Scotland: Laurentian provenance and correlation with the Neoproterozoic Dalradian Supergroup. Precambrian Research **181**, 21–42.

McAteer, C.A., Daly, J.S., Flowerdew, M.J., Whitehouse, M.J. & Monaghan, N.M. 2014: Sedimentary provenance, age and possible correlation of the Iona Group, SW Scotland. Scottish Journal of Geology **50**, 143–158.

Meinhold, G., Anders, B., Kostopoulos, D. & Reischmann, T. 2008: Rutile chemistry and thermometry as provenance indicator: an example from Chios Island, Greece. Sedimentary Geology **203**, 98–11.

Morton, A.C., Claoué-Long, J.C. & Berge, C. 1996: SHRIMP constraints on sediment provenance and transport history in the Mesozoic Statfjord Formation, North Sea. Journal of the Geological Society, London **153**, 915–929.

Paton, C., Hellstrom, J.C., Paul, P., Woodhead, J.D. & Hergt, J.M. 2011: Iolite: Freeware for the visualisation and processing of mass spectrometric data. Journal of Analytical Atomic Spectrometry **26**(26), 2508–2518.

Pell, S.D., Williams, I.S. & Chivas, A.R. 1997: The use of protolith zircon-age fingerprints in determining the protosource areas for some Australian dunes sands. Sedimentary Geology **109**, 233–260.

Rainbird, R.H., McNicoll, V.J., Theriault, R.J., Heaman, L.M., Abbott, J.G., Long, D.G.F. & Thorkelson, D.J. 1997: Pan-continental river system draining Grenville orogen recorded by U-Pb and Sm-Nd geochronology of Neoproterozoic quartzarenites and mudrocks, northwestern Canada. Journal of Geology **105**, 1–17.

Sircombe, K.N. 1999: Tracing provenance through the isotope ages of littoral and sedimentary detrital zircon, eastern Australia. Sedimentary Geology **124**, 47–67.

Sircombe, K.N. 2004: AgeDisplay: an EXCEL workbook to evaluate and display univariate geochronological data using binned frequency histograms and probability density distributions. Computers and Geosciences **30**, 21–31.

Stendal, H., Toteu, S.F., Frei, R., Penaye, J., Njel, U.O., Bassahak, J., Nni, J., Kankeu, B., Ngako, V. & Hell, J.V. 2006: Derivation of detrital rutile in the Yaoundé region from the Neoproterozoic Pan-African belt in southern Cameroon (Central Africa). Journal of African Earth Sciences **4**(4), 443–458.

Thomsen, T.B., Knudsen, C. & Hinchey, A. 2015: Detrital zircon, rutile and titanite investigations from present-day Labrador river drainages: Fingerprinting the Grenvillean front. Geological Survey of Denmark and Greenland Bulletin **33**, 77–80.

Vermeesch, P. 2012: On the visualisation of detrital age distributions. Chemical Geology **312–313**, 190–194, *http://dx.doi.org/10.1016/j.chemgeo.2012.04.021*

Zack, T., von Eynatten, H. & Kronz, A. 2004: Rutile geochemistry and its potential use in quantitative provenance studies. Sedimentary Geology **171**(1), 37–58.

Authors' address

Geological Survey of Denmark and Greenland, Øster Voldgade 10, DK-1350 Copenhagen K, Denmark. E-mail: *tbt@geus.dk*